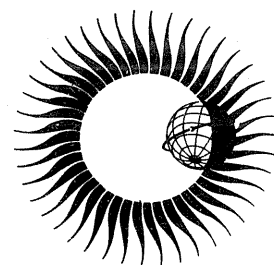


WORLD DATA CENTER A for Solar-Terrestrial Physics



MANUAL ON IONOSPHERIC ABSORPTION MEASUREMENTS



June 1976

WORLD DATA CENTER A

National Academy of Sciences

2101 Constitution Avenue, N.W.

Washington, D. C., U.S.A., 20418

World Data Center A consists of the Coordination Office

and seven Subcenters:

World Data Center A
Coordination Office
National Academy of Sciences
2101 Constitution Avenue, N.W.
Washington, D.C., U.S.A. 20418
[Telephone: (202) 389-6478]

Glaciology:

World Data Center A:
Glaciology
U.S. Geological Survey
1305 Tacoma, Washington, U.S.A. 98402
[Telephone: (206) 593-6506]

Rotation of the Earth:

World Data Center A:
Rotation of the Earth
U.S. Naval Observatory
Washington, D.C., U.S.A. 20390
[Telephone: (202) 254-4023]

Meteorology (and Nuclear Radiation):

World Data Center A:
Meteorology
National Climatic Center
Federal Building
Asheville, North Carolina, U.S.A. 28801
[Telephone: (704) 258-2850]

Solar-Terrestrial Physics (Solar and
Interplanetary Phenomena, Ionospheric
Phenomena, Flare-Associated Events,
Geomagnetic Variations, Magnetospheric
and Interplanetary Magnetic Phenomena,
Aurora, Cosmic Rays, Airglow):

World Data Center A
for Solar-Terrestrial Physics
Environmental Data Service, NOAA
Boulder, Colorado, U.S.A. 80302
[Telephone: (303) 499-1000, Ext. 6467]

Oceanography:

World Data Center A:
Oceanography
National Oceanic and Atmospheric
Administration
Washington, D. C., U.S.A. 20235
[Telephone: (202) 634-7249]

Solid-Earth Geophysics (Seismology,
Tsunamis, Gravimetry, Earth Tides,
Recent Movements of the Earth's
Crust, Magnetic Measurements,
Paleomagnetism and Archeomagnetism,
Volcanology, Geothermics):

Rockets and Satellites:

World Data Center A:
Rockets and Satellites
Goddard Space Flight Center
Code 601
Greenbelt, Maryland, U.S.A. 20771
[Telephone: (301) 982-6695]

World Data Center A
for Solid-Earth Geophysics
Environmental Data Service, NOAA
Boulder, Colorado, U.S.A. 80302
[Telephone: (303) 499-1000, Ext. 6521]

Notes:

1. World Data Centers conduct international exchange of geophysical observations in accordance with the principles set forth by the International Council of Scientific Unions. WDC-A is established in the United States under the auspices of the National Academy of Sciences.
2. Communications regarding data interchange matters in general and World Data Center A as a whole should be addressed to: World Data Center A, Coordination Office (see address above).
3. Inquiries and communications concerning data in specific disciplines should be addressed to the appropriate subcenter listed above.

WORLD DATA CENTER A for Solar-Terrestrial Physics



REPORT UAG - 57

MANUAL ON IONOSPHERIC ABSORPTION MEASUREMENTS

edited by

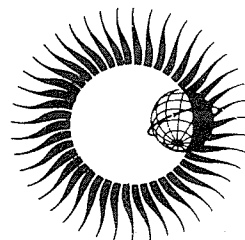
K. Rawer

Fraunhofer-Gesellschaft
Institut für Physikalische Weltraumforschung
Freiburg, Federal Republic of Germany

June 1976

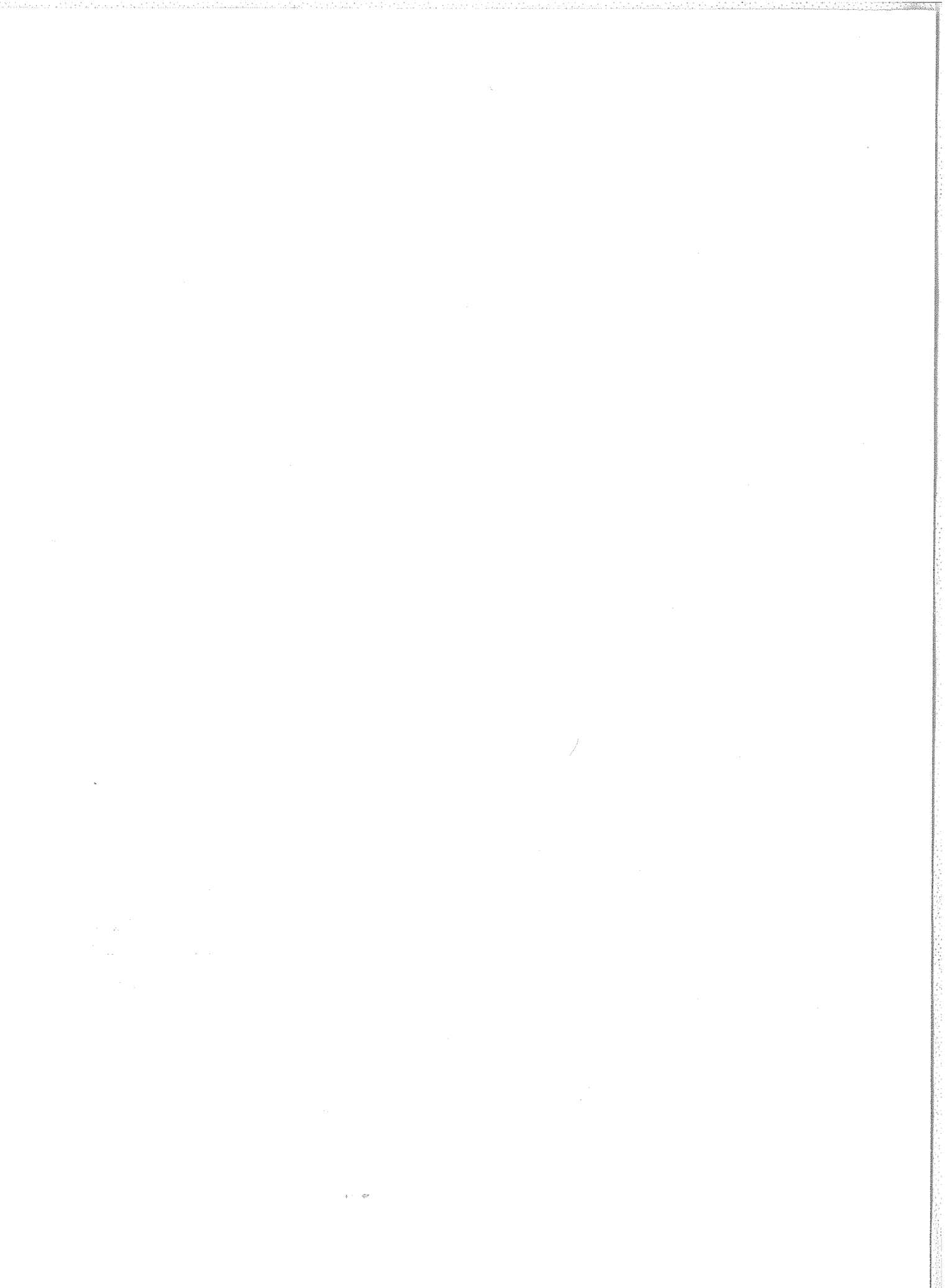
Published by World Data Center A for
Solar-Terrestrial Physics, NOAA, Boulder, Colorado
and printed by

U.S. DEPARTMENT OF COMMERCE
NATIONAL OCEANIC AND ATMOSPHERIC ADMINISTRATION
ENVIRONMENTAL DATA SERVICE
Asheville, North Carolina, USA 28801



SUBSCRIPTION PRICE: \$25.20 a year; \$12.00 additional for foreign mailing; single copy price varies.* Checks and money orders should be made payable to the Department of Commerce, NOAA. Remittance and correspondence regarding subscriptions should be sent to the National Climatic Center, Federal Building, Asheville, NC 28801, Attn: Publications.

*PRICE THIS ISSUE \$4.27



SUMMARY TABLE OF CONTENTS

| | |
|---|------------|
| FOREWORD, by A. H. Shapley | Page iv |
| EDITOR'S NOTE, by K. Rawer | v |
| Part I: <u>Generalities</u> by K. Rawer | vi |
| Chapter 1. Propagation Influences | 1 |
| Chapter 2. Theory | 7 |
| Chapter 3. Fading | 29 |
| Part II: <u>The Different Methods of Measurement</u> by W. Dieminger, E. A. Lauter, J. Mass, K. Rawer, K. Schlegel, H. Schwentek and J. Taubenheim | |
| Chapter 4. Method A1 (Pulse Reflection Method) | 44 |
| Chapter 5. Method A2 (Cosmic Noise Absorption Method) | 105 |
| Chapter 6. Method A3 (a) Oblique Incidence Field Strength Observations on Frequencies Above 2 MHz | 122 |
| Chapter 7. Method A3 (b) Oblique Incidence Field Strength Observations on Frequencies In and Below the MF Broadcasting Band | 147 |
| Chapter 8. The Partial Reflection Method | 164 |
| Chapter 9. Satellite Measurements of Absorption | 181 |
| Chapter 10. References and General Appendices | 186 |

Foreword

A project of assembling a manual on ionospheric absorption and the relevant observing techniques has been in progress for many years. Absorption measurements have long been recognized as a powerful tool in applied radio propagation work and are, in geophysics, one of the few synoptic ground-based techniques which can shed light on what is sometimes called the "ignorosphere," the region of the atmosphere not accessible to ionosondes, satellites or other global measurement techniques. Measurements of ionospheric absorption have not, however, been as widely employed as they might have been, and where they have been used it has often been with considerable difficulty, because of the lack of a suitable manual for the guidance of workers in the field. Brief instruction manuals were produced for the international programs -- the International Geophysical Year and the International Years of the Quiet Sun (see References in Chapter 10.1), but these were not attempts at a comprehensive treatment of the subject. Thus the expertise has been spread by less efficient techniques and workers have not been able to gain from the experience of others as much as they should.

The present manual has been a long time project of the International Union of Radio Science (URSI), having its origin in the URSI-IGSY Committee in the mid-1960s on which Prof. K. Rawer was consultant for ionospheric absorption. It has been one of those projects which, though recognized as intrinsically valuable, has suffered from competition with other activities in the remarkably busy decade which ensued. It is a credit to Prof. Rawer's persistence that the work has finally been brought to completion.

The English language is not native to the Editor nor any of the contributors to this work. The publication staff at World Data Center A for STP, notably Miss Helen Coffey, has suggested many small changes in the direction of idiomatic English, but it has not been practical nor was it deemed desirable to suggest wholesale changes which could so easily divert the intent and impact of the original authors. The reader can realize that typing the master copy of the manuscript was not an easy job, and will appreciate the work particularly of Miss Alice McRae and Miss May Starr.

The manual is being issued in this special data report series of World Data Center A for STP in the interest of stimulating systematic ionospheric absorption observations in more parts of the world, and in addition should result in more meaningful data for the scientific community through the World Data Center system. If this happens, our efforts, which have been small in comparison to those of Prof. Rawer and his collaborators, will be repaid through improved data services to our community of users.

A. H. Shapley, Director
National Geophysical and Solar-Terrestrial
Data Center
Environmental Data Service, NOAA
Boulder, Colorado, USA
(which operates WDC-A for STP)

June 1976

Editor's Note

For symbols, units and nomenclature, this report follows the recommendations of Document U.I.P. 11 (S.U.N. 65-3) as accepted in 1965 by the International Union for Pure and Applied Physics (IUPAP). The most important rules are (decimal numbers in brackets refer to the above document):

A physical quantity may be read as the product of a numerical value times a unit [1.1]. Symbols for physical quantities shall be printed in italics [1.2.2]. Symbols for units shall be printed in regular (steep) types [2.1.1]; they should not be accompanied by a full stop or put into plural [2.1.2].

(1) These rules allow relationships to be expressed either by equating physical quantities (non-specified equations) or by equating numerical values as obtained by dividing each physical quantity by the relevant unit. For example the relationship between frequency f , wavelength λ and phase velocity c may be written:

$$(I) \text{ in physical quantities: } f = \frac{c}{\lambda}$$

$$(II) \text{ or in numerical values: } f/\text{Hz} = \frac{c/(\text{ms}^{-1})}{\lambda/\text{m}}$$

Because (if refraction can be neglected) c is constant, one introduces its numerical value $c = 3 \cdot 10^8 \text{ms}^{-1}$ thus giving:

$$(i) \quad f = 3 \cdot 10^8 \text{m s}^{-1}/\lambda \quad \text{and} \quad (ii) \quad f/\text{Hz} = \frac{3 \cdot 10^8}{\lambda/\text{m}}$$

both forms being algebraically equivalent (since $\text{Hz} = \text{s}^{-1}$).

(2) If a unit is included with each variable (physical quantity) as is done in (ii) above, one may just say that numerical values as measured in the indicated units must be inserted into the equation. Supposing, for example, that we have measured the wavelength λ to be 50 m. From this we obtain:

$$f/\text{Hz} = \frac{3 \cdot 10^8}{50 \text{m/m}} = \frac{3 \cdot 10^8}{50} = 6 \cdot 10^6, \quad \text{i.e. } f = 6 \cdot 10^6 \text{ Hz} = 6 \text{ MHz}$$

This is an easy and straightforward use of specified equations. If other than conventional units have been used for the measurement, the transformation into conventional ones must first be performed.

NOTE: Specified equations without units (e.g. $f = 3 \cdot 10^8/\lambda$) are no longer allowed.

(3) The great advantage of this nomenclature is that it allows substitution of and computation with physical quantities and units according to the well-known algebraic rules. For example a change of units simply means substitution such that no particular reasoning is needed. One must, of course, know the relation between the original unit and its replacement.

Example 1: 1 km = 1000 m, i.e. 1 m = 10^{-3} km

gives

$$f = 3 \cdot 10^8 \cdot (10^{-3} \text{ km}) \text{s}^{-1}/\lambda \quad \text{and} \quad f/\text{Hz} = \frac{3 \cdot 10^8}{\lambda/(10^{-3} \text{ km})}$$

$$f = 3 \cdot 10^5 \text{ km s}^{-1}/\lambda \quad f/\text{Hz} = \frac{3 \cdot 10^5}{\lambda/\text{km}}$$

Example 2: 1 nautical mile = 1 $\overline{\text{nm}}$ = 1.855 km; $\text{s}^{-1} = \text{Hz}$; $10^6 \text{Hz} = 1 \text{ MHz}$

gives

$$f = 3 \cdot 10^5 \left(\frac{\overline{\text{nm}}}{1.855} \right) 10^{-6} \text{ MHz}/\lambda \quad \text{and} \quad f/\left(\frac{\text{MHz}}{10^6} \right) = \frac{3 \cdot 10^5}{\lambda/\left(\frac{\overline{\text{nm}}}{1.855} \right)}$$

$$f = .1617 \overline{\text{nm}} \text{ MHz}/\lambda \quad f/\text{MHz} = \frac{.1617}{\lambda/\overline{\text{nm}}}$$

Thus in spite of the fact that certain systems of units are now recommended by international decision (see (4)) the admitted forms of equations allow any system of units to be used.

NOTE: A particular situation exists in electromagnetism where one has rationalized and non-rationalized systems of units. We apply only rationalized units, e.g. the SI system. Warning: most of the cgs systems used in the literature are non-rationalized.

(4) The recommended system of units called SI (Système International) [9.16] is a coherent, rationalized system with the six basic units: m, kg, s, A(=Ampère), K(=Kelvin, now without the degree sign °) and cd(=candela). For practical use one often adds V(=Volt).

PART I: GENERALITIES

by

K. Rower
Fraunhofer-Gesellschaft
Institut für Physikalische Weltraumforschung
Freiburg, Federal Republic of Germany

| | Page |
|---|------|
| Table of Contents | |
| CHAPTER 1. PROPAGATION INFLUENCES | 1 |
| 1.1 Measurement Method | 1 |
| 1.2 Spatial Decrease | 1 |
| 1.3 Reflection | 1 |
| 1.4 Refraction | 4 |
| 1.5 Diffraction | 4 |
| 1.6 Scattering | 5 |
| CHAPTER 2. THEORY | 7 |
| 2.1 Mechanism of Ionospheric Absorption | 7 |
| 2.2 Absorption Coefficient | 7 |
| 2.3 Absorption Decrement | 12 |
| 2.4 Deviative Absorption | 13 |
| 2.5 Non-deviative Absorption | 14 |
| 2.6 Distinction between Contributions from Different Layers | 15 |
| 2.7 Differential Absorption | 18 |
| 2.8 Collision Frequencies | 18 |
| Appendix 2.A The Notion of "Collision Frequency" | 21 |
| Appendix 2.B Generalized Magneto-electronic Dispersion Theories | 24 |
| CHAPTER 3. FADING | 29 |
| 3.0 Nature and Origin of Fading | 29 |
| 3.1 Fading Spectrum | 29 |
| 3.2 Autocorrelation Analysis | 31 |
| 3.3 Distribution Functions | 36 |
| 3.4 Sampling Problems | 41 |

CHAPTER 1. PROPAGATION INFLUENCES

1.1 Measurement Method

The object of ionospheric absorption measurements is to determine the true absorption of radio waves in ionospheric layers, namely: attenuation by loss of energy or transfer of energy from the wave into the medium. Measurements are made by determining the attenuation suffered by such waves over their propagation path. When reducing measured data, attenuation caused by influences other than energy transfer to the medium must be eliminated as far as possible.

Measurements are generally made by receiving a radio wave after it has propagated through the ionospheric medium. The strength of the source of the radio wave (transmitters or natural sources) should be known accurately. However in most of the techniques currently used the transmitted power is not measured at the transmitting antenna itself but determined by comparison under different conditions from field strength values at the receiver. Thus the only measuring technique effectively used is field strength measurement. Absolute field strength measurements are (1) difficult to make because they demand antennas whose absolute characteristics are accurately known; and (2) would often be misleading because of environmental influences which can hardly be avoided at most sites. Therefore, most measurements are based upon relative field strength, comparing radio frequency (RF) voltages in the receiver instead of absolute measurements of the fields outside. The only condition is that on any frequency used the factors which determine the effective gain must be kept constant with time. New calibration is therefore needed at any time where any one of these parameters has been changed.

1.2 Spatial Decrease

Spatial dilution of energy is the most important attenuating influence which is not due to true losses. It is a consequence of the geometry of propagation. Waves originating from a point source propagate as spherical waves, thus the field strength E decreases inversely with distance d :

$$d \cdot E = \text{constant.}$$

This is conveniently expressed in terms of cymomotoric force (cmf) which is constant for such conditions:

$$d \cdot E = d_o E_o = \text{constant,}$$

or in dB units

$$(E_o - E)/\text{dB} \equiv 20 \log_{10}(E_o/E_d) = 20 \log_{10}(d/d_o) \quad (1.1)$$

(The unit of cymomotoric forces is Volt (V)). Eq. (1.1) is only valid if the spherical wave propagation is not disturbed by obstacles. Such obstacles may be of any kind: reflecting surfaces, refractive media, diffracting obstacles and scatter are most common forms. Their effects will be discussed in that order.

In the first two cases the propagational influence produces a divergence of the bundle of rays along which the wave energy is flowing to the receiving antenna which may differ considerably from the free-space case. The cases of diffraction and scattering are more complex. These two cases must be avoided when measuring absorption.

For plane ground the spatial attenuation can be adequately represented by replacing the actual distance, d , by the group path, P' , in Eq. (1.1). In the general case the actual effective divergence of the wave front must be calculated.

1.3 Reflection

Quite generally reflection may occur at the interface of two different media or inside a continuously variable medium.

1.3.1 Reflection at an interface is described by Fresnel's formulas. Depending on the polarization of the incident wave, these may be used to describe reflection from ground. Figure 1.1 gives the reflection coefficient and reflection loss as a function of the angle of incidence for different typical conditions.

Ground reflection is also important for understanding realistic radiation diagrams of antennas. In particular, the typical decrease of radiation at low elevation angles is due to losses in the ground.

1.3.2 Reflection in the ionosphere can be partial or total. In a medium with continuously variable refractive index (due to continuous variation of electron density) partial reflection is usually extremely small and quite negligible, except for particular conditions. These occur where a steep gradient of electron density, collision frequency or both exists. Thus partial reflection occurs at certain levels, mainly in the lower ionosphere.

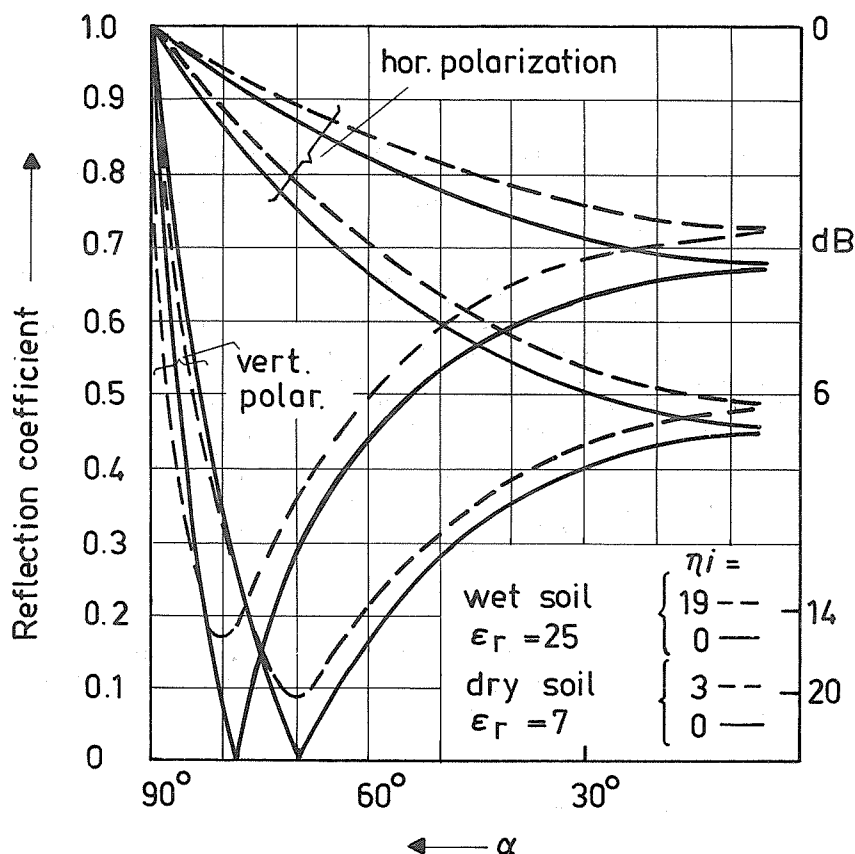


Fig. 1.1 Reflection coefficient (left hand ordinate) and ground reflection loss (right hand ordinate) for different combinations of soil and frequency as function of α , the angle of incidence. $\epsilon_r + j\eta_i$ is the complex (relative) dielectricity constant of the soil; $\eta_i = \kappa_i / (\omega \epsilon_0)$, κ being the conductivity.

Es layers if they are homogeneous in the horizontal plane may produce such partial reflections -- normally in a rather limited frequency range. Most observed "partial reflection" from Es layers is, however, due to a patchy structure in the horizontal plane (see Section 1.5 below). Note that it is essential to distinguish between o- and x-components before interpreting partial reflection traces.

1.3.3 For a radio wave entering the ionosphere (from below or from above) the refractive index decreases as the wave proceeds into the layer towards the level of maximum electron density. Increase of electron density and lowering of the frequency have similar effects. The lower the frequency of the wave, the more the ray is refracted towards the horizontal direction. Rays incident under a small angle of elevation are bent to such an extent that they leave the layer again as if they had been reflected (Figure 1.2a). Steeper rays have a better chance to pass through the layer but with a sufficiently low frequency or high electron density even a vertically incident ray can be returned (Figure 1.2b). At vertical incidence this occurs at the level where the refractive index vanishes. For a continuous plane stratification the general condition of reflection for a wave incident under an angle α_0 is (Figure 1.3, μ is the refractive index):

$$\mu_{refl.} = \sin \alpha_0. \quad (1.2)$$

Reflection occurs at that level where this condition is satisfied. Eq. (1.2) shows that the reflection level varies with the angle of incidence on the ionosphere, α_0 (Figure 1.3). For a plane ionosphere Eq. (1.1) continues to be valid provided the group path length P' is taken instead of the geometric distance d .

Thus total reflection in the ionosphere more closely resembles sharp ray bending than partial reflection. In cases where the effect of collisional absorption is strong enough, however, losses may occur near the reflection level (see Section 2.4, Deviative Absorption).

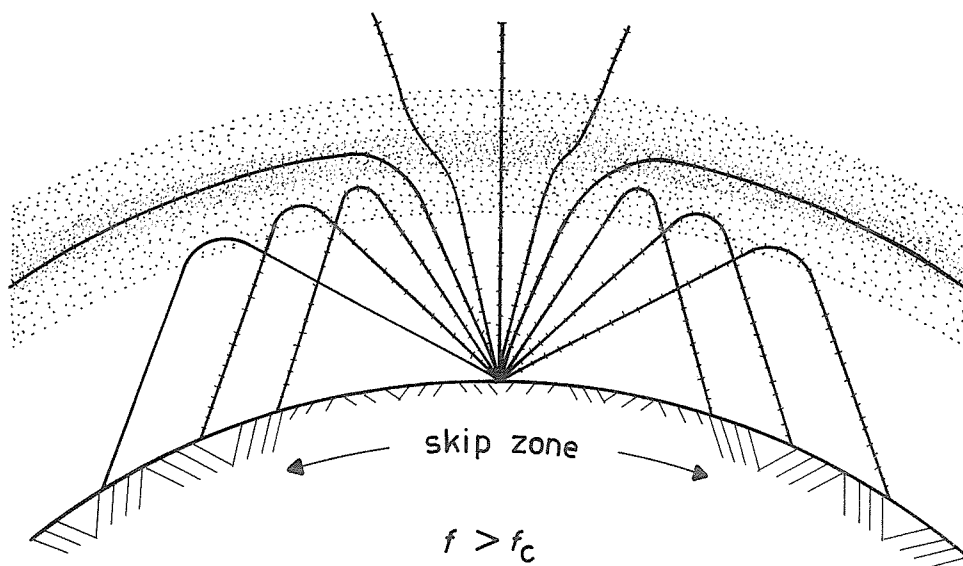


Fig. 1.2a

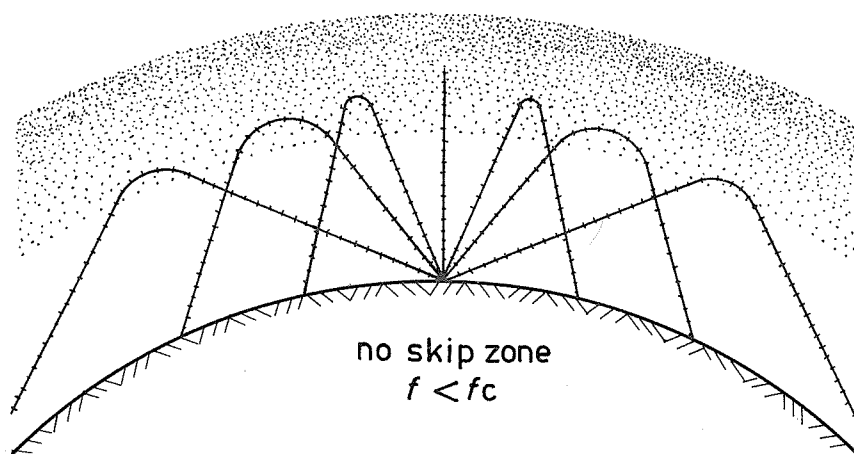


Fig. 1.2b

Fig. 1.2 Ray path due to refraction at different angles of incidence

- a) for a frequency about 15% above the critical one
- b) for a frequency below the critical one.

1.3.4 With respect to the geometry of propagation, the curvature of the effective reflecting surface is of great importance. Convex curvature increases the divergence of the bundle of rays so that the field strength decreases more rapidly with the distance than it would without curvature. Concave curvature, however, produces focusing effects. Focusing is an important feature of ionospheric "geometrical optics". Under ideal conditions the general curvature of the ionosphere should produce strong "caustic" focusing for rays near grazing incidence only. The real ionosphere quite often has much stronger curvature due to "ripples", most of which are probably produced by atmospheric gravity waves. These ripples can

produce field strength variations typically of some 10 dB. Unfortunately for absorption measurements, this kind of fading is the slowest one we have so that abnormal focusing conditions may last for a quarter of an hour or more. In such cases the observed absorption decrement may be very misleading.

The focusing effects tend to be more pronounced with multiple reflections for which the curvature effect occurs repeatedly. This is a strong argument against the direct use of multiple echoes for absorption measurements, though techniques have been developed which avoid this difficulty.

When the field strength at oblique incidence ionospheric propagation is estimated, the standard curvature of the ionosphere has a definite effect. It was determined by Rawer first for specular reflection [1947], then including refraction effects (see Section 1.4) [1948, 1950, 1952], and finally with refraction in two layers, thus including deviative absorption [Rawer *et al.*, 1952a; Rawer, 1955].

1.4 Refraction

Due to secondary radiation of free electrons oscillating with the incident wave the effective phase velocity in a plasma is greater than in free space. In other words the refractive index is smaller than unity. This produces refraction in the opposite direction to that usually found in optical examples (see Figure 1.3). In the presence of a magnetic field the medium becomes doubly refracting with two refractive indices at each level. These indices are involved functions of electron density, wave frequency, collision frequency and magnetic field parameters. Both refractive indices usually decrease with increasing electron density. Exceptions are due to the resonance phenomena for the x wave near the gyrofrequency and in the case of propagation in the "whistler mode" at frequencies below the gyrofrequency. From the viewpoint of theory refraction is closely linked with absorption (see Chapter 2 below).

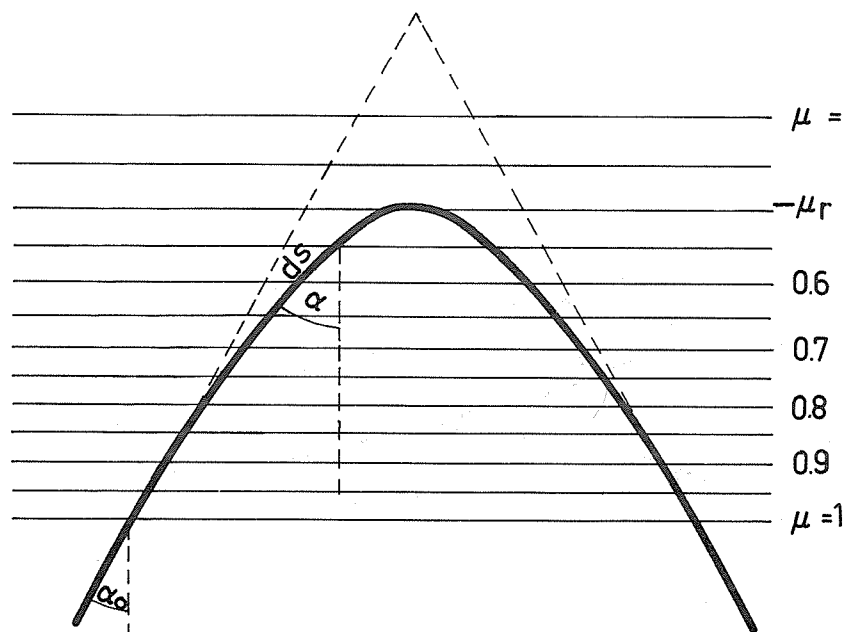


Fig. 1.3 Ray bending by refraction in an ionospheric layer: "refractive reflection", see Eq. (1.2).

1.5 Diffraction

An obstacle that is not large relative to the wavelength does not produce a clearly limited "shadow zone" because the wave bends round the obstacle. Thus its shadow may almost disappear at larger distance. Many diffraction effects can be described in a simplified, easily accessible way by using the notion of Fresnel zones. A plane surface at a given distance from the source may be subdivided into circular rings depending on the path length between the source and the point of observation. The rings are arranged so that this length differs by just half a wavelength from one circle to the next one. Figure 1.4 demonstrates the typical cases of source and observing point at ground (a), and of source at infinity with observation at ground (b). Thus the phase in any zone is opposite on the average to that of the two neighboring zones. In other words the contributions of successive zones almost cancel each another.

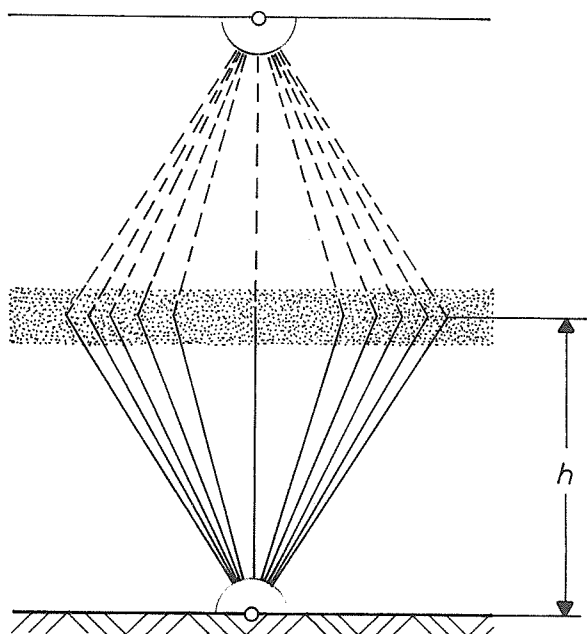


Fig. 1.4a

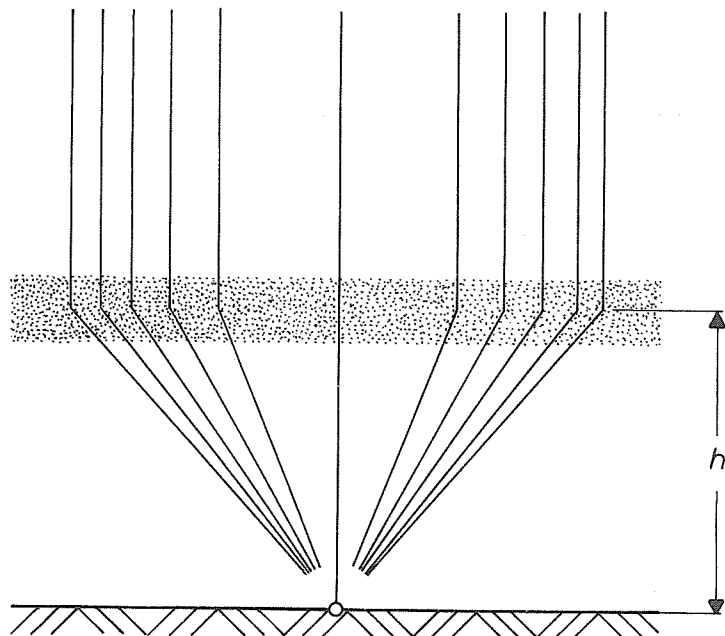


Fig. 1.4b

Fig. 1.4 Construction of Fresnel zones with observation at ground:

- a) reflection case: source and observation point are identical
- b) transmission case: source at infinity overhead the observation point.

If propagation is limited by a hole covering only very few zones, the passing of wave energy through that hole critically depends upon its diameter. The energy is less than expected from geometry if the hole covers an even number of zones; it is better than expected if this number is odd. Diffraction may be important when clouds of ionization are present. In particular, sporadic E often occurs as a "patchy" thin layer. As the frequency is increased, reflection will eventually occur from the patches with the largest electron density. These may be of the size of one or a few Fresnel zones, or even smaller. For a reflected wave these patches then act as an irregular diffracting screen.

In these complex cases "partial reflection" is apparently found, but as a consequence of inhomogeneity in the horizontal direction. For absorption measurements such conditions should be avoided wherever possible. Cases of strong partial reflection, i.e. penetration and reflection occurring simultaneously on the same frequency and for the same component, must be identified and treated correctly in the reduction of data (see Section 4).

In order to give an idea of the size of the Fresnel zones Table 1.1 lists the radii of the first four zones at normal incidence for different frequencies at different virtual heights.

1.6 Scattering

Small obstacles produce important diffraction effects. This involves sideward scattering of wave energy. If many such obstacles are present, the result may be a more or less diffuse distribution of incoherent secondary waves in all directions. This diffuse case is not often found among the propagation phenomena we have to consider here. But cases where an important amount of energy is scattered sideways and backwards are not rare.

The most important conditions where this kind of abnormal propagation occurs are:

- Spread F conditions, mainly around the peak level of the F2 layer;
- Diffuse reflections from particular forms of layers in the E region: equatorial Es (type q), auroral Es (type a), compare Piggott and Rawer [1972, Section 4.8].

In all these cases the reflection coefficient is considerably smaller than one. These conditions must therefore be recognized and be eliminated during the reduction of absorption measurements. Spread conditions may also affect waves penetrating the ionosphere (see Chapter 3).

Table 1.1

Radii (km) of the First Four Fresnel Zones
at Normal Incidence for 6 Frequencies at 2 Virtual Heights

(first line for penetration, second line for reflection)

| Frequency (MHz) | λ (m) | for h = 100 km | | | | for h = 300 km | | | | |
|-----------------|---------------|----------------|-----|-----|-----|----------------|-----|-----|------|------|
| | | Zones | 1 | 2 | 3 | 4 | 1 | 2 | 3 | 4 |
| 0.3 | 1000 | | 10 | 14 | 17 | 20 | 17 | 25 | 30 | 35 |
| | | | 7 | 10 | 12 | 14 | 12 | 17 | 21 | 24 |
| 2 | 150 | | 3.9 | 5.5 | 6.7 | 7.7 | 6.7 | 9.5 | 11.6 | 13.4 |
| | | | 2.7 | 3.9 | 4.7 | 5.5 | 4.7 | 6.7 | 8.2 | 9.5 |
| 3 | 100 | | 3.2 | 4.5 | 5.5 | 6.3 | 5.5 | 7.7 | 9.5 | 10.9 |
| | | | 2.2 | 3.2 | 3.9 | 4.5 | 3.9 | 5.5 | 6.7 | 7.7 |
| 5 | 60 | | 2.5 | 3.5 | 4.2 | 4.9 | 4.2 | 6.0 | 7.3 | 8.5 |
| | | | 1.7 | 2.5 | 3.0 | 3.5 | 3.0 | 4.2 | 5.2 | 6.0 |
| 10 | 30 | | 1.7 | 2.5 | 3.0 | 3.5 | 3.0 | 4.3 | 5.2 | 6.0 |
| | | | 1.2 | 1.7 | 2.1 | 2.5 | 2.1 | 3.1 | 3.7 | 4.2 |
| 30 | 10 | | 1.0 | 1.4 | 1.7 | 2.0 | 1.7 | 2.5 | 3.0 | 3.5 |
| | | | 0.7 | 1.0 | 1.2 | 1.4 | 1.2 | 1.7 | 2.1 | 2.4 |

CHAPTER 2. THEORY

2.1 Mechanism of Ionospheric Absorption

An electromagnetic wave in propagating through a plasma is refracted and, in general, attenuated as a consequence of forced oscillations of the electrons due to the alternating electric field of the wave. The effects depend upon the amplitude and frequency of the wave: the lower the frequency, the greater the amplitude of the forced oscillations. The energy of the wave is partially transferred to these oscillations; per unit path, the energy transfer is proportional to the electron density in the plasma. In fact, the energy balance of the wave is not seriously changed because an overwhelming part of the transferred energy is restored to the wave by secondary radiation of the electrons. Each oscillating electron acts as a secondary transmitter radiating on the same frequency as the wave. The relevant secondary fields are, however, shifted in phase relative to the original wave field. In essence, the secondary waves superimposed upon the primary ones produce a continuous phase shift along the propagation path so that the phase velocity differs from that in free space.

The transfer of energy from the wave through oscillation of electrons and back to the wave by secondary radiation is lossless provided the oscillation is not hindered. If, however, an electron suffers a collision with another particle, there is a disturbance of the process of organized reradiation; in this case there is in fact a loss of energy from the original wave. As most collisions are elastic ones, the electron's energy remains kinetic so that the lost energy finally heats the electron gas. Collisions are, therefore, events by which the wave irreversibly loses energy and is attenuated.

2.2 Absorption Coefficient

2.2.1 The attenuation can be described by an exponential decrease of the field strength, E , of the wave:

$$E = E_0 \exp(-\kappa s) \quad (2.1)$$

s being the path length and κ the absorption coefficient.

The absorption coefficient κ can be interpreted as the imaginary part of a generalized, complex wave number, k . Another generalization introduces a complex refractive index, n , which has μ for the real part and $\chi = (c_0/\omega) \cdot \kappa$ for the imaginary one, $\omega \equiv 2\pi f$ being the pulsation of the wave. Thus, the imaginary part of n is just proportional to the absorption index κ , but the coefficient decreases with increasing frequency f .

2.2.2 Since the attenuation is produced by collisions involving the oscillating electrons, the amount of attenuation necessarily depends on two factors:

- 1) the efficiency of energy transfer from the wave into electron oscillations,
- 2) the probability of collisions between electrons and other particles.

The first of these is concerned with the "source" of the lost energy and depends on the energy picked up by the electrons from the wave. The mechanism is rather complicated in our ionosphere because of the presence of the Earth's magnetic field. This field produces a kind of resonance effect at the gyrofrequency, f_B , for one of the two possible circular polarizations of a wave: namely that for which the sense of rotation is the same as that of the natural free motion of electrons in the field. The rotation frequency f_B of an electron around the magnetic field line is roughly 1 MHz at the Earth's surface. It varies with the geomagnetic location of the station.

The second factor describes the true loss mechanism, i.e. the "sink" of energy. Let $\bar{\nu}$ be an "adequate" measure of the collisions between an electron and other particles which we may provisionally call the effective collision frequency, and N the electron density. Then the "collisional loss" which is inflicted on the wave is proportional to the product $\bar{\nu}N$. The absorption coefficient should therefore be obtained by multiplication of $\bar{\nu}N$ with a "dispersive factor" describing the first influence. A detailed discussion of the notion of "collision frequency" is given in Appendix 2.A. It is shown there that the correct definition of $\bar{\nu}$ is averaged transport collision frequency.

Taking account of the influence of the magnetic field and of collisions, the conditions of radio wave propagation in a plasma must be described by a rather complicated equation, the "dispersion formula" first given by Lassen [1927] and by Appleton [1928]. Another one published by Hartree [1929] and also by Appleton [1932] is not applicable to ionospheric radio wave propagation because it contains additional terms which do not agree with observed facts (e.g. the occurrence of whistlers is not compatible with this formula). The Appleton-Lassen dispersion formula is, however, only valid for weak collisional attenuation. General dispersion equations valid for strong attenuation also have been established by Majumdar [1938], V. A. Bailey [1937], and more recently by Sen and Wyler [1960] (see Section 2.2.6 and Appendix 2.B).

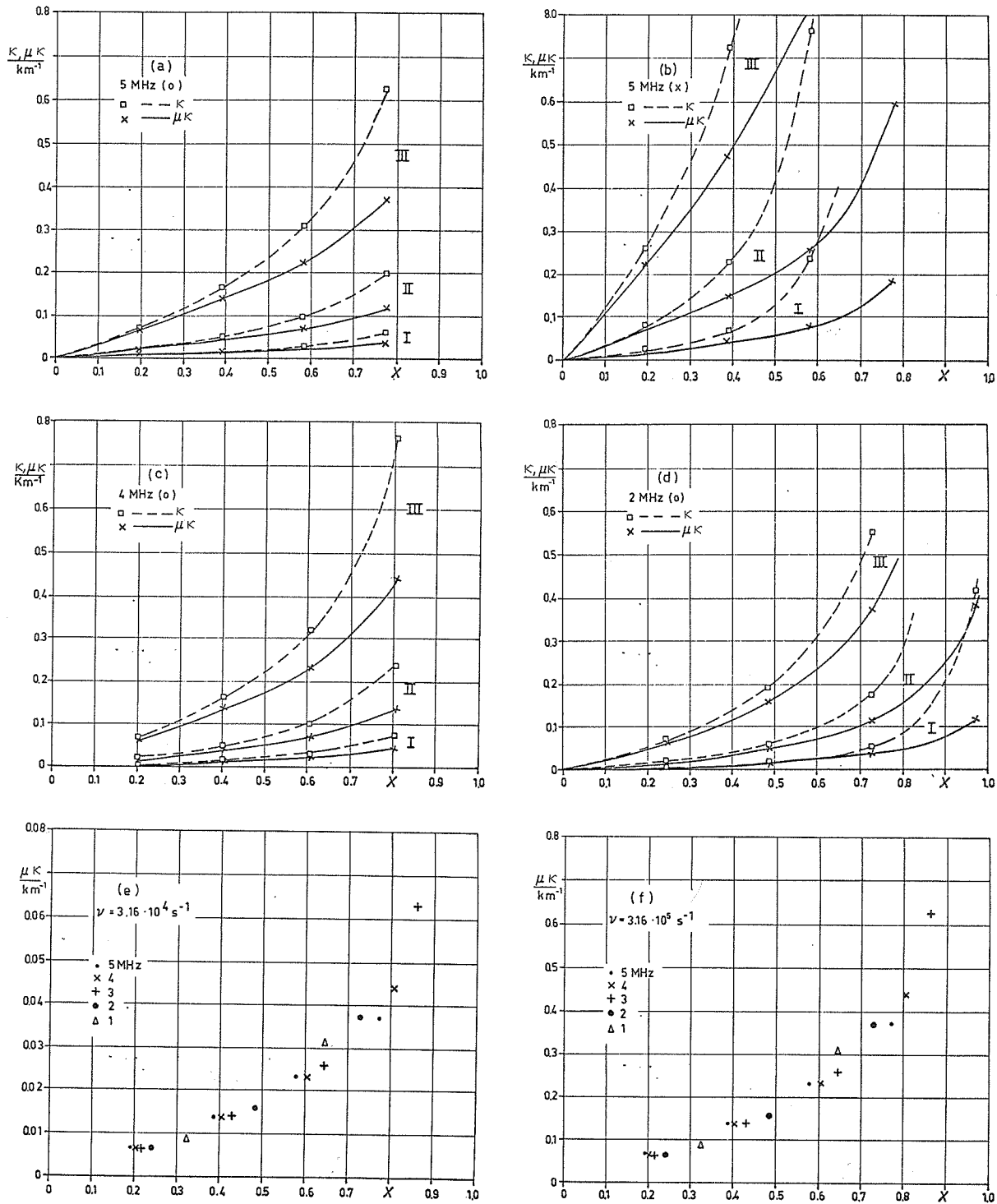


Fig. 2.1 Absorption coefficient κ obtained with the Appleton-Lassen dispersion formula as a function of the reduced electron density $X = f_p^2/f^2$. Magnetic parameters for southern Spain. Indices I, II, III identify collision frequency as $\nu = 3.16 \cdot 10^4$, $1 \cdot 10^5$ and $3.16 \cdot 10^5 \text{ s}^{-1}$ respectively.

(a) and (b) give absorption coefficient κ (broken curve) and product $\mu\kappa$ (full curve for $f = 5 \text{ MHz}$);

(a) ordinary (o) component,

(b) extraordinary (x) component,

(c) same curves for $f = 4 \text{ MHz}$, o component,

(d) same curves for $f = 2 \text{ MHz}$, o component,

(e) and (f) show product $\mu\kappa$ just for the ordinary component and $\nu = 3.16 \cdot 10^4 \text{ s}^{-1}$ and $3.16 \cdot 10^5 \text{ s}^{-1}$, respectively. The symbols identify the frequencies 1, 2, 3, 4 and 5 MHz as indicated. (Wavelength $\lambda = 300, 150, 100, 75$ and 60 m , respectively.) Note that 1 MHz is less than the gyrofrequency, the other frequencies are greater. Comparison of Figures (e) and (f) show proportionality with ν but more than proportionality increase with X . Warning: When $\kappa \cdot \lambda$ becomes greater than about 0.3, the Appleton-Lassen formula must be replaced by the Sen-Wyller formula, see text and Figure 2.3.

2.2.3 The most important effect of the magnetic field is to cause double refraction: a wave entering the ionosphere normally splits up into two waves of almost circular polarization. The two waves' components propagate almost independently of each other with opposite sense of rotation. As the electron density increases along the wave path, the polarizations of the two components change continuously, becoming elliptical and eventually, for the ordinary wave, linear at the reflection level. When sounding the ionosphere with radio waves, one thus usually obtains two separate echo traces. Above the gyrofrequency f_B these are called "o" (ordinary) and "x" (extraordinary) respectively; below f_B "x" and "z" respectively. At high latitudes a "z" mode is also sometimes seen above the gyrofrequency. Here "x" and "z" modes both stem from the "extraordinary" branch of the dispersion equation, and "o" from the "ordinary" one. (For details see Rawer and Suchy [1967]). Different absorption coefficients are valid for the two cases because of differences in the mechanism by which energy is transferred to the electrons. The "gyro-resonance" effect influences only the extraordinary component and can cause a large increase in the absorption coefficient.

2.2.4 The effect of collisional attenuation is described by the imaginary member in the dispersion equation. Therefore absorption coefficients can be computed from the complex dispersion equation, separately for each component. Figure 2.1 shows results obtained from the Appleton-Lassen formula. The first couple of subfigures 2.1 allows a comparison of the ordinary mode (Figure 2.1a) and of the extraordinary one (Figure 2.1b). The difference is quite appreciable. It would even be greater at lower frequencies. The first four subfigures (a...d) present the absorption coefficient κ , as well as the product $\mu \cdot \kappa$, both as a function of the reduced electron density X . It can be seen that the absorption coefficient κ varies linearly for small X but only in a very limited range. The product $\mu \cdot \kappa$, however, achieves a large range of linearity with X . Subfigures 2.1c and d are equivalent with 2.1a but on lower frequencies. The results are not very different because we use a reduced electron density on the abscissa, namely $X \propto N/f^2$. This is further shown by subfigures 2.1e and f in which the product $\mu \cdot \kappa$ only is shown, but for a series of frequencies between 1 and 5 MHz and for two different collision frequencies. The dispersion of the points remains small in a rather large range which extends further than the linearity range. It is also seen that the product $\mu \cdot \kappa$ is proportional to the collision frequency ν . (The ordinate scales have been chosen after the ν -ratio.) At the frequency 1 MHz (which is the only one below the gyrofrequency) one realizes that these points give no greater dispersion, but have different sign of deviation from the other frequencies for low and large X -values. It is therefore sufficient for absorption work to use an approximation to the full Appleton-Lassen formula for representing the product $\mu \cdot \kappa$. This introduces a factor $1/\mu$ into the equation for κ . A good approximation for both components is the following one:

$$\mu^2 \approx \frac{f^2 - f_N^2 \pm f \cdot |f_L|}{(f \pm |f_L|)^2} \quad (2.2)$$

and

$$\kappa = 1.344 \cdot 10^{-7} \text{ m}^{-1} \frac{1}{\mu} \cdot \frac{(\nu/\text{s}^{-1}) \cdot (N/\text{m}^{-3})}{((f \pm |f_L|)/\text{Hz})^2} \quad (2.3)$$

where f_L is the projection of the gyrofrequency vector (which is parallel to the magnetic field) on the direction of the wave normals, $|f_L|$ its absolute value:

$$f_L = f_B \cos \theta$$

and $f_L = 0$ at the magnetic equator.

Following Rawer and Suchy [1967], Eq. (2.3) may also be written in a more involved CP approximation:

$$\kappa = 1.344 \cdot 10^{-16} \text{ km}^{-1} \cdot \frac{(\nu/\text{s}^{-1}) \cdot (N/\text{m}^{-3}) \cdot (f/\text{MHz})^{1/2}}{\left[(f^2 - f_N^2 \pm f \cdot |f_L|)^{1/2} / \text{MHz} \right] \cdot \left[(f \pm |f_L|) / \text{MHz} \right]^{3/2}} \quad (2.4)$$

The upper signs are valid for the ordinary and the lower ones for the extraordinary wave components. Eqs. (2.3) and (2.4) are not valid near the reflection level. The expressions only apply when the polarization is circular or near circular and fail when linear polarization is approached. They are usually called QL (quasi-longitudinal) in the literature because the terms containing the component of the gyrofrequency parallel to the magnetic field in the dispersion equation are greater than those containing the perpendicular component. This can, however, occur when the magnetic field makes quite large angles with the direction of propagation so that it is preferable to call the approximation CP (circular polarization). Eqs. (2.2) through (2.4) are very useful for the reduction of absorption measurements, at least on frequencies above the gyrofrequency f_B . In this approximation the absorption coefficient always increases with decreasing frequency.

In practice since $f_L = 0$ at the magnetic equator Eqs. (2.2) through (2.4) go over into the simple Sellmeier (small ν) approximation

$$\kappa^{(0)} = 1.344 \cdot 10^{-16} \text{ km}^{-1} \left(\frac{1}{\mu} \right) \cdot \left(\frac{\nu}{s-1} \right) \cdot \left(\frac{N}{m^{-3}} \right) \cdot \left(\frac{f}{\text{MHz}} \right)^{-2} \quad (2.3A)$$

in the neighborhood of the magnetic equator. In the low latitude range this may still be used for the ordinary component as a reasonable approximation, but certainly not for the extraordinary component.

The approximations (2.2) through (2.4) are not correct at low heights (or low frequencies) where $\nu/2\pi$ is comparable with $(f \pm |f_L|)$. There one has to use

$$\kappa^{(0)} = 1.344 \cdot 10^{-16} \text{ km}^{-1} \left(\frac{1}{\mu} \right) \cdot \left(\frac{\nu}{s-1} \right) \cdot \left(\frac{N}{m^{-3}} \right) \cdot \left(\frac{\text{MHz}^2}{(f \pm |f_L|)^2 + (\nu/2\pi)^2} \right) \quad (2.5)$$

The corresponding Sellmeier approximation is

$$\kappa = 1.344 \cdot 10^{-16} \text{ km}^{-1} \left(\frac{1}{\mu} \right) \cdot \left(\frac{\nu}{s-1} \right) \cdot \left(\frac{N}{m^{-3}} \right) \cdot \left(\frac{\text{MHz}^2}{f^2 + (\nu/2\pi)^2} \right) \quad (2.5A)$$

2.2.5 It follows from Eq. (2.5) that, for a given frequency f and electron density N , the absorption coefficient κ as a function of ν reaches a maximum at that altitude where $\nu = 2\pi(f \pm |f_L|)$. Thus the absorption effect of a given amount of ionization is maximum at a certain altitude which decreases with increasing frequency as can be seen from Figure 2.2. In order to obtain a real absorption profile the absorption coefficients of Figure 2.2 must be multiplied by the appropriate electron density values. As N tends to increase almost monotonically with height up to the peak of the E region, real κ profiles have maximum values at heights well above those shown in Figure 2.2 (see Figure 2.6b).

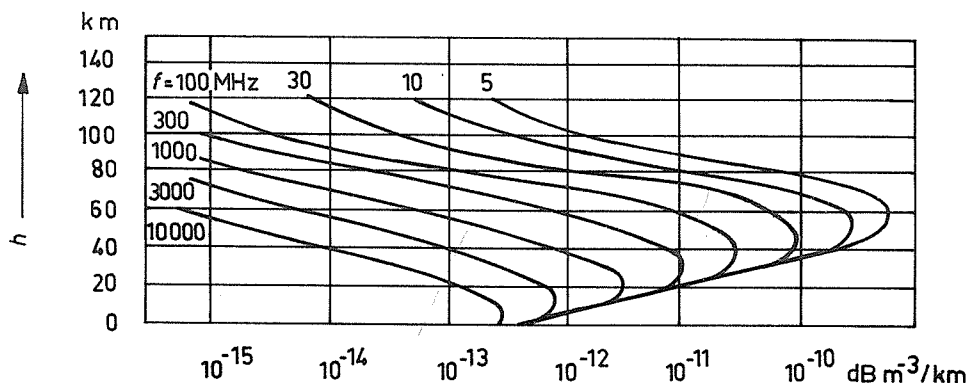


Fig. 2.2 Absorption effect of unit electron density at different altitudes, for different frequencies: Appleton-Lassen dispersion formula. Parameter = f/MHz . (Courtesy: W. Pfister.)

Eqs. (2.2) through (2.4) are only strictly valid as long as the denominator of Eq. (2.5) may be replaced by its first term, i.e.

$$\text{if} \quad \nu^2 \ll 4\pi^2 (f \pm |f_B|)^2 .$$

At heights above 75 km, this condition does not cause any difficulty so far as the ordinary wave component is concerned (upper sign). Due to gyroresonance the situation is different for the extraordinary components; the limits of validity imposed by Eq. (2.6) are given in Table 2.1.

Table 2.1

Relation between height (h) at which absorption occurs and the frequency (f) below which Eqs. (2.3) through (2.5) should not be applied to the extraordinary wave, ($f_B = 1.2$ MHz).

| | | | | | | | |
|----------------|-----|-----|-----|-----|-----|------|------|
| h/km | 70 | 75 | 80 | 85 | 90 | 95 | >100 |
| f/MHz | 4.2 | 2.8 | 1.8 | 1.5 | 1.3 | 1.25 | 1.2 |

2.2.6 In cases where the above condition is not satisfied the Appleton-Lassen dispersion formula is no longer applicable. This is due to the fact that in this formula the collision frequency is assumed to be independent of the electron velocity. This is not true and the probability of collision varies considerably with the velocity of the colliding electron and depends upon the nature of the colliding molecule or ion [Phelps and Pack, 1959]. Generalized dispersion formulas must be used under such circumstances, particularly in the medium and low frequency range. A discussion can be found in Appendix 2.B [see also Suchy and Rawer, 1971].

2.2.7 As shown by Eqs. (2.3) and (2.5) absorption and refraction are directly related. At vertical incidence for a given frequency the refractive index μ decreases along the sounding path until it becomes zero at that level where the incident wave is finally reflected. For these circumstances the factor $1/\mu$ in Eqs. (2.3) and (2.5) leads to an infinite value for the absorption coefficient κ . Although our equations are not really valid for $\mu = 0$, the absorption coefficient becomes very large near the reflection level. At this level, appreciable absorption may be found even in higher layers where the collision frequency is quite small. The dependence of κ upon the refractive index μ must therefore be taken into account in all normal cases. This is explained in Section 2.4 below; the cases where the factor $1/\mu$ may be neglected are the exception, not the rule (See Section 2.5 below).

Eqs. (2.3) through (2.5) have been derived under the assumption of small ionization and, consequently, almost circular polarization of the two wave components. This is certainly not true for the ordinary component near its reflection level where it just reaches linear polarization. Another approximation called "LP" (linear polarization) is then indicated; in the literature it is usually called "QT" (quasi-transverse) which may be misleading. Following Rawer and Suchy [1967] the "LP" expression of the absorption coefficient for the ordinary component is:

$$\kappa_{LP} \approx 1.344 \cdot 10^{-7} \text{m}^{-1} \cdot \left(\frac{1}{\mu} \right) \cdot \frac{(v/s^{-1}) \cdot (N/\text{m}^{-3})}{f^2 \cdot |\sin \theta| / \text{Hz}^2} \quad (2.6)$$

For comparison we give the expression for vanishing magnetic field influence:

$$\kappa^{(0)} = 1.344 \cdot 10^{-7} \text{m}^{-1} \cdot \left(\frac{1}{\mu} \right) \cdot \left(\frac{v}{s^{-1}} \right) \cdot \left(\frac{N}{\text{m}^{-3}} \right) / (f/\text{Hz})^2 \quad (2.7)$$

or also

$$\kappa^{(0)} = 1.344 \cdot 10^{-16} \frac{1}{\text{km}} \cdot \frac{1}{\mu} \cdot \left(\frac{v}{s^{-1}} \right) \cdot \left(\frac{N}{\text{m}^{-3}} \right) / (f/\text{MHz})^2$$

which is, of course, identical with Eq. (2.3A).

2.2.8 Comparing the CP approximation, Eqs. (2.3) and (2.4), and the LP approximation, Eq. (2.6), with the case of no magnetic field, Eq. (2.7), we find that the effect of the magnetic field on absorption is opposite in the two approximations: it decreases absorption of the ordinary component under CP conditions, i.e. at lower levels, but increases it under LP conditions, i.e. in the vicinity of the reflection level. For waves of higher frequency penetrating the whole ionosphere LP conditions are never reached [Argence *et al.*, 1953].

When the magnetic field is neglected the dispersion equation [Sellmeier, 1872] becomes very simple, namely

$$\mu^2 = 1 - X^2 = 1 - f_N^2 / f^2 \quad (2.8)$$

in which f_N is called the plasma frequency and is given by

$$f_N = 9 \text{ MHz} \cdot \sqrt{N/(10^{12} \text{ m}^{-3})} \quad (2.8a)$$

The plasma frequency is the appropriate measure of electron density when dealing with propagation problems. With this particular dispersion our Eq. (2.3) may also be written:

$$\kappa^{(\theta)} = \frac{v}{c_0} \left(\frac{1}{\mu} - \mu \right) \quad (2.9)$$

where c_0 = velocity of light in free space. In the vicinity of the magnetic equator these relations hold exactly for the ordinary component (which has linear NS-polarization in this particular case).

2.3 Absorption Decrement

2.3.1 All methods actually applied to measure ionospheric absorption use radio wave propagation through at least parts of the ionosphere. Thus, what is really measured is the total absorption along a rather long path. Electron density N and collision frequency ν usually vary by order of magnitude along that path, as does the absorption coefficient κ . The total attenuation must therefore be written as an integral expression

$$\int \kappa \, ds = -\ln (E/E^*) \quad (2.10)$$

where E is the field strength at the receiver and E^* is that which would have been observed if the medium did not absorb. Since E is smaller than E^* , both sides of Eq. (2.10) are always positive.

The integration path should, strictly speaking, follow the ray path, i.e. that of energy flux. At oblique incidence or for frequencies near the gyrofrequency, due to the anisotropy of the refractive index in a magnetized plasma, this may differ from the result of Bouguer's refractive law:

$$\mu \cdot r \sin \alpha = \text{const.} \quad (2.11)$$

which is the curved ionosphere generalization of Snell's law

$$\mu \cdot \sin \alpha = \text{const.}$$

In most practical cases, however, the refracted path, as given by Bouguer's law, can be taken as the integration path.

2.3.2 By international convention (IUPAP) the absorption loss along an ionospheric path should be designated by A and is measured in dB.

$$\frac{A}{\text{dB}} = -20 \log_{10} (E/E^*) = 8.686 \int \kappa \, ds \quad (2.12)$$

Introducing from Eq. (2.5)

$$\frac{A}{\text{dB}} = 1.16 \cdot 10^{-6} \text{ Hz m}^2 \int \frac{1}{\mu} \frac{\nu N}{(f^2 - f_L^2)^2 + (\nu/2\pi)^2} \, ds \quad (2.13)$$

or for numerical computation

$$\frac{A}{\text{dB}} = 1.16 \cdot 10^{-15} \int \frac{1}{\mu} \left(\frac{\nu}{\text{s}^{-1}} \right) \left(\frac{N}{\text{m}^{-3}} \right) \frac{1 \text{ MHz}^2}{(f^2 - f_L^2)^2 + (\nu/2\pi)^2} \frac{ds}{\text{km}} \quad (2.13a)$$

In order to evaluate the integral of Eq. (2.13) we should know the height profiles of electron density N and collision frequency ν and the magnetic field parameters. Usually only the latter are known, but not the profiles. From one measured integral value it is impossible to obtain direct profile information. Single frequency measurements are, however, useful as they allow relative variations to be detected and, in particular, effects due to geophysical events. Useful information concerning the profile can be obtained by means of multifrequency measurements of absorption and virtual height. Note that the frequency appears not only in the denominators of Eqs. (2.3), (2.8) and (2.13) but also, and often critically, in the factor $1/\mu$ [Piggott, 1953].

2.3.3 The relation between absorption measured at vertical and oblique incidence is of great importance for problems like estimation of sky-wave field strength. Martyn [1935] formulated an equivalence theorem by which absorption at oblique incidence (angle α) on a frequency f is related with that found at vertical incidence on the equivalent frequency $f \cos \alpha$. The ratio of both absorption decrements should be $\sec \alpha$. The range of validity of this theorem has been critically discussed by Appleton and Beynon [1955] and Rawer and Suchy [1958].

2.4 Deviative Absorption

2.4.1 The factor $1/\mu$ gives more weight to that part of the wave path where the electron density is greatest. If, in particular, the wave is reflected at a certain level, the contribution from the vicinity of this level is greatly increased because μ is small and the refractive bending of the ray is important. For this reason this type of absorption is called "deviative". The increased absorption is particularly evident in cases where reflection occurs in the vicinity of a layer maximum because then μ remains small over a large height range.

As the magnetic field causes the CP absorption to be less and the LP more than for the no field case, the error in total absorption when using a no magnetic field approximation is usually not very great (see Section 2.2.8).

2.4.2 In absorption measurements using method A1, deviative absorption in the E region plays a major role. For the frequencies used in this particular technique the factor $1/\mu$ reaches large values near the reflection level for the lower frequencies which are reflected from the E region. For higher frequencies which penetrate the E region and are reflected from the F region there may also occur a large $1/\mu$ amplification of absorption at altitudes near the E-region peak density. Because of such "amplification", deviative absorption is associated with high values of the absorption decrement not only below but also above the critical frequency of the E layer. The variation with frequency of the decrement is thus clearly "selective".

As an example of a fairly typical variation of the absorption decrement with frequency, Figure 2.3 shows the results for a parabolic E layer with exponential variation of the collision frequency with height. The values of $\kappa''(0)$ from Eq. (2.7) have been used so that the magnetic influence has not been taken into account. The right-hand curve (above the critical frequency f_c) is valid for upward penetration of the whole E region, lossless reflection from an upper layer (F) and downward penetration of the E region. The left-hand curve refers to reflection from the E layer at frequencies below f_c [Argence *et al.*, 1950; Bibl and Rawer, 1951].

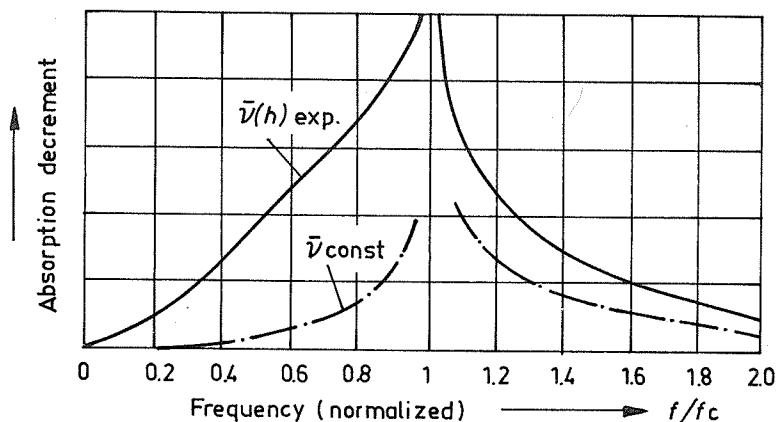


Fig. 2.3 Absorption as function of frequency for a parabolic electron density layer (critical frequency f_c , half thickness d) and constant ν or exponential decrease of collision frequency with height varying as $\exp(-z/H)$ (with $H = 2d/5$) [Argence, Mayot and Rawer, 1950].

2.4.3 Conditions are not really symmetrical around f_c as they should be for constant ν (dot-dash curve). The large increase in ν with decreasing height causes much larger decrements below f_c than above. Whenever one considers deviative absorption, this feature must be taken into account. Figure 2.4 is another example in which the components have been computed separately. An Elias-Chapman layer profile has been assumed and, again, exponential variation of the collision frequency ν with height. On the "o" trace the downward increase of ν appears quite clearly, almost producing a step. The most prominent feature

on the "x" trace, however, is a very large selective increase of the decrement near the gyrofrequency f_{B_2} called the "gyro-resonance" effect. It appears also on the "z" trace below that frequency, which is, however, only very rarely used for absorption measurements.

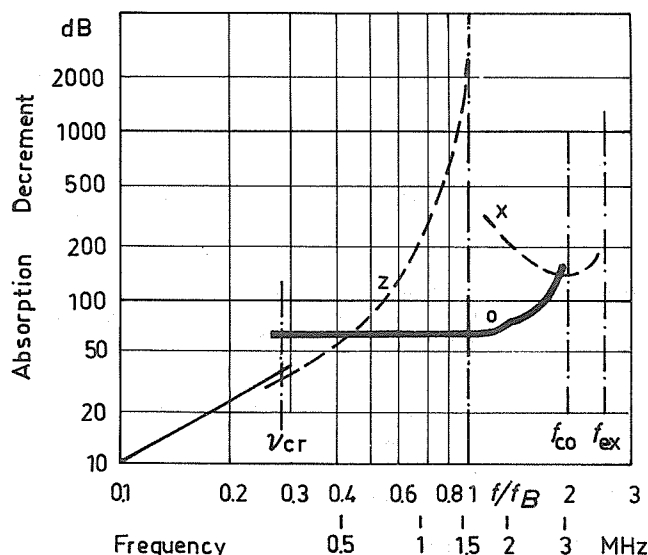


Fig. 2.4 Absorption as function of frequency for an electron density layer of Elias-Chapman type and exponential decrease of collision frequency with height. Both profiles are determined by a unique scale height. The magneto-electronic components are identified (ordinary trace bold). [Pfister, 1953].

Although different assumptions have been used in the models taken for Figures 2.3 and 2.4 the main features of both are rather similar so far as the "ordinary" component is concerned and the frequency is well above the gyro-frequency. The rather large attenuation on the lower frequencies found in Figure 2.4, compared with Figure 2.3, is at least partially due to the appreciable difference of the electron density profiles assumed.

2.4.4 "Ledges" in the E-region profile may also sometimes produce selective increases along the frequency axis. Sporadic E layers, however, are too thin to give appreciable contributions to absorption. Effective energy loss by partial reflection does occur quite often with sporadic layers and, in such cases, it is often impossible to reduce the data. On the other hand, below its blanketing frequency an Es layer is normally a better reflector than is the normal E layer.

2.5 Non-deviative Absorption

2.5.1 When using the "non-deviative" approximation, it is possible to make a considerable simplification of the formulas by suppressing the factor $1/\mu$, i.e. by putting $1/\mu = 1$. The assumption means

$$X = f_N^2 / f^2 \ll 1. \quad (2.14)$$

Following Millington [1954] we may with this assumption write

$$\kappa_{nd} = 1.344 \cdot 10^{-16} \frac{1}{\text{km}} \cdot \left(\frac{\nu}{\text{s}^{-1}} \right) \cdot \left(\frac{N}{\text{m}^{-3}} \right) \frac{\text{MHz}^2}{(f \pm |f_L|)^2 + (\nu/2\pi)^2} \cdot G(Y, \theta) \quad (2.15)$$

where G depends on $Y = f_B/f$ and on the angle θ between the magnetic field and the direction of propagation (wave normal). The curves reproduced in Figure 2.5 show that G is usually greater than 1. On the ordinary trace the largest corrections occur near $\theta = 60^\circ$ which corresponds to an inclination of 30° . The corrections are not negligible except for frequencies greater than 5 MHz.

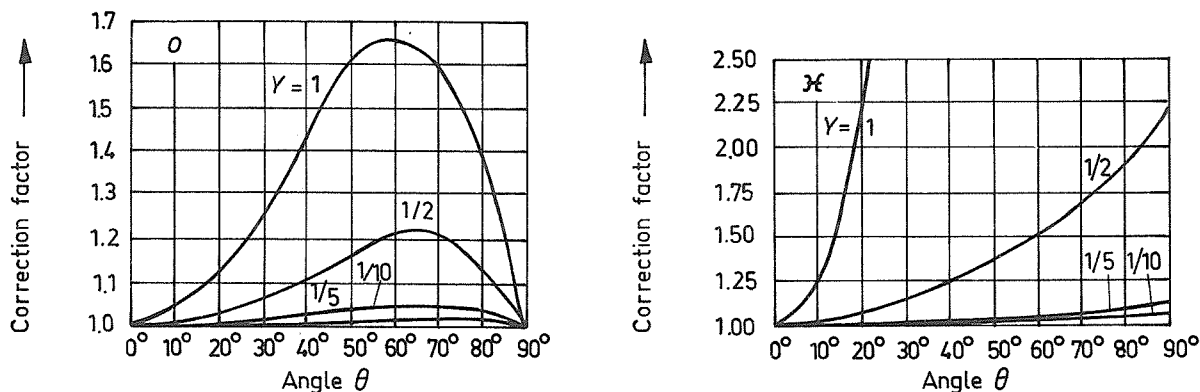


Fig. 2.5 Magnetic correction factor G in Eq. (2.15) for non-deviative absorption [Millington, 1954].

If the frequency is so high that $G \approx 1$, one obtains

$$\kappa_{nd} \approx 1.344 \cdot 10^{-16} \frac{1}{\text{km}} \cdot \left(\frac{\nu}{s^{-1}} \right) \cdot \left(\frac{N}{m^{-3}} \right) \cdot \frac{1 \text{ MHz}^2}{(f_{\pm}|f_L|)^2 + (\nu/2\pi)^2} \quad (2.16)$$

which simplifies further if $(f_{\pm}|f_L|)^2 \gg (\nu/2\pi)^2$ to give

$$\kappa_{nd} \approx 1.344 \cdot 10^{-16} \frac{1}{\text{km}} \cdot \left(\frac{\nu}{s^{-1}} \right) \cdot \left(\frac{N}{m^{-3}} \right) \cdot \frac{1 \text{ MHz}^2}{(f_{\pm}|f_L|)^2} \quad (2.17)$$

2.5.2 When reducing absorption data with the non-deviative equations, in particular Eqs. (2.16) or (2.17), the conditions of validity should be checked carefully. Knowing the magnetic inclination at the station one may decide for which frequencies the correction factor G in Eq. (2.16) must be taken into account.

There is little chance of finding a non-deviative case on low or medium frequencies. In the high-frequency range, its possible validity is limited to the D region. However, at very high frequencies the magnetic influence is small and absorption in the D and E regions is non-deviative; this is almost always true for absorption in the F region except for very high values of f_oF2 . Note that for the extraordinary component the Appleton-Lassen dispersion equation may not be adequate at very low levels where additional ionization can be present under disturbed conditions.

2.6 Distinction between Contributions from Different Layers

2.6.1 In the total absorption integral, Eqs. (2.12) and (2.13), the relative importance of contributions from different heights depends largely upon frequency. A typical daytime case is illustrated in Figure 2.6. For HF sounding frequencies there are two distinct height ranges from which appreciable contributions are to be expected: in the D region where the non-deviative formulas may be used and in the vicinity of the reflection level in the E region where we are certainly bound to take the deviative term into account. The situation is similar for higher frequencies in the HF range which penetrate the E region and are reflected from the F region. However, in this case some deviative absorption in the E region may also be important. It is also seen from Figure 2.6 that the effects of deviative absorption in the E region are not restricted to a small frequency range only. However, the variation with frequency is so different for non-deviative and deviative absorption that this difference can be taken as a criterion for distinguishing between the two parts.

One could imagine a procedure by which multifrequency data could be used to determine a profile of local absorption coefficients linking as many points as there are frequencies. However, attempts to do so have not been successful because small errors or variations during the period of observation can have large effects. Fitting simple model profiles to observed data is much less sensitive to these errors and usually gives reasonably consistent parameters for the models.

2.6.2 For the normal E layer and an exponential profile of the collision frequency Bibl and Rawer [1951] computed a typical frequency law of deviative absorption (Figure 2.4). Better agreement can be obtained with an empirical model starting with a log-log graph of observed absorption loss A against f/f_oE which is then fitted by a suitable function [George, 1971; Samuel and Bradley, 1975].

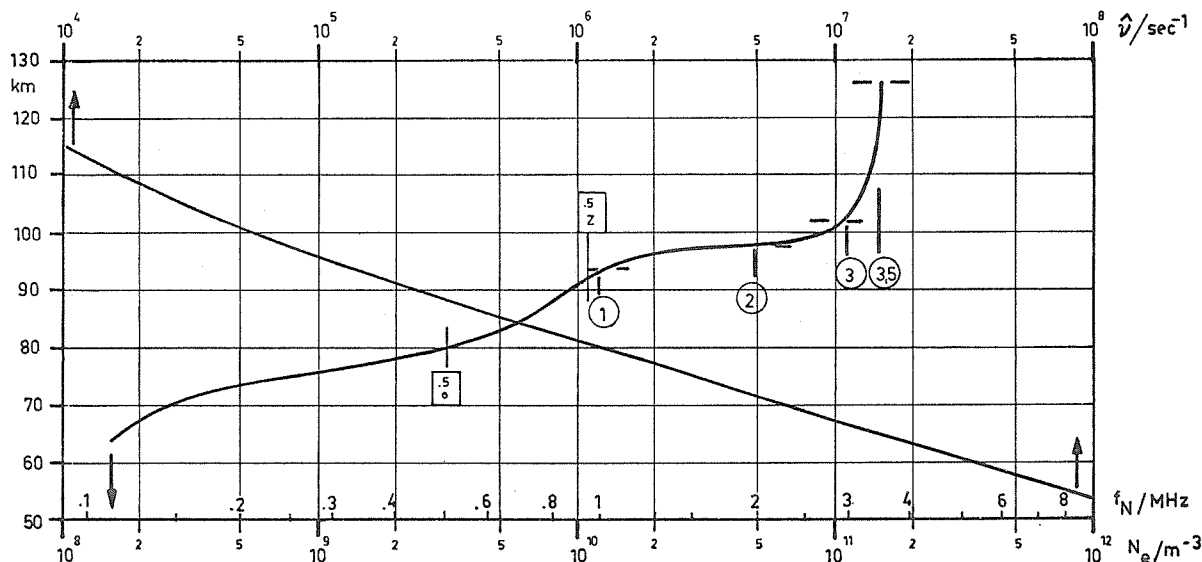


Fig. 2.6a Model N_e and \hat{h}_p from Piggott and Thrane (courtesy W. R. Piggott).

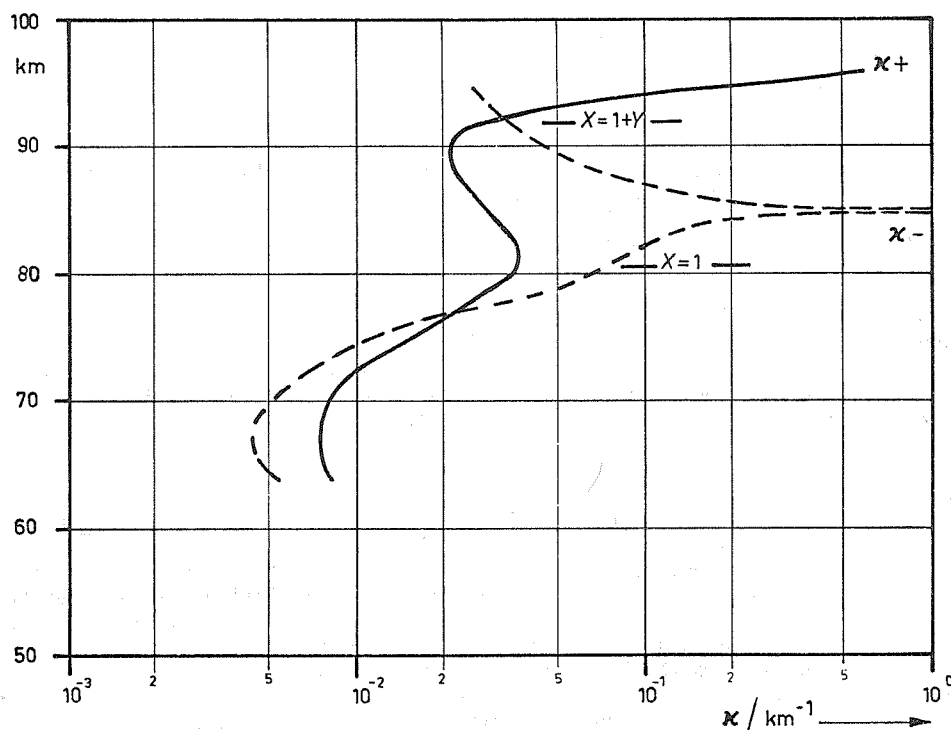


Fig. 2.6b Contributions at different heights (ordinate) to the absorption integral. Model of Figure 2.7a, frequency 512 kHz (for $\theta=32^\circ$, $B=0.52$ Gauss, after Mechtly [1959]).

2.6.3 When blanketing Es is present, the parabolic or any other continuous layer model is no longer correct because the thin Es layer prevents certain frequencies (below the blanketing frequency f_{bEs}) from penetrating deeper into the E region as they can do in the absence of Es. By truncating the profile at these frequencies (above the cusp frequency of c-type Es), one obtains a family of curves instead of only one function. This family is shown in Figure 2.7 [Bibl, Paul and Rawer, 1959]. It depends on two parameters: f_{oE}/f and f_a/f , f_a being the cusp frequency which is used as a measure of the height where truncating occurs.

Observations of low layers at VHF under disturbed conditions in particular have been interpreted using a cubic layer model, the coefficients of which are determined. For details see Chapter 5 [Parthasarathy *et al.*, 1964].

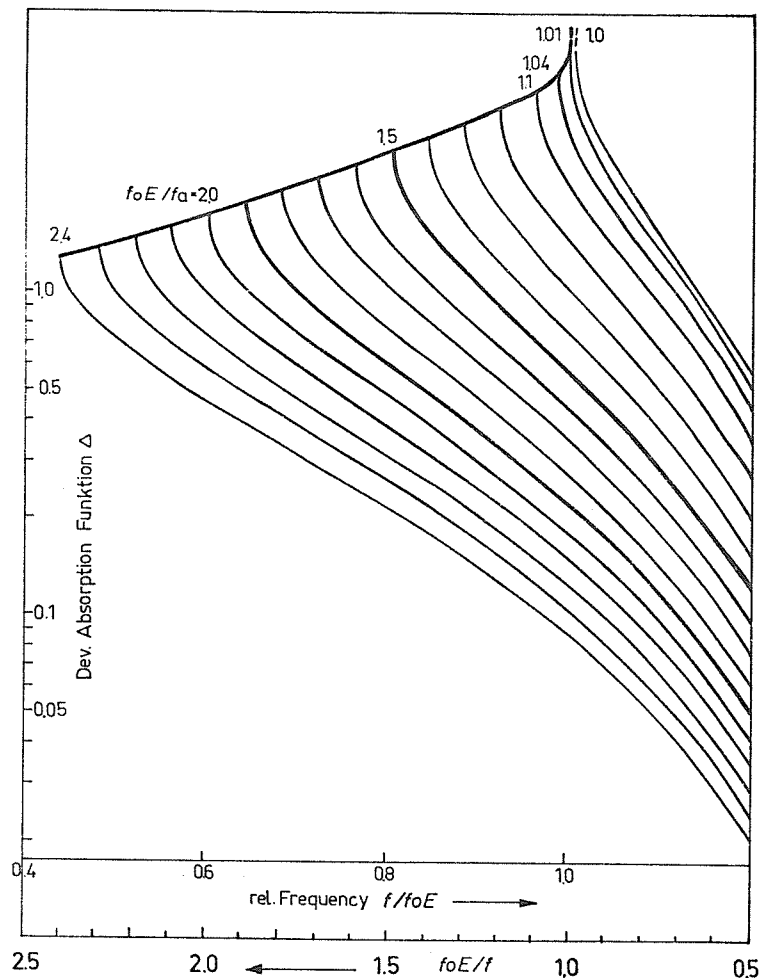


Fig. 2.7 Absorption as function of frequency for a parabolic E layer and exponential decrease of collision frequency with height (see Figure 2.3) in the presence of blanketing ("c-type") Es with "cusp frequency" f_a . The bold curve is valid in the absence of "c-type" Es. Each of the other curves belongs to the given parameter viz. the value of foE/f_a , the bold curve then being valid at the left side of the intersection point only. Magnetic field effects are neglected [Bibl, Paul and Rawer, 1959].

2.6.4 The height at which abnormal absorption is centered can often be estimated when using multifrequency riometer techniques. As shown by Eq. (2.16) and Figure 2.2 the largest increase in absorption occurs at the height where $\nu = 2\pi(f + |f_L|)$. Magnetic field effects are neglected in this model (see Section 2.4.1). As to absorption in the D region the non-deviative frequency law of Eq. (2.17) is a good approximation. With a simple graphical method (known as "spider-web" method, see Figure 4.3.2 in Chapter 4) Bibl and Rawer separate the data obtained on the different frequencies below and above foE so that two parameters are determined from the median intersection point. One, called B , characterizes absorption in the D region, and the other, called C , is an absorption parameter of the E region. The expression of the two parameters can be written:

$$A = B \frac{1}{(f + |f_L|)^2} + C \Delta_E (foE/f) \quad (2.18)$$

It must be noted that by definition B is an absorption loss standardized to an "effective frequency" of 1 MHz, its unit being dB MHz². On the contrary, C is a parameter proportional to the product of layer thickness and collision frequency (at the layer peak). Thus, the variations of actual electron density have been taken out of C (due to function Δ), but appear in the B values.

Note that the form of the function $\Delta_E (foE/f)$ depends also on the way in which the collision frequency varies with height.

2.7 Differential Absorption

2.7.1 The phenomenon of double refraction may be exploited to give an additional method of measurement. Thus, for example the Faraday effect provides a technique for measuring total electron content between source and receiver. For absorption measurements the difference of attenuation suffered by the two components can give useful data even if the absolute value of the non-absorbed field strength is unknown. The method is used particularly with VHF emissions from satellites (see Chapter 9) and with polarized riometers (see Chapter 5).

As stated in Section 2.2.3 double refraction means that a wave entering the ionosphere splits into two components which are almost circularly polarized (except near the magnetic field direction where they become linear). If the polarization of the wave at the transmitter is linear, it splits into two components of equal amplitude, E_o and E_x . By measuring the amplitude ratio of the two circular components after they have left the ionosphere, one determines the difference of attenuation of the "o" and "x" components.

2.7.2 Supposing the refraction effects to be so small that the same ray path is applicable to both components, we obtain the logarithm of the ratio of the fields by applying Eq. (2.10) to each component "o" and "x" and subtracting:

$$\int (\kappa_x - \kappa_o) ds = -\ln (E_x/E_o) \quad (2.19)$$

or with Eq. (2.12)

$$\frac{\Delta A}{dB} = -20 \log_{10} (E_x/E_o) = 8.686 \int (\kappa_x - \kappa_o) ds. \quad (2.20)$$

The method is normally applied at frequencies above about 15 MHz where κ is taken from Eq. (2.13a) giving:

$$\frac{\Delta A}{dB} = 1.16 \cdot 10^{-15} \int \frac{\nu}{\text{Hz}} \frac{N}{\text{m}^{-3}} \left\{ \frac{\text{MHz}^2}{\nu_x (f^2 - |f_L|)^2} - \frac{\text{MHz}^2}{\nu_o (f^2 + |f_L|)^2} \right\} \frac{ds}{\text{km}} \quad (2.21)$$

or with Eq. (2.4)

$$\frac{\Delta A}{dB} = 1.16 \cdot 10^{-15} \int \left(\frac{\nu}{\text{Hz}} \right) \left(\frac{N}{\text{m}^{-3}} \right) \left(\frac{f}{\text{MHz}} \right)^{1/2} \cdot \left\{ \left(\frac{f^2 - f_N^2 - f |f_L|}{\text{MHz}^2} \right)^{-1/2} \cdot \left(\frac{f - |f_L|}{\text{MHz}} \right)^{-3/2} - \left(\frac{f^2 - f_N^2 + f |f_L|}{\text{MHz}^2} \right)^{-1/2} \cdot \left(\frac{f + |f_L|}{\text{MHz}} \right)^{-3/2} \right\} \frac{ds}{\text{km}} \quad (2.22)$$

2.8 Collision Frequencies

2.8.1 The gas kinetic collision frequency is defined as the probability of occurrence of certain events. It is not identical with the "effective collision frequency" [Ginzburg, 1944] which is used in the dispersion equations and also in the above approximate equations. The "effective collision frequency" for radio wave propagation in a plasma may be greater than the gas kinetic one by a factor of up to two. Using the terminology of modern kinetic theory we may say that our "effective collision frequency" is an "average transport collision frequency" $\bar{\nu}$. For details see K. Suchy and K. Rauer [1971] and Appendix 2.A. The hatched range in Figure 2.8 describes the average variation of $\bar{\nu}$ with height.

2.8.2 In the lower ionosphere up to about 150 km collisions between electrons and neutral molecules mainly determine the collision frequency. Their probability decreases exponentially with height whereas (below the peaks of ionization) electron-ion collisions increase with height. The cross section for collisions between electrons and ions is much greater than for electrons and neutrals since it is determined by electric forces (so-called "Coulomb" forces). In the F2 layer, electron-ion collisions determine the effective collision frequency.

This can also occur in Es layers when the electron density is very high, e.g. for fB_{Es} above about 7 MHz.

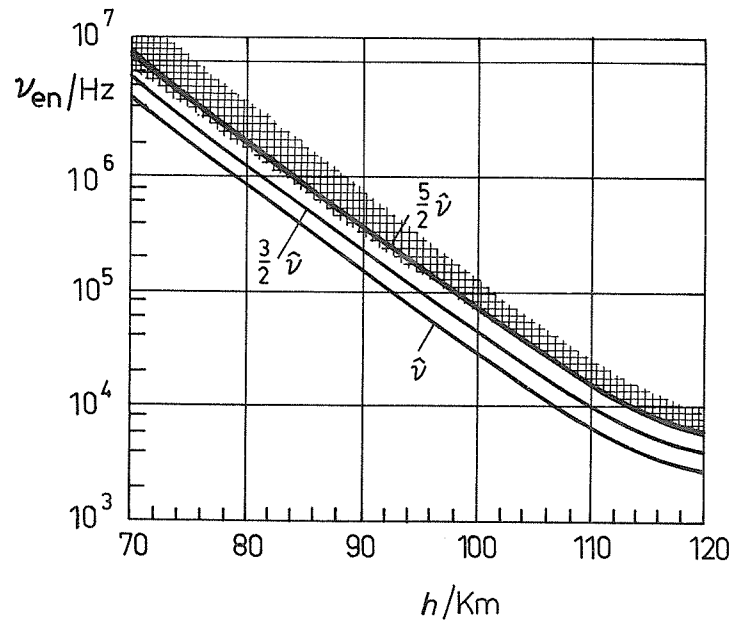


Fig. 2.8 Height variation of the "most probable transport collision frequency" $\hat{\nu}$ (lowest curve) and its multiples by $3/2$ ("mean transport collision frequency") and by $5/2$ ("averaged transport collision frequency"). [Suchy and Rawer, 1971, after M. Nicolet]. Hatched range covers indications by different authors.

Absorption due to electron-ion collisions is mainly important in experiments in which the waves penetrate the whole ionosphere, such as A2 using cosmic noise sources (Chapter 5) and in the applications of satellite transmitters (Chapter 9).

2.8.3 The equations for the absorption coefficient given above may be used with the appropriate values of $\hat{\nu}$. Suchy [1964] gives:

$$\frac{\hat{\nu}_{ei}}{\text{Hz}} = \left[54.4 + 8.5 \log_{10} \frac{(T_e/K)^{3/2}}{(N/\text{m}^{-3})^{1/2}} \right] 10^{-6} \frac{N}{\text{m}^{-3}} \left(\frac{T_e}{\text{K}} \right)^{-3/2} \quad (2.23)$$

The form of the absorption integrals is changed when electron-ion collisions are dominant since the collision frequency is itself proportional to the electron density N . The product νN is roughly proportional to $N^2/T^{3/2}$. The factor N^2 varies as $(foF2)^4$, i.e. increases very rapidly with the critical frequency $foF2$. There will be further increased deviative losses due to the decrease in μ .

For waves penetrating the ionosphere the signal may also be attenuated by screening, i.e. the cone over which the layer is transparent decreases in angle as the frequency approaches $foF2$.

2.8.4 It appears to be very difficult to take into account the influence of electron-electron Coulomb collisions. Under most conditions such collisions do not appreciably contribute to the currents induced by radio waves in the plasma, so that they do not influence the dispersion relation. Only in the vicinity of the electron gyrofrequency has an appreciable effect been shown to exist [Kelly, 1960; Wyller, 1962].

2.8.5 The particular phenomena of coupling between the two magneto-electronic modes occur under special conditions, namely at an altitude where $f \approx f_N$ ($X \approx 1$) and at the same time ν reaches a critical value (called ν_c) which depends exclusively on the magnetic field in the ionosphere:

$$\nu_c = \frac{\sin^2 \theta}{2 \cos \theta} \cdot 2\pi f_B, \quad (2.23)$$

where f_B is the gyrofrequency and θ the angle between the wave normal and the terrestrial magnetic field.

Figure 2.9 describes ν_c as a function of θ and f_B . With a given ionosphere both conditions are satisfied at just one frequency, namely that for which $f = f_N$ at the height where $\nu = \nu_c$. This particular case must be avoided when absorption measurements are made. At low and temperate latitudes it occurs on quite low frequencies which are rarely used (except possibly in Method A3, see Chapter 7). More caution is needed at high latitudes.

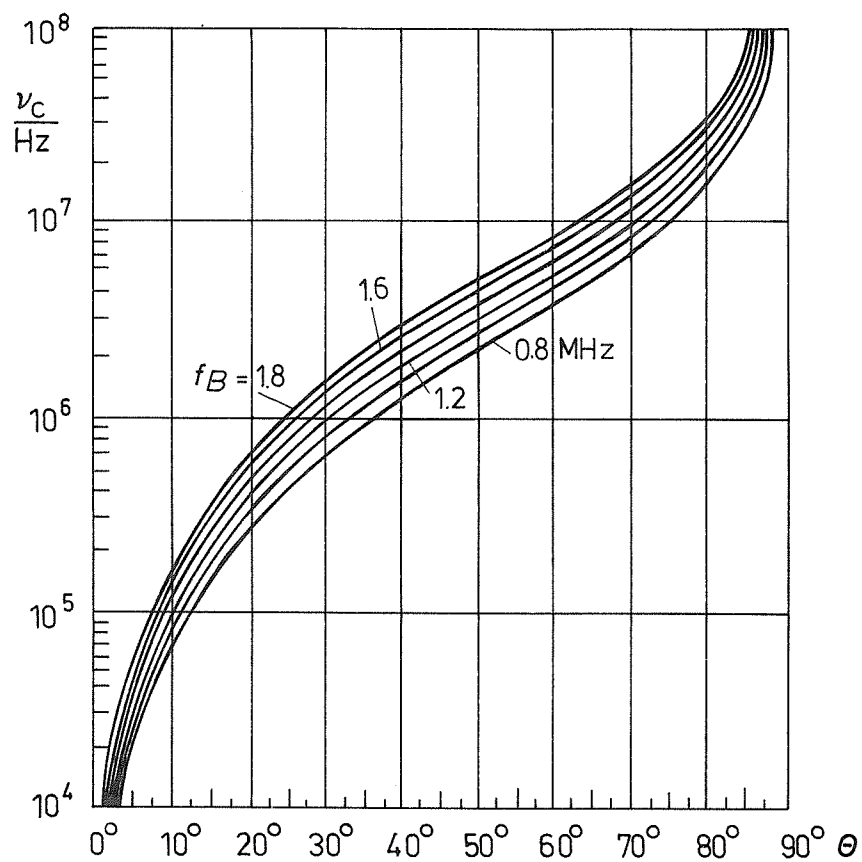


Fig. 2.9 Critical collision frequency as function of magnetic field angle θ parameter gyrofrequency f_B .

APPENDIX 2.A

2.A The Notion of "Collision Frequency"

2.A.1 The term "collision frequency" is often used in plasma treatises. The word itself gives the impression of being involved in a counting problem. This is, however, only true for the most simple interpretation when one uses the model of "rigid spheres": each particle is replaced by something similar to a billiard ball. Let us consider one red ball and many white ones. Then the number per unit time of touches between the red ball and any one of the white ones seems to be well defined; its statistical average is called "collision frequency".

However, when considering kinetic or transport problems this type of consideration is found to be oversimplified and must be abandoned. What is really needed in applications of any kind is something like an efficiency function describing the effect of collisions in the process to be computed. This effect depends strongly upon the angle by which the considered particle is deflected; this angle is related to the "collision parameter" (namely the smallest distance between the particle centers which would be obtained without deflection).

Take, for example, the problem of diffusion of one kind of gas through another one. For problems of this nature backward collisions (with a deflection angle $>90^\circ$) have greater effect than forward collisions (deflection angle $<90^\circ$). So we should use a weighting function depending upon the deflection angle: large angles should have more weighting than small angles. The final result is then obtained by integration over all collision parameters, i.e. by averaging over all possible cases. Unfortunately, there is no unique solution to the weighting problem: the weighting function must be adapted to the physical process which is considered; but to a certain extent or, better yet, inside certain limits there is an arbitrary choice.

No doubt the model of "rigid spheres" is also an oversimplification as far as the force between colliding particles is concerned. More realistic models describe the force/distance function by a continuous potential, U , usually with a power law $U \sim r^{-P}$, r being the distance and P a fixed power. For two neutral or one neutral and one charged particle, the range of distances to be considered tends to be narrowly limited. If, however, two charged particles are colliding, the Coulomb force is not limited in distance such that the whole range of distances should, in principle, be considered. (One tends to eliminate very large distances in the evaluation by applying a "screening function".) By adopting an appropriate weighting function depending on the "collision parameter" one may obtain a suitable approximation for any such problem. We see, however, that the weighting function in fact depends on both the kind of problem to which the "collision frequency" is to be applied and the physical model for particle interaction (i.e. on the kind of colliding particles). In other words there is no unique weighting function applicable to all problems, and thus there is no unique collision frequency for all applications of the notion [Suchy and Rawer, 1971].

2.A.2 Until now we have assumed that the relative velocity between the colliding particles have a given fixed value. However, since quantum mechanical interaction depends largely on the relative velocity, the force/distance function is not the same for different velocities. The only exception is Maxwell's hypothetical interaction model with $P=4$. Under more realistic assumptions we have to take account of the different possible combinations of velocities due to the thermal velocity distribution. Therefore, we must still admit one more averaging process viz. over different velocities taking due account of the statistical distribution functions of the two kinds of particles. The corresponding integration has to be extended over both velocity (or momentum) spaces. Since the distribution functions may be different from the Maxwellian distribution, f_h^M , we may have to admit correction terms. (A practical way is to use Laguerre polynomials of increasing order m .)

Using the notations introduced by Suchy and considering colliding particles of kind h and k we come to the following definitions:

$v_{hk}^{(\ell)}(g) =$ Transport collision frequency: describes the specific collisional effect for a given relative velocity, g , by applying a Legendre polynomial of order ℓ as the weighting function.

$\hat{v}^{(\ell)} =$ Most probable collision frequency: the transport collision frequency (with a weighting function of order ℓ , see above) for the most probable thermal velocity (k being the Boltzmann constant):

$$\hat{v}^{(\ell)} = v^{(\ell)}(\hat{g}) \quad \text{where} \quad \hat{g}_{hk} = \left(\frac{2kT_h}{m_h} + \frac{2kT_k}{m_k} \right)^{1/2}.$$

$v_{hk}^{(\ell/0)} =$ Mean transport collision frequency: is obtained by averaging transport collision effects (see above) over the different velocities assuming Maxwellian velocity distribution functions f_h^M , f_k^M .

$\nu_{hk}^{(\ell/m)}$ = Averaged transport collision frequency: (order m): is obtained by averaging transport collision effects (see above) over the different velocities assuming generalized velocity distribution functions with corrections up to order m (against the Maxwellian distribution f^M).

2.A.3 When applying such considerations to a plasma, averaged transport collision frequencies are usually needed. The orders ℓ and m must be adapted to the problem under discussion. Very often one may assume Maxwellian distribution so that $m=0$. The simple term ν should be reserved for the type of collision frequency as used in gas kinetics. The "most probable collision frequency" is sometimes called "monoenergetic collision frequency" in the literature and is then designated by ν_m . In this volume we prefer $\hat{\nu}$ to ν_m . It is important to realize that $\hat{\nu}$ corresponds to a simplified model which cannot give the right numerical value to be applied to wave propagation in a plasma but a smaller one. It has, however, the correct order of magnitude. The appropriate averaged transport collision frequency in cases where the conditions are not particularly specified is called $\bar{\nu}$ in this volume.

The three curves of Figure 2.8 represent the three quantities $\hat{\nu}$, $(3/2)\hat{\nu}$ and $(5/2)\hat{\nu}$ for Nicolet's $\hat{\nu}$ model profile [reproduced from Rawer and Suchy, 1967].

Since the "monoenergetic collision frequency" $\hat{\nu}$ has a straightforward definition, it is often taken as a basic parameter. Three different model profiles as $\hat{\nu}$ are shown in Figure 2.10 together with the electron density profile as used by Rose.

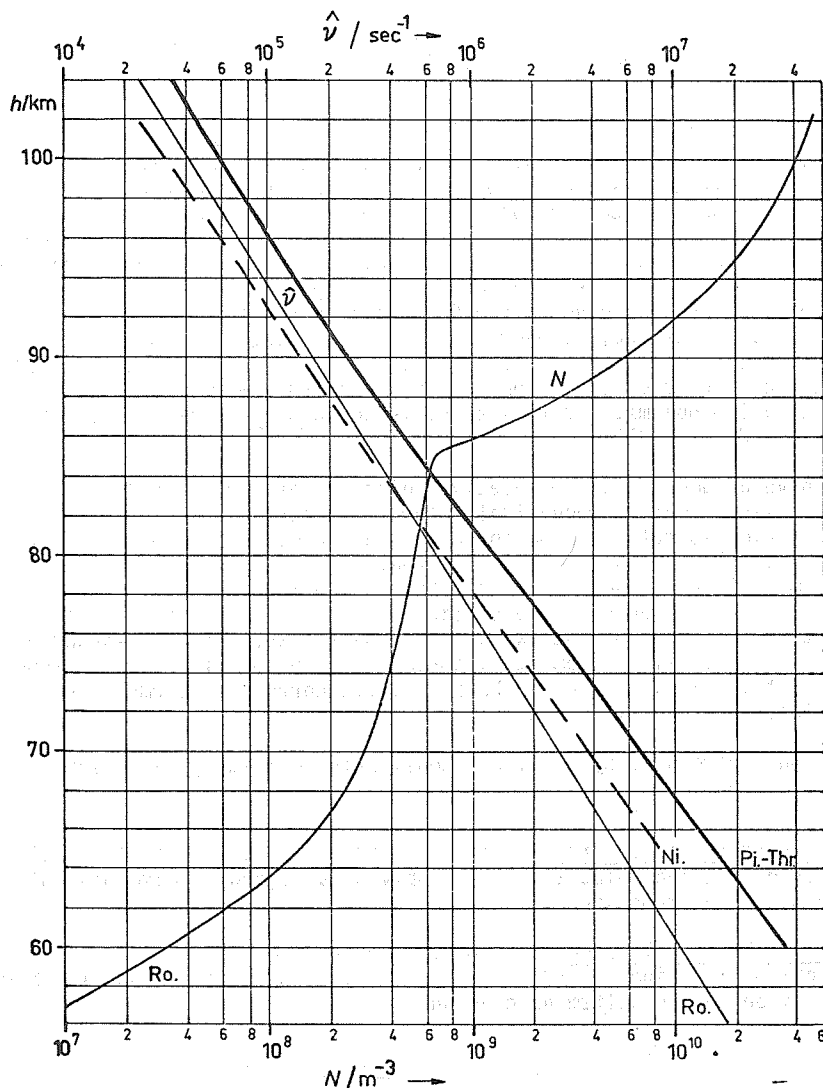


Fig. 2.10 Model for noon electron density (N) and "most probable transport collision frequency" $\hat{\nu}$ after Rose. $\hat{\nu}$ models by Nicolet and Piggott for comparison.

Expressions of numerical computations under ionospheric conditions can be found in Rawer and Suchy [1967, Sections 3, 4, 9].

2.A.4 Between the "most probable collision frequency", $\hat{\nu}$, and the "averaged transport collision frequency", $\bar{\nu}$, (in the literature often called ν_m and ν_{eff} , respectively) there exists, of course, a relation but it depends upon the assumptions made so that it would be quite involved in general form. Practical relations depend on the height range. However, when the deviations from Maxwellian distribution functions are not large and where the nature of collisions is described by the relation given in Subsection 2.2.6.2 above, one has a good approximation

$$\bar{\nu}/\hat{\nu} = \left[\left(\frac{1}{2} \right) \cdot \left(\frac{3}{2} \right) \cdot \left(\frac{5}{2} \right) \dots \frac{(3+n)}{2} \right] / \left[\left(\frac{1}{2} \right) \cdot \left(\frac{3}{2} \right) \right] \quad (2.A.1)$$

which gives for the lower ionosphere ($n=2$)

$$\bar{\nu}/\hat{\nu} = \left(\frac{5}{2} \right) \quad (2.A.2)$$

The relation can be used in most practical cases for the lower ionosphere.

2.A.5 Critical discussion of how collisional effects can be taken account of in the dispersion relation has revealed that this is a difficult problem. It can only be correctly resolved if two facts are known: the velocity distribution of the colliding particles and the dependence of the cross section on velocity. As to the first problem one assumes thermal velocity distribution for the electrons while the motion of the much slower ions can be neglected. As to the second problem some information about the physics of collision is needed.

2.A.5.1 Of course, the second problem has no importance if all colliding particles have the same relative velocity. This is the naive assumption from which the classical dispersion relations due to Sellmeier [1872, without magnetic field] or to Lassen [1927] and Appleton [1928] (with magnetic field) have been derived. If one admits a velocity distribution, in order to obtain the same relations one has to assume that the collision frequency is independent of the particle velocity. Since, however, the average time between two collisions decreases with increasing velocity, independence of the collisional frequency means that the cross section must decrease inversely with increasing particle velocity. Thus, the naive assumption in fact introduces a very particular model of the physics of collisions.

2.A.5.2 Unfortunately, laboratory experiments with electrons colliding with oxygen (O_2) and nitrogen (N_2) molecules have shown that this model is far from being true. In the velocity range which must be considered here the cross section has been found to increase with velocity. It is roughly proportional to it so that ν would vary with the square of the velocity. Let us describe the variation of collision frequency by a law

$$\nu(g) = \hat{\nu} \cdot (g/\hat{g})^x \quad (2.A.3)$$

where g is a measure of velocity and \hat{g} may correspond to an averaged thermal velocity. Then $x=0$ for the naive assumption but $x=2$ for electrons colliding with O_2 and N_2 molecules as found in the lower ionosphere. The Sen-Wyller [1960] dispersion equation uses $x=2$ so as to be in agreement with these laboratory data. It is adequate but only in cases where the particles hit by the electrons are mainly N_2 and O_2 molecules. Otherwise another generalization is needed. For example for collisions of electrons with ions (so-called Coulomb interaction) the cross section decreases very rapidly with increasing velocity and one has $x=-3$. More detailed considerations can be found in Appendix 2.B below.

2.A.5.3 Fortunately these considerations have no practical importance wherever the absorption effect remains small (i.e. where the imaginary member of the dispersion relation is small in comparison with the real one). Within this limitation the Appleton-Lassen relation though starting with a wrong assumption describes the phenomena well enough, at least for practical purposes, except that the absolute value of the "averaged transport collision frequency", $\bar{\nu}$, differs by a factor greater than one from the value of $\hat{\nu}$, the "most probable transport collision frequency" (see Section 2.A.4 above).

APPENDIX 2.B

2.B Generalized Magneto-electronic Dispersion Theories

2.B.1 Wave propagation in a magnetized plasma can be described by a three dimensional tensor of second degree characterizing the dielectric behavior of the medium or its conductivity or the mobility of the electrons in the plasma. Since they are equivalent among themselves, any one of these descriptive models may be used. Because the anisotropy of the medium is due to the magnetic field, the propagation properties must have cylindrical symmetry. (This is at least true for "normal incidence", i.e. incidence of the wave in the direction of stratification of the medium. For other incidence or for a non-linearly stratified medium, conditions are considerably more involved.) For cylindrical symmetry the tensorial components are not independent from each other so that a description by nine such components is redundant.

A non-redundant description can be obtained as follows. (We designate vectors by simple underlining, dyadics, i.e. tensors of second degree, by double underlining.) A dyadic $\underline{\underline{T}}$ with cylindrical anisotropy in the direction of \underline{b} can be written as a sum of three members, namely one member proportional to the unit dyad $\underline{\underline{U}}$, a second one corresponding to the dyadic determined by a couple of vectors \underline{b} (written as dyadic product $\underline{b} \underline{b}$), and a third one which is proportional to the "vectorial product" of the vector \underline{b} with the unit dyadic. So we may write

$$\underline{\underline{T}} = \alpha \underline{\underline{U}} + \beta \underline{b} \underline{b} + j \gamma \underline{b} \times \underline{U} \quad (2.B.1)$$

The three values

$$(\alpha - \gamma b), (\alpha + \beta b^2), (\alpha + \gamma b) \quad \text{where} \quad b \equiv |\underline{b}|$$

are known as "Eigenvalues" of $\underline{\underline{T}}$ and may be designated as

$$\tau_{-1}, \quad \tau_0, \quad \tau_{+1}.$$

These three Eigenvalues are all we need in order to describe the propagational properties of the medium.

2.B.2 Let us now consider the "mobility tensor" of a magnetized plasma with Eigenvalues β_s ($s=-1, 0, +1$). If collisional attenuation is neglected, one finds (always $s = -1, 0, +1$) three Eigenvalues all of which are real:

$$\beta_s = \frac{1}{2\pi} \frac{1}{(f - s f_B)}$$

(f_B is the gyrofrequency). In the presence of collisions the Eigenvalue must, of course, be complex so as to describe the attenuation of the wave. Using the "most probable transport" collision frequency $\hat{\nu}$ (see Appendix 2.A) it is advantageous to introduce three "reduced frequency" expressions, namely:

$$Y_{-1} \equiv \frac{2\pi}{\hat{\nu}} (f + f_B); \quad Y_0 \equiv \frac{2\pi}{\hat{\nu}} f; \quad Y_{+1} \equiv \frac{2\pi}{\hat{\nu}} (f - f_B). \quad (2.B.2)$$

According to whether one applies "naive" or "critical" kinetic theory, Eigenvalues of the mobility tensor are found. In the Appleton-Lassen theory which applies the "naive" concept of collisions

$$\beta_s^{(AL)} = \frac{1}{\bar{\nu}} \frac{1}{Y_s + j} \equiv \frac{1}{\bar{\nu}} \frac{1}{Y_s^2 + 1} (Y_s - j) \quad s = -1, 0, +1, \quad (2.B.3)$$

but in the "critical" Sen-Wyller theory one has to write instead:

$$\beta_s^{(SW)} = \frac{1}{\hat{\nu}} \left(\frac{5}{2} \cdot C_{\frac{5}{2}}(Y_s) + j Y_s C_{\frac{3}{2}}(Y_s) \right). \quad (2.B.4)$$

$\bar{\nu}$ the averaged transport collision frequency and $\hat{\nu}$ the "most probable transport collision frequency" are explained in Appendix 2.A under 2.A.2 through 2.A.4 above. $\bar{\nu}$ is often called ν_m in the literature. $C_{5/2}$ and $C_{3/2}$ are special functions (Dingle's integrals) which have been tabulated by Burke and Hara [1963]; approximations for these functions are found in Hara [1963], one curve for $C_{5/2}$ in Chapter 5 (Section 5.1.5, Figure 5.1), sets of curves in Pfister [1965]. The Sen-Wyller theory applies only if collisions occur mainly with neutral molecules N_2 and O_2 , i.e. in the lower ionosphere, below about 120 km.

2.B.3 As to wave polarization in a magnetized plasma there are always two characteristic radio waves which alone can propagate independently, i.e. without splitting. For each of these (and only for these) a complex refractive index exists which we write in the form $(\mu + j\chi)$. Here χ describes the attenuation of the wave. It is related to the absorption coefficient κ of the wave by

$$\kappa = \frac{2\pi f}{c_0} \chi \equiv \frac{2\pi}{\lambda_0} \chi \quad (2.B.5)$$

where c_0 is the speed of light and λ_0 the wavelength (both in vacuum).

2.B.4 In order to obtain χ from the Eigenvalues β_s of the mobility tensor we first note the corresponding Eigenvalues ϵ_s^v of the dielectricity tensor which are connected with the β_s by

$$\epsilon_s^v = \epsilon_0 (1 + j\omega X \beta_s), \quad (2.B.6)$$

where $X \equiv (f_M/f)^2$. The equations are written in general rationalized units (e.g. SI units), and ϵ_0 is the dielectric constant of free space. (Not to be confused with the Eigenvalue ϵ_0^v .)

Now the following definitions are introduced:

$$\epsilon_+^v \equiv \frac{1}{2} (\epsilon_{+1}^v + \epsilon_{-1}^v); \quad \epsilon_-^v \equiv \frac{1}{2} (\epsilon_{+1}^v - \epsilon_{-1}^v); \quad (2.B.7)$$

$$\xi \equiv \frac{2 \cos \theta}{\sin^2 \theta} \cdot \frac{\epsilon_0^v \epsilon_-^v}{\epsilon_{+1}^v \epsilon_{-1}^v - \epsilon_0^v \epsilon_+^v} \quad (2.B.8)$$

with θ the angle between the magnetic field and the wave normal (which is along the stratification of the medium, thus vertical). The complex quantity ξ is a kind of reduced plasma parameter which is particularly suitable for a simple description of the characteristic wave polarizations (see Rawer and Suchy [1967, Figure 14]).

This becomes apparent if we define

$$P_{\pm} \equiv \left[1 \mp (1 + \xi^2)^{1/2} / j\xi \right] \quad (2.B.9)$$

which can be shown to be the polarization of the characteristic wave (o or x) which is considered, i.e.

$$P = (E_m/E_l) \quad (2.B.10)$$

where E_m and E_l are the components of the electric wave field in the "phase plane" (i.e. in a plane perpendicular to the wave normal). The ratio may be complex because the phase difference between E_m and E_l is important in this context: under general conditions P is complex thus corresponding to elliptical polarization. Special conditions are: Real P means linear polarization and $P = \pm j$ which identifies circular polarization (the sign gives the sense of rotation). At middle latitudes the characteristic polarizations are almost circular at the level where the wave enters or leaves the ionosphere.

On the other hand we may determine the Eigenvalues of the reciprocal dielectricity tensor from those of the original tensor:

$$\eta_{\pm} = \pm \frac{\epsilon_+^v \epsilon_0^v}{\epsilon_{+1}^v \epsilon_{-1}^v} \quad (2.B.11)$$

We can now proceed to find the imaginary part, χ , of the complex index of refraction $(\mu + j\chi)$. The following four expressions can be obtained from η and P (Re means real, Im imaginary part):

$$\alpha_{\pm} = \text{Re } \eta_{\pm} + \cos \theta \left[\text{Re } \eta_{\pm} \text{Im } P_{\pm} + \text{Im } \eta_{\pm} \text{Re } P_{\pm} \right], \quad (2.B.12)$$

$$d_{\pm} = \text{Im } \eta_{\pm} + \cos \theta \left[-\text{Re } \eta_{\pm} \text{Re } P_{\pm} + \text{Im } \eta_{\pm} \text{Im } P_{\pm} \right].$$

With these one finds under the conditions considered by Försterling:

$$\chi_{\pm}^2 = \frac{1}{2} \frac{(a_{\pm}^2 + d_{\pm}^2)^{1/2} - a_{\pm}}{a_{\pm}^2 + d_{\pm}^2}. \quad (2.B.13)$$

and a more involved expression in the most general case [see Rawer and Suchy, 1967, Sect. 9].

Introducing this into Equation (2.B.5) one finds the absorption coefficient for each of the characteristic polarizations or modes.

Note: Under most practical conditions the suffix plus corresponds to that mode which is usually called "ordinary" and minus to the "extraordinary" one.

2.B.5 Equation (2.B.13) is only valid under particular conditions as exist in the lower ionosphere where collisions occur mainly with N_2 and O_2 molecules. A more general expression admitting eight parameters instead of only four in Equation (2.B.12) has been indicated by Rawer and Suchy [1967, Section 9].

In the presence of important collisional absorption the Appleton-Lassen equation gives stronger attenuation than found with the Sen-Wyller formula. Therefore, the latter must be used when dealing with strong absorption in the lower ionosphere. As to the intermediate height range where electrons collide with neutrals and ions as well, there exists a more involved theory by Shkarovsky [1961].

2.B.6 We compare now numerical results obtained from the three dispersion equations:

- (1) Sellmeier's, with no magnetic field, applying "naive" collision theory,
- (2) Appleton-Lassen's, with magnetic field, but still applying "naive" collision theory,
- (3) Sen-Wyller's, with magnetic field, applying modern collision theory particularly adapted to conditions in the lower ionosphere.

Very important differences are found at frequencies below about 6 MHz between (1) and the x components of (2) and (3), i.e. in the whole frequency range which is used for absorption measurements after methods A1, A3 and A4. The attenuation of the x component tends to be stronger than in the no-field case. As to the o component the differences are less severe becoming appreciable (in the case of weak attenuation) only below about 3 MHz. Here (1) gives higher attenuation than (2) and (3).

Considering now the differences between the Appleton-Lassen formula (2) and the Sen-Wyller formula (3), differences are small at higher frequencies where the attenuation is small but tend to be appreciable at frequencies below about 1.5 MHz. In this frequency range full Sen-Wyller theory should be used.

2.B.7 At frequencies in the approximate range from 1.5 to 3 MHz serious differences appear with electron densities above about 10^{10} m^{-3} (which in an undisturbed ionosphere occur only above 90 km) or with collision frequencies $\hat{\nu}$ above about $2 \cdot 10^5 \text{ s}^{-1}$ (occurring below 90 km). It is therefore allowed to apply some simplifications in this frequency range by which the Sen-Wyller formalism is considerably simplified. Rose [1970] assuming $N < 5 \cdot 10^9 \text{ m}^{-3}$ and the refractive index μ to be almost equal to 1 (i.e. $1 - \mu^2 \ll 1$) gives an approximation which may be used up to 90 km of altitude. In this approximation the influences of N and ν can be separated such that the imaginary part, χ , of the complex refractive index ($\mu + j\chi$) can be written as

$$\chi_{o,x} = N \cdot F_{o,x}(\hat{\nu}) \quad (2.B.14)$$

$$(1 - \mu^2)/\chi = G(\hat{\nu}),$$

F and G being functions of the "most probable collision frequency" $\hat{\nu}$ alone. Figure 2.10 gives the model profiles for N_e and for $\hat{\nu}$ as used by Rose and Figure 2.11 gives curves for $f = 1.5$ and 3 MHz computed by him for the Sen-Wyller theory (3), and curves obtained with Appleton-Lassen (2) and with the Sellmeier (1) theory for comparison. Since Rose's curves shown in Figure 2.11 are of almost identical shape, they may be approximately represented by a descriptive expression. With the abbreviations

$$x = \hat{\nu}/10^6 \text{ s}^{-1}; \quad y = \chi_{o,x}/(N/10^{12} \text{ m}^{-3}); \quad \xi = \log_{10}(x/x_b); \quad \eta = \log_{10}(y/y_b)$$

the following is a reasonably good approximation for all curves of the Rose type, x_b and y_b being the only parameters needed to identify frequency and mode:

$$\eta = \xi - 1.54 \cdot \log_{10}(1 + 10^{1.3 \cdot \xi}) \quad (2.B.15)$$

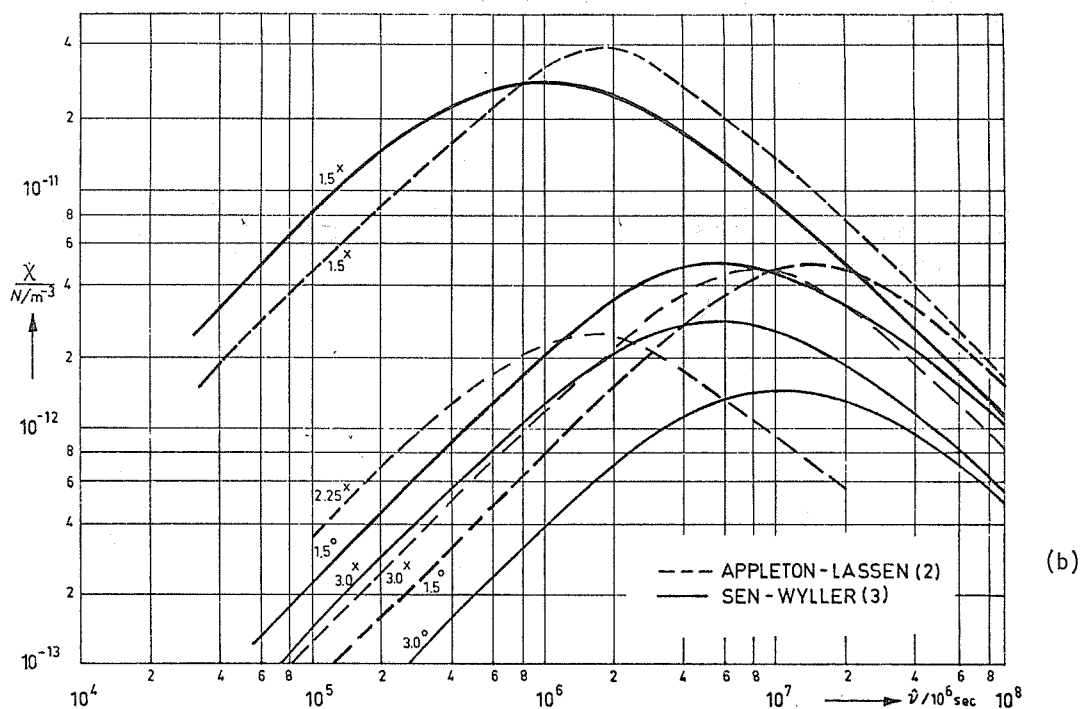
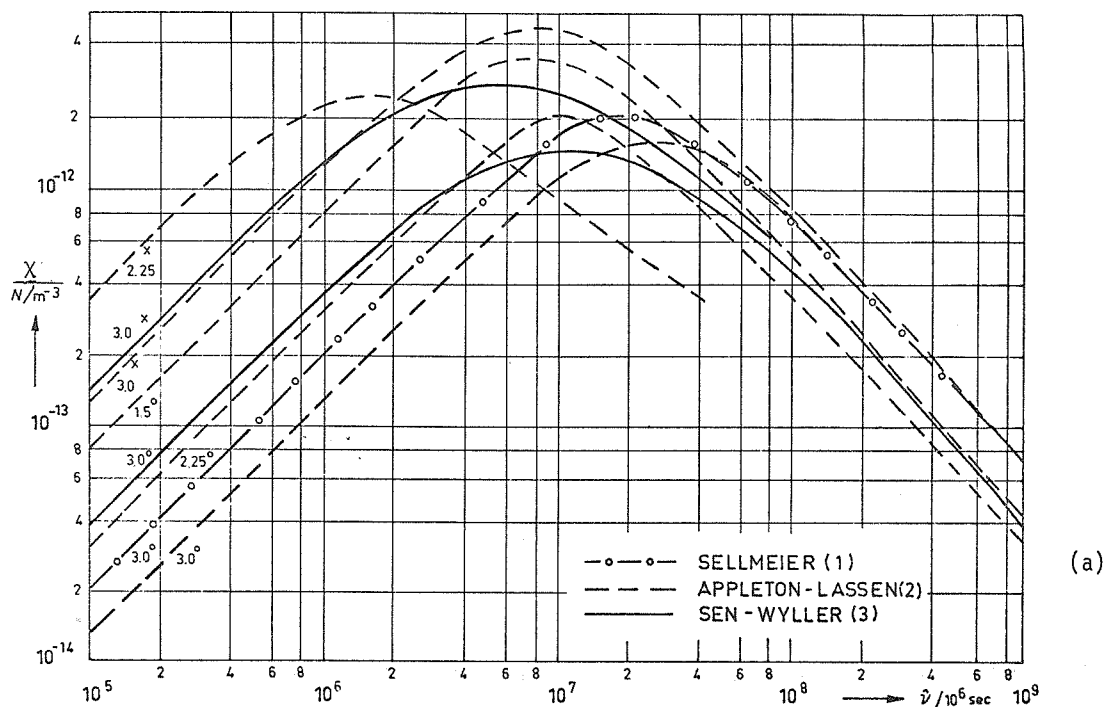


Fig. 2.11a and b Characteristic absorption function $F = \chi/N$ for the non-deviative case computed by R. Rose with Sen-Wyller theory: full curves (3); results of Appleton-Lassen theory: broken curves (2); and Sellmeier theory: dash-circle curve (1) for comparison. Valid for temperate latitude (southern Spain), but only as long as χ is proportional with N , i.e., for not too strong local absorption χ .

(a) o components for 1.5 MHz, o and x components for 2.25 and 3.0 MHz;
 (b) x components for 1.5 MHz additionally to upper part of (a).

For a given frequency in the range 1.5 to 3 MHz the values of the parameters may be interpolated from the following Table 2.2.

Table 2.2
Parameters for use with Equation (2.B.15)

| Frequency | 1.5 | 2 | 2.5 | 3 | MHz |
|---------------------------|-------|-------|-------|-------|-----|
| ω_b o-component | 6.46 | 8.22 | 9.70 | 11.20 | |
| ν_b | 14.20 | 8.34 | 5.78 | 4.22 | |
| ω_b x-component | 1.00 | 2.04 | 3.47 | 5.48 | |
| ν_b | 83.60 | 30.20 | 14.80 | 8.07 | |

This approximation may depend on the geomagnetic conditions.

Equation (2.B.15) takes into account the upper limit of attenuation introduced by the denominator which is seen for the Appleton-Lassen formula (2) from Equation (2.5). This effect is also shown in Figure 2.2 (which needs no appreciable correction since it refers to frequencies above 5 MHz).

For small enough collision frequency the influence of the denominator is negligible and we get the linear approximation

$$\frac{X}{N/m^{-3}} = K \cdot 10^{-18} \cdot (\hat{\nu}/s^{-1}) \quad (2.B.16)$$

where $K_{0,x}$ is .38 and 1.4 at 3 MHz but 2.3 and 80 at 1.5 MHz.

This may be used for the o component at values of $\hat{\nu}$ smaller than about $10^6 s^{-1}$, and $3 \cdot 10^5 s^{-1}$ for the x component. (These limits correspond to heights about 80 km and 86 km, respectively, such that the range of application of the approximation Equation (2.B.16) is limited.)

CHAPTER 3. FADING

3.0 Nature and Origin of Fading

3.0.0 Fluctuating fields are most often found in the frequency ranges in which the observations described in this booklet are made, namely MF, HF and VHF. They can be described as more or less irregular variations of the received field amplitude and phase in time, space and frequency. In order to determine a significant value of the received field strength to be used for our computations we need a representative average. It can only be obtained by suitable sampling (see Sections 3.4 and 3.5) knowing the characteristics of the specific kind of fluctuations present during the measurement (See Sections 3.1 through 3.3).

In the following we give a list of the most important propagation phenomena causing fading:

3.0.1 Interference between different modes, propagated via different paths, e.g. by reflection from the E and the F region, by multiple reflections, etc.; in these cases path differences of the components are of the order of 100 km; lapse time differences around 0.3 ms and fading stems from variations of the path lengths. Interference fading provokes strong, rather regular variations of continuous wave signals, and often very deep fading; it cannot occur with pulse methods as these select a rather narrow range of lapse time. Only interference fading with a lapse time shorter than 0.1 ms may be apparent in pulse measurements.

3.0.2 Variations of the polarization provoked by interference of the components which are due to magneto-electronic double refraction. Individually, these components tend to have elliptical polarization, but by combination any kind of polarization may instantaneously occur. Rapid changes of polarization stem from small variations of the path length difference. In a given antenna, polarization fading produces amplitude variations because the antenna selects a certain kind of polarization. The most common types of antennas select linear polarizations. It is, however, advantageous to select one of the magneto-electronic components and so avoid polarization fading at least as far as possible. Otherwise polarization fading is not avoided by pulse methods.

3.0.3 Diffraction interference between many partially or totally reflected rays, as from spread F, auroral (type a) Es, or equatorial (type q) Es produces diffuse, scattered signals. These show the most irregular fading, more shallow than interference- or polarization-fading but with very quick changes.

3.0.4 Displacement and variation of ionospheric irregularities, mainly near the reflecting level. These deform the surfaces of equal electron density provoking focusing and defocusing, i.e. amplitude variations of reflected waves. The variations are much slower than those provoked by polarization or interference fading.

3.0.5 Variations of absorption somewhere on the propagation path, mainly in the D or E region. These are also slowly variable phenomena. It is, of course, the intention of absorption observations to measure the variations of absorption but not those of focusing. Therefore both kinds of amplitude variations should be distinguished, which is not always easy.

3.0.6 The variations or, better, fluctuations of field strength present the direct aspect of a fading signal. In order to interpret the underlying phenomena and find useful parameters describing the fluctuating signal three different types of analytical representation are mainly used: Fourier analysis, auto-correlation analysis and distribution functions.

3.1 Fading Spectrum

3.1.0 By Fourier analysis of the envelope of a fluctuating signal over a long enough time period one obtains the corresponding spectrum. The relevant frequencies are found in the audio and subaudio frequency range. If it were our intention to recompose the original fading curve, both amplitudes and phases of the Fourier components are needed. However, this is not our intention here; we just need reasonable rules for sampling. The power spectrum (i.e. amplitudes alone of the Fourier components) is sufficient for this purpose.

The more regular a fading curve is the simpler is the composition of the corresponding spectrum. For a highly regular fading curve it is restricted to a few most marked spectral bands. On the other hand irregular fading curves give a broad spectrum.

The audio-frequency spectrum corresponding to the receiver output after detection results, of course, from a radio frequency (RF) spectrum appearing at the antenna and at the receiver input. For a linear receiver the shape of the output spectrum just equals one of the sidebands of the input spectrum. Of course, both are shifted along the frequency axis (see Figure 3.1).

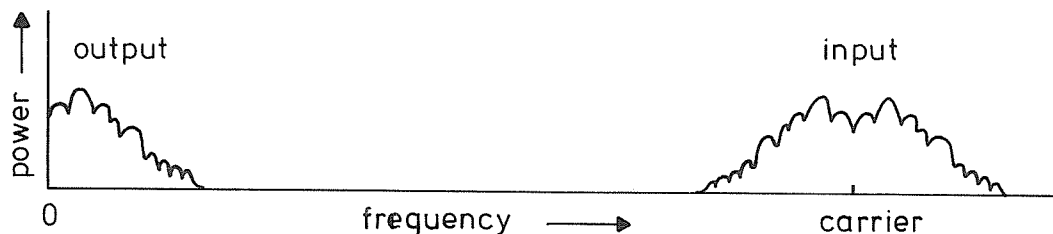


Fig. 3.1 Input and output spectrum for an AM receiver.

3.1.1 Assuming special models of the medium, radio frequency spectra can be computed essentially by determining the Doppler shift of individual wave components and modes.

The simplest case is interference fading in a two mode model: assume one mode with constant reflection height (e.g. at a stable Es layer) and another mode from a layer with variable height (e.g. an F2 layer); as the first mode can not produce a shift of frequency, it just corresponds to the original transmitted frequency f_0 . By Doppler effect the second mode is shifted to higher frequencies if the layer is going down, to lower ones if it goes up (see Figure 3.2). The distance between the two spectral lines depends upon the velocity with which the height of mode 2 varies.

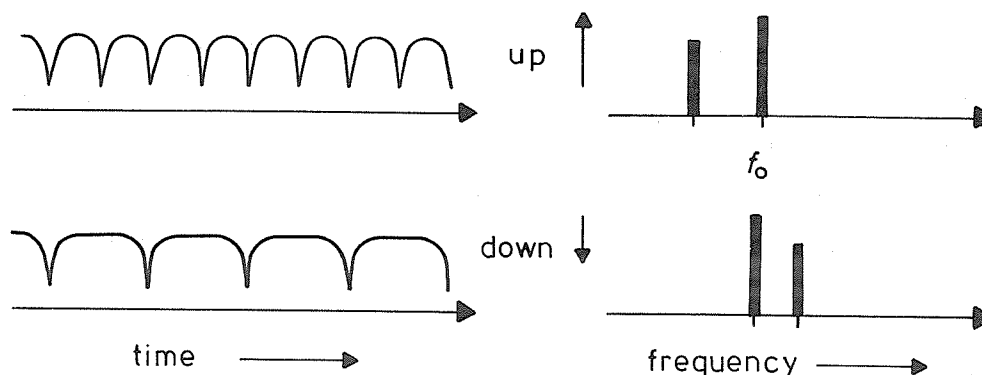


Fig. 3.2 Doppler effect causing interference fading;
at right: spectrum; at left: RF amplitude variation with time.

Ratcliffe [1948] has computed a spectrum for a case of diffractive interference assuming a scattering ionosphere with random line-of-sight velocities of the individual irregularities. The RF power spectrum is centered on the incoming frequency, f_0 , and varies with

$$\exp \left(\frac{\sigma_0^2}{8v_r^2} \left(\frac{f-f_0}{f_0} \right)^2 \right)$$

where v_r is the r.m.s. random velocity, and σ_0 the velocity of light. Ratcliffe's spectrum has the shape of a Gaussian distribution function

$$\varphi_G(x) = \frac{1}{\sqrt{2\pi} \sigma} \exp \left(-\frac{1}{2} \left(\frac{x-\bar{x}}{\sigma} \right)^2 \right) \quad (3.1)$$

where $\sigma^2 = \overline{(x-\bar{x})^2}$ is the average of the squared deviations from the mean value.

The shape of this function is shown by Figure 3.3.

3.1.2 There is a large variety of model computations. At one extreme we have models assuming only coherent modes, for example specular reflections; the spectrum is then composed of a limited number of individual frequencies (lines) (see Figure 3.2). Fading can be very deep in such cases provided the amplitudes of the modes are almost equal; fading envelopes then present some regularity. At the other extreme we have models assuming a very large number of faint individual modes, phases and Doppler shifts being at random. The spectrum is then very broad, may even be essentially determined by the bandwidth of the receiver, the original spectrum at the receiving antenna being rather flat. The corresponding fades are shallow and very irregular.

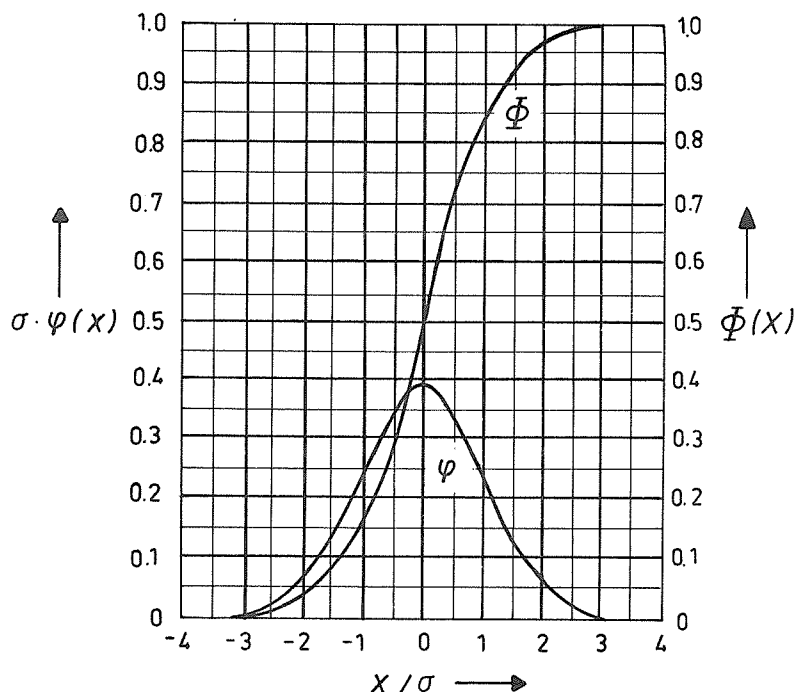


Fig. 3.3 Gaussian distribution: differential distribution function φ and integrated one Φ .

More general cases are obtained by combining coherent (specular) and incoherent (random) components. One may say that in most cases coherent components have a certain linewidth due to some fluctuations present anyway; on the other hand purely random spectra do not occur so often -- usually some specular component is present too.

3.1.3 In most absorption measuring methods the radio source just transmits one frequency; if it is pulse modulated a broadened line width is produced by the pulse shape. A pulse receiver should, therefore, always have enough bandwidth to receive the incoming RF spectrum without cutting it seriously. (This is not always the case, checking is needed). The situation is quite different with method A2 in which natural, cosmic sources are used. They have a very broad spectrum which is essentially "white" in the frequency range considered, i.e. the spectrum is just flat, the amplitude being independent of the frequency. Under these conditions the receiver acts as a bandpass so that the output spectrum is essentially determined by the transfer curve of the receiver.

3.1.4 A few examples of observed fading curves and corresponding spectra are shown in Figure 3.4. The curves have been obtained with vertical incidence pulse echoes on 2 and 3 MHz under rather different propagation conditions. Interference fading is excluded by using pulse techniques. It appears from Figure 3.4 that very different fading types must be accounted for in our sampling rules.

3.1.5 In order to get a very rough estimate of the dispersion in a fading spectrum one may use the audio-frequency spectrum, trying to replace it by a few broadened lines only. The relevant center of gravity on the frequency scale can be transformed into a time constant (by taking the inverse value). This time constant is often called quasi-period.

The spectra in Figure 3.4 have very different quasi-periods. The fading periods interesting in the present context range from a few seconds (fast fading) to the order of several minutes or even more (slow fading).

Quasi-period and depth of fast fading vary with hour and season, the fading being mostly more marked at night. Ionospheric storminess is usually accompanied by increased fading. Multiple echoes tend to show faster and deeper fading than that of first order. Slow fading is almost always present.

3.2 Autocorrelation Analysis

3.2.0 It is sometimes advantageous to consider another function which is equivalent to the spectral density function. It is obtained by applying to the power spectrum, $W(f)$, a cosine Fourier transform. This gives a function $\rho(\tau)$ which depends upon a time variable τ , the significance of which will be

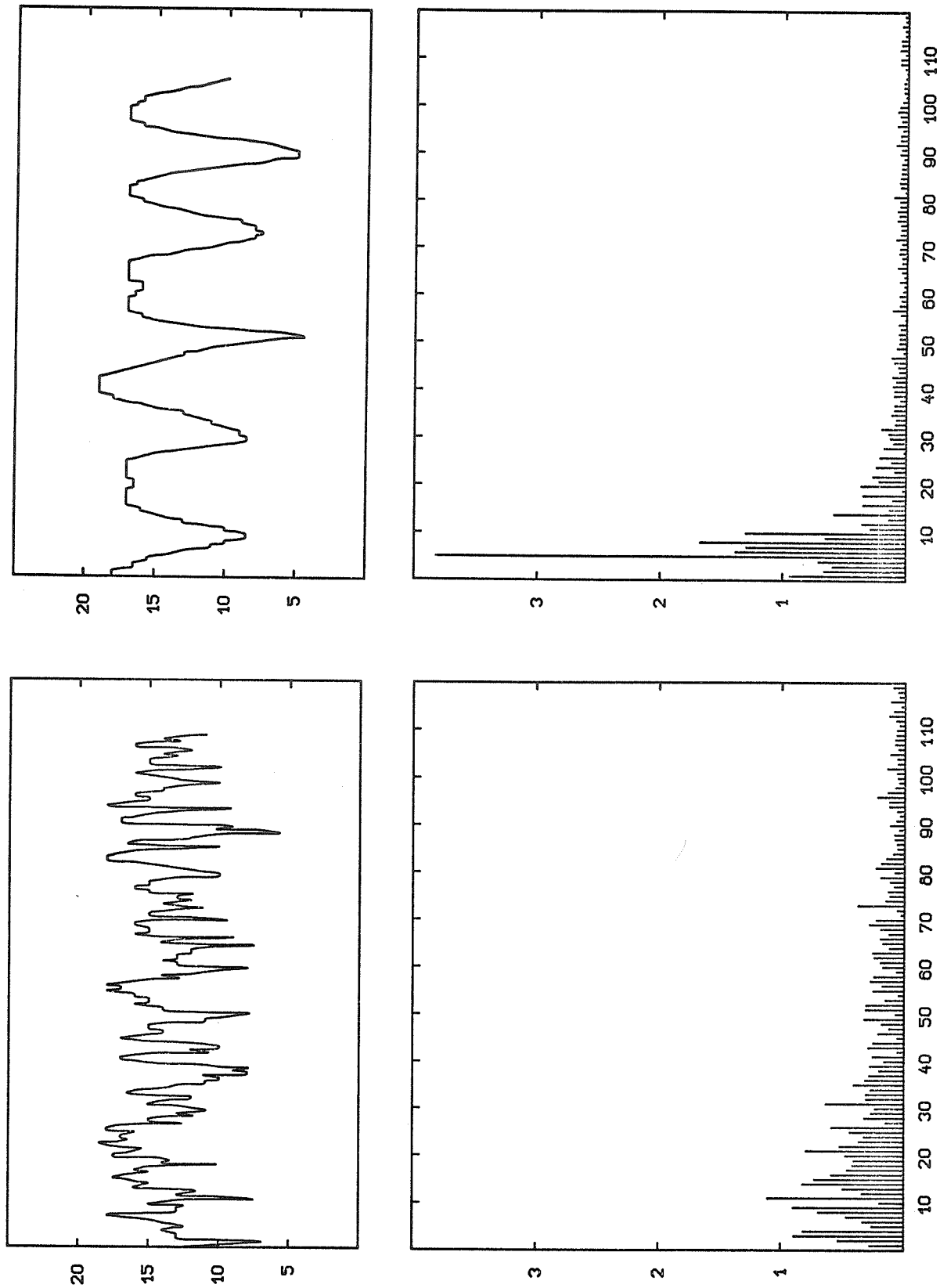


Fig. 3.4 Fading curves of individual echo pulses observed on frequencies between 2 and 4 MHz (on top) (courtesy: E. Harnischmacher, Breisach, F.R.G.), and corresponding power spectra (bottom) (a) irregular, quick fading; (b) very regular, slow fading.

explained below. This definition of the autocorrelation function $\rho(\tau)$ yields:

$$\rho(\tau) = \int_0^{\infty} W(f) \cos(\omega\tau) df \quad (\omega=2\pi f) \quad (3.2)$$

and the inverse transformation reads:

$$W(f) = 4 \int_0^{\infty} \rho(\tau) \cos(\omega\tau) d\tau \quad (3.3)$$

These are the Wiener [1948]-Hinč'in [1949] equations. They allow the autocorrelation function, $\rho(\tau)$, to be deduced if the spectrum $W(f)$ is known, and vice versa.

It can immediately be seen from Equations (3.2) and (3.3) that ρ just means power, because W means power per Hz. Thus, for $\tau=0$,

$$\rho(0) = \int_0^{\infty} W(f) df,$$

which is the total power contained in the whole spectrum.

3.2.1 Let us now describe the autocorrelation function for a few particular cases where it is most easily obtained. First consider the spectrum of a continuous wave radio transmitter with f_0 as the radio frequency. The corresponding autocorrelation function is a cosine function with period $1/f_0$, the period of the radio wave (Figure 3.5a). If in this case we ask for the audio frequency spectrum, we find just one line at zero frequency; the corresponding autocorrelation function is constant over τ (in the range considered). Next take two lines f_1 and f_2 , in the RF spectrum; this situation is often obtained by two mode propagation. The relevant autocorrelation function can be described as having two periods superposed: a short one corresponding to the average frequency, $\frac{1}{2}(f_1+f_2)$, and a long period corresponding to half the frequency difference, $\frac{1}{2}(f_1-f_2)$. When going over to the audio-frequency spectrum the "modulation" vanishes and only the slowly variable function remains (Figure 3.5b).

As a last example let us consider a "white-noise" spectrum, i.e. constant spectral density, * phases being completely at random. In this case due to lack of phase coherence the integral in Equation (3.2) vanishes everywhere, except for $\tau=0$. The autocorrelation function is just one line (Figure 3.5c). This is essentially the case of the incoming cosmic noise radiation in method A2.

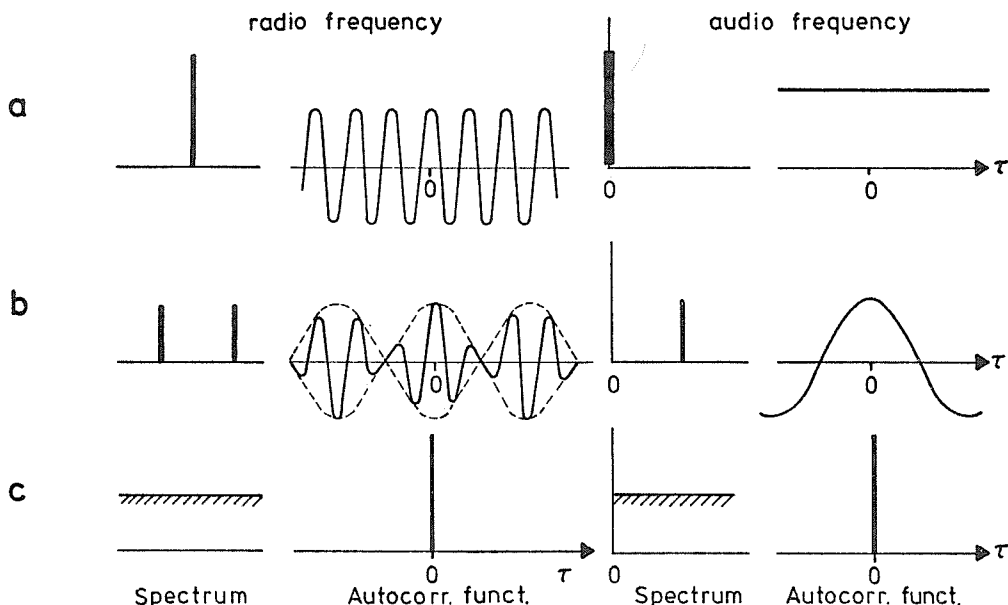


Fig. 3.5 Spectrum and autocorrelation function. At left: radio frequency aspect; at right: audio frequency aspect. Three examples: (a) continuous wave; (b) regular interference (beat) fading; (c) white noise.

* The frequency range considered never goes to infinite frequency, so that the integral in Equation (3.2) remains finite.

3.2.2 The most important advantage of the autocorrelation function stems from its direct relation with the fluctuating signal, $x(t)$. When the "d.c." component of $x(t)$ has been eliminated one finds

$$\rho(\tau) = x(t) * x(t+\tau) = \lim_{T \rightarrow \infty} \frac{1}{2T} \int_{-T}^{+T} x(t) \cdot x(t+\tau) dt \quad (3.4)$$

This definition means: in order to obtain ρ for a given τ we multiply the signal intensity at one time, t , with that at another time displaced from t by τ , and average over all possible times t . In other words, take the envelope of the fluctuating signal, shift it by τ , multiply both envelopes and determine the surface under that curve (see Figure 3.6), and so get the (audio-frequency) value of $\rho(\tau)$. This procedure can easily be executed by an automatic device containing a delaying element, D . The principle is shown in Figure 3.7. By adjusting D to different values of τ , the autocorrelation function is directly obtained. Of course, ρ can also be obtained by computation; if an automatic sampling device is at hand, the individual readings of $x(t)$ can directly be fed into a computer which is programmed after Equation (3.4).

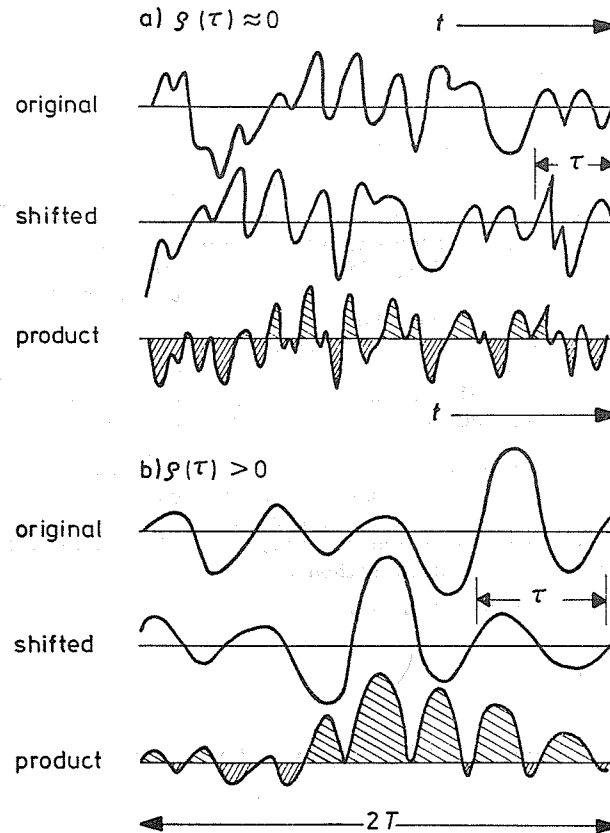


Fig. 3.6 Generating the autocorrelation function
(a) $\rho(\tau) \approx 0$; (b) $\rho(\tau) > 0$ [after W. Kleen
and K. Poeschl, 1968].

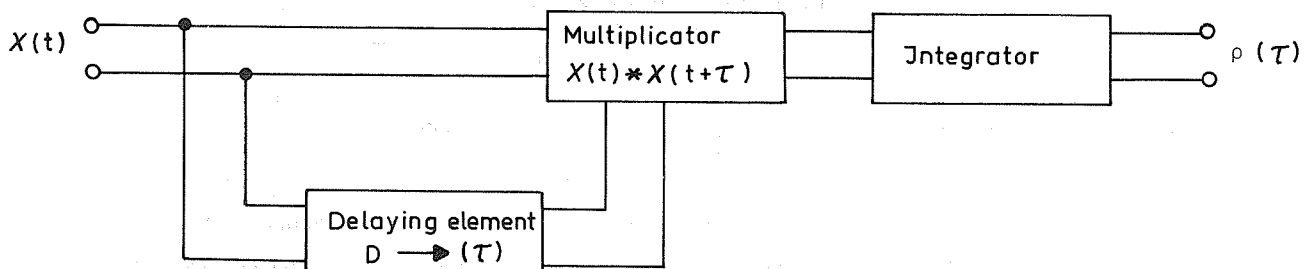


Fig. 3.7 Analogue circuit producing the autocorrelation function $\rho(\tau)$.

3.2.3 The autocorrelation function, $\rho(\tau)$, can therefore be considered to be a link between the fluctuation signal, $x(t)$, and its spectrum, $W(f)$. According to the experimental conditions it may be decided whether one or the other description is more adequate and more easily obtainable. Both can be interchanged using the Wiener-Hinčin Eqs. (3.2) and (3.3).

3.2.4 The autocorrelation function may, therefore, be used for the interpretation of observations. Ratcliffe's case of diffractive interference has for its spectrum a Gaussian distribution function, as shown by Equation (3.1) above. The computation shows that in this case the autocorrelation function is also a Gaussian distribution function (see Figure 3.3)

$$\rho(\tau) = \varphi_G(\tau/T_C) \quad (3.5)$$

where T_C is a characteristic time. An example of an autocorrelogram function derived from actual observations (HF echo sounding, McNicol [1949]) is shown in Figure 3.8. Like most observational data, it is characterized by a certain periodicity, the importance of which decreases with increasing τ . This periodic aspect in $\rho(\tau)$ reveals the presence of coherent components in the spectrum. In this particular case they are due to specular reflection.

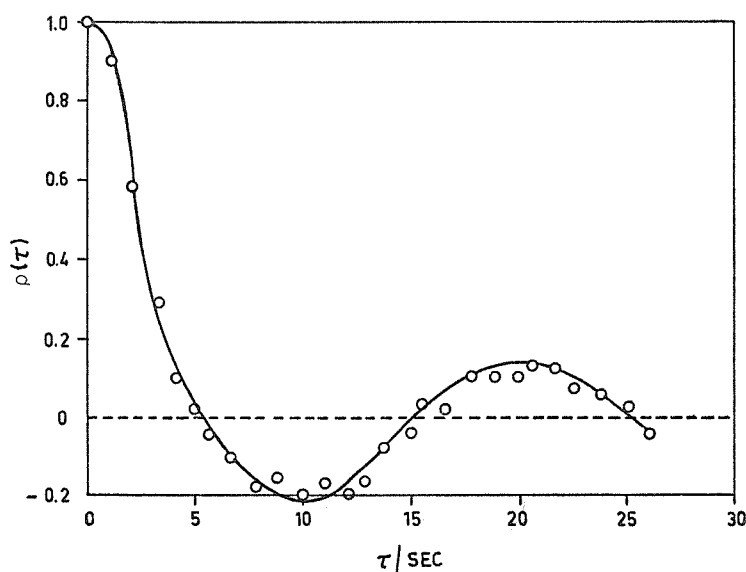


Fig. 3.8 Autocorrelogram of a fading curve [McNichol, 1949].

3.2.5 The aspect of the correlation function, $\rho(\tau)$, thus allows conclusions to be drawn concerning the spectral character of a given fluctuating signal. The greater the relative importance of coherent components is, the more periodicity appears in the shape of $\rho(\tau)$. Completely incoherent components, i.e. those with random phase, would give no periodicity at all. Strictly speaking this can not occur at the output of any receiver with limited bandwidth because the receiving system itself produces some coherence. Therefore we get a "broadened line" autocorrelation function at the output even with "white noise" at the input. As the width of $\rho(\tau)$ around its maximum at $\tau=0$ becomes smaller, the greater is the incoherence. Thus, the width of the autocorrelation function is a measure of the average coherence interval corresponding to the original fluctuating function. The coherence interval could be defined as a "memory time"; this is the delay for which the time function is mainly determined by its initial value. When describing it by sampling of individual readings, there is no sense in sampling much denser than with this time interval. In other words the knowledge of the coherence interval allows one to estimate the highest frequency component effectively present in the spectrum at least insofar as sampling procedures are considered.

3.2.6 Another advantage of the autocorrelation function is that it allows a description of the effects of receivers upon fluctuating signals in a similarly easy way as spectral functions do. Let $\underline{z}(jf)$ be the frequency transfer function of a (linear) receiver so that the power spectrum at the receiver output is

$$W_{out}(f) = |\underline{z}(jf)|^2 W_{in}(f), \quad (3.6a)$$

then

$$\rho_{\text{out}}(\tau) = \int_0^{\infty} |z(jf)|^2 w_{\text{in}}(f) \cos(2\pi f\tau) df. \quad (3.6b)$$

Using this procedure one easily computes for example the effect of a low frequency bandpass upon "white noise". The autocorrelation function at the output is in this particular case uniquely determined by the transfer function of the receiver (see Figure 3.9). This statement is of some importance for the understanding of method A2.

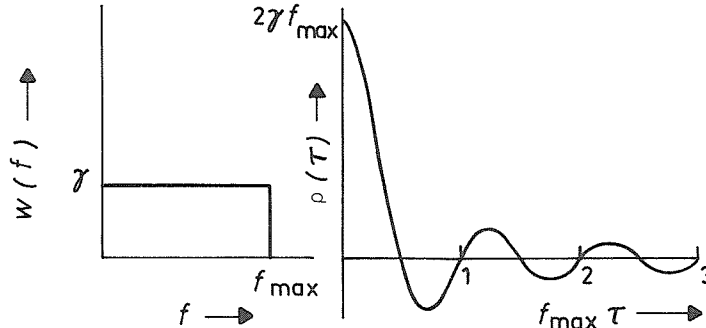


Fig. 3.9 Autocorrelation function at the output of a low-frequency bandpass (transfer function at left) fed with white noise.

3.3 Distribution Functions

3.3.0 A fluctuating field, $x(t)$, can also be described in a statistical way by indicating its differential distribution function $\varphi(x)$. This function gives information about the probability that a sample value of x taken at random is to be found in a certain (small) range of values from x to $(x+\Delta x)$. For a fluctuating field, $x(t)$, which is observed during a total time T , $\varphi(x)$ is obtained for example by first dividing the x -axis into equal intervals, Δx , and summing up over all time intervals Δt during which the curve $x(t)$ appears in a given interval. The procedure still needs normalization which is achieved by dividing by T such that finally

$$\varphi_0(x_n) = \frac{1}{T} \sum \Delta t_n(x_n \leq x < x_n + \Delta x). \quad (3.7)$$

Here $\varphi_0(x)$ is an empirical result which is usually displayed as a "staircase function". Figure 3.10 shows two examples.

3.3.1 The function φ does not contain all information about the fluctuating field contained in $x(t)$ because it only describes the rate of occurrence of different field values. In particular the spectral characteristics cannot be found from the distribution function. This is most easily seen from Figure 3.10 where two very different field variations are shown which give exactly the same distribution function $\varphi(x)$. Therefore, the knowledge of the distribution function of a fluctuating field only allows identification of a broad class of functions, $x(t)$, the detailed behavior with time being completely open.

3.3.2 It is often practical to use the integrated distribution function Φ instead of the differential distribution function, φ . Figure 3.11 shows (hatched area) the same differential distribution function as Figure 3.10. The height of each column is the probability for x to fall into a given interval. Now, by summing up over the columns from the left side up to x_1 , we determine the probability for x to take any value not greater than x_1 . At the right end the summed-up curve (thick in Figure 3.11) must always end with probability 1, i.e. 100%. It is called the integrated distribution function $\Phi(x)$. The median value x_m is easily determined from $\Phi(x)$. The probability for x to be not greater than x_m is just 50%. Thus, by intersecting the Φ curve with the 50% line one immediately reads x_m . Quartile values can similarly be found for 25% and 75%, decile values for 10% and 90% (see also Figure 3.11).

3.3.3 As seen from Figure 3.10 empirical distribution function, φ or Φ , have a "staircase shape". In fact, there is no sense in making the steps too small because the bulk of individual data tends to be rather limited. If the total number of observations is small, increasing the number of steps simply means producing detailed features which are completely fortuitous. If, however, the total number of observations could be made extremely large, the width of the steps could reasonably be made smaller and smaller, so that finally a continuous curve would be obtained. Thus, continuous distribution functions are always an extrapolation of empirical observations towards an idealized case. Problems considered in mathematical statistical theory assume such idealization. Theory shows that according to the basic assumptions made, different idealized distribution functions are obtained.

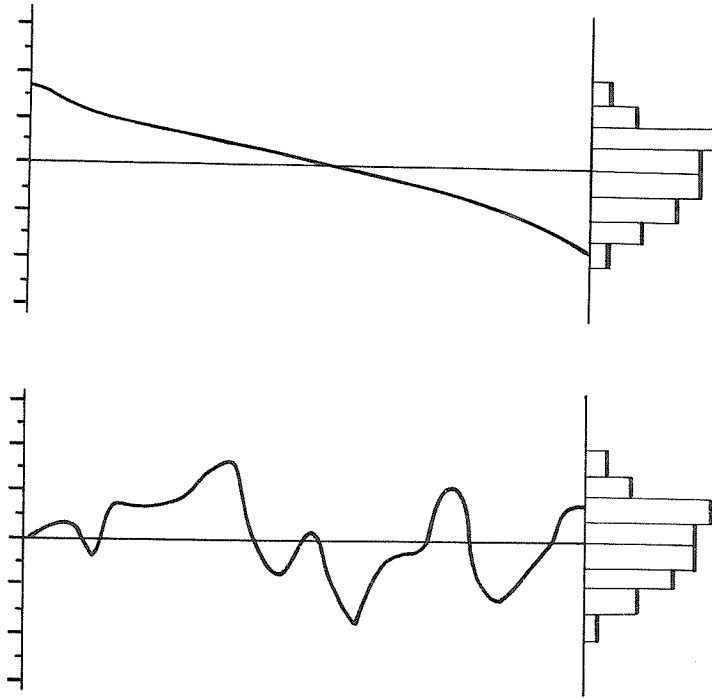


Fig. 3.10 Time function (at left) and staircase amplitude distribution function (at right).

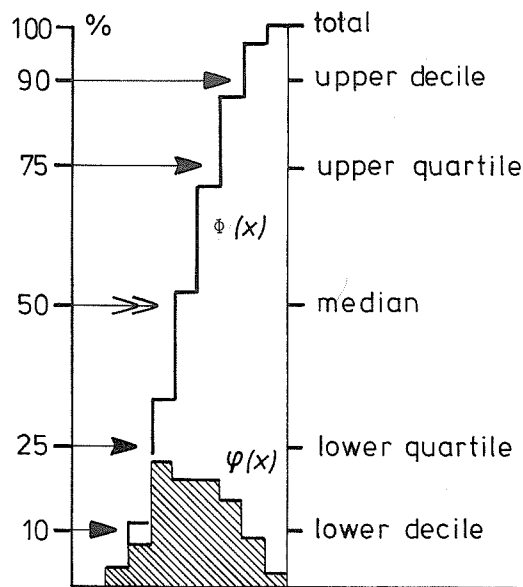


Fig. 3.11 Same differential distribution function as in Figure 3.10 (at right) and integrated distribution function (at left).

3.3.4.0 The best known of these distribution functions is the Gauss distribution function φ_G , Equation (3.1), Figures 3.3 and 3.12. It is also called "normal distribution". Being of symmetric shape it occurs often in problems of symmetric character, for example in the following case: a large number of vectors, randomly distributed in a plane, are projected onto one straight line in that plane. (This is a description of what happens to field entries with random polarization picked up by a linear antenna).

3.3.4.1 However, if instead of the field vectors themselves we take the absolute value of many vectors randomly distributed in a plane, we obtain a slightly different distribution function. This is the Rayleigh distribution whose differential form is:

$$\varphi_R(x) = \frac{2x}{x^2} \exp \left(-\frac{x^2}{x^2} \right) . \quad (3.8)$$

It differs from the Gauss function by the factor x ahead of the exponential. This factor makes the distribution skew (asymmetric) (see Figure 3.12). The Rayleigh distribution is for example used where many field entries with random phases and values occur. Since negative field values cannot occur, the distribution of fading field entries must be skew. Therefore, true random fading with incoherent entries should theoretically obey Equation (3.8).

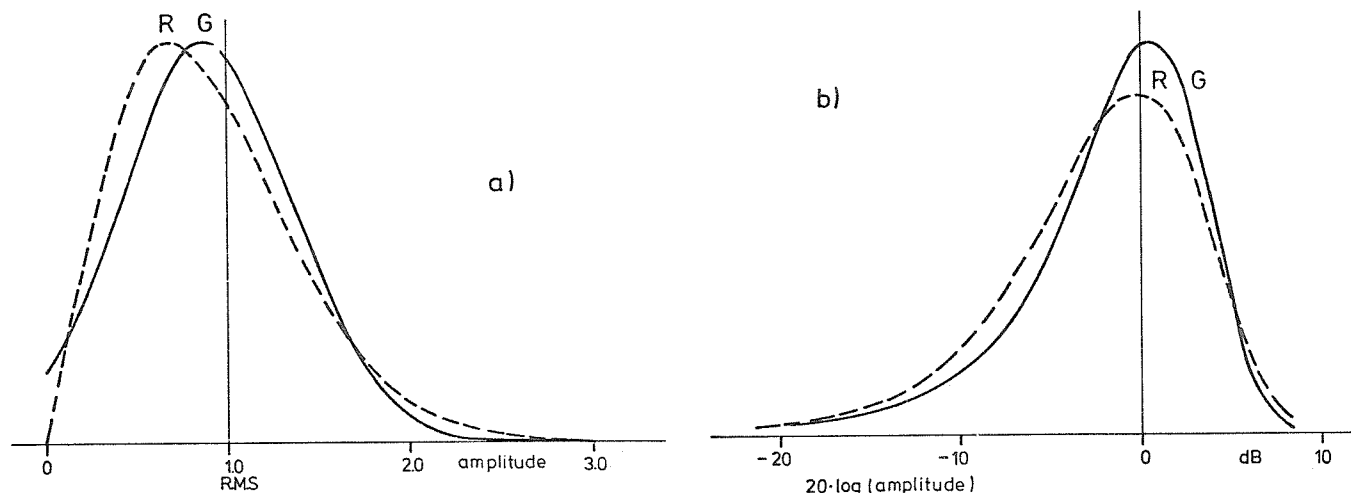


Fig. 3.12 Gauss (G) and Rayleigh (R) (differential) distribution functions (a) linear abscissa scale; (b) logarithmic (dB) abscissa scale.

3.3.4.2 In many practical cases we have a mixture of incoherent and coherent entries. Take as a typical case just one coherent component together with other incoherent ones. We then have to add one constant vector to the random vectors considered above, and take the amount of the sum of any of the latter with the constant vector. This reasoning leads to the Nakagami [1943]-Rice [1948] distribution, the argument x being the envelope tension of the received signal:

$$\varphi_{NR}(x) = \frac{2x}{x_n^2} \exp\left(-\frac{x_s^2 + x^2}{x_n^2}\right) \cdot I_0\left(\frac{2x_s \cdot x}{x_n^2}\right) \quad (3.9)$$

x_s is the amplitude of the constant coherent signal and $\overline{x_n^2}$ the squared average, i.e. the mean power of the incoherent components. I_0 is the modified Bessel function of zero order. According to the ratio x_n/x_s , the distribution lies between the Rayleigh distribution (for large values of the ratio) and a Delta function (for small values), i.e. when the incoherent component is prevailing. Figure 3.13 describes the integrated distribution function corresponding to Equation (3.9).

An often useful distribution function is derived from the normal (Gaussian) distribution by applying it not to the field or voltage values themselves but to the logarithms of these. The log-normal distribution (of an argument x) reads:

$$\varphi_{\log n}(x) = \frac{1}{\sqrt{2\pi} \sigma_1} \exp\left(-\frac{(\log x - \overline{\log x})^2}{2\sigma_1^2}\right) \frac{d \log x}{dx} \quad (3.10)$$

Here $\sigma_1^2 = \overline{(\log x - \overline{\log x})^2}$, i.e. σ_1 is the root mean square value of the deviations of $\log x$ from its mean value.

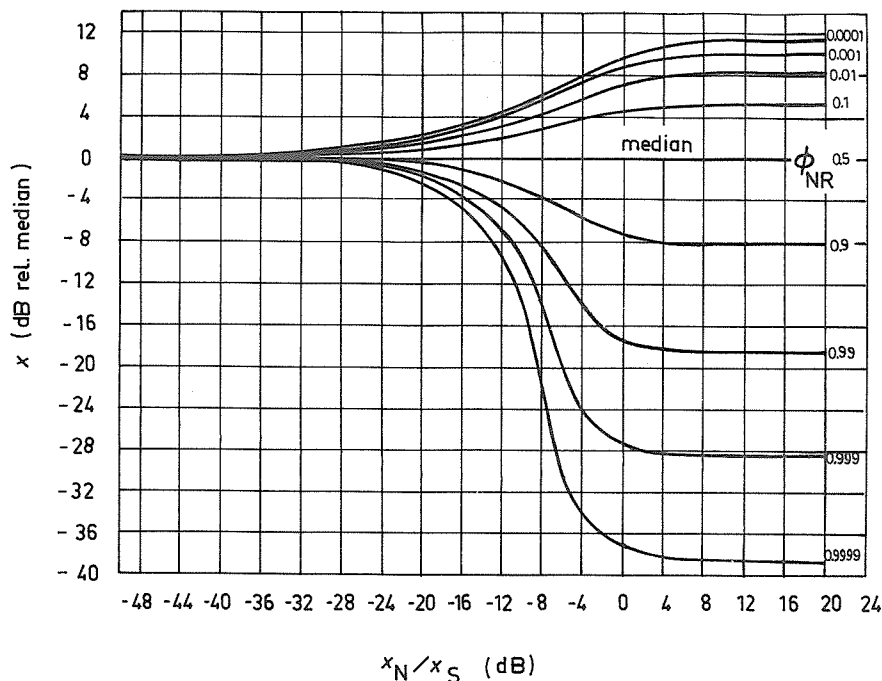


Fig. 3.13 Set of x vs x_N/x_S curves describing Nakagami-Rice distributions. Each curve has a given probability as parameter (ϕ_{NR}). Plotting ϕ against x at a given ratio x_N/x_S produces one integrated distribution function with logarithmic abscissa. Such sections approach a step function for small ratios, but a Rayleigh distribution for large values of x_N/x_S .

3.3.4.3 With respect to the levels of probability CCIR [1970] gives the following table concerning the integral distribution functions which are mostly used when dealing with fading. It gives the level (in dB against the median value) which is exceeded in a given percentage of total time:

Table 3.1

| dB Levels Against Median Value As Exceeded in the Given Percentage of Time | | | | | | |
|---|-----------------|-----------------|-----|------------------|------------------|----------|
| Distribution | 1% | 10% | 50% | 90% | 99% | Equation |
| 1. Rayleigh | 8.2 | 5.2 | 0 | -8.2 | -18.4 | (3.8) |
| 2. Nakagami-Rice | | | | | | (3.9) |
| 2a. $x_1 = \sqrt{x^2}$ | 7.0 | 4.5 | 0 | -7.5 | -17.6 | |
| 2b. $x_1 = 3.16\sqrt{x^2}$ | 3.5 | 2.1 | 0 | -2.8 | -6.0 | |
| 3. Log-normal | $2.33 \sigma_1$ | $1.28 \sigma_1$ | 0 | $-1.28 \sigma_1$ | $-2.33 \sigma_1$ | (3.10) |

This table can also be used for quick classification of an observed distribution.

3.3.5 When searching for an appropriate approximation to observed data, one needs some criterion characterizing the effective error. CCIR [1970] proposes to take the greatest deviation of the measured (staircase-like) distribution function, φ_0 , from the supposed theoretical one, φ_1 , yet demanding that the difference should decrease with the root of the number n of samples taken.

Thus

$$D(n) = \sqrt{n} \cdot \text{Max} (|\varphi_0(x) - \varphi_1(x)|) \quad (3.11)$$

is a test quantity measuring the quality of the approximation by a theoretical distribution function.

This is the Kolmogorov-Smirnov criterion.

3.3.6 Many observational statistics have been obtained and compared with different theoretical distributions. The results have been summarized by CCIR [1970].

3.3.6.1 For the HF range (decameter waves) propagated via ionospheric reflections it is stated that:

"With short analysis intervals (3 to 7 minutes), distribution functions close to the Rayleigh distribution seem to predominate. On the other hand, during longer analysis intervals (30 to 60 minutes), the distribution seems to follow the log-normal law rather than Rayleigh. The fading range is often defined as the difference (in dB) between the signal levels exceeded for 10% and 90% of the time, and values of (13 ± 3.2) dB [Grosskopf, 1953] and (16.6 ± 3.2) dB [Konopleva, 1964] have been given for long distance HF paths.

"It is of interest to note that, although the form of the measured distributions may differ from the Rayleigh distribution, the observed fading range is of the same order as the value of 13.4 dB expected for the Rayleigh distribution. However, at high signal levels the fading range has been observed to fall below the Rayleigh value, possibly due to a strong constant term arising from a specular reflection, and distributions of the Nakagami-Rice type will apply under these conditions."

3.3.6.2 Observations in the MF and LF bands (hectometer and kilometer waves) ended with a different result. Here, log-normal and Rayleigh distributions are only applicable in marginal cases. Considering observational periods of 30 to 60 minutes Sulanke and Täumer [1967, 1968] could demonstrate that an appropriate distribution function is that of a product of a slowly variable log-normal distribution function with another one of Rayleigh type describing the quick variations:

$$\Phi_{ST}(x) = \frac{1}{e\sqrt{2\pi}} \int_{-\infty}^{+\infty} \exp \left(-\frac{v^2}{2e^2} - \exp(v + 2.3026 x) \right) dv \quad (3.12)$$

The free parameter e characterizes the relative importance of the slow variations as compared with the quicker ones. The distribution becomes one of Rayleigh type, Equation (3.8) for small e ; in the opposite cases when e is large it is log-normal, Equation (3.10). See Figure 3.14 for intermediate cases. The numerical factor is $(\ln 10)/10$, x being a logarithmic function of the field strength.

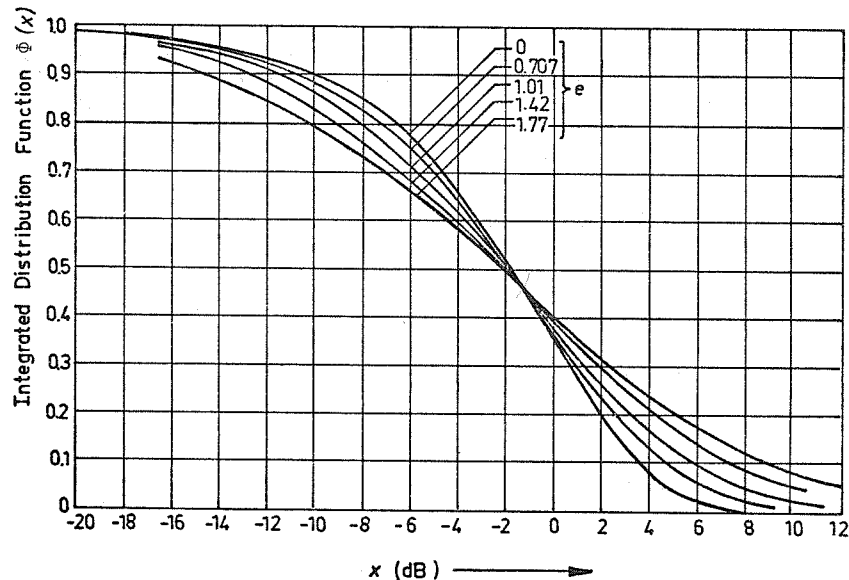


Fig. 3.14 Sulanke-Täumer (integrated) distribution functions with logarithmic (dB) abscissa.

3.3.7. It must finally be stated that observational data rather often give abnormal distributions which cannot be approximated by any of the theoretical distribution functions mentioned above. Differential distribution functions with two or even more maxima are not so rarely found. In such cases the median value may be found between two maxima so that it is less representative than in other cases. Of course, dispersion and other statistical notions too require special interpretation in these cases. As an example, consider the idealized case of a very regular interference or polarization fading. Two types of possible amplitude variations are shown in Figure 3.15, together with the relevant distribution functions. These are, of course, hypothetical cases, but by adding some fluctuations one obtains the dotted distribution curves as are sometimes observed.

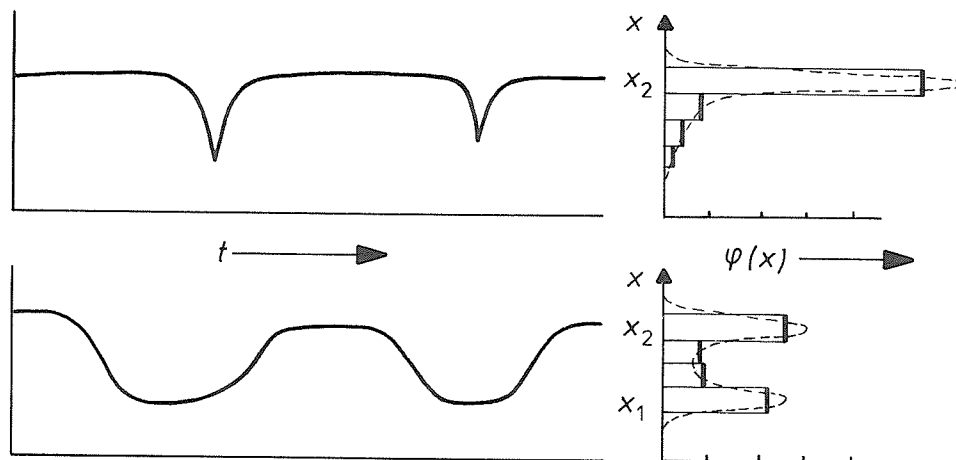


Fig. 3.15 Two different types of regular fading (at left) and their staircase distribution functions. Estimated continuous distribution functions are indicated as broken curves.

3.4 Sampling Problems

3.4.0 In order to obtain a representative value for the fluctuating field at a receiving antenna (or of the corresponding voltage at a given point in a receiver), one needs an agreement concerning an appropriate sampling procedure. Usually amplitudes are read in a sequence of time intervals the median of these readings being taken as representative for the whole time T , which is called sampling period. In most cases one has constant time intervals and the number of readings per time unit is called sampling frequency, usually expressed as the number of readings per minute. The procedure for determining sampling period and sampling frequency must be adapted to the fading characteristics.

3.4.1 The sampling period should be long enough so that a sufficient number of independent samples can be taken. A real fading curve always has some persistency as can be seen from its autocorrelation function; very quick sampling just results in repeating the same values several times without adding significant information. The period of "quasi-persistency" characterizes the time interval over which the autocorrelation function goes down to insignificant values in the HF range, in practical cases it is most often found to lie between 2 and 10 sec. Thus, an estimate of the number of possible independent observations is between 30 and 6 per minute. For this reason as far as sampling is concerned, automatic devices are not an improvement as compared with manual procedures. In order to obtain satisfying sampling most automatic devices artificially decrease the sampling frequency which, technically, could be obtained. In the MF, and LF range the period of quasi-persistency is longer (up to a few minutes in the LF range) so that longer total time is needed in order to obtain enough independent samples.

3.4.2 In order to avoid the redundancy caused by autocorrelation the sampling frequency should be rather low; 6 samples per minute is a reasonable value on HF and the higher MF waves. For MF waves 2 samples per minute may be suitable, and much less on LF waves. These values are in agreement with the highest quasi-periods occurring in the audio frequency fading spectrum. In other words in the received audio frequency spectrum the important contributions due to fading tend to be found above the following frequencies

0.1 Hz on HF waves,
0.03 Hz on MF waves,
0.01 Hz on LF waves.

The sampling frequency should be chosen below the indicated values.

3.4.3 The sampling period, T , should be long enough to cover a sufficiently large number of individual samples, so that their median value is well representative and slow (long-period) fading is eliminated. On the other hand, it should not be too long because otherwise the natural short term variations of absorption itself would also be eliminated. Unfortunately, both conditions together are too severe to be strictly applied with real measurements. Quick variations of absorption, particularly in cases of solar flare effects (sudden ionospheric disturbances, SIDs) sometimes occur in a minute or two; on HF waves this would allow about 6 samples only, which is not enough for a representative median. Thus, when the sampling frequencies were chosen so as to eliminate all long period fading we were unable to follow the quickest variations of absorption itself. In other words the quickest absorption variations and slow fading are mixed-up in the same range of the frequency spectrum and can not be distinguished with absolute certainty.

3.4.4 The requirements for sampling can be summarized as follows: Taking account of the appropriate sampling frequency (see Section 3.4.2 above), we should take so many independent samples that on one hand their median or mean value is significant, and on the other hand the time period of sampling is

not too long, so that quick variations of absorption are not eliminated. The second requirement can only be approximately satisfied, as has been stated above. The first requirement essentially means that median or mean values obtained from two different sets of samples taken under the same physical conditions should not be seriously different.

In other words we must realize that the mean (or median) value of a finite set of individual measurements is not necessarily identical with the "true" mean (or median) value which would be found from a very large (in the limit: infinite) set of observations. This problem is currently encountered in most applications of statistics, particularly with small sets of samples. In order to get a realistic evaluation one should know a "range of confidence" (often called "error range") inside which the "true" mean (or median) value is to be found with high probability. The width of this range depends, of course, not only on the number of samples, but also on the shape of the statistical distribution function. Caution is therefore needed when applying one or the other idealized distribution function to a given problem.

3.4.5 In the special case of a "normal" or Gaussian distribution the mean (or median) values of different individual sets of samples (of equal size) are symmetrically distributed around the (unknown) "true" mean (or median) value. In spite of the fact that in practice field strength distributions are often skew, means (or medians) of individual sets tend to be almost symmetrically distributed so that the "normal" distribution is a sufficient approximation in this particular context. Under such conditions Student's so-called "t-criterion" may be used in order to determine confidence limits. The criterion is described in statistical treatises; a discussion from the geophysicist's viewpoint can be found in Taubenheim's treatise [1969].

Assuming a "normal" distribution, a set of N measurements x_i may be taken so that the individual samples are independent. Let \bar{x} be their mean value then Student's criterion says that the confidence limits are given by:

$$\bar{x} \pm t\sigma_0/\sqrt{N} \quad (3.13)$$

where σ_0 is the root mean square deviation of the observed set

$$\sigma_0^2 = \frac{1}{(N-1)} \sum (x_i - \bar{x})^2. \quad (3.14)$$

The coefficient t depends on the size of the set, i.e. on N , and on the particular value of probability which has been chosen in order to obtain "confidence".

Similar reasoning applies to medians, however the corresponding range of confidence is somewhat larger than for mean values because by definition the dispersion of median values is greater. With a "normal" distribution, the t values for medians are greater by a factor of about 1.25 (i.e. $\sqrt{\pi/2}$). Table 3.2 gives t -values for mean and median values for different set sizes (N); we consider a confidence range of 95% or 99%, which is the probability to find the "true" mean (median) value inside the range given by Equation (3.13).

In such cases, however, where consecutive samples are not fully independent slightly larger ranges than given in Table 3.2 should be admitted. It must be held in mind that N in Equation (3.13) is the number of effectively independent samples, thus smaller than their real number under conditions where the independence is not fully granted [see Taubenheim, 1969].

3.4.6 We give one example to show how this criterion could be used. Let the number of independent samples be 10. Let the set of measured values be (in dB):

60 58 64 59 57 69 65 61 55 62

The mean (mn) and median (md) are 61 and 60.5 respectively. We determine the individual deviations from mn and md:

| | | | | | | | | | | |
|-------|-------|-------|-------|-------|-------|-------|-------|-------|------|-------|
| -1, | -3, | +3, | -2, | -4, | +8, | +4, | 0, | -6, | +1 | (mn); |
| -0.5, | -2.5, | +3.5, | -1.5, | -3.5, | +8.5, | +4.5, | +0.5, | -5.5, | +1.5 | (md). |

Squaring these deviations we get:

| | | | | | | | | | |
|-----|-----|------|-----|------|------|------|-----|------|-----|
| 1, | 9, | 9, | 4, | 16, | 64, | 16, | 0, | 36, | 1 |
| 0+, | 6+, | 12+, | 2+, | 12+, | 72+, | 20+, | 0+, | 30+, | 2+. |

(+ meaning +.25).

Adding up we get 156 in the first line and 158.5 in the second one. Thus after Equation (3.14)

$$\sigma_0^2 \text{ (mn)} = \frac{156}{9} = 17.33 \text{ and } \sigma_0^2 \text{ (md)} = \frac{158.5}{9} = 17.61,$$

i.e. $\sigma_0 \text{ (mn)} = 4.16$ and $\sigma_0 \text{ (md)} = 4.20$.

From Table 3.2 we find for $N = 10$ the following values of t and from Equation (3.13) the confidence range $2t\sigma_0/\sqrt{N}$.

| | 95% (mn) | 95% (md) | 99% (mn) | 99% (md) |
|-------------|----------|----------|----------|----------|
| $t =$ | 2.26 | 2.82 | 3.25 | 4.06 |
| Total range | 5.95 | 7.49 | 8.56 | 10.79 |

In spite of the much greater dispersion of the individual samples the maximum possible error which we have to admit at the data reduction is given by the figures in the last line.

Table 3.2

t -Values After Student's t -Criterion

| Number of Samples N | 95% Probability | | 99% Probability | |
|--------------------------|-----------------|--------|-----------------|--------|
| | Mean | Median | Mean | Median |
| 2 | 12.71 | 15.89 | 63.66 | 79.58 |
| 3 | 4.30 | 5.38 | 9.92 | 12.40 |
| 4 | 3.18 | 3.98 | 5.84 | 7.30 |
| 5 | 2.78 | 3.48 | 4.60 | 5.75 |
| 6 | 2.57 | 3.21 | 4.03 | 5.04 |
| 7 | 2.45 | 3.06 | 3.71 | 4.64 |
| 8 | 2.37 | 2.96 | 3.50 | 4.38 |
| 9 | 2.31 | 2.89 | 3.36 | 4.20 |
| 10 | 2.26 | 2.83 | 3.25 | 4.06 |
| 12 | 2.20 | 2.75 | 3.11 | 3.89 |
| 14 | 2.16 | 2.70 | 3.01 | 3.76 |
| 16 | 2.13 | 2.66 | 2.95 | 3.69 |
| 18 | 2.11 | 2.64 | 2.90 | 3.63 |
| 20 | 2.09 | 2.61 | 2.86 | 3.58 |
| 22 | 2.08 | 2.60 | 2.83 | 3.54 |
| 24 | 2.07 | 2.59 | 2.81 | 3.51 |
| 26 | 2.06 | 2.58 | 2.79 | 3.49 |
| 30 | 2.04 | 2.55 | 2.76 | 3.45 |
| 35 | 2.03 | 2.54 | 2.73 | 3.41 |
| 40 | 2.02 | 2.53 | 2.70 | 3.38 |
| 45 | 2.02 | 2.53 | 2.69 | 3.36 |
| 50 | 2.01 | 2.51 | 2.68 | 3.35 |
| 60 | 2.00 | 2.50 | 2.66 | 3.33 |
| 70 | 1.99 | 2.49 | 2.65 | 3.31 |
| 80 | 1.99 | 2.49 | 2.64 | 3.30 |
| 90 | 1.99 | 2.49 | 2.63 | 3.29 |
| 100 | 1.98 | 2.48 | 2.63 | 3.29 |

PART II: THE DIFFERENT METHODS OF MEASUREMENT

by

W. Dieminger, E. A. Lauter, J. Mass, K. Rower,
K. Schlegel, H. Schwentek and J. Taubenheim

CHAPTER 4. METHOD A1 (PULSE REFLECTION METHOD)

by

K. Rower

(Consultant on A1 and A3 Absorption to the URSI-STP Committee until 1969)
Fraunhofer-Gesellschaft, Institut für Physikalische Weltraumforschung, Freiburg, F.R.G.

Table of Contents

| | Page |
|--|------|
| 4.1 Principle of Measurement | 45 |
| 4.2 Experimental Procedures | 47 |
| 4.2.1 A1 system | |
| 4.2.2 Constant gain linear receiver technique | |
| 4.2.3 Quasi-logarithmic receiver technique | |
| 4.2.4 Constant output technique | |
| 4.2.5 Automatic devices | |
| 4.2.6 Constant output automatic devices | |
| 4.2.7 Constant gain automatic devices | |
| 4.3 Experimental Techniques | 51 |
| 4.3.1 Bandwidth considerations | |
| 4.3.2 Wave form generators | |
| 4.3.3 Pulse transmitter | |
| 4.3.4 Antennas | |
| 4.3.5 Pulse receivers | |
| 4.3.6 Indicator and recording devices | |
| 4.4 Maintenance and Checking | 57 |
| 4.5 Procedures in the Reduction of Measurements | 59 |
| 4.5.1 Correct identification | |
| 4.5.2 Basic equations | |
| 4.5.3 Reference field | |
| 4.5.4 Equivalent height | |
| 4.5.5 Accuracy rules | |
| 4.5.6 Recommended reduction schedule | |
| 4.5.7 Examples | |
| 4.5.8 Data for interchange | |
| 4.6 Calibrations | 70 |
| 4.6.1 Absolute calibration | |
| 4.6.2 Relative calibration | |
| 4.6.3 Reference value | |
| 4.6.4 Height scale calibration | |
| 4.7 Data Handling and Interpretation | 75 |
| 4.8 Programs and Data Interchange | 78 |
| 4.9 A Few Results | 80 |
| Appendix 4.A Transistorized IF-Pulse Amplifier | 101 |
| Appendix 4.B D.C. Voltage Controlled RF Amplifiers | 101 |
| Appendix 4.C Digital Sampling System with Cyclic Commuting of Thresholds | 103 |

4.1 Principle of Measurement

4.1.1 A radio wave reflected in the ionosphere suffers on its way up and down from absorption particularly at certain height levels (see Sections 2.3 ... 2.6 and Figure 2.6b). If propagation is observed at oblique incidence, the angle between the ray and the vertical varies along the path for two reasons: first because the ionosphere is curved, second because refraction occurs (see Figure 1.3). Observations at vertical incidence can be interpreted more easily as the geometry is much simpler. Consequently for the vertical incidence method A1, we have to apply waves which do not penetrate the ionosphere at vertical incidence (as shown in Figure 1.2b) but are reflected in one of the ionospheric layers. This is equivalent to saying that we must use frequencies below the lowest critical frequency that the ionosphere may have at the hour when observations are undertaken; the same is true for calibration time, i.e. at night (see Section 4.6). As the critical frequencies are largely variable, we cannot expect to fulfill this condition with a given frequency at all hours and seasons unless we choose a rather low one. With the exception of high latitudes, frequencies around 2 MHz will be reflected practically at any time. This is the reason why the main effort of A1 measurements is made on these frequencies.

4.1.2 It must, however, be noted that the diurnal, seasonal and solar cycle variations of ionospheric electron density necessarily cause important variations of the height where a wave of given frequency is reflected. This does not only influence the deviative absorption near the level of reflection (see Section 2.4) but also the sounding path length. For example, around noon a frequency may usually be reflected in the E region, say around 110 km of height; it will suddenly be reflected at 100 km if blanketing (sporadic) Es occurs. By this change, an important contribution to deviative absorption may be cut off (see Section 2.6 and Figure 2.7). The change thus produces a decrease of the absorption decrement on that frequency. Another example is the change from F-region reflection to E-region reflection in the morning when the E-layer critical frequency, f_oE , rises through the working frequency, and the reverse change in the afternoon. Large changes in absorption occur at these times because the F reflections have passed through a thicker absorbing region. There is also strong deviative absorption near f_oE for both types of reflection. This depends on the actual conditions near the reflection point. In noontime measurements no attempt should be made to make measurements when this occurs.

4.1.3 The choice of operational frequencies is mainly a question of ionospheric conditions. The standard frequency (2.2 ± 0.2) MHz, originally selected for the IGY, has proven extremely valuable and should be chosen as a first priority. At low latitudes absorption on this frequency is sometimes very great so that a slightly higher frequency may be preferable. In sunspot minimum the standard frequency may be too near to the critical frequency f_oE or f_oF2 and suffer from increased deviative absorption, particularly in winter. It should, however, be kept in mind that for synoptic studies of absorption it is most helpful to have data on the same standard frequency from everywhere and at all times. Thus the (2.2 ± 0.2) MHz frequency should only be rejected if very serious reasons are against it, for example when absorption at noon is too great to be determined with reasonable accuracy for an extended period (say most days in several months). In diurnal sequences of measurements data taken when the working frequency is near f_oE are not interpretable. If this occurs for more than an hour, it is desirable to make measurements on a second frequency at these times.

4.1.4 A second frequency should be used whenever possible because

- a) it enables changes in the absorbing layers to be distinguished from changes determined by slight perturbations in the reflection conditions of the standard frequency,
- b) it enables a more sophisticated analysis of the data to be made (see Section 4.7 below).

At certain times of day either frequency may not be usable because it is too near f_oE . The choice of the second frequency involves a compromise so that over a year the favorable period is maximized. In practice a frequency about 0.5 MHz above the standard frequency is frequently a good choice. When it is not possible to obtain two frequencies reflected from the E layer, e.g. over wide areas in solar minimum years and at high latitudes in most years, it is preferable to choose the second frequency so that it is usually reflected from the F region. In this case it is necessary to avoid frequencies which are near f_oE or f_oF1 for long periods of time, and the second frequency may then be several MHz higher than the first. Of course, where facilities are available to change frequency and calibrate several frequencies, more valuable data can be obtained by using different second frequencies at different seasons. It is very important that at least the primary frequency is kept constant for as long as possible so as to provide direct comparisons for different seasons, solar activity and diurnal variations.

The diurnal variation of absorption for a frequency reflected from the E region in the middle of the day and the F region near sunrise and sunset is shown in Figure 4.1. Two maxima are seen when the working frequency is well below f_oE at noon. For a higher frequency which approaches f_oE near noon there is a single maximum at noon but its value is increased by deviative absorption. Such a maximum cannot be interpreted without taking this into account -- a complicated procedure in practice.

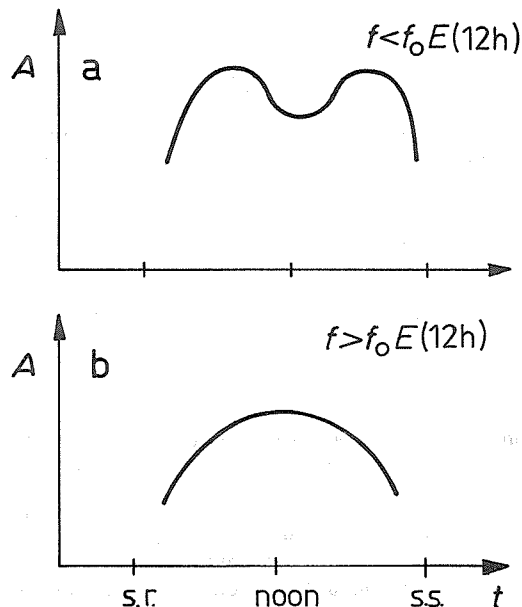


Fig. 4.1 Typical diurnal variation of absorption
 (a) for a frequency less than f_oE
 (b) for a frequency greater than f_oE
 at noon (s.r.=sunrise, s.s.=sunset).

4.1.5 The variations of f_oE and f_oF2 at high latitudes are usually too great for any single frequency to be found which will be observable at all times of day and all seasons. In this case several frequencies must be used when measurements are needed at all epochs. The principle to be observed is to use two frequencies whenever possible, allowing a considerable overlap in time when the primary frequency must be changed. The secondary frequency for one period becomes the primary frequency of the next period.

In particular in winter the normal E-layer critical frequency tends to be below the usable range of frequencies and the value of f_oF2 can be very low. Medium wave interference may then prevent measurements from being possible. However, useful data has been obtained in some localities using frequencies down to about 0.8 MHz. Caution is needed when interpreting data from frequencies below about 1.5 MHz because the simple formulas given below break down in this case (see also Section 2.2.4-6).

At times when f_oF2 is very small and no ordinary echo appears on the given frequency, the (extraordinary) x echo may be used instead. For synoptic purposes an effective o absorption may be obtained by multiplying the observed x absorption by the factor $[(f-f_L)^2/(f+f_L)^2]$ i.e. by using Equation (2.17). As some deviative absorption is always present, this procedure is not adequate to make the o and x data strictly comparable; the computed values are always less than would be found for the corresponding o measurements. Values obtained in this manner should be described by the letter J. Without the correction factor the appropriate symbol is X. Such values are considerably greater than the corresponding o-mode values.

4.1.6 Frequencies in the MF broadcasting band can be used for absorption measurement with some restrictions:

- More involved equations must be used to take account of the magnetic field effect because the gyrofrequency is found in this band. It is therefore not possible to use the simplified Equations (2.2) ... (2.5) given in Section 2.2.4, as well as the Equations in subsequent paragraphs deduced from these. For precision see Section 2.2.4, Figure 2.1.
- Application of the Appleton-Lassen dispersion equation is doubtful on these frequencies. The Sen-Wyller formula should be used systematically (see

Section 2.2.6). It is, unfortunately, considerably more involved and in practice demands the use of the computer (see Appendix 2.B).

- c) The mode of reflection which is strongest is often the z mode. This occurs in two ways:
 - (a) if the plasma frequency f_N and working frequency f are comparable at the level where $\bar{v}=v_C$, there is efficient coupling to the z mode.
 - (b) if the height of reflection is below the level where $\bar{v}=v_C$, a z mode is seen.

Both become more common at higher latitudes because the height where $\bar{v}=v_C$ increases with latitude (see Figure 2.9).

Absorption for the z mode is usually less appreciable than that for an o mode reflected from the same level.

For all these reasons the use of method A1 in the MF broadcasting band is only recommended at stations where appropriate theoretical and computational facilities exist.

4.1.7 Multifrequency observations of absorption and vertical height undoubtedly provide the most valuable data available from method A1. Six or more frequencies reasonably spaced between 1.6 and 6 MHz allow detailed studies of the different contributions to absorption (see Figure 2.6) so that physical interpretation can be reached. In particular distinction between deviative and non-deviative contributions (see Section 2.6 and Figure 2.7) can only be obtained with this technique. Multifrequency observations are therefore strongly recommended to all stations which can afford both the technical facilities and the effort required for reduction and interpretation.

Two-frequency programs have given interesting results in synoptic data studies and this continues to be true for special events or new stations. However the progress of our knowledge of the undisturbed lower ionosphere certainly demands more stations using true multifrequency techniques.

4.1.8 Practical limitations of A1 observations occur on frequencies where particular conditions are given.

Geophysical factors have a tendency to be variable with time so that they are not restricted to certain frequencies. They are, however, frequency ranges where partial reflection from Es occurs rather often in summer or where diffuse Es occurs (particularly at equatorial and auroral latitudes). In these conditions valuable data can not be expected on such frequencies. Also in the immediate neighborhood of a critical frequency, for example f_oE or f_oF1 , quick changes of absorption may destroy the value of the sample.

Interference by terrestrial radio transmissions can be a serious handicap for absorption measurements. Broadcasting bands (particularly that near 6 MHz) are not usable in most parts of the world. Regional or local emissions may produce severe interference and these frequencies should be avoided. These local conditions should certainly be taken into account when choosing a frequency. Particularly when automatic equipment is used, it is important to check that periods of serious interference can be identified in the records and be cut out where interference was so strong that the data were vitiated.

4.2 Experimental Procedures

4.2.1 An A1 system basically consists of a pulse transmitter with an antenna arranged to radiate vertically upwards, a corresponding receiving antenna and a pulse receiver with a reading or recording system (see Figure 4.2). Details of some importance are explained in Section 4.3 below. There is, however, one general requirement that the recorded signal should be related to the echo signal at the input of the receiver in a unique way (in both directions and without "hysteresis"). There is another general requirement concerning all parts of the system, namely long term stability, if possible over many months. It is much easier to keep equipment constant than to estimate the magnitude of any changes which may have occurred.

It is essential that the relation between the input signal and the recorded signal should be unambiguous and invariable. Unless the design is considered carefully, it is easy to introduce time constant effects which cause the output to depend on the shape of the signal, sense of fading and presence or absence of interfering signals. The latter can occur in HF stages due to signals which do not appear in the output of the receiver. It is therefore essential to check the receiver. During night hours commercial receivers when connected to the antenna can have sensitivities which differ 12 dB or more from the sensitivity with no antenna or from that effective during the day.

If such effects are avoided, relative variations of the field strength of a certain echo reflected in the ionosphere can be measured. First of all the system measures total attenuation, including spatial attenuation, focusing etc. (see Chapter 1). When the system has been calibrated (see Section 4.6 below) the total attenuation can be translated into total absorption along the wave path, provided effects such as focusing and fluctuating effects of fading have been eliminated by suitable sampling (see Chapter 3).

Three different procedures are mainly used. They differ by the manner in which the receiver gain is arranged and so use different ways of recording. These will be explained in more detail, first for "manual" and then for "automatic" devices.

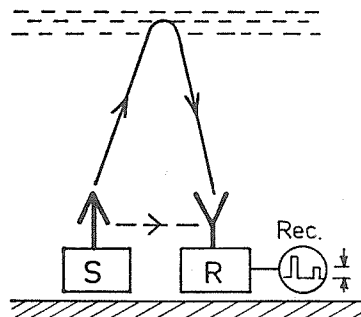


Fig. 4.2 Schematic diagram of an A1 system (S = pulse transmitter, R = receiver, Rec. = recorder)

4.2.2 Constant gain linear receiver technique means that the gain of a linear receiver is kept constant or switched in large steps. As the pulse fades, the output pulses, usually read at the scaled screen of a cathode ray tube, vary. Individual readings are taken at suitably fixed time intervals which should be longer than the quasi-persistence of the signal, i.e. its "coherence interval" (see Section 3.3.6). An interval of 10 sec is often used.

4.2.2.1 The receiver should have a wide dynamic range, the output being proportional to the input at any gain setting. A description of a widely used receiver is given by W. R. Piggott [1955a]. The overall sensitivity of the receiver can be changed in large steps, e.g. 20 dB. A passive attenuator between antenna and first stage is a good solution provided it is constant over the frequency range and is well matched at both ends.

For receivers with d.c. coupling after the detection stage the sensitivity can be calibrated with a signal generator at its input, adjusting the input voltage so that given amplitudes are found on the screen. The easiest way is to use a CW signal at the input. This is, however, not absolutely correct for pulses, except when the pulse length and the receiver bandwidth are adjusted so as to show a short flat top at the output. Of course, this must be checked. Otherwise, pulses similar in shape with those of the transmitter should be used for calibration.

4.2.2.2 The median amplitudes of the reflected signals are found by taking the median of the relevant individual mm readings on the screen and translating them with the calibration factor appropriate to the gain setting. In practice this setting is changed when measuring different orders of reflection. It is recommended to use a dB scale when transforming the average echo height on the screen to the corresponding input RF voltage. The setting factors are then replaced by additive constants (preferably 20 dB per step).

4.2.3 Quasi-logarithmic receiver technique works similarly to the linear one just described in Section 4.2.2 except that the complicated gain-setting procedure is avoided. Precise design and calibration are necessary to make the receiver characteristic stable, reliable and independent of signal and interference modulations over a wide range of signal inputs. An important dynamic range compression is needed, for example 60 dB at the input should be compressed so that one has about 2 mm per dB on the screen at the output. Calibration, reading and translating are as described in Section 4.2.2. More details are found in Section 4.3.5 below. A description of an appropriate receiver developed by K. Bibl is found in Section 19 of Rawer and Suchy [1967]. For transistorized equipment see Appendix 4.A.

4.2.4 Constant output technique can be applied to a receiver of any characteristic provided the gain can be adjusted in a reproducible manner and its value is readable. The easiest way is a scaled, adjustable attenuator at the input. Having selected a certain echo, the operator adjusts the gain so that the echo amplitude on the screen hits a fixed mark. Reference to a widely used receiver is given under Section 4.2.2.1 above. Attenuators are normally scaled in dB so that here also dB readings are appropriate.

Standard ionosondes have been adapted to allow manual measurements with this technique provided that transmitter and receiver can be tuned exactly to a fixed frequency and that tuning, transmitted power and receiver gain are reproducible, free of "hysteresis" and reliable. This means normally that automatic volume controls must be disconnected and the detector may need to be d.c. coupled to a cathode ray tube, the sensitivity of which is well stabilized.

4.2.5 Automatic devices use electronic gates to select the desired echo. The gate width should be as small as possible. It must, however, admit the height variations occurring for geophysical reasons (unless automatic setting is used). For echoes from the E region a gate of 85 ... 145 km of virtual height is adequate. If, however, the faint partial reflections from lower altitudes are to be studied, the beginning of the gate should be as low as 65 km. For F echoes a large range (180 ... 280 km at temperate latitude) is needed. Another difficulty with gating of F echoes is the possible occurrence of 2 E or 2 Es echoes which necessarily fall into the F gate. There is no automatic device known which could readily make this distinction. Checking is needed, for example by comparison with the ionogram taken at the hour of measurement.

Devices which integrate over the whole gate width are almost inadmissible because interfering transmissions largely influence the integrated amplitude. Therefore, peak reading devices must be used. A simple but reliable device can be obtained with photoelectric control of the pulse peak on a cathode ray tube. More modern means use peak voltage discriminators followed by an averaging circuit.

4.2.6 Constant output automatic devices use a servo loop which is controlled by the peak amplitude of the gated pulse signal at the output. The loop either controls the gain of the receiver or an attenuator between antenna and receiver. It is important that the actual gain or the ratio of attenuation can be recorded with good accuracy.

4.2.6.1 Gain setting somewhere inside the receiver is not easy to obtain reliably due to the fact that exact calibration is needed and the relevant parameter must be recorded. If the receiver has a linear characteristic, an attenuator at the receiver input could certainly be controlled by a servo motor and gear; its position must be recorded in a suitable manner. A more modern device would be a linear RF amplifier with voltage controlled amplification at the receiver input (see Appendix 4.B). A typical circuit of a voltage-controlled solid state amplifier is shown in Figure 4.3. Maximum amplification could be such that the amplifier normally acts as an attenuator. It is, however, not easy to build a completely reliable system free of unwanted coupling and independent of temperature and frequency.

The latter difficulty can be overcome with a logarithmic receiver: In this device the voltage-controlled amplifier could be at the (video) output side, just before the indicator. The method of averaging raises special problems. If the average value is determined, the actual value obtained depends on the type of receiver used and the depth of fading since the averaging procedure gives different results for direct and for logarithmic averaging. Theoretically the ideal is to measure the mean power; so a logarithmic receiver (see Appendix 4.A) is more accurate than a linear one when fading depth is changing.

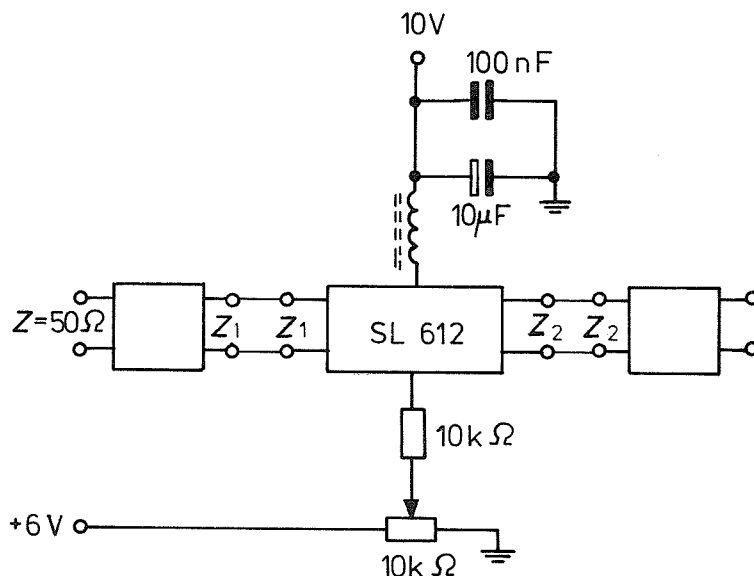


Fig. 4.3 Circuit diagram of voltage-controlled linear amplifier (L. Unger; see Appendix 4.B).

4.2.7 Constant gain automatic devices are not easily operated when using a receiver with a linear characteristic because changing of gain in steps is unavoidable in this case (see Section 4.2.2). With a logarithmic receiver, however, a large compression of range is easily obtained so that all interesting echo amplitudes can be distinguished and be sampled at the output.

4.2.7.1 Meter recording allows some integration (over a few sec) by the time constant of the meter. Follow-up meters using servo techniques allow rather long time constants; they may also be used for digital recording with an analog-digital converter. Any meter record must, however, again be sampled as much longer sampling periods are needed (see Section 3.4.3). This means additional reduction work, even if an approximate mean or median can often be drawn by eye estimation of the recorded curves. The greatest handicap of standard meter recording is its vulnerability to rather weak continuous wave interference -- peak reading meters have only rarely been used.

4.2.7.2 Photographic recording is used at some places. The screen of an amplitude deflection cathode ray tube is photographed with a fixed position frame during the whole sampling period. A fading signal appears on the film as a pulse with a diffuse peak. Its width in amplitude corresponds to the fading range of the signal. For fading distributions with one maximum only the median can easily be estimated in the central part of greatest blackening. With some experience the median can also be reasonably estimated when two maxima are present in the distribution.

The advantage of this recording system is that manual sampling is not needed. It is, however, difficult to apply when sampling periods of several minutes are required. The longer the period the greater is the chance to have a distribution with more than one maximum, or a height change, due to variations of the reflection conditions. In one (multifrequency) application the recording system is applied with two or three split sampling periods of 20 sec each, separated by an interval of 2 ... 3 min [Rawer, 1951].

With a particular electronic complement to an ionosonde A. K. Paul was able to obtain frequency-dependent peak amplitude records on the classical ionogram traces with the usual device for photographic ionogram recording [see Rawer and Suchy, 1967]. A typical record is shown in Figure 4.11, Section 4.9.1.1.

4.2.7.3 Modern recording systems use electronic voltage discriminators which are now available as integrated circuits. As the fading range normally is about ± 6 dB, it is sufficient to place the discriminating voltage levels in 6 dB steps (as measured with the input signal). Thus with 10 discriminators a total range of 54 dB can be covered. If each discriminator has its own register (counter), the whole field strength distribution function can be recorded. The integrated distribution function (see Section 3.3.2) is obtained if all discriminators are working in parallel. By introducing a selecting stage looking for an incremental change between registers the differential distribution function ϕ may also be obtained directly (see Section 3.4). The last procedure may be less reliable than the direct one. By gate switching the chains of discriminators and counters could be used in turn for different echoes as well as for noise (see Appendix 4.C).

4.2.7.3.1 The pulse repetition period of usual sounding equipment is far too short compared with the coherence interval (see Section 3.2.5) or with the quasi-period (see Section 3.1.5) of actual fading. A pulse repetition of one per sec would be more than enough. With higher pulse repetition frequencies redundant information is obtained and some preselection is recommended, for example by a 1 over 10 dividing gate at the input. Otherwise the counters must have more digits than physically significant. Of course the nonsignificant digits can also be cut out at the data reduction.

4.2.7.3.2 Digital recording followed by data processing on a computer is recommended when counting devices are used. These are, of course, binary in first instance. According to the available periphery devices, one out of the following arrangements may be chosen:

- Binary coded recording directly on magnetic tape, or on punched tape with special code;
- Binary coded decimal (BCD) converter with magnetic tape recorder or punched tape recorder with special code;
- Decimal converter with printer;
- Decimal converter with magnetic tape recorder using a suitable code;
- Decimal converter followed by Baud-code converter and punched tape recorder in telex code.

Punched cards could also be used but these are not recommended due to the interruptions of data flow unavoidable with such cards.

NOTE: Modern development moves towards real time data preprocessing so that only highly significant results are digitally recorded.

4.2.7.3.3 Automatic devices producing distribution functions make a large amount of data available. Computer reduction would not only produce median values for the different echoes but also allow fading studies to be made. In particular, empirical distribution functions could be compared with theoretical ones (see Section 3.3), their skewness determined etc. Full statistical reduction of such data is probably more a research than a routine task.

4.2.7.3.4 For routine stations simplified sampling systems may be chosen. One which has been used in conjunction with multifrequency observations is explained in more detail in Appendix 4.C. The idea is that diversity in time may be used to avoid the heavy burden of many counters in parallel. It is important that the coherence interval (Section 3.2.5) be large compared with the pulse repetition period so that sufficient sequential readings can be made without serious changes of the signal amplitude. But even if such changes occur the system by statistical integration would give correct final results. It applies, however, a particular rule for obtaining "average field strength".

With a commutating electronic switch the different discriminators are interchanged. Thus each pulse passing through any discriminator is counted by one and the same counting device. The first digits of the total count obtained after a long enough sampling period are taken as average. With logarithmic level setting, for example in 6 dB steps, one can obtain an average quite close to the median with an accuracy better than 1 dB (see Appendix 4.C).

The procedure must, of course, be applied to a few gate positions in turn (e.g. E echo, F echo and interference level). It is advantageous to have a second commutator and three separate counters to allow these data to be obtained during one and the same sampling interval. Otherwise variations of reflection and absorption conditions could provoke incoherent data. This system with three counters could even be applied in multifrequency systems by using the counters successively on the different frequencies. After having automatically recorded the last counting results, the counters must, of course, be reset to zero with each frequency commutation.

4.2.7.3.5 Digital ionosondes [Bibl, 1971] are adequate for producing large numbers of echo amplitudes in a form suitable for computer handling. In order to apply these to absorption measurements care must be taken that enough samples are obtained on each measuring frequency and the sampling period be of the order of 10 min at least. In order to achieve this, data must be taken from a frequency range of about 0.1 MHz instead of from one fixed frequency value only. The sampling rules as well as gating have to be specified in a computer program. Checking of echo identification will certainly be needed. No program is known as yet which would achieve this automatically. A development for real time data preprocessing is under way.

An example of amplitude data obtained with this technique is given in Figure 4.12 in Section 4.9.1.2.

4.3 Experimental Techniques

4.3.1 Bandwidth considerations As explained in Section 4.2.1 an A1 system contains a pulse transmitter and receiver. Both should not only be tuned to the same frequency but also considered as a one-channel system.

4.3.1.1 This means that the bandwidth of the receiver should be adapted to the spectrum of the RF-pulse transmitted from the sender such that the main part of this spectrum should pass through the receiver with roughly constant amplification. This condition is not so easy to satisfy because with usual sound-ing pulses of about 100 μ sec the main part of the spectrum covers a rather large range (of several times 10 kHz). On the other hand interference is quite important on frequencies usable for A1 systems so that vulnerability to interference increases quickly with increasing bandwidth. A compromise is therefore needed. Its limits are rather narrow. Looking at Figure 4.4 which describes typical conditions we may say that a 3 dB bandwidth of about 20 kHz is needed to reproduce a rectangular pulse of 100 μ sec length in order to get amplitude reproduction accurate to a few percent.

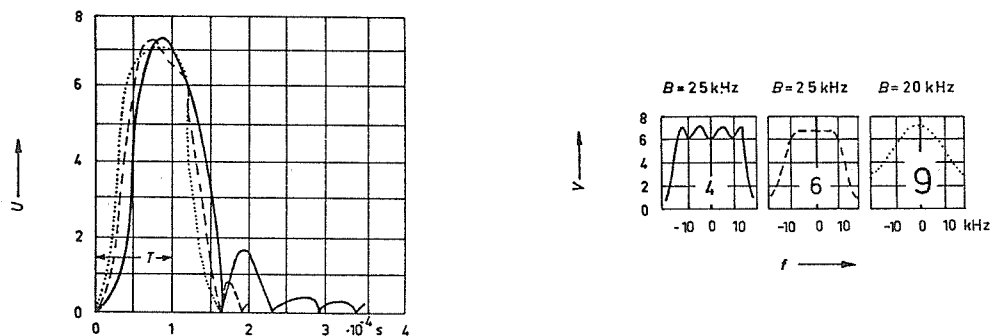


Fig. 4.4 Reproduction of a rectangular pulse by receivers of different bandwidth B and design [Huber and Rawer, 1950]. Band curves in side diagrams. The large digits give the number of standard amplifying elements (tubes or transistors) needed to get equivalent amplification. T is the length of the input pulse.

Where interference is intense and the available transmitter power is limited, the optimum compromise is often to use pulses up to 300 μsec length for which the bandwidth can be less than 10 kHz.

4.3.1.2 The shape of the transmitted pulse has some importance. Truly rectangular pulses produce a very broad spectrum which cannot be reasonably pushed through the receiver without losses. The tails at both ends of the RF spectrum are therefore useless and provoke unwanted interference for other radio systems on neighboring frequencies. Thus a smaller steepness of rise and fall would be welcome. Of the pulse shapes shown in Figure 4.5 a "half-sine" shape would be better from this point of view. On the other hand it is very important for absorption measurements that peak amplitudes of transmitted and received pulse are well defined. Otherwise they can not easily be measured, and it is difficult to take account of the pulse deformation necessarily occurring in the receiver (see Section 4.3.5). The best choice is an almost rectangular pulse shape with some round off.

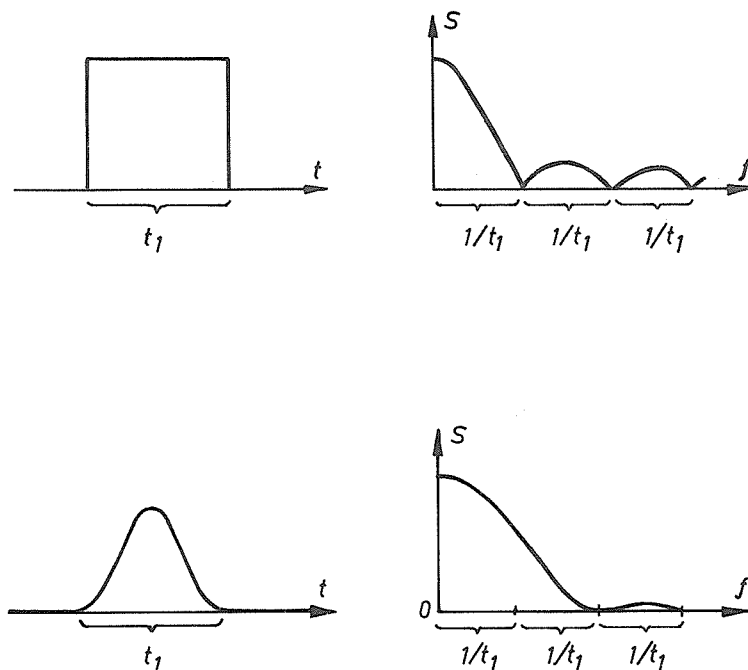


Fig. 4.5 Envelopes of transmitted rectangular and \cos^2 pulses (at left), and relevant Fourier spectrum (amplitudes only, at right).

If a capacitor chain discharge is used for high-power pulse production (see Section 4.2.1.2), such shape can be produced by suitable choice of the elements of the chain. Pulses for A1 measurements should not be too short: 200 μsec is better than 100 in order to guarantee the peak value to be correctly reproduced by the receiver (see Section 4.3.5.3).

4.3.1.3 The design of the receiver is important for the quality of pulse reproduction. Phase distortion may produce strong deformation and delay even if the bandwidth is kept large enough, (see Section 4.3.5.3). One must also be extremely cautious with video amplification (see Section 4.3.5.4).

4.3.2 A few wave form generators are always needed in an A1 system:

4.3.2.1 A basic clock frequency is often convenient to make the pulse sequence reliable. In the past it has often been derived from the a.c. powerline, giving 50 or 60 Hz according to the regional arrangements. Now most stations have independent clocks, often quartz clocks. By frequency division almost any frequency could be produced. Due to the rather long coherence interval of fading, a 1 Hz repetition would by far be quick enough. At this time, however, most A1 stations use a repetition frequency between 25 and 100 Hz.

4.3.2.2 A pulse shaper is needed to produce pulse keying of the transmitter. Grid control is less advantageous than direct anode control of all pulsed stages including the power stage. It is now usually obtained with a particular power supply using the discharge of a capacitor chain as in Figure 4.6. The pulse shape can be computed by admitting a step function at the switch. Until now thyatrons have been used as switches, preferably with hydrogen filling. With advancements in technology semiconductor switching devices can now be used instead. These have longer lifetimes than thyatrons.

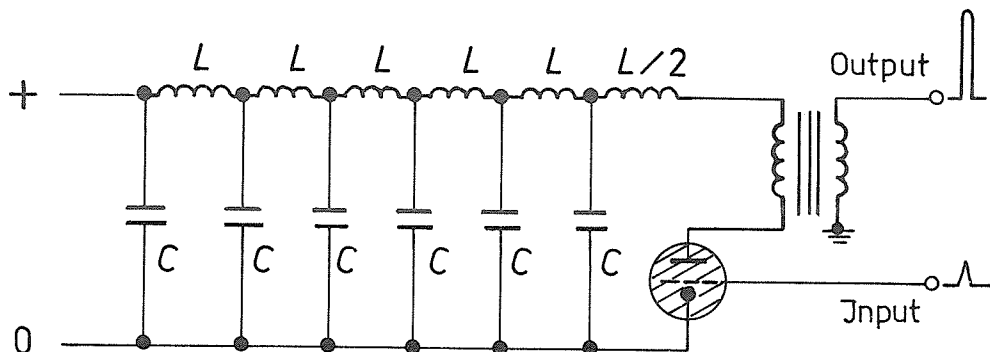


Fig. 4.6 Pulse-producing discharge chain with thyatron and pulse transformer.

4.3.2.3 Electronic gates are essential for almost all automatic devices (see Section 4.2.5). They produce rectangular wave forms of constant length and amplitude derived from the basic clock frequency which controls pulse transmission. It is important that the delay of the opening of a gate be reasonably well fixed against the leading clock pulse. Delay intervals are between 0.5 and 2 msec (see Section 4.2.5). If some caution is applied, resistor - capacitor time constants in monostable multivibrators are good enough to produce these. They have the advantage of being easily adjustable by a potentiometer. This is also true for the duration of the gate pulse which usually lies between 0.5 and 1 msec. More sophisticated devices use height marker pulses to derive gates with very stable position. Electronic gates can now very easily be built up with integrated circuits applying external timing elements.

4.3.2.4 Height markers are needed for accurate height measurement. These are pulse sequences, usually with one of the following frequencies and corresponding virtual height interval:

| | | | | | | | | |
|-----------|---|----|----|----|----|-----|-----|-----|
| frequency | { | 15 | 6 | 3 | 2 | 1.5 | 1 | kHz |
| interval | { | 10 | 25 | 50 | 75 | 100 | 150 | km |

Height markers must, of course, have a stable phase relation with the master clock frequency.

4.3.3 The pulse transmitter needed for A1 measurements may be a tunable or a fixed frequency transmitter.

4.3.3.1 Broadband power stages can easily be built up if suitable radar tubes are at hand. Such tubes must allow for a large cathode current during a pulse duration as long as 100 to 200 μ sec, which is a serious limitation for most modern radar tubes. "Oldtimers" have often been used, for example USA-tube "715". Its follower type 4PR60A (identical with Philips QEP (20/18)) achieves more than 30A plate current with plate voltage up to 5 kV.

In order to match with the antenna feeder line an RF power transformer is needed. Due to the large power which is transferred, the transformer must have a rather large ferrite core. A very practical arrangement with easily available ring cores is shown in Figure 4.7.

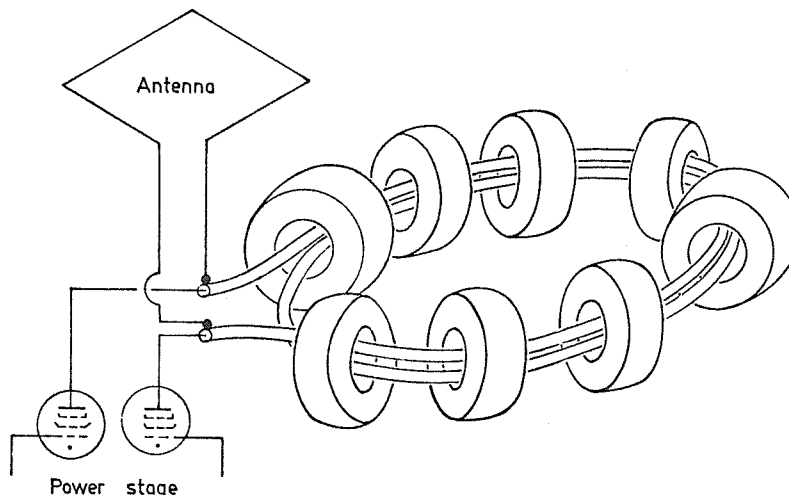


Fig. 4.7 K. Bibl's power transformer using the conductors of a concentric cable as primary and secondary, and an unconventional iron circuit consisting of ferrite cores in parallel.

The output is always symmetric. At the present time it is not yet feasible to replace such tubes with a peak power of about 10 kW by transistors. However, such replacement is recommended as soon as suitable transistors become available.

All other stages can now be built using transistors. Frequency changes can easily be made by replacing just a push-in unit, without retuning, or by operating a switch commutating of such units.

4.3.3.2 Pulse modulation by grid modulation is feasible but no more appropriate. Anode modulation by a high power pulse modulator as described under Section 4.3.2.2 above is recommended. A pulse transformer is needed for matching the transmission line to the impedance of the pulsed stages. It must be large enough in order to transfer the total power to be transmitted. The divided iron core should have a small air slit. Otherwise saturation affects the system. The transformer normally has different voltage outputs according to the stages which must be fed. In case mixed semiconductor and tube techniques are applied it is recommended to cut the pulse amplitudes for the transistor stages by inserting Zener diodes, the voltage of which is adapted to the maximum voltage applicable to the silicon transistors used.

It is important for A1 measurements that the pulse is well shaped and has a flat top. This can be achieved by choosing suitable values of the elements, see caption to Figure 4.6.

4.3.3.3 Power control is more important in A1 systems than in normal ionosondes.

4.3.3.3.1 Small changes in the characteristics can alter the radiated peak power with almost no visible effect upon time-integrating readings. It is recommended to provide meters for different parameters separately, e.g. d.c. voltage of power generator, cathode current of output tubes, radio frequency output current (see Section 4.4.2). The latter measurement may be obtained in a simple way with low voltage lamps, the brightness of which is monitored. (Brightness measurement with an optical pyrometer is quite accurate and can reasonably well be calibrated with d.c.).

4.3.3.3.2 Peak voltmeters are relatively easy to build and give readings which are independent of pulse length, a considerable advantage. Some redundancy is needed, e.g., minor changes in antenna geometry can seriously alter the output current or voltage without changing the actual power radiated.

4.3.3.3.3 A most important control concerns pulse duration. It can, for example be obtained by direct coupling of a piece of wire to a deflecting electrode of a simple cathode ray tube (without preamplifier). Variations of pulse duration necessarily influence all averaging meter readings. As the A1 system depends on instantaneous pulse amplitude and not on average power, such variations would not affect the system itself. Their knowledge is, however, needed to interpret the meter readings. Grid-modulated power stages are rather unstable in this respect; anode-modulated ones are much safer.

One must, however, consider also the possible occurrence of unwanted VHF oscillations which can be very dangerous. They are "killed" by suitable VHF filters directly on the main electrodes of the tubes (50 Ω resistors short-circuited by about six windings of copper wire on the same axis).

4.3.3.4 Control readings should be made rather often in order to ensure stable peak power of the transmitter. It is evident that for an A1 transmitter and receiver the a.c. power line voltage should be regulated by a suitable system. Electronic devices are preferable to magnetic ones because these latter have a tendency to provoke variations of the regulated voltage when the line frequency or the content of harmonics are variable.

4.3.4 Antennas are needed at the transmitting as well as on the receiving side of the A1 system. It is not recommended to use the same antenna in both directions, though devices are known with which this is feasible.

In general the transmitting antenna would be designed to give the maximum radiated power to the ionosphere, the receiving antenna to give maximum signal-to-noise ratio. If the sensitivity is limited by noise picked up by the ground system, there is no advantage in increasing the antenna pick up factor; in fact this may cause cross modulation and hence lower signal-to-noise ratio in the receiver.

Fields due to atmospherics or to man-made noise tend to be vertically polarized and arrive at low angles of elevation so that balanced horizontal antennas are advantageous for reception. Preferentially, they are perpendicular to the transmitting antennas.

4.3.4.1 The radiation diagram of the antennas should have maximum radiation to the zenith. Different types of antennas with such diagram are known; all of them have symmetric feeding.

4.3.4.1.1 Rhombic and delta antennas, if correctly built, should have almost constant input impedance in the whole frequency range. However, as ground properties are frequency dependent and correct matching is not easy to obtain, non-negligible variations of the input characteristics cannot be excluded a priori. For a given mast height and horizontal span, a delta is more efficient than a rhombic at the lower frequencies, and vice-versa as the frequency increases.

4.3.4.1.2 Horizontal dipole antennas are narrow-band tuned systems. The input impedance is real and minimum on the resonance frequency; it becomes complex and of much greater absolute value on frequencies away from the resonance. Folded dipoles cover a somewhat larger band than simple ones. Dipole systems with thick cylindrical arms (obtained with, say ten or twelve wires on a circle of about 1 m diameter) are recommended because they have much lower characteristic impedance than a single wire system. Consequently variations of impedance with frequency are much smaller for such thick dipoles (French name: "antenna trombone").

The terminated folded dipole combines the wide-band response of other terminated antennas with the advantages of horizontal dipoles. It is obtained by terminating a folded dipole at its center with a resistor of about 100 Ω . The input and output impedance is approximately equal to that of the terminating resistor. For receiving it is convenient to use a center-tapped balanced transformer, primary 100 Ω with secondary to match the preferred feeder. The center tap should be grounded to minimize rain or snow static.

4.3.4.1.3 The height above ground of the antennas is a parameter that has great importance for their radiation diagram. It should not be much less than 1/10 wavelength, since otherwise the radiation resistance becomes very small. At frequencies where the height is equal to half wavelength, interference between the direct and ground-reflected wave will cause a minimum in the upward radiation. In practice minimum gain and the frequency where it occurs depend largely on the effective ground level and on ground conductivity. Changes of the water level in the soil can be quite important and, on a given frequency, sometimes produce seasonal variations of upward radiated power.

The better the ground conductivity is, the greater the effect of such ground influences on particular frequencies. For a fixed frequency with horizontal antenna it is recommended to make the height above ground about 1/8 wavelength (instead of 1/4, the optimum for ideal ground).

4.3.4.2 Polarization of most antennas is linear at vertical direction.

4.3.4.2.1 Near the magnetic (dip) equator the characteristic polarizations of a vertically propagating wave are also linear (N-S and E-W, magnetically). At all other latitudes, however, the characteristic polarizations at the lower side of the ionosphere are elliptical; at temperate and high latitudes they are almost circular. It is therefore possible to select one of the magneto-electronic components by applying circular polarization at the transmitting or receiving antenna. According to the sign of rotation the ordinary or extraordinary component is selected, the ordinary component being the "ionic" polarization. Its sense of rotation is the same as that of the free motion of a positive charge around the vertical component of the local magnetic field of the Earth. This is independent from the wave propagation direction so that the expressions "left- or right-handed" are misleading.

4.3.4.2.2 To obtain circular polarization from linear antennas, one uses a pair of perpendicular antennas at 90° phase shift. Small-band resonant 90° phase-shifting circuits were formerly used, but are rather sensitive to detuning. +45° and -45° phase-shifting networks are known which easily cover a large band; 1:3 with 30 dB rejection can be achieved. An example is shown in Figure 4.8. Details of computational procedure including matching can be found for example in H. J. Orchard [1950].

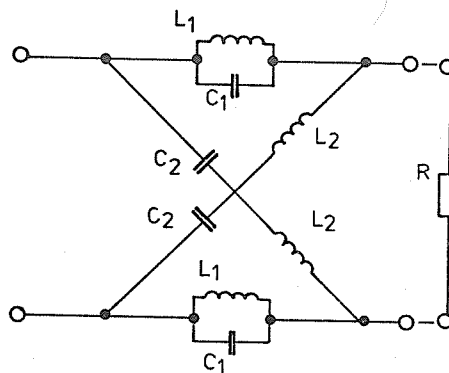


Fig. 4.8 Network for phase shifting by +45° and -45° in a broad frequency range [Orchard, 1950].

4.3.4.3 A few technical details may be worth mentioning.

4.3.4.3.1 Mechanical stability, in particular of connections, is essential and avoids fluctuations of the radiated power due to bad contacts with feeder lines, antenna wires and the ground system. Steps should be taken so that fouling with other metal structures cannot occur.

4.3.4.3.2 D.c. grounding of all antennas is recommended both for safety reasons and to minimize rain or snow static. For symmetrical antennas without a convenient symmetrical connection, two symmetrically connected high power resistors can be used, e.g. for deltas or rhombics about 1000 Ohm, 25 Watt. Where thunderstorms are expected, a spark gap to a directly grounded conductor is a useful additional safety device. Two or three couples of sharp tips with an 8 mm interval between each couple are often used to this end.

4.3.4.3.3 In non-resonant antennas the terminating resistance should be non-inductive and not sensitive against overloading during atmospheric discharges. Volume resistor types are better than surface resistors.

4.3.4.3.4 Strong coupling between the transmitting and receiving antenna may cause overloading of the receiver shortly after the sender pulse. The receiver can often be modified so as to minimize this difficulty, e.g. by the use of diode clamps. Coupling is minimized when applying linear antennas in crossed position. It is, however, unavoidable when crossed antenna arrangements are used to produce circular polarization. In this case, a distance of more than one wavelength is recommended between transmitting and receiving antenna. Metallic structures in the immediate neighborhood may considerably influence the state of polarization and the radiation diagram, and should therefore be avoided whenever possible.

4.3.5 Pulse receivers

4.3.5.1 Quite generally it is the task of a pulse receiver to amplify pulsed RF signals picked up by the receiving antenna, detect them and transfer the detected signals to the recorder. It is an evident requirement that the pulse shape at the output should be reasonably similar to the envelope of the RF pulse at the input. Due to bandwidth limitations there is always some smoothing of shape.

Receivers usable for A1 measurements should further correctly reproduce the amplitudes of the incoming echo pulses, independent from the average signal level. This particular condition excludes the use of automatic volume control in the manner it is used in commercial and broadcasting receivers. Quite generally, circuits with time constants between pulse duration and pulse recurrence period must be avoided.

4.3.5.2 Almost correct reproduction of the amplitudes of Fourier components in the received band is certainly a necessary condition. However, correct pulse reproduction can only be obtained if phase distortion is also kept small. The phase must be a slowly variable, almost linear, function of frequency inside the band. In a heterodyne receiver the critical elements limiting the band are the intermediate frequency (IF) bandpass filters. In telecommunication receivers one usually has combinations of over-coupled (or slightly detuned) high quality circuits; the corresponding phase curve is far from being linear. Therefore circuits with critical or under-critical coupling (and without detuning) should be used in the IF stages of pulse receivers. In order to achieve the wanted bandwidth (see Section 4.3.5.3) they must be artificially damped (by parallel resistors). Therefore, with given amplifying elements the amplification is considerably smaller than in a telecommunication receiver so that a pulse receiver needs more amplifying elements [Huber and Rawer, 1950].

4.3.5.3 The bandwidth of a pulse receiver depends on the shape of the pulse which is to be reproduced (see Section 4.3.2.4). Of course, there are limits. Very large bandwidth means strong interference and heavy noise. Necessarily, a pulse receiver is a compromise [Huber and Rawer, 1950] between reproduction quality and sensitivity.

4.3.5.4 The video stages of a pulse receiver for A1 measurements must amplify the whole low frequency band including d.c. (direct current). Otherwise the reproduction of pulse amplitudes would be depending upon CW (continuous wave) background. With tubes d.c. amplification is rather troublesome, so it is recommended to use not more than one video stage after detection. The situation is different with modern "integrated circuit" semiconductor amplifiers. These contain up to three transistors in cascade which can be operated safely because inside coupling is carefully compensated, provided unwanted outside coupling is avoided. Good temperature compensation is important in this context.

4.3.5.5 Stability is a very important feature of an A1 receiver, the output voltage of which should be a unique function of the RF voltage at the input. Overloading by unwanted signals (telecommunication or broadcasting) or by the direct pulse is avoided by holding the time constants either small enough or large enough.

4.3.5.5.1 Feeding voltages, in particular screen voltages in a tube receiver, must be kept very constant with a time constant of a few seconds. Grid bias is not recommended; automatic (positive) cathode bias is preferable. It is, however, very difficult to produce a long enough time constant to make the amplification independent of background signals. It is easier to have no capacitor at all at the cathode and so make the time constant smaller than pulse duration. Cathode bias is produced by a simple resistor. Such stages have negative feedback which is welcome in logarithmic receivers because it just makes the sensitivity decrease for large RF input.

4.3.5.5.2 Similar considerations can be made for transistor receivers: automatic emitter bias (without shunt capacitor), voltage stabilization with Zener diodes and temperature compensation. The latter can be obtained quite accurately with well-adapted NTC resistors. See Appendix 4.A for an example of a transistor receiver.

4.3.5.5.3 Integrated linear circuits are now used more and more in the RF and IF stages of a receiver to cover all amplification and detection functions with one or two monolithic elements. Instead of

the classical device with several IF filters separated by transistors, no more than one IF filter can be used in this modern technique. This filter must be a combination of several resonant circuits, weakly coupled and adequately damped. It is not very easy to avoid unwanted effects with such design, so that at present time several IF stages with individual filters may be built up with often better stability (see Appendix 4.A). With future improvements, however, this technique will also almost certainly become practicable. Of course, temperature compensation is particularly important in this context.

4.3.5.6 The desired sensitivity curve of a receiver must be achieved in a reproducible and stable way. In the input stages the amplification is usually almost linear as RF voltages are small. In the IF stages, however, this is no longer true. One achieves either linear amplification throughout (techniques described in Section 4.2.2 above) or quasi-logarithmic (Sections 4.2.3 and 4.2.7).

The big difficulty with a linear receiver is to hold all potentials constant over a long time. For a quasi-logarithmic receiver compression of amplitudes can be achieved with some care by cathode or emitter negative feedback (avoiding shunt capacitors). Automatic volume control in the usual way must be excluded.

With integrated linear circuits much care is needed to obtain suitable negative feedback. Anyway, for very small inputs the sensitivity curve is always almost linear.

4.3.6 Indicator and Recording Devices

4.3.6.1 Formerly, amplitudes were directly indicated by deflection on the screen of a cathode ray tube and were read optically. Automatic photographic recording (see Section 4.2.7.2) is an equivalent technique.

4.3.6.2 While this technique is yet widely used, it will be replaced more and more in the future by automatic amplitude discriminating and counting devices (see Section 4.2.7.3). These can now most easily be built with integrated digital circuits (see Appendix 4.C for an example). Care is recommended when calibrating discriminators. The use of Zener diodes to produce reference voltages is also recommended. The final recorder for counting devices is a digital one: punched paper or magnetic tape are preferable to punched cards. Printing devices are only recommended when manual reduction is intended. Wherever computers are used, digital output data carrier should be compatible with the computer.

4.3.6.3 Pen recorders are sometimes used after gating, either with recording of current or with a potentiometer servo-system. Pen recorders of the latter ("followup") type can quite easily be adjusted to almost any desired scale using preset taps. While this is a great advantage and simplified receiver design, it is not very easy to have automatic readout of pen records. Siemens has a photoelectric system with digitalization in 100 steps. Not the margin but the center of the recorded trace is digitized. This is particularly important for broad traces as produced by quick fading.

4.4 Maintenance and Checking

4.4.1 The accuracy of absorption measurements depends critically on the stability of the equipment. It is easier and safer to keep equipment constant than to estimate the magnitude of any changes which may have occurred. Though the significance of readings is rather limited (several dB for individual readings, about 1 dB for the median of a good sample of such readings), changes of sensitivity are dangerous in the long run. Long term changes of geophysical nature can be detected provided the long term stability of the equipment is maintained. Another even more serious danger is provoked by diurnal variations of the power line voltage which could influence the calibration constant (see Section 4.6), and so make the observed diurnal variation wrong.

While it is not difficult to check the receiver sensitivity with a good signal generator, it is not so easy to ensure that antenna and transmitter characteristics remain constant. Good maintenance needs regular and careful checking. To some extent procedures should depend on the particular conditions of equipment and station. The station chief has to think about harmful effects which may be dangerous at his station, even if not mentioned in this text. In the following we indicate some rules which have proved to be adequate at many stations.

4.4.2 Single indices of transmitter behavior are seldom sufficient to ensure a constant power output, since small changes in the characteristics of the radiating system can alter the readings of radio frequency voltage and current without significantly changing the radiated power. On the other side an increase of pulse width would provoke a proportional increase of all average current readings without increasing the peak amplitude of the radiated pulse which is of main importance (see Section 4.3.3.3).

It is desirable to measure a number of different parameters in order to be certain that peak output power remains constant. Depending on the type of transmitter used, the following controls may be particularly useful:

- (i) Pulse width;
- (ii) average RF output (usually current);
- (iii) average cathode current of output tubes;
- (iv) anode voltage of output tubes (direct for d.c. feeding, peak amplitude for pulse feeding);
- (v) peak RF amplitude at grid of output tubes.

4.4.3 The amplification of the receiver is the most important member in the whole chain. It should be kept as constant as possible over years of operation. Any changes must be accurately determined and check notes maintained in the files. These should contain all information which a successor to the present time operator may need for future reevaluations.

4.4.3.1 The normal procedure is to connect a high quality standard signal generator to the input of the receiver and measure the overall sensitivity at all frequencies at which regular observations are to be made. A middle class signal generator is good enough provided its dynamic range is large enough (60 dB at least). It should allow the input voltage of the divider to be adjusted after the indication of an accurately reading RF meter (contained in the generator itself). The generator needs a well stabilized power supply, otherwise the fluctuations due to variations of the signal generator could be larger than the true changes of receiver sensitivity. Such cases have occurred. By successive repetition of the receiver calibration procedure it can be found out whether this generator is stable enough. At such calibrations, repetitions with different positions of the continuous attenuator should be made, preferably by operating the decimal (20 dB) switch first in one, then in another position of the small scale attenuator. In this matter one minimizes inaccurate scaling of this latter which occurs rather often with inexpensive standard signal generators. Accurate values should be obtained at least for every 2:1 amplitude change (i.e. 6 dB) at the input. Values for smaller changes may be deduced from the receiver response curve, i.e. a plot of output voltage (linear) against input (in dB).

4.4.3.2 A quick check of the stability of calibration is most easily obtained by operating the decimal ratio commutator switch of the signal generator which tends to be more reliable than the continuous 20 dB attenuator. This at least should be made weekly, preferably on a fixed day. In case a change appears against the last calibration it is recommended to control stage gains and crucial voltages or currents at various points inside the receiver in order to know where to repair. Recalibration is needed after any change of the receiver, e.g., replacement of a transistor or tube, retuning of the receiver circuits, etc.

The frequency of the generator after a reasonable heating period must be constant enough to stay well inside a few kHz (1/3 bandwidth of the receiver) during one minute at least. Otherwise tuning errors would occur.

Tuning could be avoided by using a standard noise source instead of the signal generator. It is, however, not usual for such sources to cover the large dynamic range needed for the receiver.

4.4.3.3 If a multifrequency technique is used, it may be advantageous to determine the amplification curve of the receiver on the intermediate frequency (IF) only. This can be achieved by coupling an IF signal to the RF input of the mixing stage in a suitable way, for example with a small coupling capacitor. When doing this, one assumes the preamplifier and mixing stages to be linear which is usually true for echo signals (not for the direct signal of course). Absolute RF input voltages are not obtainable with this particular technique. These are, however, not needed when nighttime echo amplitudes are used for calibration, as is now the general use (see Section 4.6). In any case the relation between transmitted power and echo amplitude must be obtained by one of the allowed calibration methods (see Section 4.6) and, for this purpose, signal amplitude at the IF input is as good as RF amplitude at the receiver input.

4.4.3.4 Input and output devices need some checking too. If attenuators are used in the receiving set, these must be checked from time to time, though they tend to be more reliable than the receiver itself. Also, output devices like cathode ray tubes, voltage discriminators, etc. need checking at reasonable intervals. Notes should be kept of all such calibrations and checks. Voltage discriminators in automatic (digital) devices must be recalibrated once per month and readjusted if a change has been found. The importance of the change should be noted to allow for correction of past data.

4.4.3.5 Maintenance of the receiver means also that the supply voltage must be satisfactorily stabilized. Electronically stabilized power supplies are recommended. In receivers using tubes the heating voltage also needs to be kept constant. Transistorized receivers with Zener diodes as stabilizing elements do not need stabilization of the power line voltage if the latter does not change by more than $\pm 15\%$.

4.4.3.6 Temperature changes could provoke serious effects in the receiver. Circuits and filters containing divided iron cores are equally sensitive, as are most transistors. Temperature compensation is the better way to avoid changes of sensitivity due to temperature variations.

A first step is made by avoiding critical conditions in the transistors: the working point should be determined in a way that temperature changes do not alter the collector current. A second step is compensation of the measured temperature drift of sensitivity by shifting one (or two) transistor working point with temperature sensitive resistors which are now available with any desired characteristic.

If temperature compensation has not been achieved, transistor receivers should be kept at constant temperature, e.g., in a thermal state regulated to something like $\pm 3^\circ$ centigrade.

4.4.4 Antennas and ground system are of some importance.

4.4.4.1 This is particularly true on the transmitter side. Resonant antennas like half-wave dipoles (see Section 4.3.4.1.2) should be correctly matched to the feeder. Detuning tends to occur at the (rare) occasions when the antenna is covered with ice. Thick antennas have broader resonance and are therefore preferable. Another convenient solution is non-resonant antennas like rhombic or delta antennas (see Section 4.3.4.1.1). It is, however, important that terminating resistors are non-inductive. They should be checked once a month with a d.c. ohmmeter. Metal structures in the neighborhood of the antennas may have considerable effects upon the radiation diagram; thus any alteration in a field of antennas may produce changes of radiation though the antenna itself remains unchanged.

4.4.4.2 The ground system is less important if the transmitting antenna has symmetric feed. At any rate a reliable and stable connection with ground should be achieved (see Section 4.3.4.3).

4.4.4.3 Similar considerations are valid for the receiving antenna which, however, must not necessarily be matched to the receiver input if it has reasonable length. It should, of course, be kept constant. This is much easier if capacitive coupling with metallic structures, wires and walls is minimized. Different forms of receiving antennas are conceivable including modern "active antennas", i.e., metal structures small with respect to the wavelength, which are part of a tuned transistorized preamplifier normally inside the structure. A loop antenna could also be used as a tuned receiving antenna. (These devices are not suitable for multifrequency techniques.) Because of their sensitivity to temperature changes, ferrite antennas are not recommended except when temperature compensation is achieved.

4.4.5 The alternating current (a.c.) power supply must be checked or, better, its voltage recorded if constant a.c. voltage is not guaranteed. If stabilization is not applied, it should be remembered that transmitted power varies at the least with the square of the power line voltage.

Best solution is an a.c. voltage stabilizer. There exist now rather inexpensive electronic devices which regulate a.c. to a few percent. At some stations the variations of the power line voltage are probably so important that they fall outside of the admitted input range of the stabilizer at certain times. In these cases one puts a step-transformer which allows hand regulation in front of the stabilizer; it must, of course be adjusted by hand. Under such conditions the power line voltage and the stabilized voltage should be noted or recorded with every measurement.

4.4.6 A maintenance plan should be established at each station. It should specify days when certain checks must be made. For example:

- (i) Transmitter working parameters (Section 4.4.2): weekly;
- (ii) Receiver sensitivity (response curve, Section 4.4.3.2): weekly;
- (iii) Voltage stabilizer: twice a week;
- (iv) Output and recording devices: monthly;
- (v) Terminating resistors of non-resonant antennas: monthly;
- (vi) Attenuators, inspection of antennas and ground system: every second month.

4.5 Procedures in the Reduction of Measurements

4.5.1 It is the primary aim of AI measurements to determine for a well-determined reflection mode the absorption loss, A . Thus correct identification of the mode is needed. This means that the path of the considered pulse must be identified. Standard procedures are based upon 1E (or 1Es) and 1F echoes only. For special investigations second order echoes are sometimes useful, higher orders only very rarely. Combined modes like (Es+F) or M (=2F-Es) occur rather often when more or less transparent Es is present. They should always be disregarded.

In view of the standard echoes, distinction between 1E and Es is important. This may be rather difficult, sometimes impossible, by inspection of the pulse amplitude display only. Inspection of the ionogram taken at about the same time is most helpful in these cases. When a cusp type Es (type "c") is present, echoes on a frequency lower than the cusp frequency are 1E, those on a frequency above that limit are identified as 1Es. As to the first order F-echo the danger is that it may be confused with 2E or, more often 2Es. Here again inspection of the ionogram allows critical cases to be interpreted correctly.

Echoes from Es are often due to partial reflection, i.e., part of the wave energy is reflected, part is penetrating and may be reflected from an upper layer (see Section 1.5). These conditions are not suitable for determination of absorption and must be cancelled (see Section 4.5). Finally by double refraction (see Section 2.2.3) there appear two magneto-electronic modes, o and x (z echoes are not used for absorption measurements). In the majority of observations the reduction is adapted to one mode only, namely o, which in the average suffers less from absorption than x except for cases of strong deviative absorption. Therefore it is justified to suppose the contribution of the o mode to be predominant if two conditions are satisfied: 1) both modes stem from almost the same equivalent reflection height so that the echo pulse shows no splitting, and 2) absorption is not negligible. When absorption is very small, both modes arrive with almost equal field strength and the observed amplitude is on the average 3 dB greater than the amplitude of the o mode alone.

If splitting of both components occurs, identification is easy provided no F1 layer is present: the lower one of the split echoes is the extraordinary (x); the upper one is the ordinary (o) and should be used in standard reduction. When, however, F1 is present, inversion of equivalent heights may occur in a small frequency interval of about 1 MHz around the critical frequency $f_{x\text{F1}}$. As the diurnal variation of $f_{x\text{F1}}$ tends to be known inspection of the ionogram is not really needed though it might be quite helpful in complicated cases.

4.5.2 The basic equations of method A1 describe the field strength of a wave reflected at vertical incidence from an ionospheric layer (see Section 1.3.3). The expression for the field strength takes account of spatial decrease (see Section 1.2), loss at ground reflection (see Section 1.3.1) and loss due to ionospheric absorption (see Section 2.1). According to Equation (1.1) the spatial influence is simply given by an inverse distance law (see, however, Sections 1.3.4 and 4.5.2.2); account is taken of refraction in the layer by using equivalent height, h' , instead of true reflection height. Ground and ionospheric losses may be described by apparent reflection coefficients ρ_g and ρ_i . These parameters are given by the ratio of the amplitude of the reflected wave in the presence of the attenuating medium (ground or ionosphere) to that which would be obtained with specular reflection.

4.5.2.1 Using simple ray theory and neglecting the curvature of the ionosphere (see Sections 1.3.4 and 4.5.2.2) one obtains for the field E_r of the r -th multiple reflection:

$$r \cdot h' \cdot E_r = \rho_i^r \cdot \rho_g^{r-1} \cdot E_0 \cdot d_0 \quad (4.1)$$

where $E_0 d_0$ is the cymomotoric force at vertical direction; this can also be expressed by saying that E_0 is the field strength at a convenient reference height, d_0 , above the transmitter (usually $d_0 = 1$ km). Using Equation (2.10) the ionosphere reflection coefficient ρ_i is obtained from

$$-\ln |\rho_i| = \int \kappa \, dh \quad (4.2)$$

Equation (4.1) is normally used in logarithmic form, using dB units:

$$F_r \equiv 20 \log_{10} \left(E_r / \frac{\mu V}{m} \right) = F_0 - 20 \log_{10} \frac{r h'}{d_0} - (r-1) A_g - r A_i \quad (4.3)$$

where

$$F_0 \equiv 20 \log_{10} \left(E_0 / \frac{\mu V}{m} \right) \quad (4.4)$$

identifies the reference field at height h_0 ($=1$ km);

$$A_g = -20 \log_{10} \rho_g \quad (4.5)$$

is the ground reflection loss expressed in dB. A_g is positive since $\rho_g < 1$.

Using Equation (4.2), we find

$$A_i = -20 \log_{10} \rho_i = -8.686 \int \kappa \, dh \quad (4.6)$$

as the ionospheric loss suffered by the wave during one reflection. For a first order echo, Equation (4.3) reads simply:

$$F_1 = F_0 - 20 \log_{10} (h'/d_0) - A_i \quad (4.3a)$$

Equations (4.1) and (4.3) neglect several influences which might be of importance in certain cases. These are:

4.5.2.2 Curvature of the reflecting surface. As shown in Section 1.3.4 this may lead to variations up to 10 dB if ripples are present. Such effects must experimentally be eliminated by suitably long sampling time. It is, however, difficult to obtain satisfying results from higher order echoes because ripples with wavelength of the order

of 1000 km are almost always present. These are not so dangerous at the observation of the first order echo ($n=1$). In bad cases even a first order measurement may be seriously influenced by focusing or defocusing.

Effects of the large scale curvature of the ionosphere would almost be negligible but the real reflecting surface is quite often severely disturbed by gravity waves. If the real radius of the curvature is, say 1000 km (instead of 6600), and the virtual height 250 km, a 4F echo would be strongly focused at ground, and its field strength higher than that of lower orders. This sometimes even happens with 2F and 1F echoes. The absorption loss determined by comparing both echoes is then found to be apparently negative. In fact, nighttime observations with higher order echoes have been used to determine the instantaneous curvature of the real ionosphere [Rawer *et al.*, 1952b]. It has been found for the F region that positive and negative curvatures occur, a median radius being about 700 km.

4.5.2.3 Wave polarization at the receiving antenna is due to superposition of the two magneto-electronic components which have almost circular polarization when leaving the ionosphere (except for the magnetic dip equator). More or less irregular changes of polarization produce fading at the antenna terminal, i.e., the receiver input (see Section 3.0.2); these are rather easily eliminated by suitable sampling procedures.

4.5.2.4 Specific magnetic field influences upon propagation have the effect that the ray path is slightly different from the wave normal as a consequence of anisotropy due to the magnetic field. These effects are normally negligible.

4.5.3 The reference field E_0 (or F_0 in dB units) can be computed if radiated power and antenna diagram are known; otherwise it must be determined by measurement.

4.5.3.1 Let P be the effective power radiated upwards by the transmitting system (in units of Watt), then the reference field is:

$$F_0 = (K + 10 \log_{10} P/W) \text{ dB}/\frac{\mu\text{V}}{\text{m}} . \quad (4.7)$$

The value of K depends upon the kind of antenna used, its height above ground and ground properties. Table 4.1 is valid for a reference distance of 1 km; it takes account of the fact that with a linearly polarized transmitting antenna only half of the radiated energy enters one of the magneto-electronic modes. More precisely, when arriving in the ionosphere a linearly polarized wave splits up into two components, o and x , which are almost circularly polarized. Thus when a transmitting antenna with circular polarization is used, 3 dB must be added to K values read from Table 4.1.

Table 4.1

K Values For Use in Equation (4.7)

In units of dB above 1 $\mu\text{V}/\text{m}$ produced by 1 W radiated power at 1 km above the antenna

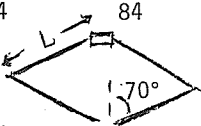
| Antenna | $\lambda/2$ Dipole (or folded dipole) | | | | Typical Vertical Rhombic | | | | |
|--|--|-------|---------|-----|--|-------|---------|-----|---------------|
| Height above ground | Ground Quality (Ground conditions may vary with season by one class) | | | | | | | | Side Length |
| | Soft water | Humid | Average | Dry | Soft water | Humid | Average | Dry | |
| $\lambda/4$ | 82 | 81 | 80 | 79 | 85 | 84 | 84 | 83 | λ |
| $\lambda/8$ | 79 | 78 | 78 | 77 | 84 | 84 | 84 | 84 | $3/4 \lambda$ |
| $\lambda/16$ | 74 | 74 | 74 | 75 | 85 | 84 | 84 | 83 | $1/2 \lambda$ |
| For a short horizontal dipole, K values are smaller by about 1 dB. | | | | | Valid for  Variation of angle produces changes to ± 2 dB. | | | | |

Table 4.1 may be used to obtain an estimate. Usually it is not quite so easy to determine the total radiated power P because one ignores the precise efficiency conditions of real antennas and ground. This at least is the usual situation.

Two solutions have been proposed to determine the reference value from observed reflected signals only.

4.5.3.2 Comparison of first and second order echoes apparently allows us to determine both absorption loss and reference value provided the distance attenuation term is simply $1/D$. In logarithmic terms Equation (4.3) reads for the first and second order echo

$$F_1 = F_0 - 20 \log_{10} (h'/d_0) - A_i$$

$$F_2 = F_0 - 20 \log_{10} (2h'/d_0) - 2A_i - A_g$$

from which follows

$$A_i + A_g = F_1 - F_2 - 6 \quad (4.8)$$

and

$$F_0 + A_g = 2F_1 - F_2 + 20 \log_{10} (h'/d_0) - 6 \quad (4.9)$$

F_1 , F_2 can be measured with the methods explained in Section 4.2. The equivalent height, h' , is easily obtained as the pulse reflection height. A_g must be estimated. It may be neglected in the case of good grounding.

Considering Equations (4.8) and (4.9) this procedure seems to be satisfactory. If one plots the logarithmic field values F_1 against F_2 from Equation (4.9) one expects to obtain a straight line with slope 2. Experience, however, has shown that this is not so with observed data [Piggott, 1960; see Figure 4.9; Pillet, 1960, 1962]. The difference is due to the fact that the distance dependence does not simply go with $\log h'$ but admits focusing and defocusing effects (see Section 4.5.2.2 above). Curvature effects tend to be worse for the F- than for the E-region echoes.

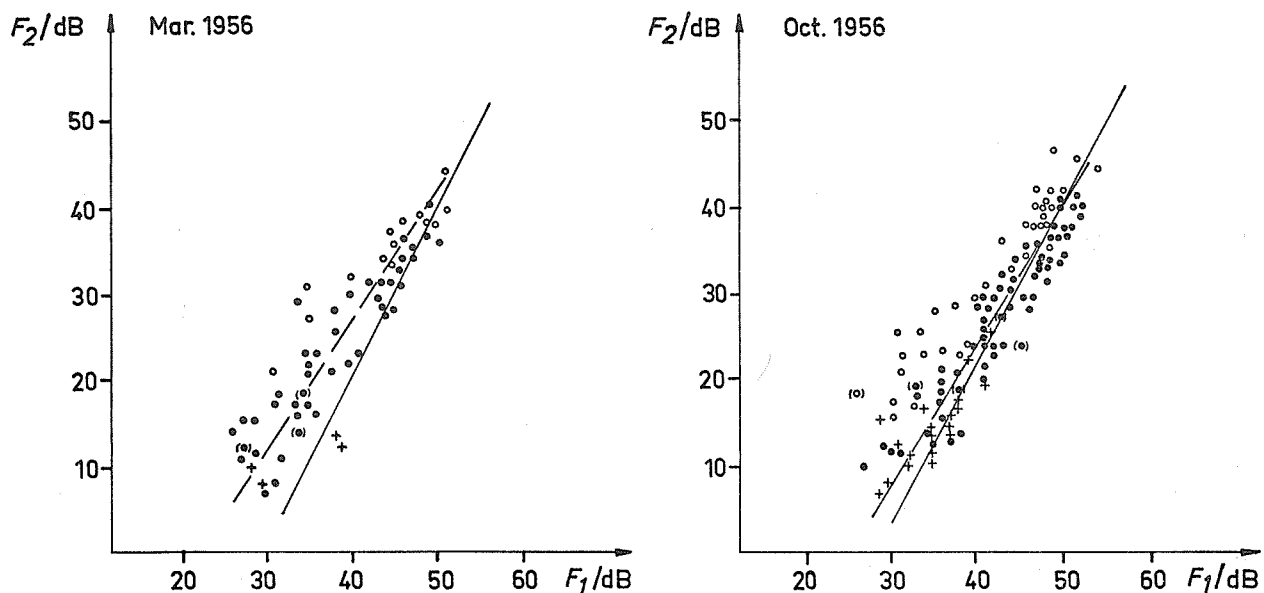


Fig. 4.9 Comparison of first order (abscissa) and second order (ordinate) echo amplitudes on 3 and 4 MHz. Dots and circles: E-region echoes (circles: presence of focusing); crosses: echoes from blanketing Es; parentheses: transparent Es present [Pillet, 1960]. Broken line with median slope, full line with theoretical slope of 2.

Of course the computations of the reference value from first and second order echoes must break down if focusing is appreciable. Therefore, the first and the second order comparison method is not recommended. It should no longer be used for standard absorption measurements.

4.5.3.3 Comparison with unabsorbed conditions is a better method.

4.5.3.3.1 At temperate and low latitudes during late night hours (preferentially after midnight) attenuation due to absorption is supposed to be quite small at frequencies above about 1.5 MHz. In that case the field strength of the first order echo, which is most often 1F but sometimes 1Es, can be used to compute the reference value provided spatial attenuation is known. Now, for a first order echo focusing is almost always small so that the $1/h'$ law can be used for the field E_1 . This is the hypothesis used when deriving Equation (4.3a).

From:

$$F_N = F_0 - 20 \log_{10} h'_N/d_0$$

follows:

$$F_0 = F_{1N} + 20 \log_{10} h'_N/d_0 \quad (4.10)$$

Where the subscript N means unabsorbed nighttime conditions.

This method for determining the reference value is recommended by URSI since 1958.

4.5.3.3.2 The reflecting properties of ground have no influence at all since only the first order echoes are considered. They could only interfere if the radiation efficiency of the antenna depends sensibly on ground conditions in the immediate neighborhood of the station. If so, a seasonal effect might appear.

4.5.3.3.3 Nighttime ionospheric absorption has been taken out of Equation (4.10). It is, however, evident that it has been supposed to be invariable and very small. If this hypothesis is fulfilled, variations of F_0 must be attributed to changes of the technical conditions. Unfortunately, there is some evidence that the hypothesis is not accurate, at least not to a few dB (see Section 4.6.3.5).

4.5.4 The equivalent height, h' , appears in Equations (4.1) and (4.3). It is determined in the usual way from the echo delay time. It should be remembered that absolute errors of the order of 5 km could easily occur by receiver delay time. It is therefore recommended to apply the calibration method explained in Section 4.6.4 which allows the zero of the height scale to be determined rather accurately. It is recommended that height measurements always be made with about the same echo amplitude; if feasible this amplitude should be adjusted to a standard level when measuring the virtual height.

4.5.4.1 The accuracy needed for this determination is, however, rather poor because $\log h'$ is in the equations. As the statistical significance of an individual determination of absorption is rather limited and of the order of ± 1 dB, it is just not worthwhile to require for routine measurements better accuracy than between 5 and 10% for h' readings. Table 4.2 gives a sequence of height values with 1 dB scale: This table shows that for echoes from the E region (and $d_0 = 1$ km) 47 dB is almost always correct within ± 1 dB, while for echoes from the F region the variations of h' must often be taken into account.

Table 4.2

Distance term $\Delta(h') \equiv 20 \log_{10} h'/d_0$

(In 1 dB steps, for $d_0 = 1$ km and for $d_0 = 200$ km, i.e. $h_0 = 100$ km)

| h' | $d_0=1$ km | $h_0=100$ km | h' | $d_0=1$ km | $h_0=100$ km | h' | $d_0=1$ km | $h_0=100$ km |
|------|------------|--------------|------|------------|--------------|------|------------|--------------|
| 89 | 45 | -1 | 159 | 50 | 4 | 282 | 55 | 9 |
| 94 | | | 168 | | | 299 | | |
| 100 | 46 | 0 | 178 | 51 | 5 | 316 | 56 | 10 |
| 106 | | | 188 | | | 335 | | |
| 112 | 47 | 1 | 200 | 52 | 6 | 335 | 57 | 11 |
| 119 | | | 211 | | | 376 | | |
| 126 | 48 | 2 | 224 | 53 | 7 | 398 | 58 | 12 |
| 133 | | | 237 | | | 422 | | |
| 141 | 49 | 3 | 251 | 54 | 8 | 447 | 59 | 13 |
| 150 | | | 266 | | | 473 | | |
| | | | | | | 501 | 60 | 14 |

4.5.4.2 If individual h' readings are made with each determination of absorption, then this value can be translated using Table 4.2 (to the desired accuracy of 1 dB). As finally the determination of the absorption decrement is made with Equation (4.3a), the difference $(F_0 - 20 \log_{10} h'/d_0)$ enters into the computations. Some stations make the computation with $d_0=200$ km instead of 1 km. This is equivalent to stating that the reference field is obtained at ground after reflection from a lossless mirror at $h_0=100$ km. This gives the values listed in the third column of Table 4.2. Numerical calculation is somewhat easier.

4.5.4.3 If at an absorption station ionograms are regularly recorded, the height readings can be taken from a simultaneous ionogram or from the ones immediately before and after the absorption measurement. Most absorption frequencies are chosen in such a way that large height variations do not occur. The only significant changes are between regions E and F, for example in the presence or absence of (sporadic) Es. If account of these is taken by distinguishing between both regions, it is normally not necessary to take daily readings of h' . It is sufficient to take the median $h'(f)$ at the given frequency f from the monthly ionograms at the given hour and use it for all days of that month. When the computations are made monthly, this represents a considerable simplification because $F_0(f)$ also is, normally, the same for the whole month. The only exceptions are frequencies and hours for which a retardation cusp tends to occur, e.g., in F1.

4.5.4.4 Nighttime measurements are made to obtain the reference values F_o (see Section 4.5.3.3). A reading of h'_N is needed to insert into Eq. (4.10). The same reasoning applies as explained above under Sections 4.5.4.2 and 4.5.4.3. It is again easiest to take the monthly median equivalent height, $h'_N(f)$ from the ionograms at the night hour when the measurements are made. There are, however, two difficulties:

- (i) The irregular presence of the sporadic layer Es may on a given frequency provoke splitting of the set of nighttime observations into one for reflection from Es and another one from F. The height reduction must be made separately for both sets.
- (ii) A greater variability of h' occurs because rather generally electron densities in the F region are much smaller at night than by day. Therefore at night the operating frequency comes nearer to the critical f_oF2 . If the relevant variation of h'_N is larger than $\pm 10\%$, the method of Section 4.5.4.3 is not recommended but individual readings should be made. It is better in this case to use only that part of the observations for calibration for which the lower h'_N values occur and limit these to a $\pm 10\%$ range. See Section 4.6.4 for reasons and more details concerning calibration measurements.

4.5.5 Accuracy rules:

Since A1 measurements deal with phenomena which are largely influenced by fading, it would not be justified to claim a high degree of accuracy for individual observations. Even the median of a set of measurements has some numerical uncertainty due to the remaining sampling error. In view of this error of the reflection coefficient up to 2 dB is felt to be tolerable without any qualification or description.

4.5.5.1 The following general schedule should be applied in view of the estimated (absolute) error, ϵ of the ionospheric loss, A_f :

| Situation | | Action |
|-----------|--|--|
| (i) | $\epsilon < 2 \text{ dB}$ | : take measured value as correct |
| (ii) | $2 \text{ dB} < \epsilon < 4 \text{ dB}$ | : describe by appropriate letter and qualify as uncertain (letter U) |
| (iii) | $4 \text{ dB} < \epsilon$ | : replace measured value by appropriate letter |

These rules may be applied quite generally to meet any kind of uncertainty of measurement.

4.5.5.2 A special situation arises in the presence of a sporadic Es layer which is not completely blanketing on the frequency used.

4.5.5.2.1 If the Es echo is predominant, it should be used to determine absorption. There would be, however, additional attenuation of the Es echo due to its transparency. In this case the error ϵ is the loss due to poor reflectivity. It can be estimated from the amplitude ratio of the first order E and F echoes. For this comparison we must bear in mind that the virtual height of the latter is approximately twice that of the Es echo, and we have therefore to allow for a "bias", viz., the difference in spatial attenuation.

4.5.5.2.2 To a partial reflection process corresponds a reflection loss A_R (expressed in dB); the difference of the logarithmic field strength of the E and F reflection $\langle \text{Es} \rangle - \langle \text{F} \rangle$, can then be evaluated (see Table below) and hence the relevant errors deduced as a function of this difference. If apparently partially reflected signals are not due to partial penetration at vertical incidence, e.g., if oblique reflections are present, the actual errors will be less than those computed. If one has no additional evidence that this occurs, the worst case given in the tables should be assumed to be applicable.

Due to the 6 dB bias in favor of the Es signal, all limits set by our accuracy rules refer to positive field strength ratios, i.e., the Es-echo amplitude exceeds that of the F echo, even under conditions where a qualified measurement is obtainable from the latter but no more from the Es echo.

Relation between the logarithmic field strength difference (in dB), $\langle \text{Es} \rangle - \langle \text{F} \rangle$, as a function of the loss at partial reflection, A_R (also in dB):

| A_R | 1 | 2 | 3 | 4 | (5) | dB |
|--|----|----|-----|-----|-----|----|
| $\langle \text{Es} \rangle - \langle \text{F} \rangle$ | 20 | 13 | 8.5 | 6.0 | 4 | dB |

4.5.5.3 The following particular rules may then be deduced from the general rules given above.

4.5.5.3.1 Absorption value determined from Es echoes:

| When $\alpha = \langle Es \rangle - \langle F \rangle$ (in dB) | | | | Action |
|--|----------|--------|----------|--|
| (i) | α | \geq | 12 dB | : Take measured value as correct |
| (ii) | 12 dB | $>$ | α | $>$ 6 dB : Qualify by U and describe by L |
| (iii) | α | \leq | 6 dB | : Determine absorption not from Es but from F echo |

NOTE: The symbol $\langle \rangle$ means field strength or voltage in dB above a reference level.

4.5.5.3.2 When the Es echo has large partial reflection loss, we have to use the F echo. Of course, there is now additional attenuation due to partial penetration at the Es layer, A_p , and this occurs on both up and down paths. Thus the logarithmic error of the F amplitude is $2 A_p$.

Relation between $\langle Es \rangle - \langle F \rangle$ (in dB) as a function of the loss at penetration A_p (in dB):

| | | | | | | |
|--|------|---|---|---|-----|----|
| $2 A_p$ | 1 | 2 | 3 | 4 | (5) | dB |
| $\langle Es \rangle - \langle F \rangle$ | -2.5 | 1 | 4 | 6 | 7 | dB |

which with our general rules now leads to the following set of special rules.

4.5.5.3.3 Absorption value determined by F measurements:

| When $\alpha = \langle Es \rangle - \langle F \rangle$ (in dB) | | | | Action |
|--|----------|--------|------------------|--|
| (i) | α | \leq | 1 dB or negative | : Take measured value as correct |
| (ii) | 1 dB | $<$ | α | \leq 6 dB : Qualify by U and describe by A |
| (iii) | α | $>$ | 6 dB | : Determine absorption from Es echo. |

4.5.6 A recommended reduction schedule shall be summarized in the following:

As the determination of F_0 is explained in Section 4.6.3 below, we restrict ourselves to determination of the absorption loss, A , during an hour where absorption is appreciable. It is therefore supposed that one set of amplitude readings of the first order echo exists. Furthermore at least a monthly average of equivalent height and an amplitude value for the noise level exists.

4.5.6.1 In the set of successive individual readings identify which of the first order echoes stem from the E layer or from Es and which from the F region (by inserting in different lines). This gives at most three different classes of readings. Mark Es echoes with the letter A. Check with ionogram, if available.

4.5.6.2 Decide whether a median of the echo amplitudes can reasonably be determined. Rejection may occur for one or several of the following reasons:

- (i) Identifications are so largely spread that none of the three classes, E, Es, F, contains at least 50% of all individual readings.
- (ii) Missing numerical values prevent the most frequent class from reaching that percentage. (Echoes disappearing in noise can be counted as numerical here when the observed noise level is substituted accompanied by qualifying letter E and descriptive letter B.)
- (iii) The median is not more than 2 dB above the measured noise level (see Section 4.5.6.3.3).

4.5.6.3 Consider all possible needs for qualification of the data. Check in particular that echoes chosen for reduction stem from the ordinary component and are not affected by partial reflection. In critical cases an ionogram should be considered to achieve this end (see also Rule 4.5.6.3.3 below).

4.5.6.3.1 As to the identification of magneto-electronic components (see Section 2.2.3), main sources of wrong identification are the following situations:

- (a) Es and F echo appear simultaneously, but the Es echo is an extraordinary one: the F echo must not be rejected in this case.
- (b) F1 is present and causes splitting and strong retardation: the first F echo may be extraordinary in that case so that the upper F echo would be the right one.

4.5.6.3.2 If partial reflection from Es occurs, both echo amplitudes Es and F are affected. However, with the accuracy limits adopted in Section 4.5.5.1 one or the other echo can be accepted. The criteria for acceptance have been explained in Section 4.5.5.3. They result in the following rules (for ordinary component always):

- (i) If $F_1(Es) \leq F_1(F)+1$, one does not compute $A(Es)$ but computes $A(F)$, which is unqualified.
- (ii) If $F_1(F)+1 < F_1(Es) \leq F_1(F)+6$, one also computes $A(F)$, which is, however, qualified by U and described by A.
- (iii) If $F_1(F)+6 < F_1(Es) < F_1(F)+12$, one does not compute $A(F)$ but $A(Es)$, which is, however, qualified by U and described by L.
- (iv) If $F_1(Es) > F_1(F) + 12$, one computes $A(Es)$; the numerical value is unqualified.

These rules take account of the fact that, by geometry, the unabsorbed F echo is weaker than that from Es by about 6 dB. They do give allowance for errors up to 4 dB (see Section 4.5.5.1).

The rules are summarized in Table 4.3. They apply for measurement of absorption only, not for calibration measurements, i.e. determination of F_0 (see Section 4.5.3.1).

4.5.6.3.3 Too weak echoes cannot be read with enough reliability.

- (i) When the median is not more than 2 dB above the noise level, F_{ns} , they are rejected by Rule 4.5.6.2 (iii); the notation is

$$(F_{ns})ES$$

where (F_{ns}) means the numerical value of the noise level (in the same dB scale as used).

- (ii) When the median F_1 is only between 2 and 4 dB greater than the noise level,

$$F_{ns} + 2 < F_1 \leq F_{ns} + 4,$$

the median is qualified by U and described by S.

- (iii) When Es is the only reflecting layer, it is sometimes difficult to decide whether reflection is partial or total. Inspection of the ionogram and consideration of the amplitudes compared with those obtained at other occasions may help. If no clear decision can be reached, the measurement is rejected and replaced by L. This condition is almost impossible during daylight hours on the frequencies normally used for absorption measurements. It is, however, not infrequent on the higher of these frequencies at night. Since nighttime observations are used for calibration purposes, it is better to reject doubtful values than to retain them.

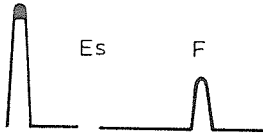
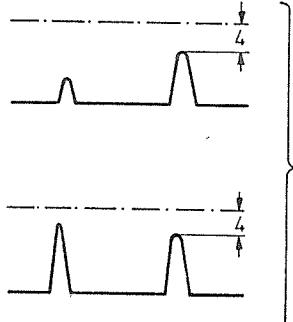
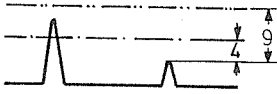
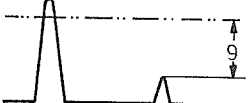

4.5.6.4 Compute the median amplitude of the first order echo by the known rules:

- (i) First put all individual samples in the order of increasing numerical value (values qualified by E at beginning, those qualified by D at the end).
- (ii) For an uneven number of samples the central value is the median.
- (iii) For an even number of samples the mean of the two central values is the median.

The median may be determined on an arbitrary scale of amplitudes. From the sensitivity curve of the receiving system it is finally translated into a dB scale (with at least 1 dB accuracy). The so-determined median in dB units is called F_1 .

Table 4.3

Notations for Absorption Loss in Cases of Partial Reflection

| Echoes | Amplitudes | Notation | |
|---|--|-----------|-----------|
| | | (Es) | (F) |
|  | no Es echo | --- -- | (value)-- |
|  | $\langle Es \rangle < \langle F \rangle + 4$ | --- -A | (value)UA |
|  | $\langle F \rangle + 4 < \langle Es \rangle$ $\langle Es \rangle < \langle F \rangle + 9$ | --- -A | --- -A |
|  | $\langle Es \rangle > \langle F \rangle + 9$ | (value)UA | --- -A |
|  | no F echo | (value)-- | --- -A |

4.5.6.5 Statements concerning the reliability of the median (by qualifying and descriptive letter symbols):

- (i) If more than 50% of all possible numerical values are missing for any reason (except absorption, letter B), then the median is to be qualified by U and described by the relevant descriptive letter. Values dropping into another class are replaced by the relevant letter (A, L, ...) (see Section 4.7).
- (ii) If the median is within 4 dB of the noise level, it is qualified by U and described by S.
- (iii) If not enough numerical values were obtained to form a median (see Rules 4.5.6.2 above), insert the most frequent descriptive letter symbol instead of numerical median value.

4.5.6.6 Take the corresponding equivalent height value, either from a (quasi-) simultaneous measurement or from the monthly median ionogram (see Sections 4.5.4.2 and 4.5.4.3), and read the relevant distance term, $\Delta(h')$, from Table 4.2.

4.5.6.7 Take the reference field value F_0 valid for the period considered and reduced to the ordinary component only (see Section 4.6). (With same value of d_0 as used when performing the readings in Table 4.2).

4.5.6.8 Compute the absorption loss, A , from Eq. (4.3a) in the form

$$A = F_0 - F_1 - \Delta \quad (4.11)$$

All three terms on the right side are dependent on the frequency f , so that each of these terms tends to be different for different frequencies. For individual days, read-out and computation are usually made to 1 dB, i.e., with whole dB values. (Monthly median computation would then, however, necessitate an accuracy of 0.2 dB).

4.5.6.9 Another computing method uses the (unabsorbed) nighttime median amplitude, F_{1N} (in dB), and compares it directly to F_1 measured in the presence of absorption. Also the relevant equivalent height, h'_N , needs to be known and translated with Table 4.2 into Δ_N . Computation of the reference value F_0 can so be avoided.

4.5.6.9.1 If both magneto-electronic components could not be resolved when reading F_{1N} , absorption loss is computed from

$$A = F_{1N} - F_1 + \Delta_N - \Delta - 3, \quad (4.12A)$$

because the average result of combining both components (at night, i.e., in the absence of absorption) is an increase by 3 dB against the desired ordinary component.

4.5.6.9.2 If during the night measurement both components were at different heights, one has to use

$$A = F_{1N} - F_1 + \Delta_N - \Delta \quad (4.12B)$$

This latter procedure is, however, not recommended because splitting of equivalent height mostly means that the operational frequency was rather near to f_{oF2} so that selective absorption in F and possibly extra loss by height dispersion may have influenced the night value F_{1N} .

4.5.7 A few examples shall illustrate the procedure:

4.5.7.1 First example: Readings (in mm) taken at 10 s intervals from the screen of a cathode ray tube. Sample size: 9. Let the noise level be 7 mm (smallest echo amplitude which can be read). On a frequency below foE let the time sequence of individual readings in the E line be:

17 20 22 28A 30A 7 15 S 10.

Descriptive letter A indicates presence of a (rather strong) Es echo. These values are eliminated, as well as S (meaning interference by an unwanted transmitter). Thus, the underlined 3 values must be dropped. The remaining ones are ordered:

7 10 15 17 20 22.

Since the two central values are 15 and 17, the median is 16 mm. 6 out of 9 values could be used -- this is 67%: reliability is good according to Rule 4.5.6.5(i).

Translate the mm readings into a dB scale using the sensitivity curve of the receiving system. Only the median and the noise level need such translation:

median 16 mm \longrightarrow 15 dB
noise 7 mm \longrightarrow 6 dB.

The difference is 9 dB so Rule 4.5.6.5(ii) also indicates full reliability. Let the equivalent height be $h' = 110$ km; one reads Δ from Table 4.2 as $\Delta = 47$ dB (with $d_0 = 1$ km).

Let the reference value (reduced to ordinary component, and $d_0 = 1$ km) be $F_0 = 78$. Equation (4.11) then gives:

$$A(E) = 78 - 16 - 47 = 15,$$

as a final result. This value for $A(E)$ is fully reliable so it is not qualified.

4.5.7.2 Second example: The frequency is above f_{oE} . Automatic recording is producing a sample of 20 values, directly in dB. Echoes from the regions E (Es) and F are distinguished; those from region E are, of course, all Es echoes.

| | | | | | | | | | | | | | | | | | | | | |
|--------|---|---|---|---|----|----|----|----|---|----|---|---|---|---|----|---|----|---|---|---|
| E (Es) | 7 | 8 | 9 | 8 | 11 | 12 | 14 | 10 | 9 | 6 | 7 | 5 | 6 | 5 | 8 | 8 | 6 | 5 | 7 | |
| F | - | - | 6 | 8 | 9 | 5 | 5 | - | 7 | 11 | 6 | - | 5 | 8 | 14 | 6 | 11 | 5 | - | 7 |

The values replaced by E, i.e., below current noise level, have been marked by a dash (-) alone. We now produce a trial median for the upper line. Arranging in order can be done by marking values in the order of increasing size up to the tenth value (half of the total number which is 20). To this end, we have used a bar above the number. This gives here: three E's, two 5's, three 6's and two 7's, which is just 10 values. The next value is 8. The median of $F1(Es)$ lies between 7 and 8. Rule 4.5.6.4 (iii) gives $F1(Es) = 7.5$.

Similar procedure for the second line gives: Five dashes, four 5's and three 6's, which is 12 values. The median is in the last group, thus $F1(F) = 6$.

Now consider the rules for partial reflection in Section 4.5.6.3.2. Rule (ii) applies as $F1(F) + 1 = 7 < F1(Es) = 7.5$; $F1(F) + 6 = 12$. According to the rule, $A(Es)$ should not be determined but $A(F)$. Let the height be $h' = 235$ km which gives from Table 4.2 (for $d_0 = 200$ km, or $h_0 = 100$ km) $\Delta = 7.5$.

Let the reference value (ordinary component for $d_0 = 200$ km) be

$$F_0 = 36 \text{ (with } d_0 = 200 \text{ km)}.$$

Eq. (4.11) gives $A(F) = 36 - 6 - 7.5 = 22.5$.

As stated above (Rule 4.5.5.3.2(ii)) we have to qualify this result so that we should write:

$$A(F) = 22.5UA; \quad A(Es) = L.$$

However, we have not yet considered the noise level, F_{ns} , Rules 4.5.6.3.3. We consider two cases:

(a) Noise level 5dB: Then $F_{ns} + 2 = 7 > F1(F) = 6$, Rule 4.5.6.3.3(i) applies and the final result is:

$$A(F) = 22.5ES; \quad A(Es) = L.$$

(b) Noise level 3.5 dB: Then $F_{ns} + 2 = 5.5 < F1(F) = 6 < F_{ns} + 4 = 7.5$ and Rule 4.5.6.3.3(ii) applies resulting in:

$$A(F) = 22.5US; \quad A(Es) = L.$$

4.5.7.3 Third example: The frequency is below f_{oE} . Sample size: 7

Readings, x, in linear scale (with decadic switching of sensitivity). Noise level is 19 scale units. Es echoes appear during sampling time:

| | | | | | | | |
|--------|-------|----|-----|-----|----|-----|-----|
| E(Es): | - | - | - | 28 | 24 | 98 | 110 |
| F | : 163 | 95 | 121 | 178 | 90 | 42A | - A |

We arrange the data in order of increasing amplitude

| | | | | | | | |
|--------|------|----|-----|-----|-----|----|-----|
| E(Es): | E | E | E | 24 | 28 | 98 | 110 |
| F | : 90 | 95 | 121 | 163 | 178 | | |

Data marked A are omitted from the count for F echoes. It appears that both lines contain more than 50% significant readings so that according to Rule 4.5.6.2(i) both medians could be determined, giving:

$$\bar{x} = 24 \text{ scale units for } E(Es) \text{ and } \bar{x} = 121 \text{ for } F.$$

Transformation into the dB scale is achieved by computing $20 \cdot \log \bar{x}$ and gives: 27.6 dB for E; 41.6 dB for F and 25.8 dB for the noise level.

According to Rule 4.5.6.2(iii) (identical with Rule 4.5.6.3.3(i)), the Es echo is to be rejected because the median and noise level difference is $27.6 - 25.8 = 1.8$ dB, thus the median is less than 2 dB above the noise level.

Let the virtual height for the F echo be $h' = 260$ km, which gives $\Delta = 8.5$ dB (from Table 4.2, with $h_0 = 100$ km).

Suppose that only one night calibration has been made, which gave $F_{1N} = 315$ scale units with $h'_N = 295$ km. Both translated into dB ($h_0 = 100$ km):

$$F_{1N} = 50 \text{ dB};$$

$$\Delta_N = 9.5 \text{ dB}.$$

Finally from Section 4.5.6.9.1, Eq. (4.12A), we compute the absorption loss in dB for the F echo:

$$A(F) = 50 - 41.6 + 9.5 - 8.5 - 3 = 6.4.$$

This value is not to be qualified! If $A(E_s)$ is reported at all, it is to be replaced by letter S.

4.5.8 Data for interchange are, by convention, the direct results of absorption measurements, i.e., absorption loss A with indication of reflecting layer.

4.5.8.1 A basic report is to be established for every observation. It is recommended that h' values be given with every reported A value. Name of station, date, hour and operating frequencies and identification of calibration used should appear on all tabulations. If available, the reference value F_0 is to be noted, also the sampling index (number of individual readings in a sample), except when it remains fixed. An example of a basic report is reproduced in Table 4.4.

4.5.8.2 After computation of the absorption loss, A , the results are summarized in a monthly report giving all indications listed in Table 4.5. This as an example is given for observations at a fixed hour once a day, most often near noon. Observations at constant solar zenith angle can be reported in similar format. Monthly reports in the format of Table 4.5 are recommended to be interchanged between stations, and through World Data Centers (WDCs). They describe the most significant results, viz: day-to-day changes, monthly median and statistical dispersion by (upper and lower) quartiles.

Where observations are made on the same day at different hours, for example hour by hour, the tabulation shown in Table 4.5 is split into different tables, one for every hour.

4.5.8.3 Such tables should be interchanged through WDCs for particular days and periods according to international conventions -- see *International Geophysical Calendar*, prepared by the International Ursigram and World Days Service (IUWDS). The calendar including suggestions from spokesmen of the various scientific disciplines is published yearly in advance -- see *URSI Information Bulletin* or *STP Notes*.

The following recommendations are valid at present for absorption (A_1) data:

- Hourly observations at least on all Regular World Days (RWD).
- Continuous observations during solar eclipse days.
- Regular Geophysical Days (i.e., each Wednesday) are recommended for special efforts, e.g., observation of the diurnal variation.
- Particular "post mortem" periods for interchange are agreed internationally for analysis of especially interesting periods. These are also identified by IUWDS as "Retrospective World Intervals". Addresses of WDCs can be found in Appendix III, Chapter 10.

4.6 Calibrations

4.6.1 Absolute calibration of the whole system is not impossible but difficult. As at least the average geometric attenuation decrement can be calculated, the absorption loss A would be the only unknown if transmitter (peak) power, efficiency of transmitting and receiving antennas, receiver sensitivity and recorder calibration were known. The corresponding measurements are discussed in this order.

4.6.1.1 Transmitted power could be quite easily measured if continuous wave (CW) transmission was used. Unfortunately, the measurement of the peak power of a pulse transmitter is more involved.

4.6.1.1.1 One procedure is to determine average power with a standard radio frequency (RF) power meter and determine the effective pulse-to-total-time ratio.

This latter determination can be made by time comparison on the screen of a cathode-ray tube. Unfortunately, most modern oscillographs have no direct input to the deflecting plates which is needed for this. It is not acceptable to pass the signal through a receiver or a wide band amplifier because such devices enlarge pulse width too much. The best method is to disconnect the vertical deflection plates from the amplifier output and connect two pieces of wire of about 1 m with each of them. In the environment of the transmitter this is enough coupling to see the RF pulse on the screen, provided the sweep on the horizontal deflecting plates is synchronized with the pulse recurrence frequency. Verify that each of the plates has a d.c. connection with zero potential through suitable resistors (about 1 M Ω). As a secondary standard, low voltage lamps may be used for measuring the average (RF) current. These can be calibrated with a (RF) meter; their luminosity can be measured very accurately with a pyrometer.

Table 4.4

Absorption Measurement: Basic Report

Station name: Date:

1st frequency: MHz

Reference value F_0 (d_0 = km)

Time of measurement: legal time h (.....° Meridian)

UT h.

Echo amplitude readings:

E(Es)

F

h' = km Noise level

2nd frequency: MHz

Reference value F_0 (d_0 = km)

Time of measurement: legal time h (.....° Meridian)

UT h.

Echo amplitude readings:

E(Es)

F

h' = km Noise level

3rd frequency: MHz

Reference value F_0 (d_0 = km)

Time of measurement: legal time h (.....° Meridian)

UT h.

Echo amplitude readings:

E(Es)

F

h' = km Noise level etc.

4.6.1.1.2 The other procedure is direct measurement of peak power. The classical method uses a cathode ray, again with direct access to the vertical deflecting plates. Deflection sensitivity can be calibrated with a direct current (d.c.) voltage. Peak to peak (p.p.) voltage of RF is then easily measurable; effective voltage is $0.35 (= \frac{1}{4} \sqrt{2})$ of this value. One measures voltages only: First the voltage at the transmitter output (one line against ground) after dividing it down to a suitable value of the order of 100 V (p.p.). A capacitive voltage divider is preferable as the load is the capacitance of the deflecting plates. Usually one just couples to the "hot" line with a small capacitor using the load as the second capacitor. RF current can be measured by inserting a resistor suitable for RF (R) into the output-antenna connection and then measure voltage against ground at both ends. The voltage difference times

Table 4.5

Absorption Measurement: Monthly Report

Station name: Month:
 Latitude: Longitude: Legal time: (.....° Meridian):.....h

1st frequency: MHz 2nd frequency: MHz etc.
 Hour of measurement: h h Legal time
 Hour of measurement h h UT
 Reference value ($d_0 =$ km) $F_0 =$ $F_0 =$ dB

| Date | Absorption loss A/dB; Virtual height h'/km; Sampling index | | | | | | Remarks |
|------|--|---------|----|---------|---|---------|---------|
| | Layer E | | Es | | F | | |
| | A | h' ind. | A | h' ind. | A | h' ind. | |
| 1. | | | | | | | |
| 2. | | | | | | | |
| 3. | | | | | | | |
| 4. | | | | | | | |
| 5. | | | | | | | |
| . | | | | | | | |
| . | | | | | | | |
| . | | | | | | | |
| . | | | | | | | |
| 30. | | | | | | | |
| 31. | | | | | | | |

median
count

upper quartile:

lower quartile:

the quantity R is the current. The resistor should be small against the load, non-inductive and good enough for high voltage; if stable enough, full section resistors are good to achieve this. The method supposes the load to be ohmic. This can be checked by substitution of a high-power ohmic resistor. Voltages and currents must remain unchanged when the right resistance value is substituted.

With modern digital techniques other methods of peak power determination are now available. The reading on a cathode-ray tube is replaced by digital voltage discriminators (Schmitt-trigger). It is, however, important to check that no error is introduced by the capacitance of semiconductor elements, and by time constants of the latter.

4.6.1.2 The vertical gain of the transmitting antenna is not easy to measure. Computation (see Table 4.1 in Section 4.5.3.1) is not feasible in most cases from lack of information about properties of the ground which acts as a "mirror". The only exceptions are water surfaces. Generally ground conductivity can only be estimated, and the effective depth below ground level of the "mirror" surface is difficult to measure; it also depends on humidity and frequency.

4.6.1.2.1 The only reliable measurement of antenna gain is field strength measurement at a few 100 m vertically above the antenna with a calibrated receiver (field strength meter) aboard a balloon or a plane. Special experience and good logistics are needed; CW transmission is preferable for calibration.

4.6.1.2.2 If the polarization of the transmitting antenna is circular, the whole energy is transferred to one mode, usually the ordinary one. This has the so-called "ionic" polarization, i.e., in a horizontal plane the electric field rotates in the same sense as a positive charge would freely spin around the vertical component of the terrestrial magnetic field. Seen from above, the "ordinary" sense of rotation of the electric field in the antenna is anti-clockwise in the (magnetically) northern hemisphere, clockwise in the southern one. The sense is independent from whether the wave travels up or down.

If as at most stations the transmitting antenna is linearly polarized, only half of the radiated power enters each of both magneto-electronic modes, which means, a 3 dB loss. Account of this loss has been taken in Table 4.1, Section 4.5.3.1.

4.6.1.2.3 It is important in this context to measure the efficiency of power delivery from the transmitter output to the antenna, i.e., losses and mismatch in the feeder. This is best done with an auxiliary CW transmitter between 5 and 100 W, and standard instrumentation for such measurements (e.g., those used by radio amateurs).

4.6.1.3 Some problems discussed above refer to the receiving antenna too. The easiest way is to use it as a transmitting antenna with a suitable auxiliary CW transmitter and apply the method described in Section 4.6.1.2 above. As indicated above in Section 4.5.3.1, a 3 dB loss due to selection of polarization occurs for a linearly polarized antenna, but not with a circularly polarized one.

4.6.1.4 Receiver sensitivity is described by the output-to-input response curve (sensitivity curve). See Section 4.4.3.1.

4.6.1.5 Recorder sensitivity is the last member of the whole system calibration chain. Methods have to be chosen according to the recorder used (see Section 4.6.2.3). Quite generally one aims to establish a unique relation between receiver output and recorder indication, whether this latter be analogue or digital.

4.6.1.6 The procedure of whole system calibration described above is not recommended for routine stations. It may, however, be interesting for research stations, particularly when the limitations of the routine calibration method are to be investigated. This latter will be described under Section 4.6.3 below.

4.6.2 Relative calibration uses only a small part of the whole chain described under Section 4.6.1 above, namely receiver and recorder calibrations. Instead of measuring transmitted power and antenna efficiencies, a "reference value" is determined which is essentially a received input voltage for a standard propagation case with vanishing absorption (see Section 4.6.3 below).

4.6.2.1 In these methods one uses input RF voltages as a replacement of field strength values, so avoiding the determination of the gain of the receiving antenna. This also has the advantage that the polarization of the antennas (see Section 4.5.3.1) has no influence.

4.6.2.2 Receiver sensitivity is measured with a high quality signal generator as explained in Section 4.4.3.1.

4.6.2.2.1 If video amplification is made with a broadband d.c. amplifier, there is no difficulty in obtaining the output-to-input response curve.

4.6.2.2.2 If, however, video amplification suppresses d.c., the situation is considerably more involved because a CW signal generator is useless then, and a special pulse signal generator with the same pulse shape as the main transmitter must be built. It is therefore not recommended to use such amplification at all. High gain integrated semiconductor d.c. amplifiers are now available with good stability and reliability so that there is no longer need to suppress the d.c. component.

4.6.2.2.3 It is important to note that relative calibration must only take account of such stages in the receiver where the amplification depends on the signal amplitude. A constant factor applicable in the same way to all amplitudes could be omitted for relative calibration. Now in classical receivers pre-amplification on the radio frequency (RF) tends to be linear, i.e., gain is independent of amplitude. (This is at least true for echo signals but not for the direct signal from the transmitter.) Therefore

considering echoes only, the sensitivity curve can be determined beginning with the first intermediate frequency (IF) stage. Of course, this is only feasible if RF tuning is always correctly obtained so that no errors could be provoked by detuning. The advantage of this recommended method is its simplicity when multifrequency techniques are used: an IF signal produced by a standard signal generator is coupled into the first mixing stage as described in Section 4.4.3.3. This simplified procedure is recommended for constant (or logarithmic) gain devices (Sections 4.2.2 and 4.2.3). It can, however, not be applied when constant output techniques are used (see Sections 4.2.4 and 4.2.6).

4.6.2.3 Calibration of the recorder unit depends upon the type used (Section 4.3.6). It is recommended to calibrate receiver and recorder as one chain. Where this is not feasible, one of the following methods may be used.

4.6.2.3.1 Cathode-ray tubes are most easily calibrated with a d.c. source (voltage stabilized power supply or batteries) or with a.c. (alternating current) voltage, taken from a transformer fed by the power-line or with a well-calibrated audiofrequency generator. It is advantageous to read peak-to-peak values. Note that peak-to-peak a.c. voltage is 2.83 times the effective voltage.

4.6.2.3.2 Meter recorders are similarly calibrated by inserting a sequence of different a.c. voltages and recording the output.

4.6.2.3.3 Automatic digitizing recorders use a limited number of levels which should be adjusted according to a given scale, for example, a fixed interval between steps (see Appendix 4.C). The interval could be such that a round number of steps makes 10 dB. 5 dB or 3.3 dB steps is often an appropriate choice.

The voltage discriminator circuits, mostly Schmitt-triggers, must then be adjusted, together with the receiver, by injection of an RF voltage at the receiver input or an IF voltage at the first mixing stage. From one step to the next one this input is increasing by the step difference, for example:

0 - 5 - 10 - 15 - 20 - 25 - 30 - 35 - 40 - 45 - 50 - 55 - 60 dB

successively. In each position the corresponding discriminator is adjusted to respond exactly to that level. This can usually be done by changing a voltage, e.g., with a potentiometer.

4.6.2.3.4 Constant output receiving systems (see Section 4.2.4) very often use a commercial attenuator so that the (negative) gain is directly readable. An amplifier with voltage controlled amplification (see Appendix 4.B) is indicated for automatic devices. In that case the control voltage is the quantity to be recorded -- often by a meter recorder or a digital meter producing punched or magnetic tape. In this case also by inserting different RF or IF voltages the meter is calibrated together with the receiver. Calibration results should be recorded.

4.6.3 Determination of a reference value is the recommended method to be used for the computation of absorption loss A in Eq. (4.11) of Section 4.5.6.8. It can only be obtained if a relative calibration as discussed in Section 4.6.2 has been executed.

4.6.3.1 The reference value is determined by measuring a first order echo amplitude under conditions where absorption is very small (see Section 4.5.3.3). This is supposed to be so at almost all latitudes during undisturbed nights, preferentially after midnight on frequencies above 1.5 or 2 MHz. The sun should be at least 5° below the horizon, so no calibration at all is possible with this method during polar day or dawn conditions.

Reflection, of course, should be total, not partial. Echoes from Es can therefore only be admitted if reflection is total, which is seen under unattenuated conditions by the occurrence of several multiples. Note that the amplitude of the multiples suffers from ground attenuation, but not that of the first order echo. Unattenuated multiples can only be expected at ship or cape stations (e.g., Dakar).

An F echo in the presence of an Es echo should not be used for calibration, except when the Es amplitude is 8 dB or more below that of F. (The Rules 4.5.6.3.2 do not apply to calibration measurements.) Deviative absorption in F must be avoided too, so cases where the frequency is near f_oF2 are better omitted.

4.6.3.2 The echo amplitude is observed and recorded in the usual way and identified as described in Section 4.5.1. Special attention must be paid to the magneto-electronic modes. Except for systems with at least one circularly polarized antenna, both modes, o and x, are present with almost equal amplitudes. Since usually the o mode is used for the daytime absorption measurements, it must be used for calibrations as well. Distinction is easy in cases where both components arrive with different equivalent height. If, however, both are confused, the echo amplitude shows (polarization) fading, the average amplitude being increased by 3 dB (sum of energy). Eq. (4.12A) is applicable only, but Eq. (4.12B) can be used when components are separate (see Section 4.5.6.9).

Of course, this influence must also be corrected for in the determination of F_0 to be inserted into Eq. (4.11) as a reference value. By definition F_0 is obtained in a logarithmic amplitude scale and refers to the ordinary component only. Choosing Eq. (4.12A), one automatically deduces 3 dB from the measured amplitude value in case both components were confused during the determination of the reference value.

4.6.3.3 The scale used for reading F_0 must, of course, be identical with that used for the daytime absorption measurements. If receiver calibration is executed by inserting a signal on the (first) intermediate frequency (IF), the same dB scale has to be used for calibration. Often the receiver is switched to reduced sensitivity at night. If this is so, the reduction must be determined (with IF calibration) and taken account of when determining F_0 . (This point must also be considered when applying Eq. (4.12) of Section 4.5.6.9).

4.6.3.4 The accuracy of the reference value F_0 depends primarily on its statistical reliability.

This, again, is a sampling problem. Unfortunately, most of the fluctuations in a series of determinations of F_0 can be ascribed to the influence of slow fading. Sometimes the amplitude may deviate for more than one hour, for example by focusing or defocusing (see Section 1.3.4). The coherence interval is quite long under such conditions so that only one or two independent samples could be expected from a measuring period of about 10 min. It is therefore necessary to make calibrations during several nights a month. A good practice is to do so every night. This is particularly necessary when measuring frequencies above about 3 MHz which at night may be quite often near $foF2$ or even above, so that only on the rare occasions where totally reflecting Es appears a usable calibration value can be obtained.

Thus, sampling inaccuracy due to the limited number of usable determinations of F_0 may sometimes be a serious limitation. Provided the technical conditions can be kept constant, one should then make an effort to determine F_0 with data from more than one month.

4.6.3.5 At a few stations determinations of the reference value have been made over years. Inspection has shown that some systematic variations seem to be present: Certainly seasonal, possibly also with the solar cycle. Thus there is evidence that this calibration method has its limitations, too. The changes are of the order of more than 1 dB.

Figure 4.10 presents the relative variations of the F_0 values obtained (by Eq. (4.10)) at Freiburg from 1956 through 1971; technical conditions were kept constant from 1956 to 1964 (replacement of transmitting station) and from 1964 to 1971. A systematic variation appears clearly after 1964, with the reduced transmitted power, rather similarly on all three frequencies. There is a seasonal variation with maximum in winter and, apparently, a long term variation, too. Further investigations of such effects are urgently needed.

4.6.4 Height scale calibration is needed because the equivalent height determines the distance term Δ of Table 4.2. Height markers are usually produced on the recorder or on the ionosonde if equivalent height is obtained from ionograms. The height marker generator can be made very accurate and reliable if the frequency is derived from a quartz. In that case no frequency calibration is needed.

However, the relative position of the direct pulse to the height markers must be accurately known, otherwise readings could be influenced by a systematic error. Best technique is to select a record with multiple Es echoes and by comparison of successive multiples determine the zero value of the absolute height scale. Multiple F echoes have a tendency to be slightly deviating from the vertical so that these cannot be recommended for determination of the zero position. Details concerning measurement procedure may be found in Section 4.5.4.4.

4.7 Data Handling and Interpretation

4.7.1 Basic data are absorption loss values, A , obtained from Eq. (4.11) or Eq. (4.12), whichever is relevant. For each period of measurement and operation frequency one A value is to be given, accompanied by at least an identification of the reflecting layer. It is, however, recommended to indicate if possible the equivalent height, h' , and the sampling index (number of samples) too. A format can be found in Table 4.5 of Section 4.5.8.2. It is recommended to determine monthly medians as shown in the model table.

In order to get enough independent samples one period of measurements should last about 10 to 15 min. Multifrequency measurements are preferentially made by sampling one frequency after the other in quick turn, a procedure which gains time because it is just as important to get enough interval between the individual samples. If, for example, four frequencies are radiated in turn, 30 s each, in 10 min one has 5 definitely independent sets of readings with 90 s each.

4.7.2 Some limitations may be due to the actual behavior of ionospheric conditions, in particular to phenomena like partial reflection or scattering.



Fig. 4.10 Monthly reference values F_0 obtained from observed echo amplitude after midnight by applying height correction to a standard height value. Freiburg 1956 through 1971 (ordinate), six digits are reproduced month by month (abscissa, fifth line). Field strength symbols refer to three sounding frequencies: 1.7, 1.0, and 2.4 MHz (see fourth line on top). Digicoder outprint: 16 symbols correspond to dB code as given in the third line on top.

4.7.2.1 Partial reflection has been discussed in detail in Section 4.5.6.3.2. Data can be rescued with the aid of the Rules summarized in Table 4.3. Uncertain values must be characterized with letter symbols as indicated there.

4.7.2.2 Scattering is produced by an irregular structure of the electron density distribution, in particular a "cloudy" structure. If a wave encounters such "clouds", it may be seriously attenuated by scattering losses. A direct assessment of these losses is not possible in the frame of absorption measurements. Fortunately, the presence of the characteristic complex reflection is clearly visible on records so that the phenomenon can easily be noted. In cases of weak scatter, one only describes the A value by the letter F; if the scatter is more serious so that the quality becomes doubtful, the description is (value)UF.

4.7.3 The expected accuracy of a measurement is first of all given by the presence or non-presence of the qualifying letter U. The sampling index can also be taken as a qualification. This is the number of individual (almost independent) amplitude readings. For continuous (automatic) measurements it is recommended to assume the coherence interval to be 5 s, and to note the number of seconds of recording time divided by 5. This is, however, not applicable on frequencies below 2 MHz where the coherence interval tends to be greater. The sampling index allows an estimate of the internal accuracy of an individual determination of A or the average accuracy of a station. It has no influence upon the monthly median.

4.7.4 When determining monthly medians to qualify their reliability, the limitations due to ionospheric influences must be taken into account. General rules for computing monthly medians can be found in Piggott and Rawer [1972]. Only a summary is given here:

4.7.4.1 Non-numerical values (absorption loss A) are treated as follows:

- values replaced by B, D, R should be treated as high values;
- values replaced by E should be treated as low values;
- values replaced by any other letter are ignored.

4.7.4.2 Numerical values (absorption loss A) qualified by

- D or E and described by A, C, F, H, R or S should be treated with the trial median procedure as explained in Piggott and Rawer [1972];
- D and described by B or R are treated as high values;
- E and described by A or not described at all are treated as low values;
- U are retained for the median.

4.7.4.3 If more than 50% of all input values of the monthly median are qualified by D, E or U, the median itself is qualified by U and described by the descriptive letter appearing most often.

If not more than 7 numerical inputs are available for a month, the median is also qualified by U and described by N. If less than 5 numerical inputs are available, no numerical median should be given (letter N only).

4.7.5 Like ionogram parameters, letter symbols are used in order to qualify or to describe a numerical value. A list of definitions adapted to the particular situation with absorption measurements is given in Appendix I Chapter 10.

4.7.6 Summarizing absorption parameters are sometimes used to give an overall description of a set of measurements obtained on two or more frequencies. They are particularly used to describe data obtained with multifrequency techniques. Either they are deduced from individual values or from monthly median $A(f)$ values so as to obtain a global monthly parameter. It is a common feature of these parameters that they assume some theoretical (or empirical) law to describe the variation of absorption loss A with frequency f . Note that for good reasons, established international interchange is concerned with A values only. Summarizing parameters are optional additions.

4.7.6.1 The simple non-deviative relation has been reported in Section 2.5

$$A(f) \propto (f \pm f_L)^{-2}, \quad [2.17]$$

f_L being the longitudinal component of the gyrofrequency (see Eq. (2.3) in Section 2.2.4). This procedure often used for summarizing neglects, of course, deviative absorption in the E region. No precise rule for eliminating this effect can be given. It is sometimes recommended just to omit values for which the operating frequency f was within $\pm 10\%$ of f_{oE} , but this excludes only the most disturbing features.

With all admitted A values on the different frequencies the hypothesis (for the ordinary component) is

$$A(f) = \frac{D}{(f \pm f_L)^2}$$

so that

$$D(f) = (f \pm f_L)^2 \cdot A(f) \quad (4.13)$$

The procedure to determine D is to compute $D(f)$ for each operational frequency $f_1 \dots f_n$, and then take the mean value

$$D = \frac{1}{n} \sum_{m=1}^n D(f_m). \quad (4.14)$$

NOTE: In the literature letter A is generally used instead of our D , and L instead of our A . The replacement has been made in order to obey a new general recommendation by IUPAP whereafter loss decrements should be designated by A . (A should, of course, not be confused with the letter symbol A of Appendix I).

4.7.6.2 Using more involved theory one has to take account of deviative absorption in the E layer, and non-deviative absorption in the D and lower E region. The influence of totally reflecting sporadic Es must also be taken into account because reflection from such a layer presents smaller loss than from a thick E layer. A model theory and procedure have been established by Bibl, Paul and Rawer [1959]. The theoretical frequency dependence is given by

$$A = \frac{B}{(f \pm f_L)^2} + C \cdot \Delta_E (f_{oE}/f). \quad [2.18]$$

In Section 2.6 the physical significance of the parameters B and C is explained in more detail.

The procedure to determine the parameters B and C from a set of measured $A(f)$ values is described in detail in the above reference. The "spider web" procedure recommended by the authors is essentially a two dimensional median. It was first described by Bibl and Rawer [1951] who indicated a simple ionogram method for determining the values ("spider-web" method, see Figure 4.32 in Section 4.9.6.4). Another version of such a method starts from an empirical model built with data of the station itself [see George, 1971; Samuel and Bradley, 1975].

4.8 Programs and Data Interchange

4.8.1 The objectives of absorption measurements are:

- (i) Study of a natural atmospheric phenomenon as such;
- (ii) Investigation of solar-terrestrial and geophysical relations with the status of the height levels where absorption occurs;
- (iii) Assessment of basic data applicable to propagation problems of radio waves.

4.8.1.1 Before sounding rockets were available for atmospheric research, measurement of absorption was one of the few methods allowing conclusions about collision frequency in the ionospheric plasma, at least in the lower ionosphere. Also electron density in the D region could hardly be obtained with other methods.

Since rockets allow local measurements, the limitation of ground-based observations giving height-integrated results only is felt to be more serious. However, even today very few rocket ascents are made where electron density at very low ionospheric altitudes could be measured at all. Calibration problems of probes are particularly difficult in the D region so that additional information concerning a height-integrated value is precious. As to collision frequencies, local measurements give very poor information due to the change of environment in the presence of a space vehicle. The more successful rocket methods are in fact propagation experiments between ground and a rocket.

The number of such experiments which have been flown up to now in the lower ionosphere is far too small to give reliable information about average collisional values or statistical distribution. At present rocket data are very desirable, informing us about height profiles in the lower ionosphere. Height dependent data available at a few places from partial reflection technique (see Chapter 8) are probably of even greater importance. But the mass of data needed to provide averages or significant statistical distributions stems from absorption measurements obtained with methods A1 and A2 at these altitudes.

4.8.1.2 Solar-terrestrial relations involving ionospheric absorption are of two kinds: long term variations with solar activity as shown by almost all ionospheric parameters, and short term variations related to solar events, in particular with flares. "Sudden ionospheric disturbance" (SID) is a large increase of absorption mainly in the D region, and this has been the first clear relation found between a terrestrial phenomenon and solar flares.

Of course, continuous methods of measurement such as method A3 (see Chapters 6 and 7) are more adequate to study flare effects. Method A1 is particularly apt to assess effects of solar activity with a time scale between days and many years.

4.8.1.3 Relations with geophysical phenomena are not so easy to assess because many of these depend also on solar influences, so that an observed correlation does not necessarily indicate a cause-effect relation. There is now one phenomenon for which many cases of clear correlation with absorption have been found, namely stratospheric warmings. These occur quite often simultaneously with a period of increased absorption in the D region, the "winter anomaly" (see Section 4.9.3.3).

4.8.1.4 Absorption data are needed for radio wave propagation forecasts, in particular field strength estimation on HF (or decameter) waves (HF = high frequency range). For such forecasts individual events are less important now than data allowing full statistical description, namely averages and statistical distribution. A1 results are quite adequate to give at least a good part of the required information. Most A1 stations measure regularly at noon so that the monthly average absorption at noon can be well specified as well as the width of the statistical distribution, e.g. quartile or decile ranges upwards and downwards. For forecasting purposes the diurnal variation would also be of great interest. Unfortunately, only a few A1 stations make enough hourly observations to give valuable information on that influence. The decrease of absorption after sunset is another feature which is of interest in this context.

4.8.2 A program of observations must be established according to equipment facilities and manpower available at a station. It must, however, take account of the character of the phenomena which shall be investigated.

4.8.2.1 In order to obtain reasonable statistical significance, the number of independent samples should range between 10 and 50 (see Section 3). Because instantaneous fading is so prominent, it is essential to make the sampling period long enough so that a reasonable number of independent samples is gathered. This means that the time interval must be long compared with the "coherence interval" (see Section 3.2.5). This is usually achieved with a sampling period of 15 min. If several frequencies are observed in turn, the sampling period for multifrequency observations must not be much longer than on a single frequency. The total number of samples is less important so that with modern automatic equipment the interval between individual readings is often artificially increased in order to avoid too large a number of input data.

4.8.2.2 Choice of working frequencies is, of course, dependent on equipment and manpower, and also on frequency regulations. At many places broadcasting makes observations difficult below 1.6 MHz. If a frequency is free locally, noon measurements are often quite possible but calibration at night may be difficult. It is usually advantageous to use a late night hour, e.g., 0300 LMT.

4.8.2.2.1 For A1 stations using only one frequency the international recommendation given for the International Geophysical Year (IGY) has proved successful and, therefore, is always valid. It specifies 2.2 ± 0.3 MHz. Near local noon this frequency is, almost everywhere, reflected in the E region, either from the normal E layer or from a "low-type" Es. The greatest amount of comparable A1 data hitherto has been collected on this frequency (see George [1971] for examples, including mapping).

4.8.2.2.2 When the working frequency is within about $\pm 10\%$ of f_oE or f_oF1 , data obtained are useless for synoptic purposes. The choice of a second frequency is therefore made so that this condition does not occur for long periods. It is not possible, in general, to choose a frequency which is reflected from the E layer in both summer and winter and also obeys this rule. Hence it is normally best to pick a frequency reflected from E in summer, F in winter. The interpretation of the absorption of the F-layer reflection is considerably more complicated than for the E, and small changes in absorption cannot be measured. At low latitudes the choice of first frequency may also have to be moved above 2.2 MHz since the absorption on this frequency can be too large to be measured by the equipment.

Frequencies above 4 MHz are not reflected from normal E, but from F or from Es. The contribution of deviative absorption is important near noon. Thus interpretation of data from these frequencies is more involved than from the lower ones. It is therefore recommended to avoid a second frequency in this range.

4.8.2.2.3 On the other hand, if multifrequency technique is used, the study of more complicated phenomena is feasible and interesting. Multifrequency observations should have at least four frequencies, better six. The range between 1.7 and 5.5 MHz is recommended.

4.8.2.3 The diurnal time schedule should be regularly adhered to every day. Minimum is one observation at local noon plus, if possible, one calibration during the night. Where two frequencies are in use, the minimum is one observation on each frequency near noon. It is preferable to do four (a, b, a, b). With multifrequency observations the minimum is one sequence at noon (a, b, c, d, e, f), preferably with the standard 2.2 MHz observation repeated. Calibration observations at night should be taken every month for which the frequencies are reflected at night. Note that calibration sequences on the same night are often partly correlated so that every attempt should be made to calibrate on at least four or five nights, each month.

4.8.2.3.1 If the diurnal variation is to be investigated, hourly measurements should be made between sunrise and sunset. With automatic equipment data should be averaged at hourly intervals, each interval centered at the hour and the absorption tabulated. For multifrequency sequences it is convenient to omit any frequency near f_oE or f_oF1 so that the sequence can be repeated at hourly intervals. With manual equipment it is usually only possible to observe an hourly program one day a week. It is recommended to take every Wednesday because many geophysical observations made once a week are now made on that day.

4.8.2.3.2 Scientifically it is very valuable to make observations at constant solar zenith angle χ throughout the year, but this is difficult in practice as the hour is continuously shifting from day to day. The minimum solar zenith angle at noon in winter is convenient at temperate latitudes. At low latitudes observations at a convenient χ between $\cos \chi = 0.4$ and $\cos \chi = 0.3$ should be chosen. Accurate timing in true local time is essential; a few minutes shift can change χ considerably in summer months. In view of the particular aim of such a program use of local mean time is not sufficient: the program must be established in true local time, i.e. it has to take account of the equation of time [see, for example, Piggott and Rawer, 1972].

4.8.3 International data interchange has become current practice since the IGY. Results of measurements usually in the format described by Table 4.5 of Section 4.5.8.2 are either interchanged between scientific organizations running stations or through an established international organization, the WDC service.

4.8.3.1 Tables of daily noon values of absorption, virtual height and sample count should be sent to one or all of the four World Data Centers (WDCs) responsible for absorption. If one copy is sent, the WDC should be notified so that it can send copies of the data to the remaining three WDCs. Corresponding tables of the calibration observations should be sent at convenient intervals. Where diurnal variations

are measured on 4 or 5 days per month, median or average values at hourly intervals should be tabulated and sent to the WDCs. For automatic recording at least the median values at each hour should be circulated, preferably the day by hour tables from which these medians were reduced.

It is essential that every table is accurately described with

- (a) station name and latitude and longitude
- (b) time used
- (c) parameters and frequencies used
- (d) type of sequence (e.g. noon, diurnal, constant χ , calibration)
- (e) month and year.

4.8.3.2 At present the international interchange rules for absorption (A1) are as follows.

Requested are:

- (a) Monthly tables of noon observations in one of the following forms:
 - (i) For one or two frequency programs: Tables of each frequency of absorption loss A in dB, sample count, and virtual height, together with monthly medians, median count and quartiles of A , and the calibration constants for the month.
 - (ii) For multi-frequency programs: Tables of absorption loss A in dB for all frequencies, plus corresponding tables of virtual heights, together with monthly medians, median count and quartiles of A , and the adopted calibration constants for the month.
- (b) Summary of calibration constants.
- (c) For stations making continuous recording of absorption, hourly values of absorption loss A in dB for each frequency should be tabulated together with monthly medians, median count and quartiles for each hour based on all the days listed. If this analysis is not made, copies of the original recordings may be substituted provided that adequate intensity and time scales are included (refers to methods A2 and A3).
- (d) For manual stations the highest priority is to make and circulate noon data. The next priority must be determined by local conditions and should be chosen from:
 - (i) measurements, preferably equally spaced about noon, at times which enable the diurnal variation to be checked,
 - (ii) measurements at constant solar zenith angle, for example 75° (these are difficult to organize but scientifically most useful),
 - (iii) diurnal variation measurements for at least five days per month, giving priority to the RWDs.

The resulting data should be displayed in appropriate tables, together with monthly medians, median count and quartiles. Changes in recommended program or in data interchange are published periodically in the *Guide to International Exchange of Data in Solar-Terrestrial Physics* obtainable from the WDCs, current issues; STP Notes. Special programs are published in the International Calendar, issued yearly, URSI Bulletin, INAG Bulletin and STP Notes.

Data transmitted to a WDC are available to all interested scientists from all countries. It is, of course, usual to quote the origin of data used for scientific investigations if the latter are published. A list of WDCs with addresses is found in Appendix III at the end of this volume.

4.8.3.3 A list of stations can be obtained on request from the nearest WDC.

4.9 A Few Results

In order to give some idea of what can be achieved with A1 measurements, we give in the following a short description of a few results obtained from such observations. It is, of course, not intended to give a summary of all published data or of the scientific conclusions obtained from these. Such summaries can be found in the scientific literature [Piggott, 1964; Rawer, 1969 (findings obtained during the years of the Quiet Sun -- IQSY-- 1964/65); Mitra, 1970; Harnischmacher, 1974].

It is our aim in the following paragraphs to give observers some guidance towards interpretation of their measured data and, eventually, warn against misinterpretation.

4.9.1 The absorption loss, A , depends on frequency. With observations on one or two frequencies only, it is not possible to determine A as a function of f . Even with multifrequency measurements it is not quite easily derived. Nevertheless, this function is most important. It should be known for any interpretation of data, even if these have been obtained at a fixed frequency.

Different experimental procedures have been used to determine the frequency dependence of A .

4.9.1.1 Amplitude records in ionograms allow an estimate to be made of instantaneous conditions. Paul [1964] has obtained such records by producing a (logarithmic) amplitude indicator signal which appears in the usual $h'(f)$ plot on the echo traces (see Figure 4.11). There are quick variations which stem from the different causes of fading (see Chapter 3). It appears from Figure 4.11 that these produce quite important variations of amplitude with frequency. It must be noted that the pattern changes quickly with time so that successive records show quite different details. In order to eliminate fading effects and conserve the important features, observations at a fixed frequency must be averaged over some time. For A1 measurements the arrangement should be such that averaging is made after suitable sampling. Apart from this, deviative absorption can be seen near foE , but also near rather small stratifications (often called "ledges"). There is, finally, a general increase of amplitude with increasing frequency, at least near f_{min} at the lower end of the frequency scale. This is the effect of non-deviative absorption. The apparent decrease with increasing frequency above about 4 MHz is, however, due to a technical reason, namely decreasing power of the ionosonde.

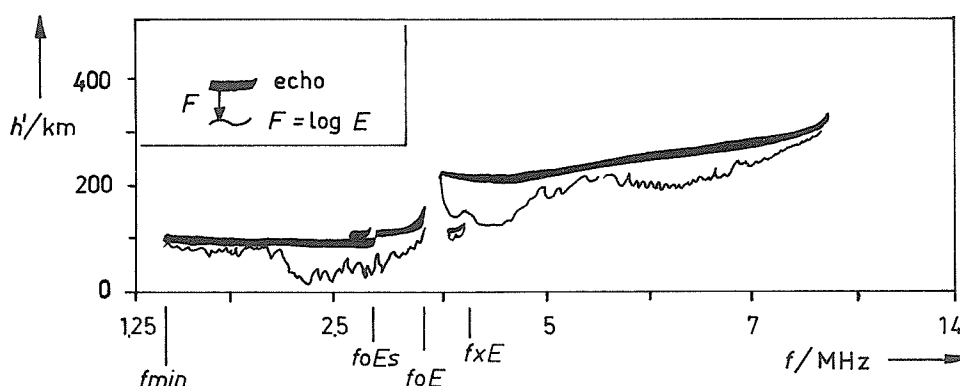


Fig. 4.11 Combined h' and amplitude record for noon conditions obtained by Paul [1964]. Indication of the (logarithmic) amplitudes by the difference between the thick echo trace and the thin curve below.

4.9.1.2 Another source of information is amplitude data at a large number of frequencies, as now automatically produced by digital ionosondes [Bibl, 1971]. These give amplitude (not absorption loss) as a function of frequency and hour. Figure 4.12a shows averaged amplitudes of echoes from the E region in a frequency vs. hour diagram obtained during one day in January where Es did not appear. Absorption means small amplitude, and this is observed near f_{min} at the lower border of the plot. Higher amplitudes corresponding to smaller absorption are found near the upper limit, i.e., at higher frequencies. However, at the upper limit of the plot near foE there appears a quick decrease of amplitude due to deviative absorption.

Figure 4.12b is a similar diagram obtained the same day for echoes from the F region. Contrary to the E region one gets nighttime data of considerably greater amplitude than found by day. Highest amplitudes occur between after midnight and before sunrise hours. For this reason A1 calibration measurements are usually made during these hours. By comparison with daytime amplitude data one may derive absorption loss values of about 20 dB near 3.5 MHz and somewhat larger near 3 MHz. Going up in frequency, there is a slow increase with frequency of daytime amplitude (with maximum in the 6 to 8 MHz range). This is explained by the combined influences of absorption decreasing with increasing frequency and a technical decrease of transmitted power (which is much less important here than for the equipment which produced the data used in Figure 4.11).

4.9.1.3 We may summarize by saying that the main features of non-deviative (D region) and deviative (E region) absorption described in Chapter 2 are clearly visible in $A(f, t)$ plots. However, other features are superposed. These are due to fading on the one hand and to particular instantaneous structures in the ionosphere on the other. "Traveling disturbances" probably produced by internal gravity waves in the atmosphere may be the explanation for most of these latter. It is these features which make it so difficult to reach complete interpretation with isolated observations on a fixed frequency.

4.9.2 The diurnal variation is not regularly observed at most A1 stations, at least not day-by-day. If it is, it often suffers from the deforming influence of deviative absorption and of "ledges", as has been shown in Section 4.9.1.1 above. Monthly mass plots show considerable spread, but also a

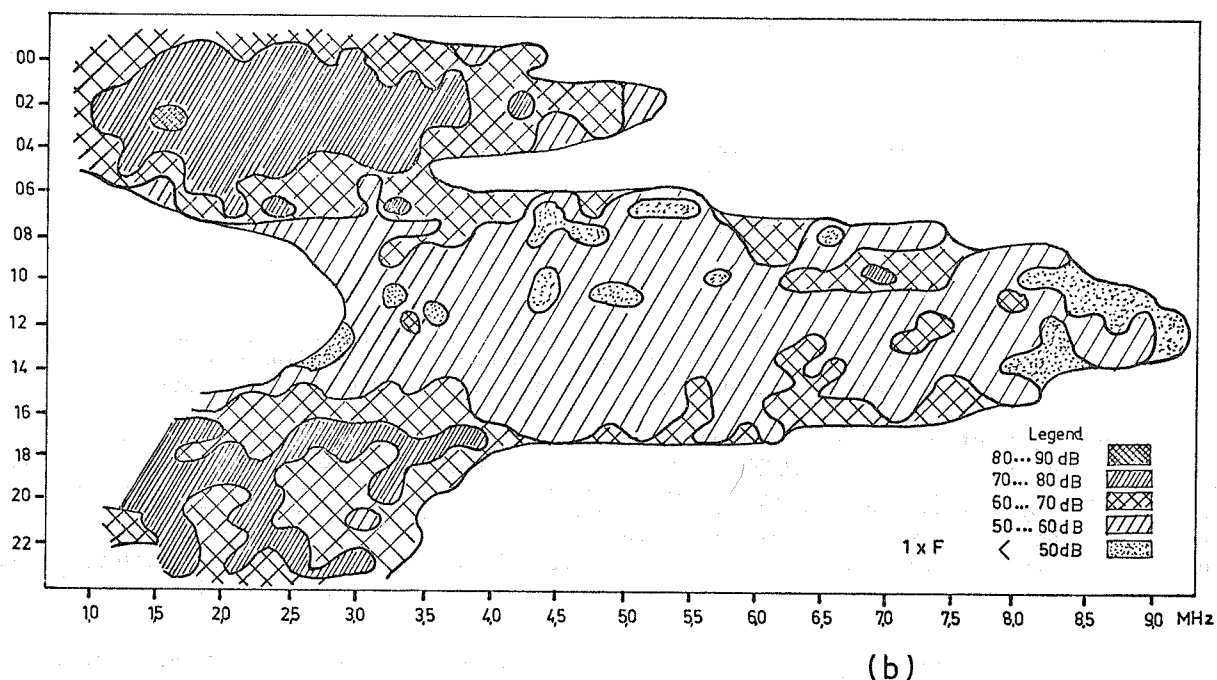
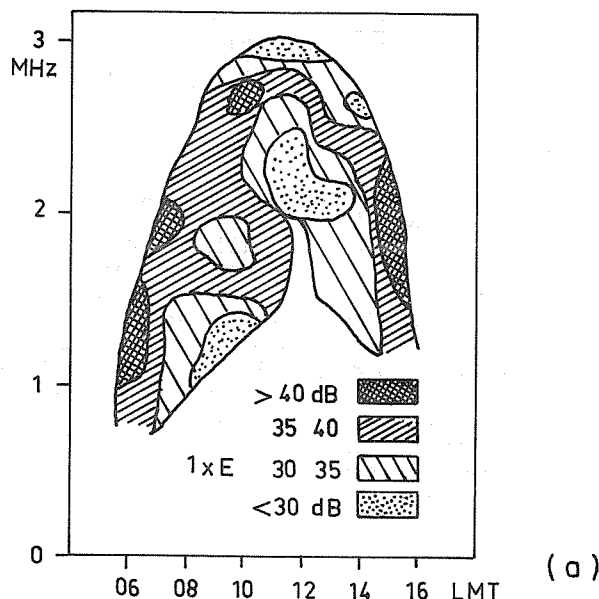


Fig. 4.12 Average echo amplitudes in a frequency vs. hour diagram obtained 10 January 1970 at Freiburg with a Bibl digisonde.

- (a) echo from the E region (essentially normal E echoes)
 (b) echo from the F region.

regular diurnal variation clearly exhibiting solar zenith angle control (see Figure 4.13). The conclusion is that diurnal variations observed on one fixed frequency are not accessible to simple interpretation but need more involved procedures distinguishing deviative and non-deviative absorption.

4.9.2.1 Figures 4.12 (see Section 4.9.1.2 above) are good examples showing diurnal variation and frequency influence for an individual day. From such digital ionosonde data the variation of received field strength as a function of the hour is easily derived. We show in Figure 4.14 the average diurnal variation on seven frequencies obtained in February 1971 at Freiburg. The increase during daylight hours of absorption with decreasing frequency appears clearly (Harnischmacher, private communication). Figure 4.15 is a more detailed diagram just for 2.1 MHz showing the observed variation of the F2 echo (orig.) and the E and Es echo which appear around noon. Taking account of the fact that the F2 echo stems from greater height, the field strength values have been reduced for this effect. This gives the upper curve labelled (red.) which fits rather well with the Es curve, giving maximum absorption of almost 30 dB around noon. It also appears that Es echoes tend to be stronger than E echoes [Pillet, 1960, 1962].

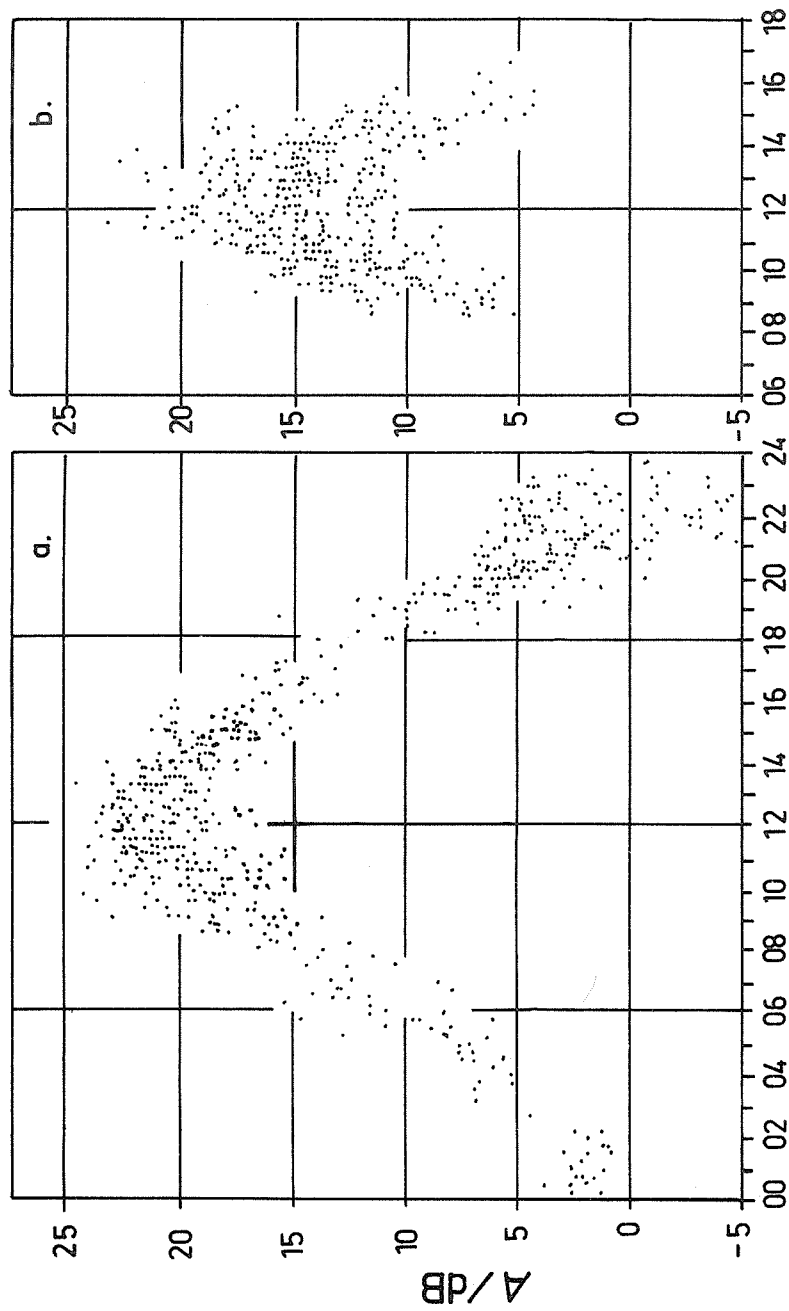


Fig. 4.13 Monthly mass plots of A1 absorption on 3.86 MHz June 1964 (left) and December 1965 (right). Station Juliusruh.

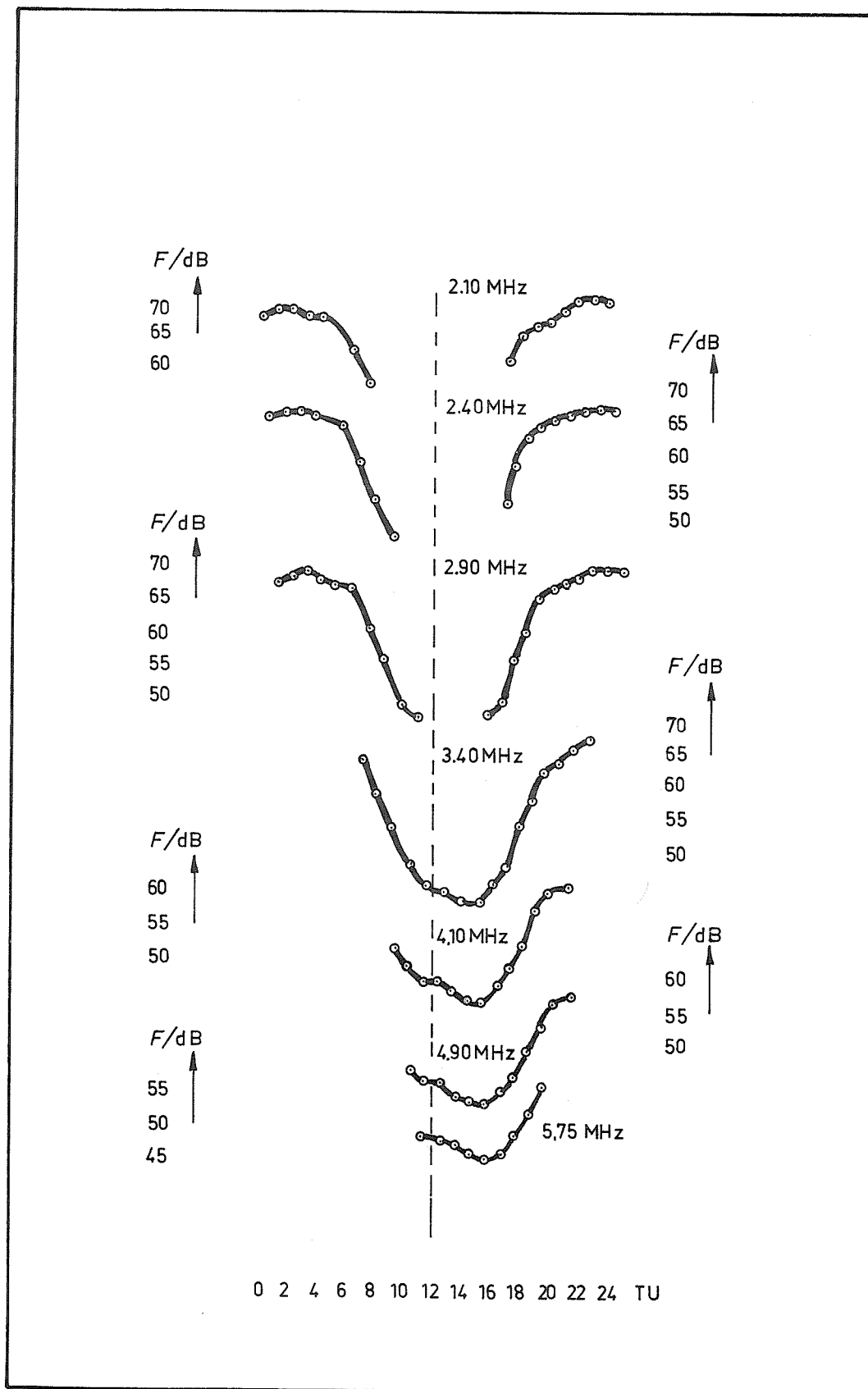


Fig. 4.14 Monthly median variation of F-echo amplitude obtained on seven frequencies by digisonde technique at Freiburg (February 1971).

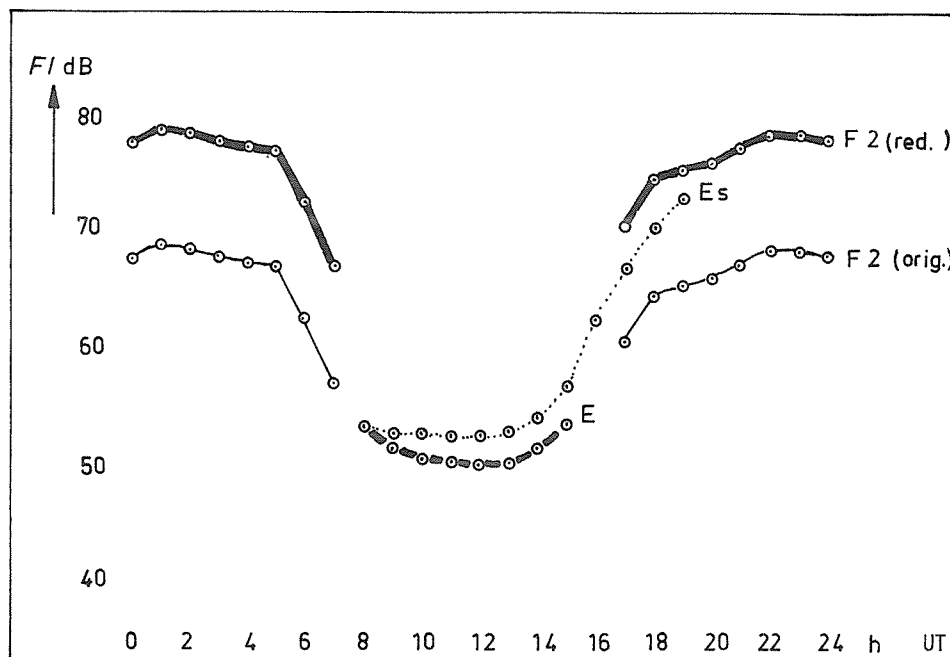


Fig. 4.15 Monthly median variation of echoes from different layers obtained on a frequency of 2.1 MHz (see text).

4.9.2.2 It may be of interest to use the critical frequency of the normal E layer, foE , as a kind of independent variable which could, at least in a crude manner, describe several influences together, namely: diurnal, seasonal (see Section 4.9.3) and solar cycle variation (see Section 4.9.4). This description has first been introduced in connection with propagation prediction problems by Kazanzev [1947, 1956]. See also Sections 4.9.3 and 4.9.4.

4.9.3 A seasonal variation tends to appear with data of slightly more than one month provided the day-to-day fluctuation is averaged out. Figure 4.16a gives digisonde data in a day by hour diagram after averaging over 5-day intervals. Figure 4.16b has been obtained from the same data after a second averaging process over two hours and two 5-day intervals. The seasonal variation is clearly apparent.

Therefore the seasonal variation can also easily be obtained from absorption measurements made at noon only. If undisturbed days are selected, the average variation is remarkably regular but slightly delayed against the solar zenith angle variation (See Figure 4.17).

4.9.3.1 The solar zenith angle controls the seasonal variation to a large extent -- provided the long term influence of the solar cycle (see Section 4.9.4) can be disregarded and the winter anomaly (see Section 4.9.3.3) is not too important. Figures 4.18 through 4.20 have been obtained from multifrequency observations. Schultz and Gallet [1970] first determined the global absorption parameter D (which does not distinguish between deviative and non-deviative contributions, see Eq. (4.13 and 4.14) in Section 4.7.6.1). The sequence of monthly average D values has subsequently been analyzed in terms of long term and seasonal variation, the long term variation, D_{13} , being the sliding average over 13 months; the seasonal variation is then obtained by comparison of the actual value D with the sliding average:

$$I = D/D_{13} \quad (4.15)$$

Finally the I values are ordered and averaged by month, thus giving \bar{I} . In Figures 4.18a,b \bar{I} and $\cos \chi$ are compared. It appears that at middle latitudes a large variation in $\cos \chi$ results in a small variation of absorption, while the opposite is true at low latitude. Figures 4.19a,b,c are double logarithmic graphs of $2 \bar{I}$ against $\frac{1}{2} \cos \chi$. The non-winter months lie very close to a straight line, the slope of which gives a power law in $\cos \chi$:

$$\bar{I} = K \cos^n \chi \quad (4.16)$$

With the data in Figures 4.19a,b,c they find

| | K | n |
|--------------|------|------|
| for Slough | 1.35 | 0.72 |
| for Freiburg | 1.25 | 0.66 |
| for Dakar | 1.10 | 1.53 |

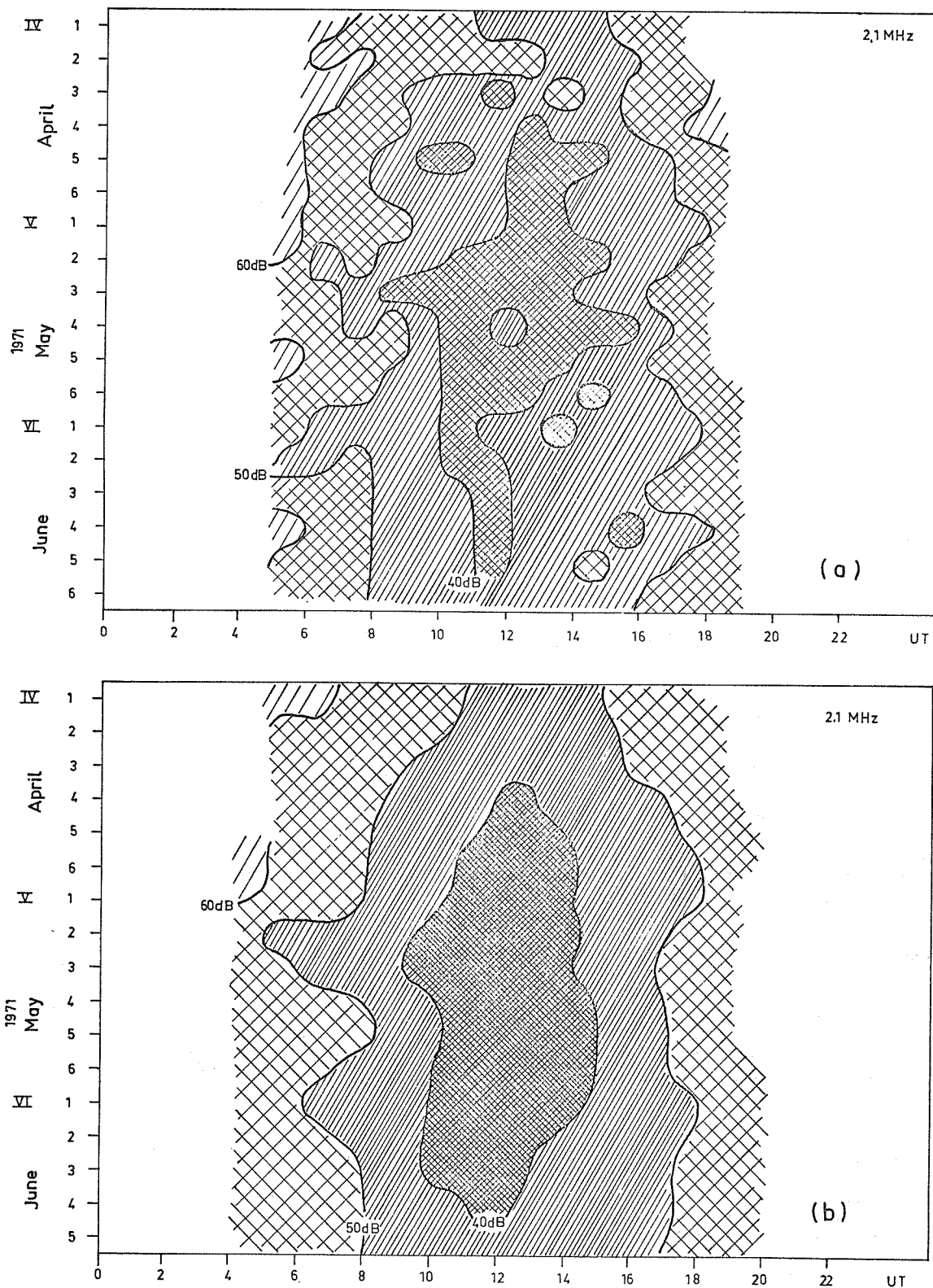


Fig. 4.16 Variation of echo amplitude on 2.1 MHz by day (ordinate) and by hour (abscissa) obtained with digisonde technique at Freiburg
 (a) after averaging once over 5 days
 (b) after a second two-dimensional averaging process over 4 adjacent values [Harnischmacher, 1974].

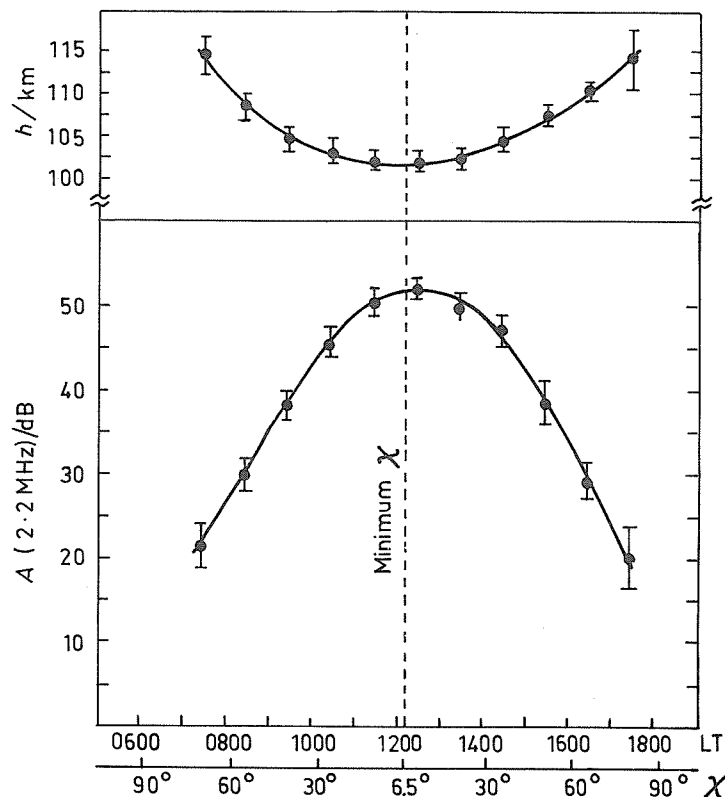


Fig. 4.17 Mean diurnal variation of virtual reflection height and absorption on 2.2 MHz for 15 undisturbed equinoctial days from 1968 through 1970 at Colombo [Gnanalingam, 1972].

At the European stations the winter months deviate markedly from the straight line; this is due to the winter anomaly (see Section 4.9.3.3). The authors introduce a "winter effect coefficient" W , defined by

$$D = D_{13} K \cdot W \cos^n \chi \quad (4.17)$$

where K is independent of the season (but depends on the solar cycle). Typical K values are given above (for W see Section 4.9.3.3 below).

Due to the fact that in the equatorial belt the Sun twice a year reaches $\chi = 0$; the Dakar curve (Figure 4.19c) exhibits two seasonal maxima (see also Figure 4.18b). Figure 4.20 summarizes data from 11 stations analyzed with Eq. (4.16). The exponent n depends on the latitude. A descriptive formula is

$$n = 2 \cdot \cos^{2.4} \chi. \quad (4.18)$$

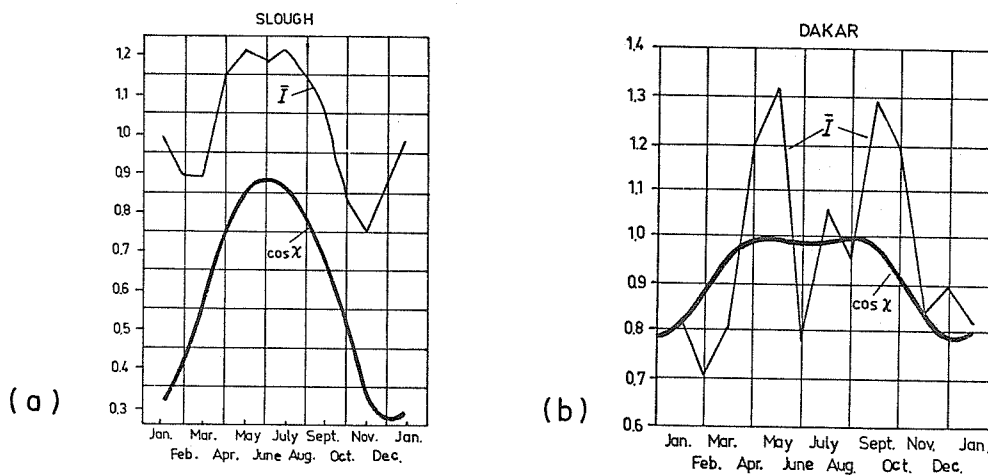


Fig. 4.18 Seasonal component \bar{I} of multifrequency absorption. Parameter D compared with the cosine of the solar zenith angle, $\cos \chi$

- (a) for the temperate latitude station Slough
- (b) for the low latitude station Dakar [Schultz and Gallet, 1970].

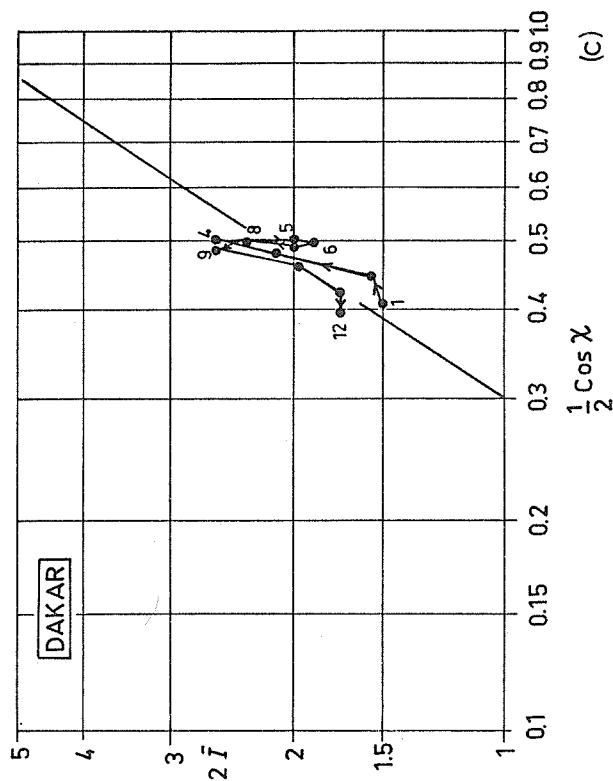
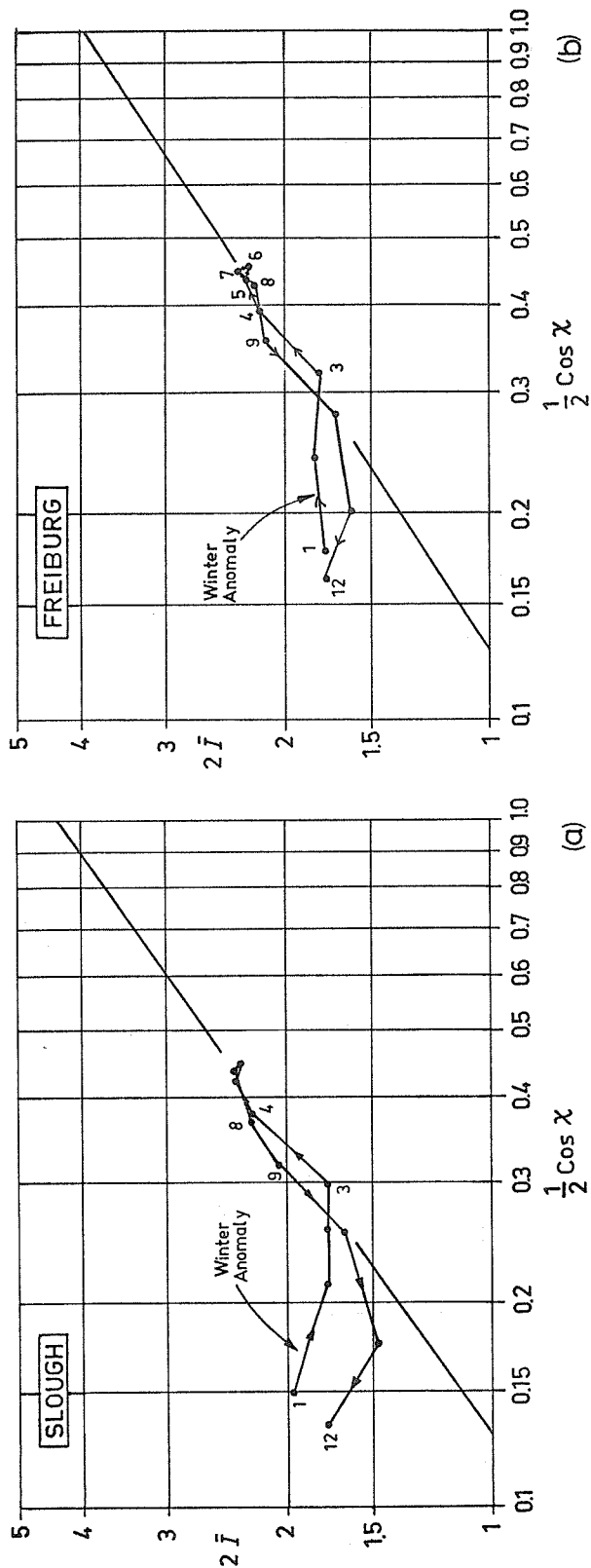


Fig. 4.19 Seasonal variation of absorption (\bar{I} , see Figure 4.18) as a function of $\cos \chi$. Temperate latitude stations Slough (a), Freiburg (b) show winter anomaly; not so the low latitude station Dakar (c). Digits designate month by number [Schultz and Gallet, 1970].

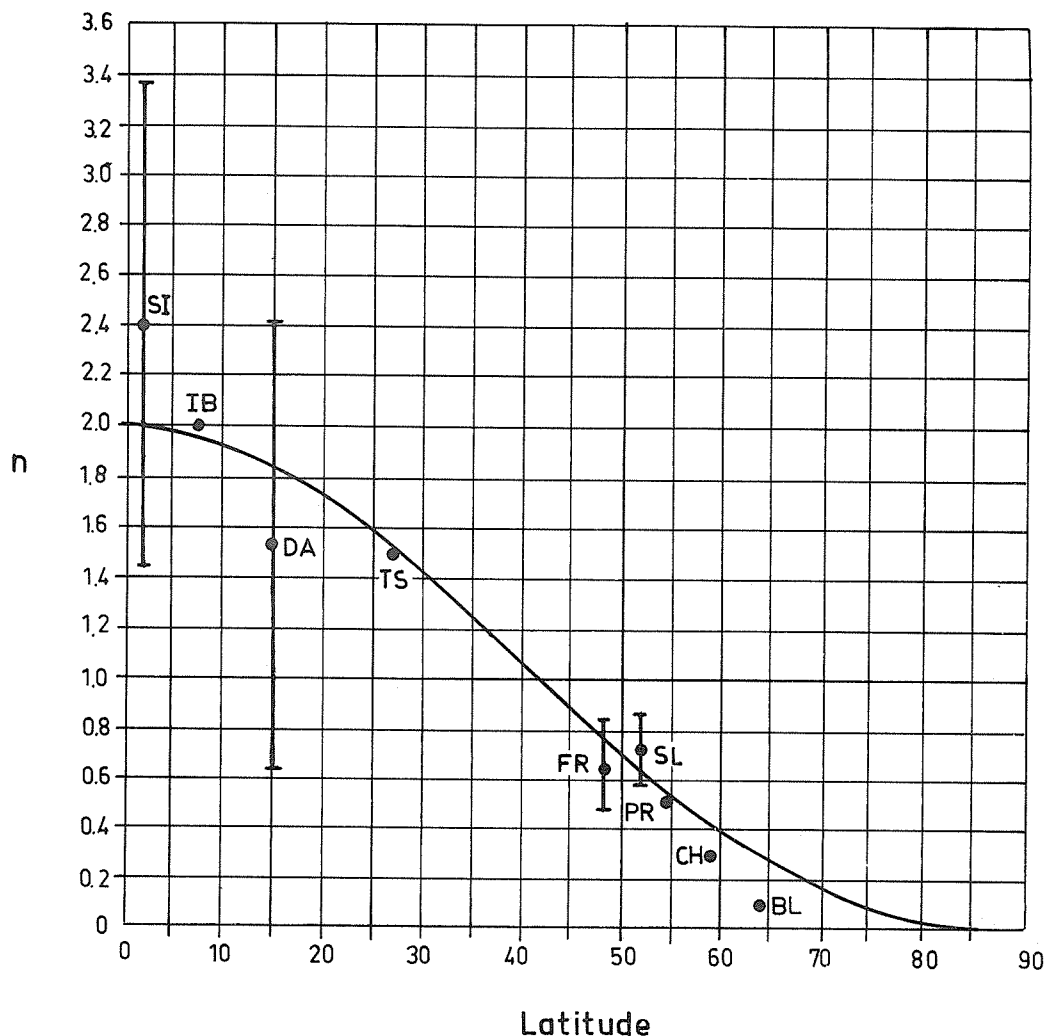


Fig. 4.20 Variation of the exponent n in the seasonal factor $\cos \chi$ with geographic latitude. Each station contributes one point. A range of (95%) confidence is indicated by a vertical bar for those stations for which enough data are available. The curve corresponds to Eq. (4.18). [Schultz and Gallet, 1970].

4.9.3.2 Deviative absorption in the E region often causes a complex behavior. On frequencies below 3 MHz the deviative contribution is larger in winter because then, near noon, f_oE comes nearer to the operational frequency than in summer so that the diurnal variation of A could be opposed to that of $\cos \chi$ (see Figure 4.1, Section 4.1.4). Quite differently, on frequencies slightly above 4 MHz the $\cos \chi$ effect is enlarged because the frequency is nearer to f_oE in summer.

This is quite clearly seen in a summary diagram representing the absorption loss A (parameter) with the monthly median critical frequency f_oE (see Section 4.9.2.2) as abscissa and the operation frequency f as ordinate. Figure 4.21 is an example obtained from routine multifrequency noon observations by statistical averaging of data obtained in 13 years of observation after discrimination according to the monthly mean f_oE value [Harnischmacher and Rawer, 1972]. In order to avoid the winter anomaly (see Section 4.9.3.3 below) only monthly data from six "summer" months (April through September) have been used. In the diagram a "ridge" appears along the line where $f = f_oE$. This is the deviative effect, though smoothed out twice because monthly median A values -- which are smoothed -- have again been averaged. For individual days, the deviative effect is more pronounced (see Figures 4.11 and 4.12a).

4.9.3.3 The winter anomaly concerns D-region absorption mainly. It occurs at subauroral latitudes. The effect has been shown in Figures 4.19a, b and is described in more detail in Chapter 6. It does not occur day-by-day but has a tendency to be present on sequences of consecutive days, thus influencing the average seasonal variation. The seasonal maximum of absorption at a subauroral station may even be found in winter. The overall average seasonal variation then has two maxima, one in summer and one in winter.

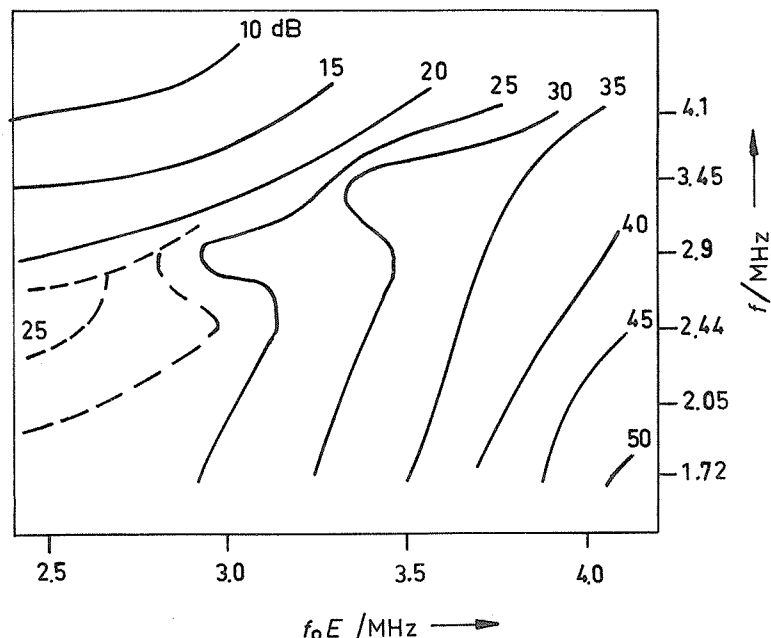


Fig. 4.21 Absorption A as function of the critical frequency f_oE (abscissa) and the operational frequency f (ordinate). Diagram obtained by smoothing of monthly medians of the routine measurements at Freiburg 1956 through 1970. [Harnischmacher and Rawer, 1972].

Applying Eq. (4.17) Schultz and Gallet [1970] find the following values for W :

| | Nov. | Dec. | Jan. | Feb. |
|----------|------|------|------|------|
| Slough | 1.14 | 1.64 | 1.69 | 1.18 |
| Freiburg | 1.18 | 1.48 | 1.39 | 1.17 |

If (with f_oE as independent variable) the seasonal variation in summer is extrapolated into the winter period, one obtains a minimum value of A which is essentially a lower boundary of the dispersion range of individual observed values during the winter period. By subtracting this minimum from observed monthly medians the additional absorption due to the winter anomaly can be derived. Figure 4.22 is a by-product of the analysis which ended with Figure 4.21. At Freiburg in midwinter the averaged anomaly reached a maximum of 25 dB at $f = 2$ MHz (data for a station nearer to the auroral zone can be found in Chapter 6, Sections 6.10.1.3 and 6.10.2, as well as Figures 6.15 and 6.16).

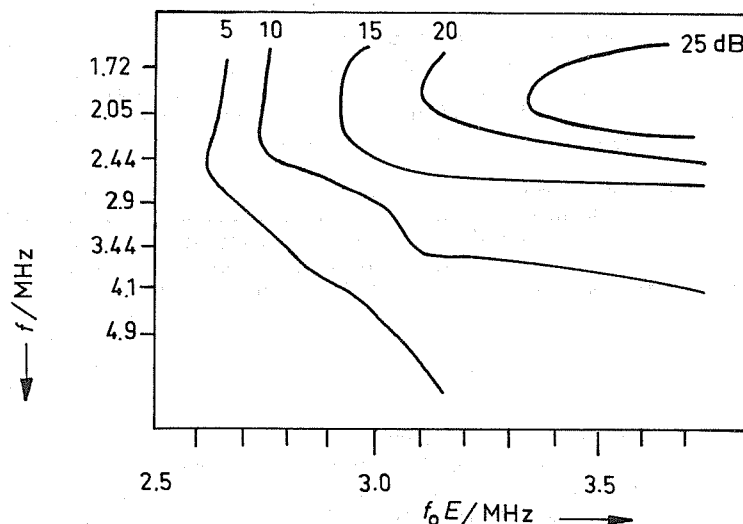


Fig. 4.22 Averaged winter anomaly at Freiburg, obtained after deduction of the overall seasonal behavior. Same data as in Figure 4.21 [Harnischmacher and Rawer, 1972].

4.9.3.4 Since in summer sporadic Es occurs very often, it may also influence the observed seasonal variation. On a lower frequency where echoes normally stem from normal E, conditions are seriously changed in cases where a well-reflecting (low) Es layer cuts off that part of wave path in the E region which gives the main contribution to deviative absorption. Thus, on the average, echoes from Es have greater amplitude than those from normal E, and this means some decrease of absorption loss in the summer statistics (see Figure 4.23 from Pillet [1960]). Similarly for a frequency above f_oE , reflection normally occurs in the F region and is largely influenced by deviative absorption in the underlying E layer. This part is, however, cut off when totally reflecting Es is present (see Figure 4.9, Pillet [1960, 1962]).

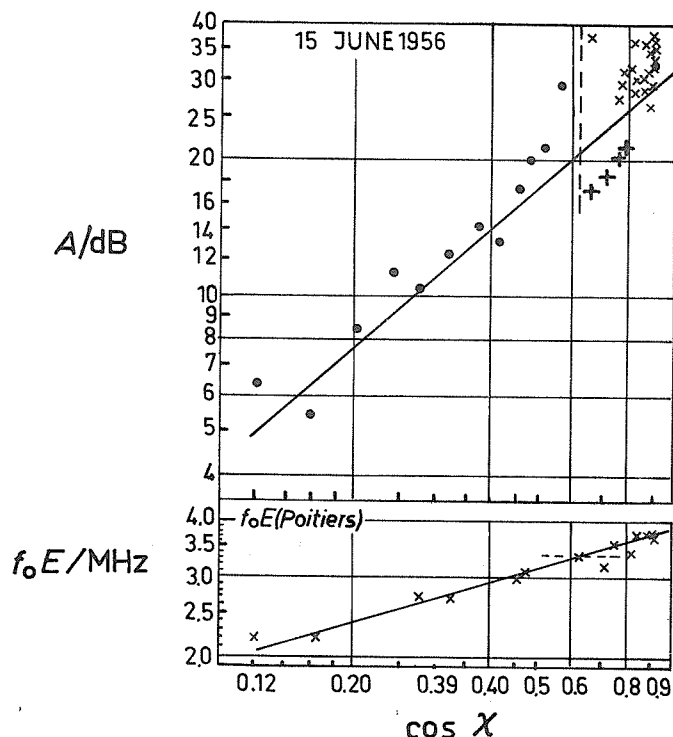


Fig. 4.23 Diurnal variation of absorption on 3.4 MHz, double logarithmic plot against $\cos \chi$ (Poitiers, 15 June 1956). Dots: F-region echoes; oblique crosses: echoes from normal E; vertical crosses: echoes from blanketing Es. Deviative absorption appears with the first two kinds while Es echoes give considerably lower absorption because most of the deviative contributions are cut out [Pillet, 1960].

4.9.3.5 Apart from parameters characterizing the absorption effect, efforts have been made to determine certain physical parameters from absorption results. This is difficult since A is defined as a height integral. Deviative absorption was used to estimate the effective collision frequencies in the E region [Rawer *et al.*, 1952b] but the numerical value depends critically on the shape of the electron density profile.

4.9.4 The long-term variation of absorption is almost entirely due to the variation of solar activity and its eleven year cycle. Solar activity has been characterized by the Zürich "relative sunspot number" R , derived from optical inspection of the Sun's disk. More recently, solar radio noise radiation on 10.7 cm wavelength is often used; this is the "Covington index", ϕ . (The unit of the measurable flux is $10^{-22} \text{ W m}^{-2} \text{ sr}^{-1} \text{ Hz}^{-1}$. CCIR recommends, however, to take ϕ just as a dimensionless parameter characterizing solar activity.)

4.9.4.1 Noon observations in the MF range, e.g., near 2 MHz, show very clearly an increase of absorption with increasing solar activity. On these frequencies at noon absorption mainly occurs in lower layers and is non-deviative. An example (IGY and IQSY measurements on 2.3 MHz) is shown in Figure 4.24.

Conditions are more involved on higher frequencies where the deviative contribution becomes important and, therefore, the variation of the critical frequency f_oE as compared with the working frequency f .

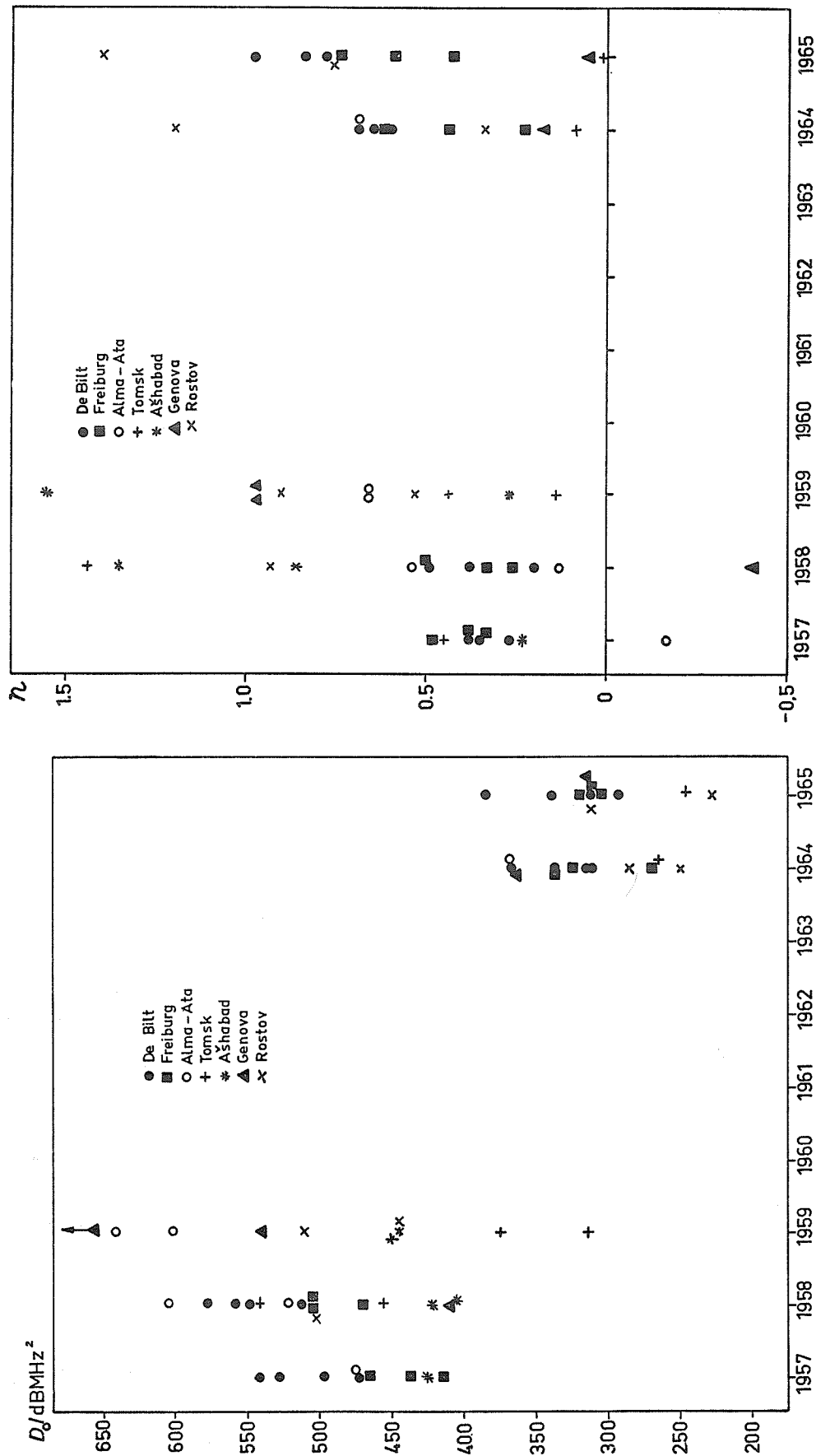


Fig. 4.24 Seasonal and long term variation of absorption on 2.3 MHz at seven (northern) mid-latitude stations described by $D_0 \cos^2 \chi$, for non-winter months. (a) D_0 ; (b) n , 1959 through 1965. Solar activity was maximum 1957/58 and minimum 1964.

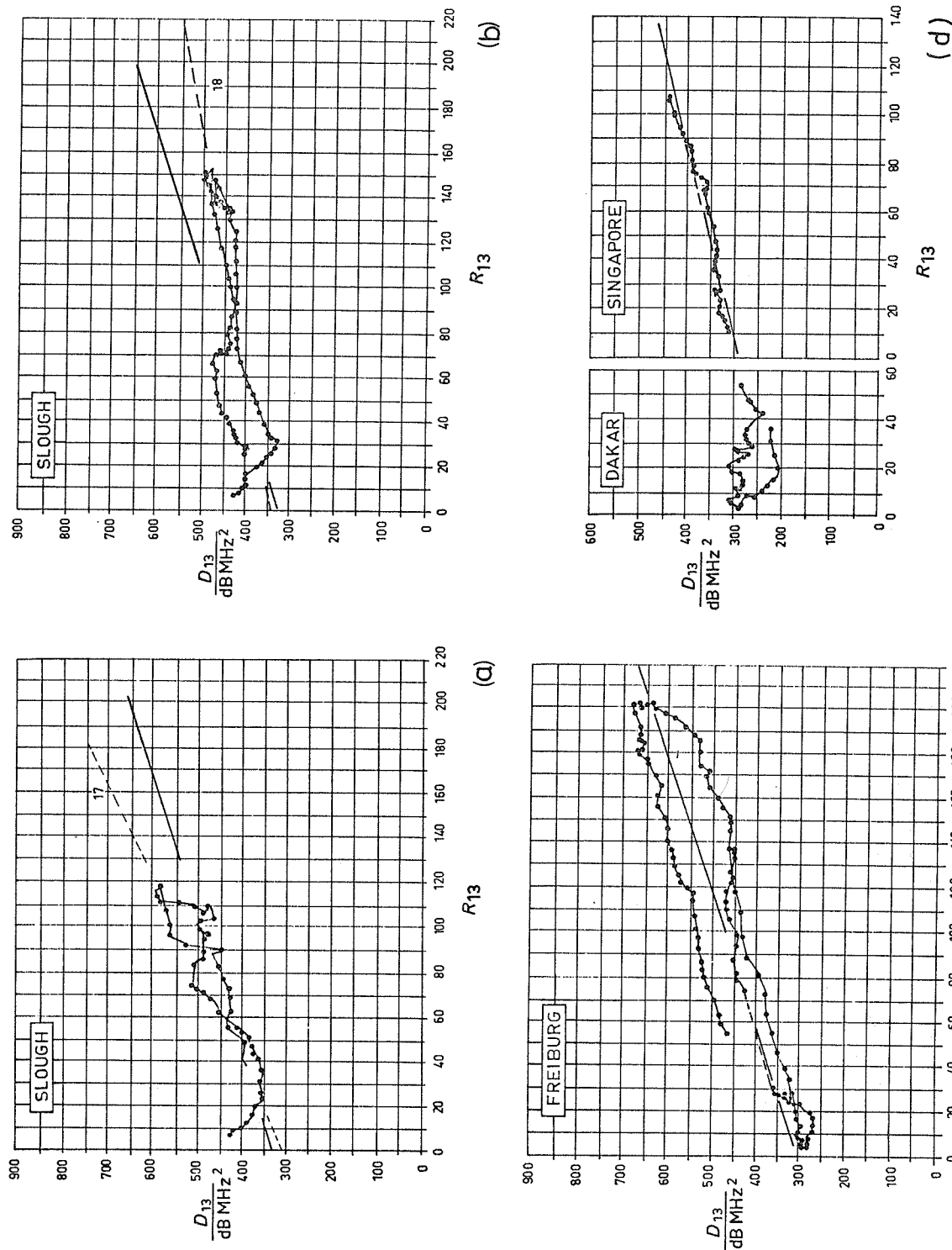


Fig. 4.25 Running averages of global absorption, D_{13} , as a function of equally averaged solar activity R_{13} ; (a) Slough, 1935 through 1944 (sunspot cycle 17); (b) Slough, 1944 through 1953 (sunspot cycle 18); (c) Freiburg, 1949 through 1961; (d) Singapore, 1950 through 1953 (right), and Dakar, 1951 through 1955 (left).

In (a) and (b) the full line gives the average of the whole measuring period of Station Slough. [Schultz and Gallet, 1970].

4.9.4.2 A summary description using f_oE as an indicator of (season and) solar activity has been given in Figure 4.21. This is a better description because the selective absorption peak is better localized in this presentation. Deviative and non-deviative contributions to absorption can be distinguished with multifrequency observations. Once identified, the results obtained may be used when making single frequency observations too. Multifrequency observations made over many years have been described by Appleton and Piggott [1954], by Rawer [1951], by Bibl, Paul and Rawer [1959, 1965] and, recently, by Harnischmacher and Rawer [1972].

4.9.4.2.1 It has been tried to determine non-deviative absorption which has a simple monotonic frequency dependence just by "overlooking" the deviative peaks. This procedure gives, of course, an empirical description by only one parameter, D , which is obtained by assuming all observed absorption to be non-deviative (see Eqs. (4.13) and (4.14) in Section 4.7.6.1). Sliding averages of monthly D values, D_{13} , are well correlated with solar activity, R_{13} (see Figures 4.25a, b, c, d). The relation is approximately linear and may be described by

$$D_{13} = D_0 (1 + bR_{13}). \quad (4.19)$$

Schultz and Gallet [1970] give the following values for the parameters at stations of different latitude:

| | Slough cycle 17 | Slough cycle 18 | Slough all data | Freiburg | Singapore | Dakar |
|------------------------------|--------------------|--------------------|--------------------|----------|-----------|-------|
| D_0 dB MHz ² | 303 | 342 | 326 | 304 | 289 | 270 |
| $1000 \cdot b$ | 8.04 | 2.75 | 5.02 | 5.5 | 4.43 | |

Figure 4.26 shows results obtained for a low latitude station by comparing with the Covington index (deduced from solar radio flux on 10.7 cm wavelength). In this figure D has been transformed by Eq. (4.13) to a hypothetical absorption loss value on 2.2 MHz.

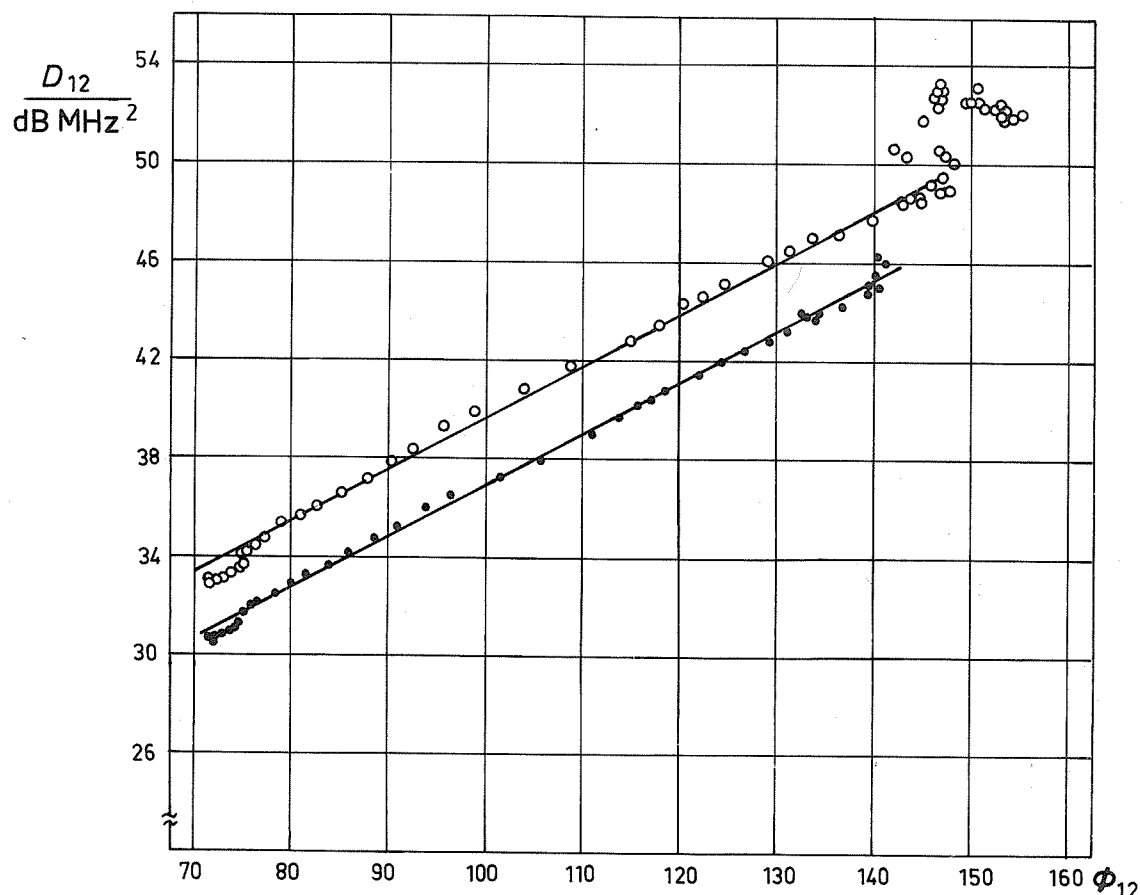


Fig. 4.26 12 months running average of multifrequency absorption at noon (normalized to 2.2 MHz) against the same average of the Covington index. Colombo, 1964 through 1970 (circles). The dots have been obtained from the 10 days by month showing smallest absorption (1964 through 1968). [Gnanalingam, 1972].

4.9.4.2.2 Another more involved approach distinguishes both contributions by building a model theory. One then tries to adapt the results of theory to the observed data. B and C of Eq. (2.18) (see also Section 4.7.6.2) are parameters intended to separate the non-deviative contribution, B , occurring in the D and lower E region from the deviative one, C , of the E region. More detailed explanations have been given in Chapter 2, Section 2.6.4. In order to obtain usable rules, certain model hypotheses have been used. These may influence the results to a certain extent, but not too much. B and C are clearly dependent on solar activity. The correlogram against foE shown in Figure 4.27 may be taken as proof: Even without sliding averages the correlation is quite good. Only winter months are aberrant because of the winter anomaly (see Section 4.9.3.3). The long term variation (obtained after averaging out the seasonal effects) shows a clear solar cycle effect for B (see Figure 4.28).

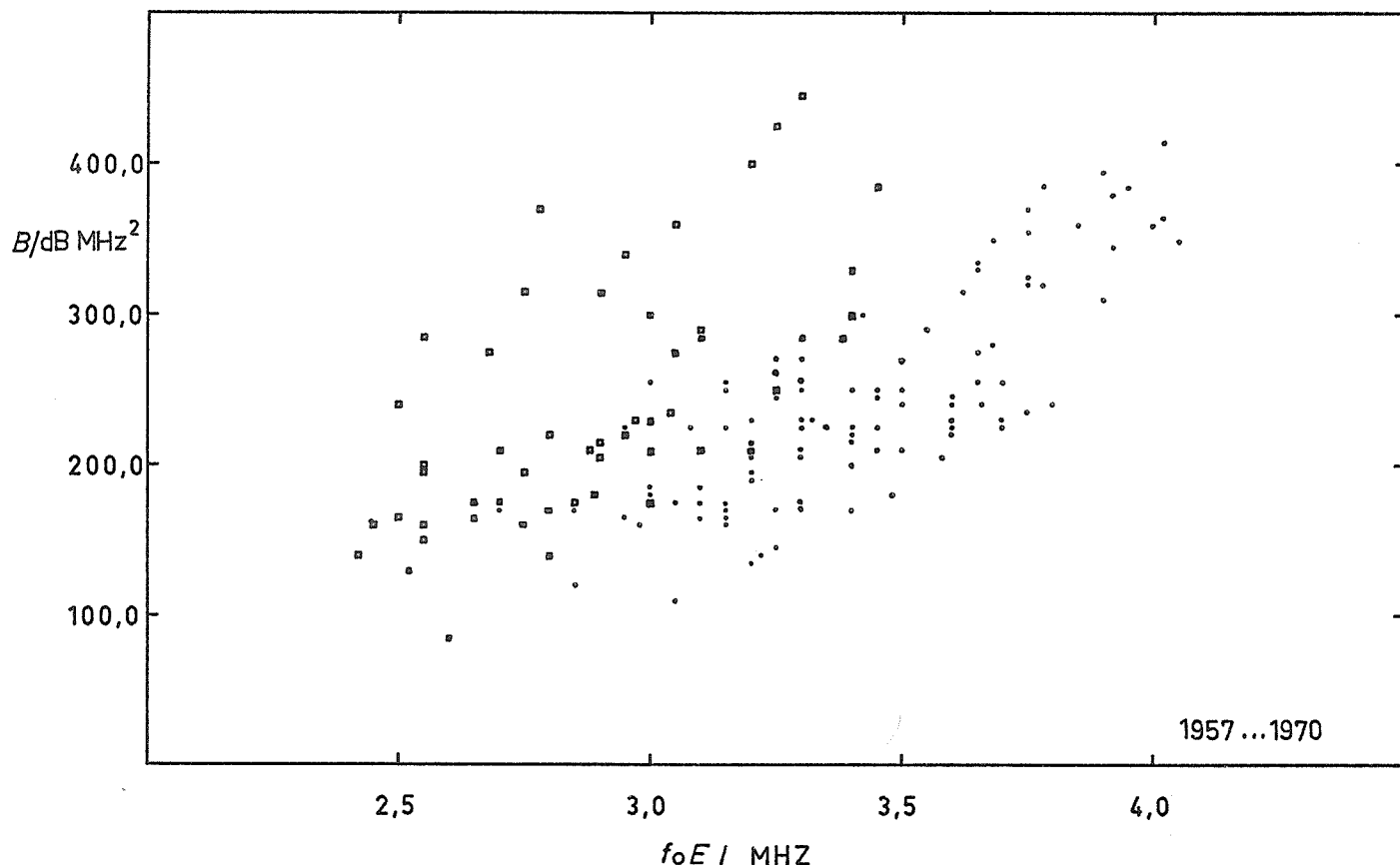


Fig. 4.27 Monthly median noon values of the non-deviative absorption parameter B plotted as correlogram against monthly median noon foE . Freiburg, 1957 through 1970. Dots: non-winter months; squares: winter months.

4.9.5 Though events are better accessible to methods A2 and A3 or other methods of measurement which are continuous in time, A1 observations can give some valuable information.

4.9.5.1 A solar eclipse may be described roughly by saying that night conditions are established during a short daytime period. One expects, therefore, a decrease of ionization in the D region and in the E region simultaneously. The first effect makes the non-deviative absorption decrease, but the second may provoke an increase of deviative absorption. On operating frequencies lower than foE the decrease of foE provokes an increase of deviative absorption. In cases where foE crosses the operating frequency, two peaks both due to deviative absorption tend to appear, one during the decrease of foE at the beginning of the eclipse, the other during the re-increase at the end (see Figure 4.29). This shows that on a fixed frequency eclipse conditions may even give increased absorption. Such data are better interpreted in terms of the parameters B and C of Eq. (2.18). See also Piggott [1956] and Rawer [1956].

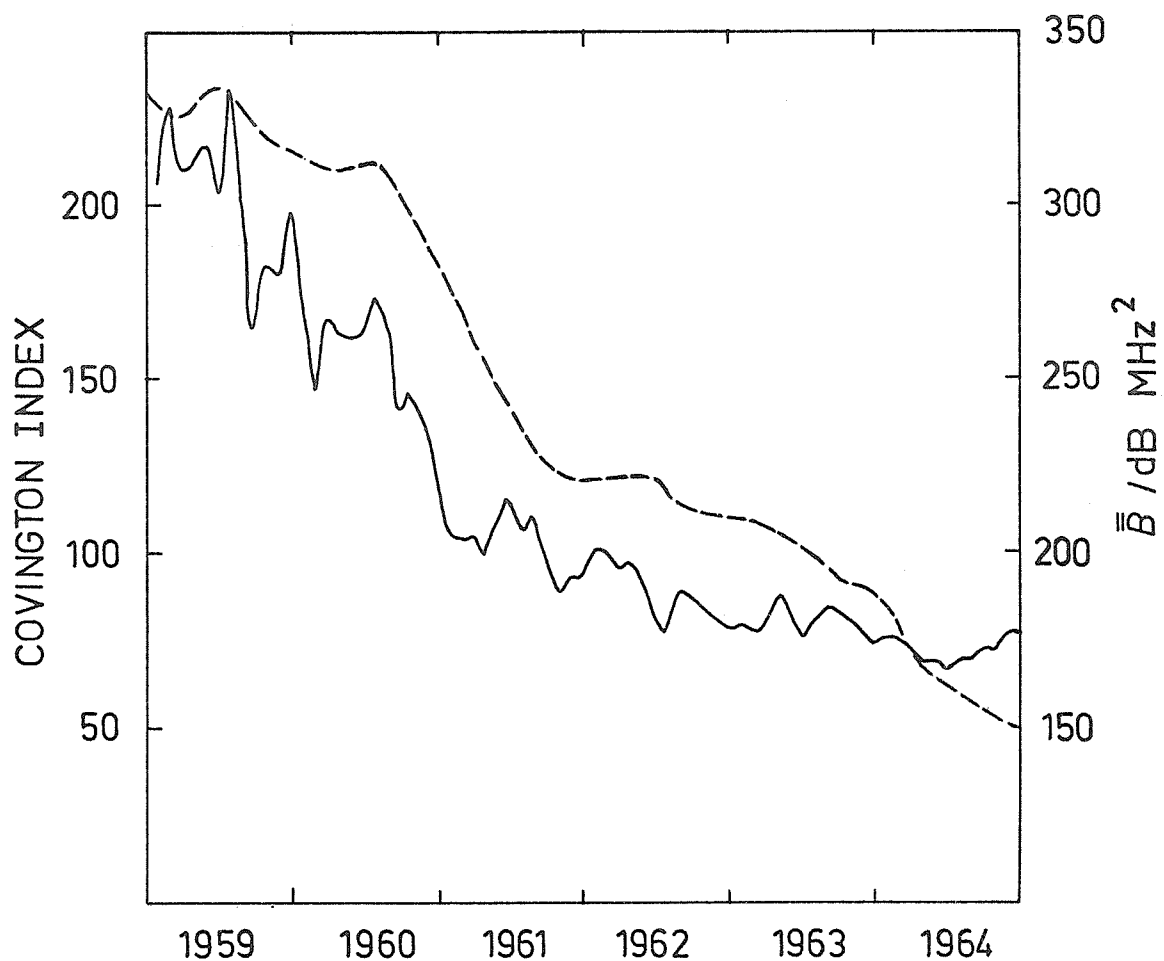


Fig. 4.28 12 months running averages of the non-deviative absorption parameter B measured at Freiburg (broken curve) and the monthly values of the Covington index of solar noise activity (full curve).

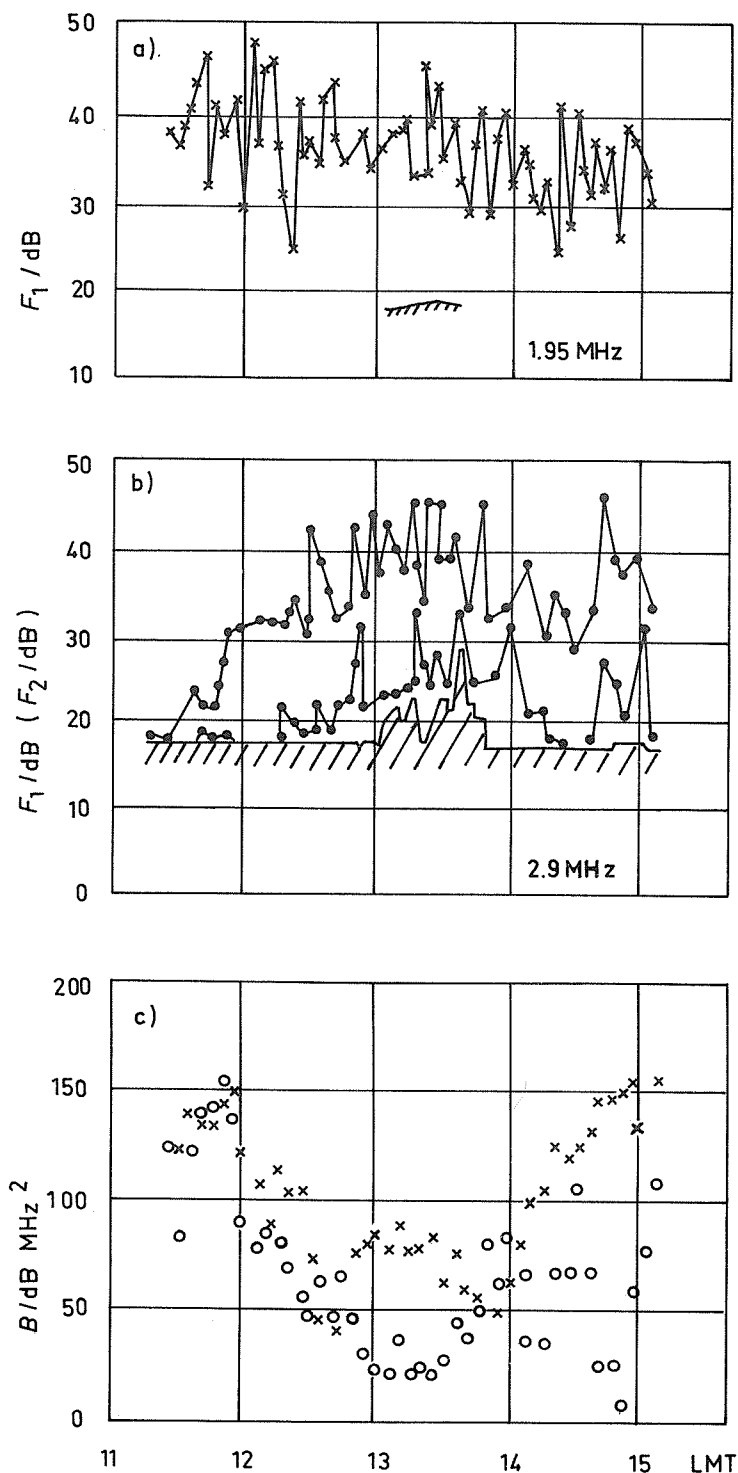


Fig. 4.29 Field strength of first order (F_1) and second order (F_2) echoes observed at Freiburg during the partial solar eclipse of 30 June 1954. (a) for 1.95 MHz (first order only), (b) for 2.9 MHz first and second order, the latter appearing only during the eclipse. The hatched line identifies the observed noise level. (c) gives the parameter B of non-deviative absorption (as found from the observed total absorption A by deducing a model-computed deviative term, taking account of the observed variation of f_oE). While field strength curves are in apparent contradiction, the latter analysis shows rather consistent values of both frequencies: 1.95 MHz crosses, 2.9 MHz circles [Rawer, 1956].

4.9.5.2 A Sudden Ionospheric Disturbance (SID) is a solar flare effect resulting in a considerable increase of non-deviative absorption in an enhanced D region; only a very small increase of E-region ionization is observed simultaneously. The effect has a sudden onset and lasts between a few minutes and half an hour. During strong SIDs no echoes are obtained at all at the frequencies normally used for A1 measurements. Less strong effects are observable (see Figure 4.30). For comparison with solar and other geophysical phenomena precise timing is important. (Better timing can be achieved with methods A2 and A3.) On the other hand, by analyzing multifrequency A1 data in terms of B and C the conditions of D- and E-region absorption can be distinguished as discussed in Section 4.7.6.2. An example is shown in Figure 4.31.

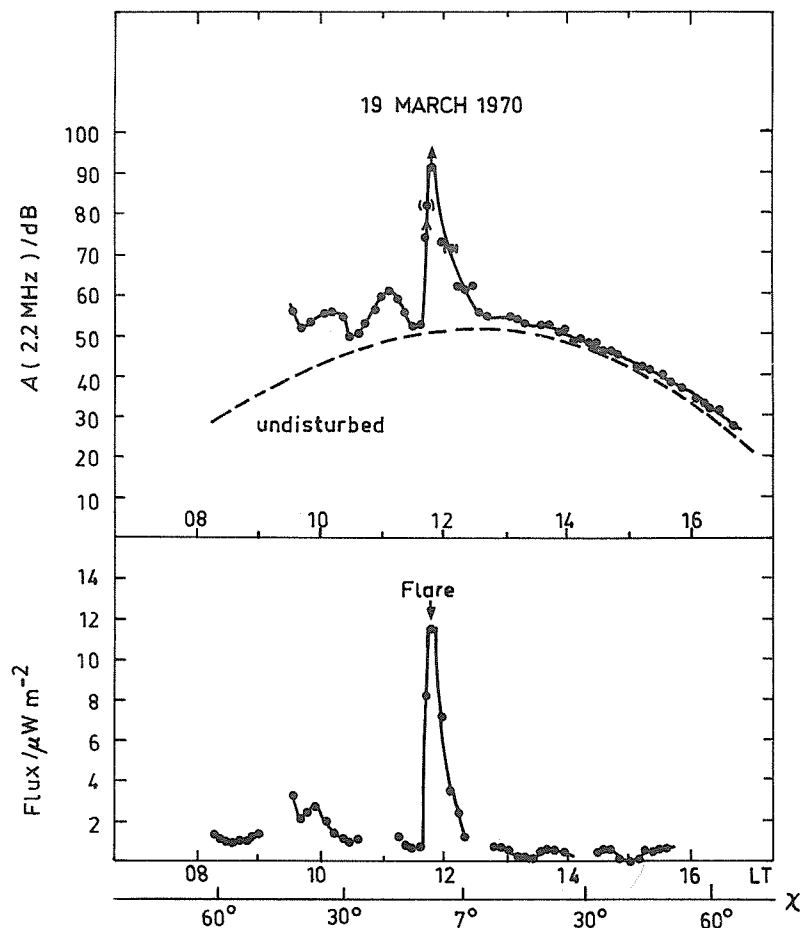


Fig. 4.30 Diurnal variation during SID day at a low latitude station (Colombo). Upper part shows multifrequency absorption characterized by the parameter D but reduced to effective absorption on 2.2 MHz, A . Lower part gives solar soft X-ray flux in the wavelength range 0.1 to 0.8 nm (averaged data from satellite SOLRAD 9). [Gnanalingam, 1972].

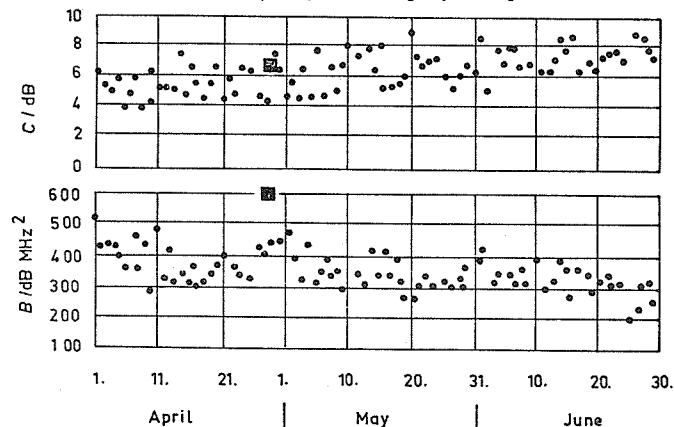


Fig. 4.31 Daily noon values of deviative and non-deviative absorption parameters C and B (Freiburg, summer 1958). The two squares identify an SID event of medium strength. [Bibl, Paul and Rawer, 1959].

4.9.5.3 Auroral and other polar disturbances produce highly variable, localized "patches" of strong absorption due to energetic corpuscles, electrons mainly, reaching the lower ionosphere and increasing the ionization considerably. Method A1 allows moderate events to be followed but breaks down for strong events because then absorption becomes so strong that almost no echoes appear. Method A2 is better adapted to these conditions.

4.9.6 Intercomparison of data between distant stations may give information about the dependence of absorption on the geographic location [Rawer, 1951; Piggott, 1955b, 1960, 1964; Delobau and Suchy, 1956].

4.9.6.1 A short and medium distance intercomparison experiment between European stations was made in 1955 and is reported in Vol. III, part III of the *Annals of the IGY* (p. 218). It showed that at a frequency of 2.4 MHz for undisturbed days the probability of larger deviation from a reference station increased almost linearly with distance and at 1600 km reached about 50% for deviations exceeding 4.5 dB, but only 25% for such of 6 dB and more. Day-to-day changes of absorption were quite coherent over the distance -- though North-South gradients were stronger on disturbed days.

4.9.6.2 At larger distances appreciable and systematic variations have been found. Shirke and Henry [1967] report on 3 MHz data from a ship crossing the geomagnetic equator in the Pacific. Due to the effect of the magnetic field in the Sen-Wyller formula, maximum absorption was expected on the magnetic equator. A minimum was observed instead and a maximum between 10° and 30° of geomagnetic latitude. Also, the character of the diurnal variation was found to be different in both zones.

4.9.6.3 An intercomparison of measurements made on the recommended standard frequency of 2.3 MHz has been made by Piggott. A few results are found in Piggott [1964] and George [1971]. Such measurements allow significant relative variations to be seen and reproduce the influences of solar zenith angle, solar activity, geographic location, and of disturbances.

4.9.6.4 In a multifrequency data reduction with the "Spider Web Method" derived from Eq. (2.18) in a diagram with axes $A/\Delta E$ and $A \cdot (f + f_L)^2$ the measured absorption value A on each frequency determines one straight line. The median intersection point of all lines gives B and C . Piggott [1964] has shown that this gives very good intersection if the magnetic field influence is accounted for in ΔE (see Figure 4.32). See also George [1971], and Samuel and Bradley [1975].

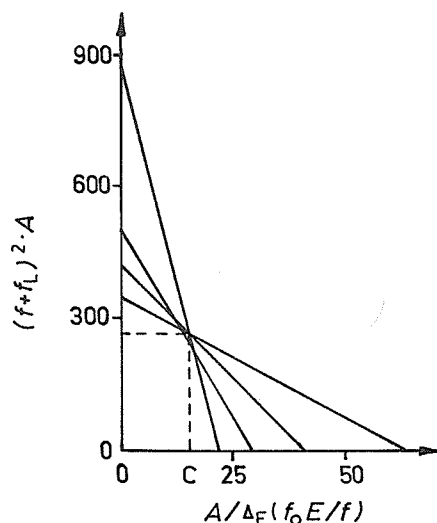


Fig. 4.32 Spider Web nomogram for determining the parameters of non-deviative and deviative absorption, B and C . Inverness at noon during equinox [Piggott, 1964].

4.9.7 Comparison with data from other techniques measuring absorption is encouraged. See Chapter 5 for method A2, Chapters 6 and 7 for A3, Chapter 8 for A4 and Chapter 9 for the new method using emissions from satellites. The techniques differ, however, in particular as their sensitivity to collisional absorption varies with the altitude in the ionosphere.

4.9.7.1 Method A2 uses very high frequency (VHF) waves or frequencies at the upper limit of the HF range. As shown in Section 2.2.5, Figure 2.2, these frequencies have a preference for rather large

collision numbers or large electron density. Therefore A2 is often sensitive to phenomena which play only a minor role for methods A1 and A3 (e.g., very low level ionization). On the other hand, phenomena at higher levels (e.g., attenuation and scattering in the F2 layer) cannot influence A1 or A3 data, but may occasionally be of considerable importance when method A2 is applied. For all these reasons comparisons of A1 and A2 data are not straightforward except for typical events like SID, Polar Cap Absorption (PCA) or auroral blackout.

4.9.7.2 Method A3 compares quite well with A1 data provided the A3 data have been obtained under favorable propagation conditions. The criteria are described in detail in Chapters 6 and 7.

4.9.7.3 Method A4 gives very valuable information concerning the D and lower E region. Therefore data are expected to be comparable with the non-deviative part of A1 absorption. Simultaneous application of both methods at one place would be of great interest (see Chapter 8).

4.9.8 The standard parameter f_{min} is read on all ionograms which are produced according to established international rules [Piggott and Rawer, 1972]. f_{min} is the lowest frequency in the MF/HF range at which the ionosonde is able to identify an ionospheric echo assumed to be due to total reflection.

4.9.8.1 Clearly f_{min} is an absorption parameter. When absorption on lower frequencies increases, the echo amplitude must decrease, often below the minimum detectable value. Since under the circumstances near f_{min} non-deviative absorption is decisive, the decrease of amplitude is greater as the frequency becomes lower. For an ionosonde with frequency independent sensitivity the change in absorption can be directly determined from that of f_{min} . Unfortunately, the transmitted power of practically all ionosondes decreases at the lower end of the frequency range so that two effects are always superposed, one of which is purely due to experimental limitations (antenna dimensions). Since both effects work in the same direction by this superposition, the desired absorption effect is increased and can be more easily identified. However, the relation between f_{min} and absorption loss is rather involved. It cannot simply be deduced from theory.

4.9.8.2 With a reliable sounder, however, it is not too difficult to make an empirical calibration by comparing f_{min} values with absorption losses measured simultaneously on suitable frequencies. The example shown in Figure 4.33 has been obtained by Piggott from routine measurement. The ionosonde was not specially monitored for these observations, and the gains were changed as necessary for the production of good ionograms.

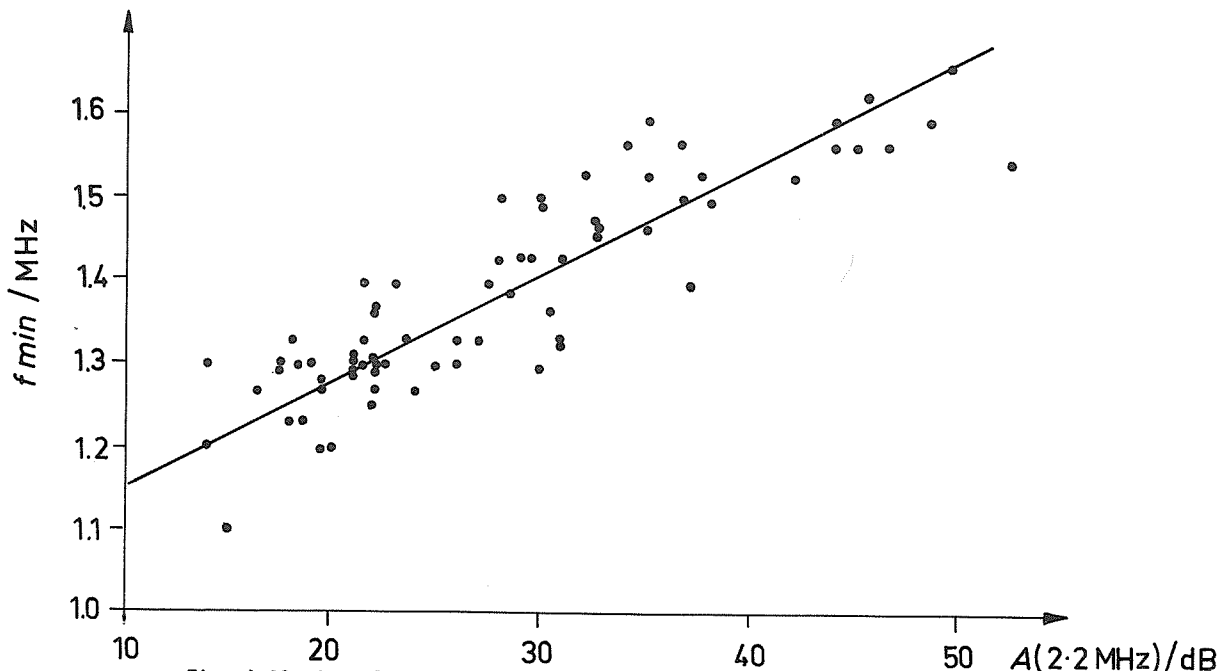


Fig. 4.33 Correlogram of f_{min} and A (2.0 MHz) obtained at Slough during winter 1954/55.

4.9.8.3 More care must be taken if f_{min} data are intended to be used as a quantitative index of (non-deviative) absorption. It is essential that the sensitivity of the ionosonde be kept constant for periods as long as possible. Month-to-month changes in gain should be stated and clearly identified. The inevitable day-to-night adjustment of ionosonde gain should be carried out at the same hour for each day in a given month; switching times must be known. Gain calibration can be achieved by measuring the input at a convenient frequency needed to give a standard output at each of the gain settings used.

4.9.8.4 Care must also be taken that f_{min} is not seriously influenced by interfering unwanted transmitters, in particular by broadcasting stations. Part of the data may be obsolete when f_{min} happens to occur in a broadcasting frequency band.

Transistorized IF Pulse Amplifier

The schematic diagram illustrates a three-stage electronic circuit. The first stage, labeled '1st stage', is an IF 800 kHz amplifier featuring a transformer and a 100 ohm resistor. The second stage, labeled '2nd stage', is a gain setting stage with a 10k resistor and a 10nF capacitor. The third stage, labeled 'phase coherent frequency transposition', includes a 100 kHz output and a 900 kHz oscillator input. The circuit is powered by a 9V battery and includes various resistors and capacitors for signal processing.

Trials to replace transistor stages by integrated circuits have failed to give comparable quality at pulse reproduction.

d.c. Voltage Controlled RF Amplifiers

L. Unger, Freiburg, F.R.G.

4.B.1 Figure 4.35 shows a straightforward RF amplifier, the working point of which is varied by control of the base potential. Downward regulation is not indicated since the input impedance is then seriously influenced; also, overdriving is often reached. Upward regulation is recommended. It avoids overdriving since increasing the emitter current produces an increase of the base-emitter potential so that higher input voltages become feasible. Also cross-modulation remains small. The only disadvantage is that more power is needed for regulation. The working point for low input voltages is chosen at maximum amplification (left in Figure 4.35b). It is important that the tuned circuit at the collector is attenuated by the decoupling $C_C R_C$ combination. Its attenuation increases with increasing collector current. One reaches a 50 to 70 dB regulation range with this device.

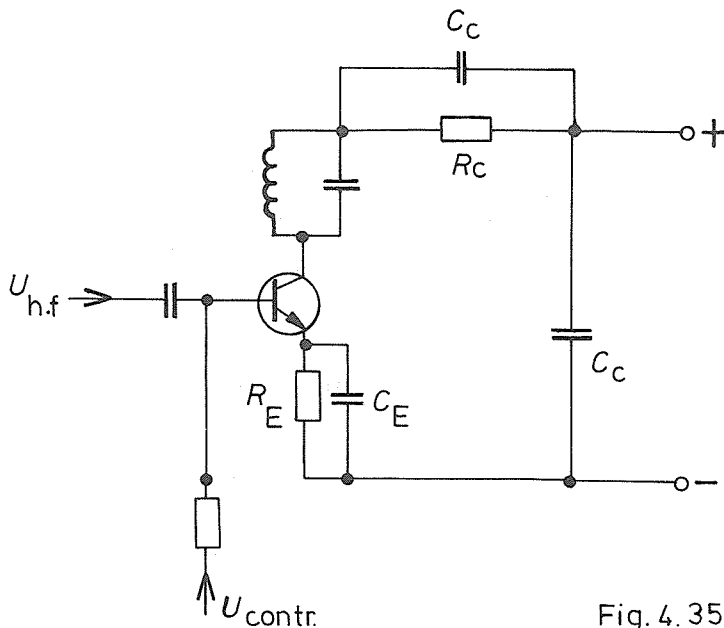


Fig. 4.35a

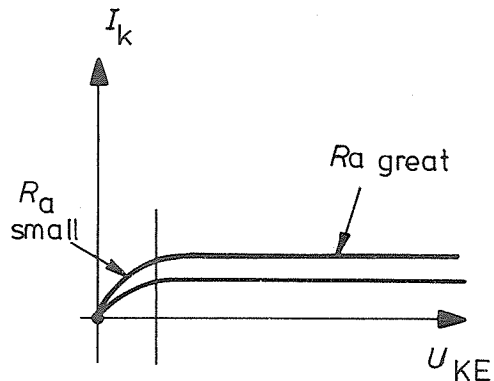


Fig. 4.35b

Fig. 4.35 d.c. regulated RF amplifier with one transistor designed by L. Unger, (a) circuit, (b) characteristic.

4.B.2 Figure 4.36 shows an active two-port network working as a regulated attenuator. The control potential influences the effective impedance ratio of both diodes. This device could be used between the first two amplifying stages of a receiver. For classical IF frequencies pin-diodes may be applied. Attenuators with pin-diodes have two advantages: they admit very reliable and invariable regulation characteristics and have constant input and output impedance. There is, of course, some minimum unavoidable attenuation of about 2 dB, but maximum attenuation can be made as high as 50 dB with cross-modulation of only 1% ($U_E = 1V$). The lower frequency limit with pin-diodes is about 1 MHz. The device has the advantage that the signal-to-noise ratio is improved at low HF inputs.

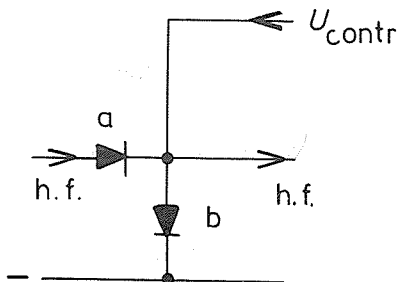


Fig. 4.36 Two-port attenuator with (pin-)diodes designed by L. Unger.

4.B.3 Most integrated circuits do not admit a larger regulation range, usually only 20 to 40 dB (with emitter-followers at input and output). The only integrated circuit series we know which admits better range is the SL600 from Plessey. In Figure 4.37a the integrated circuit is an SL612 admitting a large regulation range with an operating voltage of 5 to 10 V and 10 MHz bandwidth.

A 70 dB range is obtainable at the working point 250 mV with only 1% cross-modulation, amplification being practically linear in a 50 dB range. With the SL611 or SL612 a 40 dB range can be reached even at frequencies above 10 MHz. Suitable working impedances at both sides of the integrated circuit are indicated in Figure 37b.

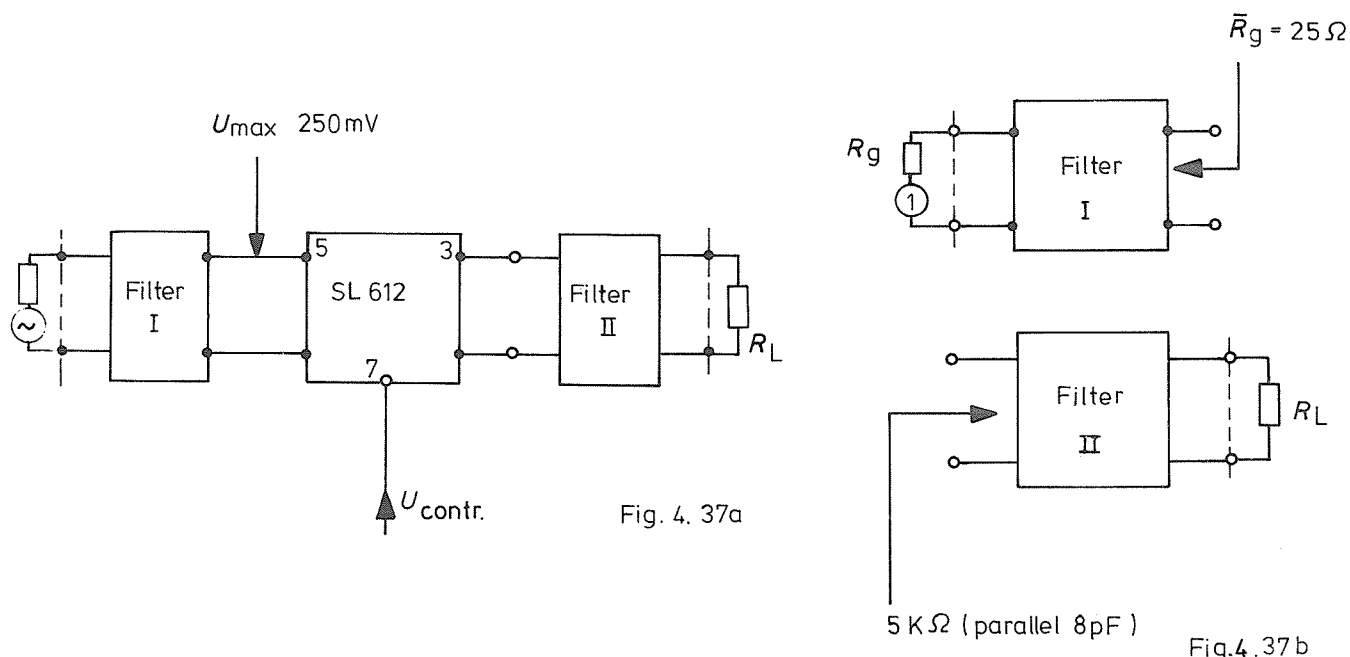


Fig. 4.37 d.c. regulated RF amplifier in integrated circuit techniques designed by L. Unger, (a) full circuit, (b) input and output loading.

Appendix 4.C

Digital Sampling System with Cyclic Commuting of Thresholds

With this automatic device it is intended to determine directly the median pulse amplitude. One uses a set of discriminators adapted to different signal amplitudes, i.e., thresholds which are usually chosen equidistant in dB at the receiver input. A straightforward statistical counting system would require one counter per level. Signals "pass" as long as the echo amplitude is above the threshold; they do not when it is below. A given counter would therefore indicate the number of pulses during the sampling period whose amplitudes exceeded the given level. The median level would be that for which half of the total number of pulses would "pass"; the other half would be rejected. In order to economize counters and sophisticated circuitry, a simplified system is proposed which uses cyclic level commuting. With regularly increasing threshold values (during a cycle) for example, we expect "passing" for the lower threshold values, "non-passing" for the higher ones. Thus the overall probability for echo pulses to "pass" during several full cycles is directly related to the median echo signal level. This statistical statement also remains true when fading is present, except that in this case the order of "passing" (+) and "non-passing" (-) is less regular. We give an example for 10 thresholds distant from each other by 4 dB:

a) No fading, signal just above level 12 dB

| | | | | | | | | | | |
|---|---|---|----|----|----|----|----|----|----|----|
| 0 | 4 | 8 | 12 | 16 | 20 | 24 | 28 | 32 | 36 | dB |
| + | + | + | + | - | - | - | - | - | - | |

b) Fading present, same average level, 6 cycles:

| | | | | | | | | | | |
|--------------|---|---|---|---|---|---|---|---|---|---|
| + | + | - | + | - | + | - | - | - | - | |
| + | + | + | + | + | - | - | - | - | - | |
| + | + | + | + | - | - | - | - | - | - | |
| + | - | + | - | + | - | - | - | - | - | |
| + | + | + | - | - | - | - | - | - | - | |
| + | + | + | + | + | - | + | - | - | - | |
| <hr/> | | | | | | | | | | |
| Total Number | 6 | 5 | 5 | 4 | 3 | 1 | 1 | - | - | - |

The following drawings (designed by H. Afzali during advanced degree research at Breisach) may be considered for further information.

Figure 4.38a is a block diagram of the electronic system.

Figure 4.38b gives the voltage curves for selected points as designated in Figure 4.38a.

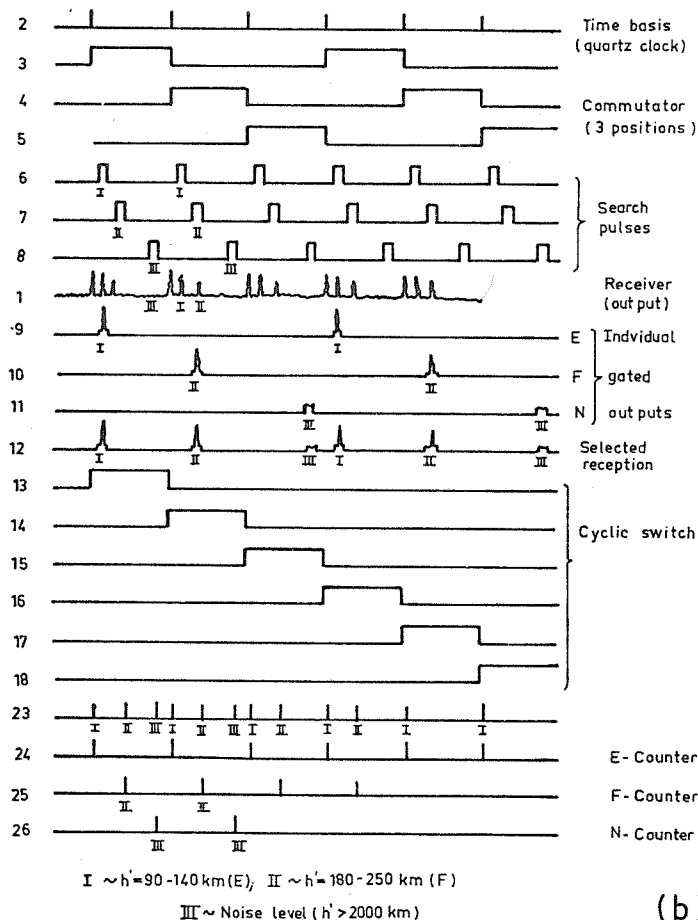
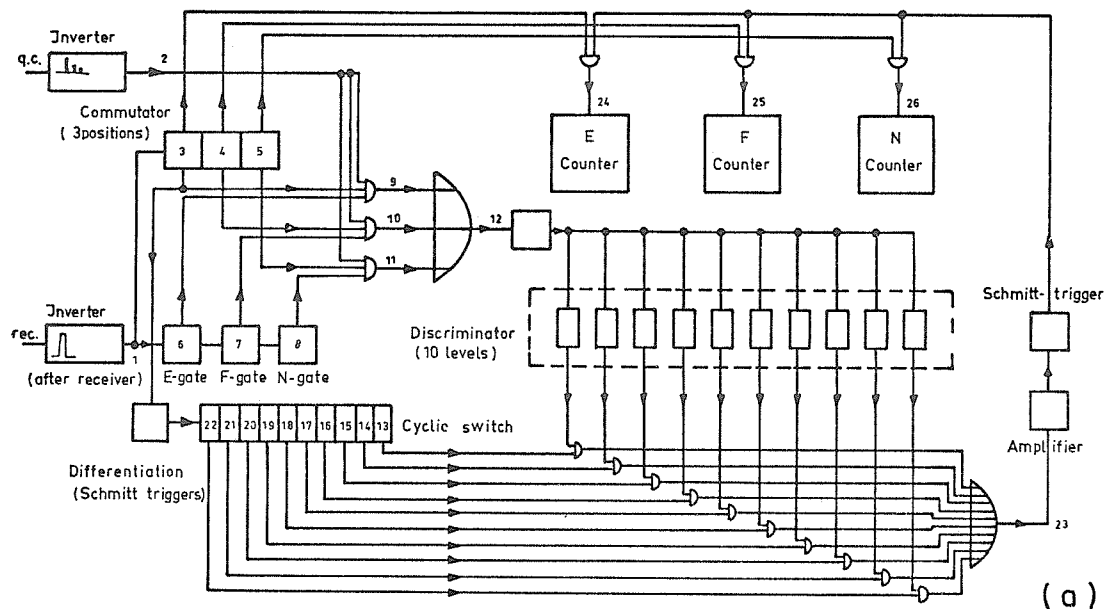


Fig. 4.38 Automatic 10-level pulse height counter designed by H. Afzali, (a) circuit, (b) voltage variations at points indicated in (a).

CHAPTER 5. METHOD A2 (COSMIC NOISE ABSORPTION METHOD)

compiled (1970) by

J. Taubenheim
(former URSI-STP Consultant on Ionospheric Absorption Measurements)
Zentral-Institut für Solar-terrestrische Physik, Berlin-Adlershof, G.D.R.

on the basis of contributions by

G. C. Reid
Aeronomy Laboratory, NOAA, Boulder, Colorado, U.S.A.

A. P. Mitra and Co-workers
Delhi, India

K. R. Ramanathan and Co-workers
Ahmedabad, India

and Others

Table of Contents

| | Page |
|---|------|
| 5.0 Introduction | 106 |
| 5.1 Theory of the A2 Technique | 106 |
| 5.2 Measurement of Cosmic Noise Power -- Principal Problems | 108 |
| 5.3 Receiving Systems | 110 |
| 5.4 Scaling of the Records | 113 |
| 5.5 Interpretation and Scientific Use of A2 Absorption Data | 116 |
| 5.6 Specialized Developments of the A2 Technique | 120 |
| 5.7 International Interchange | 121 |

5.0 Introduction

Instructional material on the theory and operation of the A2 (cosmic noise) method of measuring ionospheric absorption appeared in the *IGY Instruction Manual on the Ionosphere* (Volume III of the *Annals of the International Geophysical Year*), and was subsequently updated in the *IQSY Instruction Manual* (Volume 1 of the *Annals of the IQSY*). The purpose of the present document is to provide an essentially new version of this material which includes recommendations based on the results of many years operation of the A2 technique.

A brief introduction to the theory of the method is followed by a discussion of the techniques recommended for installation and operation of A2 equipment, and by a description of the methods of data reduction that are commonly employed.

5.1 Theory of the A2 Technique

5.1.0 Radio noise of extraterrestrial origin is continuously incident on the top of the ionosphere over an extremely wide range of frequencies. The ionosphere reflects back into space all of the radiation at frequencies below the F-region critical frequency, but cosmic noise at frequencies appreciably above this lower limit can readily be detected by a simple radio receiver at ground level. In the upper HF and lower VHF bands the major contribution to cosmic noise comes from our own galaxy and reaches its maximum signal strength in the direction of the plane of the galaxy (the Milky Way). Smaller contributions are due to the more intense discrete sources of both galactic and extragalactic origin and to the Sun, though on the relatively rare occasions of major solar activity this latter contribution may dominate the noise signal (cf. Section 5.1.2 below). With the exception of the Sun, variable radio sources (like variable radio stars or the planet Jupiter) are found only with the use of high-resolution radio telescopes, which are usually not applied in A2 absorption measurements. The galactic radio noise picked up in the usual antenna beams does not vary with time.

5.1.1 The cosmic radio noise power incident from a given direction in space, as measured with a fixed receiving system on the Earth at a given sidereal time, ought therefore to be constant if there were no absorption in the Earth's atmosphere. Consequently, the strength of cosmic noise actually measured at the surface of the Earth ought to be a reliable indicator of the integrated absorption produced by the intervening ionosphere. This fact was first realized by Shain [1951] in Australia and the temporal variation in absorption was studied by him and by Mitra and Shain [1953] using this technique at a frequency of 18.3 MHz. Since then, the usefulness of the method has been greatly increased by employing servo-comparison techniques as embodied in the "riometer" (see Section 5.3.2 below) developed by Little and Leinbach [1959] primarily for the study of the disturbed high-latitude ionosphere, and a considerable body of literature pertaining to the technique now exists.

5.1.2 Radio noise from the Sun at wavelengths of the order of 10 m can normally be neglected, since the undisturbed noise power from the Sun is less than 1 per cent of the noise power from the diffuse background observed on a wide beam antenna. When active sunspot groups are present, and at the times of solar flares and similar events, however, the Sun's radio output at these frequencies may increase enormously and finally dominate the total noise received, thus rendering the determination of absorption impossible during these times. Since information on ionospheric absorption is often desired at the time of such events, this effect must be regarded as a serious drawback of the measuring technique. It can be limited, however, to the strongest events by making use of an antenna with a polar diagram directed as far away as possible from the ecliptic plane, e.g., an antenna beamed toward the pole star.

5.1.3 A source of variations in received noise power is the scintillation of discrete extra-terrestrial radio sources due to diffraction effects in the ionosphere. These scintillations take the form of variations (period about 30 s) in the intensity of the localized sources, but average out for the diffuse background radiation. When one of the more intense sources such as the Cygnus or Cassiopeia source is in the antenna beam, these scintillations may result in fluctuations of the order of two or three per cent of the input power; however, their effect is rarely serious, since the power received from a source averaged over several fluctuation periods is unaffected by the presence of scintillations.

5.1.4 The intensity of the radio noise originating in the ionosphere will normally be very small compared with that of extraterrestrial radio origin, except perhaps at low frequencies. Usually it can be neglected (see Sections 5.2.1.2 and 5.2.2 below).

5.1.5 The absorption suffered by a radio wave in traversing the ionosphere is usually expressed in decibels (dB), and is found from the expression

$$\frac{A}{\text{dB}} = 10 \log_{10} (P_0/P) \quad (5.1)$$

where P is the signal power received and P_0 is the power that would be received in the absence of the ionosphere. The absorption can be related to the physical parameters of the ionosphere through the dispersion theory in one or other of its forms (see Section 2.2 above). The following relation between

the amplitudes E^* and E of the incident and received waves has been established in Section 2.3:

$$E = E^* \exp(-\int \kappa ds) \quad (2.13)$$

where ds is an element of path length in the ionosphere, κ is the absorption coefficient, and the integration is carried out for the entire path between the source and the receiver. In the range of validity of the CP ("quasi-longitudinal") approximation to the Appleton-Lassen formula (see Section 2.2.3 above) the absorption coefficient is given by Equation (5.2):

$$\kappa = \frac{q^2}{2\epsilon_0 m_e c_0} \frac{1}{\mu} \frac{N\nu}{\nu^2 + (\omega \pm \omega_L)^2} \quad (5.2)$$

The equation is written in rationalized units (κ has m^{-1} for dimensions in SI units). N is the electron number density, ν the electron collision frequency, ω the radio wave angular frequency, ω_L the component of the gyrofrequency vector in the direction of propagation, and μ the refractive index of the medium; q and m_e are respectively the charge and mass of the electron, c_0 the speed of light in free space, and ϵ_0 the permittivity of free space, which is expressed in SI units as $8.86 \cdot 10^{-12} \text{ AsV}^{-1}\text{m}^{-1}$ (i.e. farad per meter). The positive and negative signs in the denominator of Eq. (5.2) refer respectively to the "ordinary" and "extraordinary" components of the received signal (see Section 2.2.2 above). Combining Eqs. (5.1), (2.13) and (5.2) and expressing the constant numerically, we find (see Equation (2.16)):

$$\frac{A}{dB} = 4.58 \cdot 10^{-5} \int \frac{1}{\mu} \frac{N}{m^{-3}} \frac{\nu/s}{\nu^2 + (\omega \pm \omega_L)^2} \frac{ds}{m} \quad (5.3)$$

In the case of cosmic noise observations, which are necessarily confined to frequencies appreciably above the F-region penetration frequency, the absorption is non-deviative and μ can be taken as unity. Also at the commonly used operating frequency of 30 MHz, ω_L can safely be neglected in comparison with ω for most purposes.

Generalized magneto-electronic theory, which includes the effect of the variation of collision frequency with velocity, should be used in preference to the Appleton-Lassen theory if accurate absorption calculations are required. The development by Sen and Wyller [1960] (see Section 2.2.5) is much more adequate under conditions met in the lower ionosphere. For the case of non-deviative absorption (and $\omega \gg \omega_L$), it leads to the replacement of Eq. (5.2) above by (cf. Appendix 2.B.2 above):

$$\kappa = \frac{5q^2 N}{4\epsilon_0 m_e c_0 \omega} \alpha C_{5/2}(\alpha) \quad (5.4)$$

Here α is the dimensionless ratio $(\omega/\hat{\nu})$, and $C_{5/2}(\alpha)$ is one of a class of integrals occurring in semiconductor theory and tabulated by Dingle, Arndt, and Roy [1957] and by Davies [1965]. Relationships between the collision frequencies to be put into the absorption expressions, $\bar{\nu}$ and $\hat{\nu}$ (called ν_m in the literature), are found in Appendix 2.A above.

The quantity $\hat{\nu}$ appearing here is the collision frequency associated with electrons at the peak of the Maxwell-Boltzmann distribution, i.e., of energy kT , where k is Boltzmann's constant and T is the absolute temperature. The altitude profile of $\hat{\nu}$ in the lower ionosphere has been discussed by several authors, e.g., Thrane and Piggott [1966]. For many practical purposes it is quite well approximated in the lower ionosphere by the relation

$$\frac{\hat{\nu}}{s^{-1}} \equiv \frac{\nu_m}{s^{-1}} = 8.40 \cdot 10^7 \frac{p}{\text{Torr}} \quad (5.5)$$

where p is the atmospheric pressure at the height level which is considered. Values for p may be taken from CIRA 1972 (COSPAR International Reference Atmosphere).

Eqs. (5.1), (2.15) and (5.4) lead to the following expression for absorption A :

$$\frac{A}{dB} = \frac{1.149 \cdot 10^{-4}}{\omega/s^{-1}} \int \frac{N}{m^{-3}} \alpha C_{5/2}(\alpha) \frac{ds}{m} \quad (5.6)$$

For convenience a graph of the function $C_{5/2}(\alpha)$ is included as Figure 5.1.

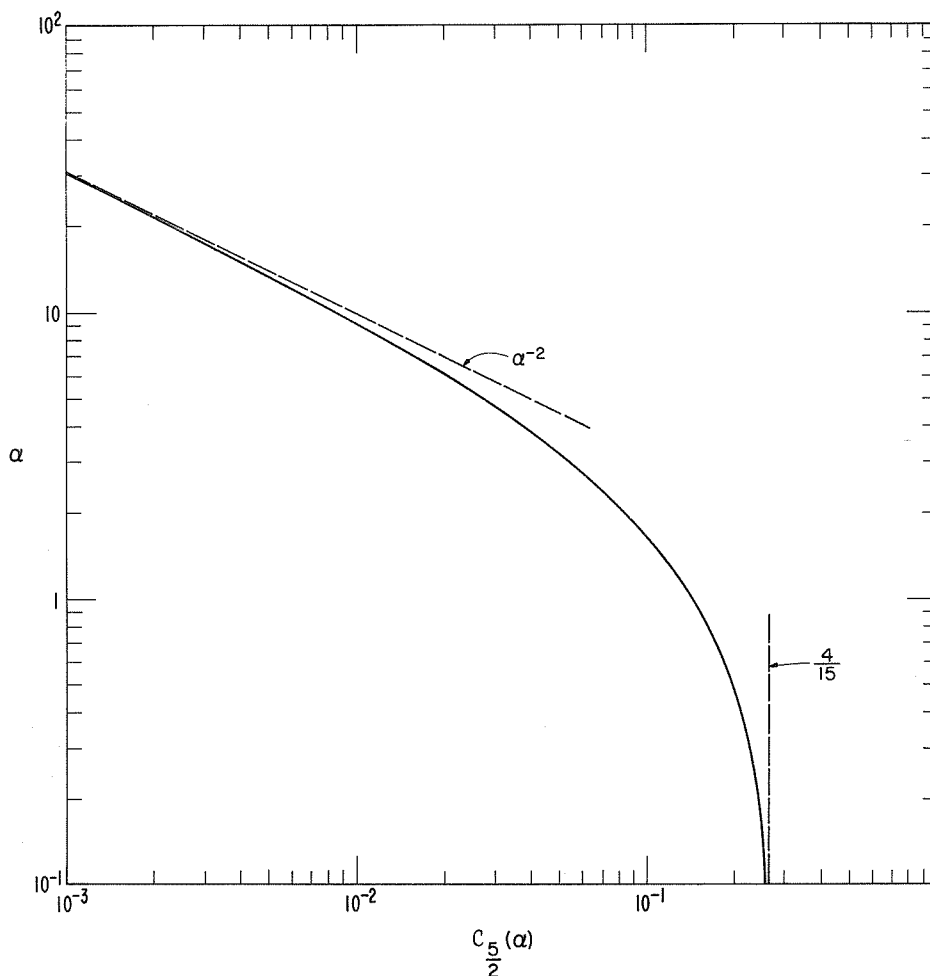


Fig. 5.1 Graph of the function $C_{5/2}(\alpha)$ occurring in the advanced theory of ionospheric absorption (cf. text)

5.2 Measurement of Cosmic Noise Power -- Principal Problems

5.2.0 The relations given in Section 5.1 above allow the calculation of the absorption suffered by a radio wave of any frequency in traversing the ionosphere in any direction, provided that the ionospheric parameters are known. Various practical considerations, however, enter into the measurement of absorption by the A2 technique. Some of the principal problems of cosmic noise power measurement will be discussed in this section, while the following Section (5.3) will deal with the receiving systems in practical use.

5.2.1 It is convenient to use the "equivalent temperature" concept in discussing noise powers. The power of a noise signal can be expressed as

$$P = kTB \quad (5.7)$$

where k is Boltzmann's constant ($k = 1.38 \cdot 10^{-23}$ J/K), B is the effective bandwidth, and T is the equivalent temperature of the noise source. The equivalent temperature of the galaxy is a strong function of frequency, varying approximately as $f^{-2.7}$ from about 30,000 K at 30 MHz to about 200 K at 200 MHz.

5.2.1.1 If the antenna were ideal (without ohmic losses) and the cosmic noise source filled its effective beam, it would be in thermodynamic equilibrium with the source, and its equivalent temperature would be identical to that of the galaxy. In practice, however, all antennas have an efficiency factor less than unity, representing ohmic losses in a fictitious resistor at the ambient temperature, T_a . If we denote this efficiency factor by e , and the galactic equivalent temperature by T_g , then the antenna equivalent temperature becomes $T_{\text{Ant}} = eT_g + (1-e)T_a$. The power from the antenna must be delivered to the receiver through a cable (transmission line) which also has a transmission factor b , less than unity, and a temperature T_c , so that it acts as an attenuator and a generator of radio noise. Thus the power appearing at the receiver input is equivalent to a temperature given by b times the antenna equivalent

temperature plus $(1-b)$ times the cable temperature. Thus even in the absence of the ionosphere the equivalent temperature measured is

$$T_0 = bcT_g + b(1-c) T_a + (1-b) T_c \quad (5.8)$$

instead of simply T_g , as would be measured with an ideal system.

5.2.1.2 In the presence of an absorbing ionosphere an additional complication is introduced. The ionosphere can be thought of as having a transmission factor, a , again less than unity, and a temperature T_i , which is simply the temperature of the electrons in the absorbing region. In this case, the incoming galactic signal, T_g , is replaced by

$$aT_g + (1-a)T_i.$$

Thus the true ionospheric absorption would be given by

$$\frac{A}{dB} = 10 \log_{10} \frac{T_g}{aT_g}. \quad (5.9)$$

The absorption measured by an ideal system with no losses would be

$$\frac{A'}{dB} = 10 \log_{10} \left[\frac{T_g}{aT_g + (1-a) T_i} \right]$$

but the absorption measured by a practical system would be

$$\frac{A''}{dB} = 10 \log_{10} \left[\frac{bcT_g + b(1-c)T_a + (1-b)T_c}{abcT_g + (1-a)bcT_i + b(1-c)T_a + (1-b)T_c} \right] \quad (5.10)$$

5.2.1.3 Finally, the received noise power will add to the noise power generated within the receiver itself, which is given by the expression:

$$P_r = (F-1) kTB \quad (5.11)$$

where T is the room temperature and F is the noise factor of the receiver.

If the above system is now used to observe extraterrestrial radio noise, the total power output of the receiver may be written as:

$$P_0 = G(P_s + P_i + P_a + P_c + P_r + I) \quad (5.12)$$

where

$$P_s = cbaT_s kB \quad - \text{ noise power from the sky}$$

$$T_s \quad - \text{ effective noise temperature of the sky}$$

$$P_i = cb(1-a)T_i kB \quad - \text{ noise power from the ionosphere}$$

$$T_i \quad - \text{ temperature of the absorbing region}$$

$$P_a = b(1-c)T_a kB \quad - \text{ noise power generated by the ambient temperature, } T_a, \text{ at the antenna}$$

$$P_c = (1-b)T_c kB \quad - \text{ noise power from the cable}$$

$$P_r = (F-1)T kB \quad - \text{ noise power from the receiver}$$

$$I \quad - \text{ interference}$$

$$G \quad - \text{ power gain of the receiver.}$$

5.2.2 Under most circumstances, the complicating factors appearing in Eqs. (5.9) through (5.12) can be ignored since the cosmic noise temperature at about 30 MHz ($T_s \sim 10^4$ K) is much higher than any of the other temperatures ($T_i, T_a, T_c \sim 10^2$ K). They cannot be ignored, however, when attempting to measure the intense absorption accompanying some PCA (polar cap absorption) events when the quantity a can become

extremely small or when operating at frequencies much higher than 30 MHz where the galactic equivalent temperature is comparable with the other temperatures. In riometer systems the input noise signal is continuously compared with the output of a local noise diode whose current is adjusted in such a way as to preserve equality between the two signals. In practice the noise power supplied by the diode is augmented by the thermal noise from the diode load resistor, and this can also become an appreciable contribution under conditions of very high absorption when the diode is nearly switched off entirely. It can readily be seen that this contribution partially compensates for the locally generated terms in Eq. (5.10).

Notwithstanding the relatively minor importance of these factors under normal operation of a riometer, care should be taken to minimize their effect by such precautions as employing low-loss antenna feedlines (see Section 5.3.5 below), maintaining good matching at both ends of the cable and ensuring that the diode load resistor is not at an excessively high ambient temperature. In addition, local sources of interference should be avoided as far as possible (see Section 5.3.3 below). If all of these conditions are fulfilled, the absorption measured by a 30 MHz riometer can be safely deduced simply from the ratio of the observed output current to the quiet-day output current provided the absorption is less than about 10 dB.

5.3 Receiving Systems

5.3.0 Taking into account that all unwanted contributions to the total output power in Eq. (5.12) either are small or can be kept small compared with the cosmic noise power, P_s , the measurement of cosmic noise can principally be done by means of any low-loss receiver matched through a low-loss transmission line to an antenna with a fixed upward beam (vertical or oblique, see Section 5.3.5 below), calibrating the receiver with the help of a local standard noise generator, and correcting, if necessary, for the contributions of P_i , P_a , P_c , P_r , and I .

5.3.1 Simple receiving systems of this kind are operated at several stations. For the determination of normal absorption in medium and low latitudes, however, the accuracy depends very critically on the short-term and long-term stability of the receiver gain. Great care must therefore be taken for a proper stabilization of all units of the receiving system by using electronically stabilized power supplies, crystal-controlled local oscillators, temperature stabilization of the equipment, and avoiding variations of the transmission losses between antenna and receiver (e.g., by burying the cable in the ground). Calibrations by means of the noise diode should be made regularly, at least once a day, preferably several times a day, at a sufficient number of fixed output levels covering the whole range of the cosmic noise power normally recorded. Where possible, calibration should be made in such a way that the antenna is replaced by the standard noise source so that the calibration signal is fed through the whole receiving channel including the transmission line. The receiver noise factor is to be kept as low as possible and to be checked frequently. If these requirements cannot be fulfilled, a simple receiving system of this kind may serve as an indicator for short-term absorption effects, like flare effects or auroral and polar absorption events, but it will be useless for an accurate measurement of ionospheric absorption.

5.3.2 The riometer [Machin, Ryle, and Vonberg, 1952; Little and Leinbach, 1959] was developed to avoid the problems of receiver gain stability described in the foregoing paragraph. The essential feature of the riometer is a servo control unit that continuously compares the noise received from the antenna with the noise generated by a local noise diode and adjusts the latter to maintain equality. Variations in receiver gain affect both noise signals equally, and thus only have the second-order effect of changing the amplitude of the "error" signal. Calibration is carried out by replacing the antenna by a second local noise source whose output can be adjusted either manually or automatically to certain pre-set levels; the servo noise source will track these known input signals, producing a calibrated response that can be used to reduce the varying signal recorded by the antenna to actual power levels.

A simplified block diagram of a typical riometer is shown in Figure 5.2. The outputs from the antenna and from the local noise diode are alternately switched into the receiving system through a radio frequency switch controlled by a reference audio oscillator. The error signal resulting from inequality between the two inputs is detected in the receiver, amplified, and applied to a phase detector driven by the same reference oscillator. The phase detector produces a d.c. signal whose polarity is determined by the phase of the error signal, and this is applied to the servo noise diode in such a way as to reduce the error signal to zero, thereby maintaining the noise diode output equal to that of the antenna. The noise power generated by the diode is proportional to its plate current, and this is the quantity normally recorded as the output of the riometer. The chart reading is calibrated in terms of the test diode plate current as described above, and the absorption is then calculated from Eq. (5.1) above, where P is now the square of the observed current, I , and P_0 the squared current that would have been observed in the absence of the ionosphere, as described in Section 5.4 below:

$$\frac{A}{dB} = 20 \log_{10} (I_0/I) \quad (5.1a)$$

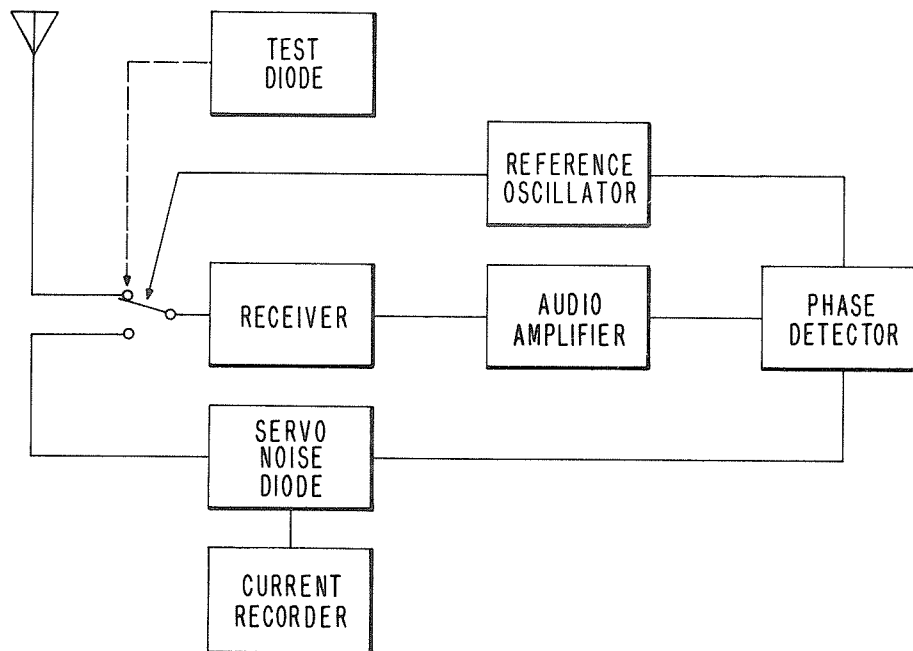


Fig. 5.2 Simplified block diagram of a typical riometer.

5.3.3 Obviously, there are several adjustable parameters in the riometer, and these must be set to the optimum values for the operating conditions. Since noise signals are being measured, there is an inherent statistical fluctuation in the output, given by

$$\frac{\Delta P}{P} = (B\tau)^{-1/2} \quad (5.13)$$

where B is the effective input bandwidth, and τ is the output time constant. This fluctuation can be reduced by increasing either B or τ ; a practical restriction on the input bandwidth is generally the requirement that there be no interfering signals (see below), and the need for a fairly rapid response to changes in absorption similarly restricts the usable range of output time constants. In practice, bandwidths of a few hundred Hz and time constants of a few s have generally been found satisfactory, but interfering signals can often be a serious problem even with these values especially at frequencies below 30 MHz since the wanted signals in this kind of absorption measurement are weak. Whereas local interference by man-made "technical" noise (power lines, electrical machinery etc.) can be largely avoided by choosing an appropriate observing site, the interference by radio communication often raises severe problems. Some riometers therefore use a sweep frequency receiver (with a sweep of a few hundred Hz) combined with a minimum signal detection, and this has been found to produce some improvement in the operation.

5.3.4. The choice of operating frequency is also restricted by practical considerations. Eq. (5.3) indicates that the frequency should be as low as possible if one wishes to detect the effects of weak ionization. An absolute limit is set by the highest critical frequency of the ionosphere (usually f_oF_2), but even at frequencies considerably above this limit, operation is often severely hampered by propagated interference. Experience has shown that a frequency of 30 MHz is normally free of these effects, though during periods of high sunspot number propagated interference may become a serious problem during daytime conditions even at this frequency. Unfortunately the absorption produced by the normal quiet D region of the ionosphere only amounts to a few tenths of a decibel at 30 MHz, and this fact, coupled with the rather regular smooth diurnal variation of this absorption, makes it extremely difficult to measure with precision. Therefore, wherever practical in view of these problems, the use of frequencies somewhat below 30 MHz is desirable.

The riometer, in fact, was designed as a technique for studying the disturbed ionosphere, and especially such high-latitude phenomena as polar cap and auroral absorption associated with particle precipitation. At temperate and low latitudes it also provides an excellent means of studying solar flare effects which are short-term increases in absorption of relatively large magnitude (SCNA = sudden cosmic noise absorption). But studies of the quiet ionospheric absorption should be undertaken only if a considerable amount of time can be devoted to maintaining operation of the equipment at a high level of efficiency or if special efforts can be made as described in Section 5.5 below. Obviously, the study of quiet absorption will be much more efficient with the use of the (more sensitive) methods A1 and A3, where their application is practical.

At the opposite end of the scale, several polar cap absorption (PCA) events during the last decade have produced absorption at 30 MHz that was so intense as to be virtually immeasurable. Continuous monitoring of absorption during an event of this kind requires the addition of a second riometer operating at a considerably higher frequency where the absorption is appreciably less. In practice, a frequency of about 50 MHz has been found to be adequate for this purpose.

5.3.5 The antenna is an important component of the receiving system. Many different types of antennas have been used successfully in the past, and it would probably not be desirable to attempt to standardize the antenna design. It is important, however, to have a reasonable estimate of the pattern of the antenna being used so that the observed absorption can be corrected to the vertical absorption that would be observed by a pencil-beam antenna pointing at the zenith. This latter quantity is the only parameter that can be safely intercompared between stations operating with different equipment, and between riometers operating at different frequencies at the same location. If studies of solar-flare effects (SCNAs) are being contemplated, the possibility of excluding the Sun as far as possible from the antenna beam ought to be investigated, since solar flares are often accompanied by intense outbursts of radio noise covering a very broad band that can include the operating frequency of the riometer. In such cases the cosmic noise signal can be completely obscured for the most critical phase of the event (cf., Section 5.1.2 above).

At temperate and high latitudes this can be avoided to some extent by arranging that the main beam of the antenna point at the celestial pole rather than at the zenith, with the additional advantage that the amplitude of the diurnal variation in cosmic noise signal is minimized and the strong point sources of noise (radio stars) are removed from the most sensitive region of the antenna beam. The chief disadvantage of such an arrangement is the necessity for making a rather large correction to reduce the observations to zenith absorption, and the consequent need for fairly accurate knowledge of the antenna pattern.

5.3.5.1 As an illustration of a fairly typical riometer antenna, Figure 5.3 shows a sketch of a double-dipole design that is in wide use in the high latitude observations. The antenna consists of two center-fed half-wave dipoles spaced 0.4λ apart and 0.15λ above a ground screen. Its pattern is approximately 60° in width between half-power (3 dB) points in all planes and is such that the zenith pencil-beam absorption, A_z , is related to the observed absorption, A_0 , by an approximate expression which has been derived from data presented by Ecklund and Hargreaves [1968]:

$$A_z = 0.67 A_0^{1.06} \quad (5.14)$$

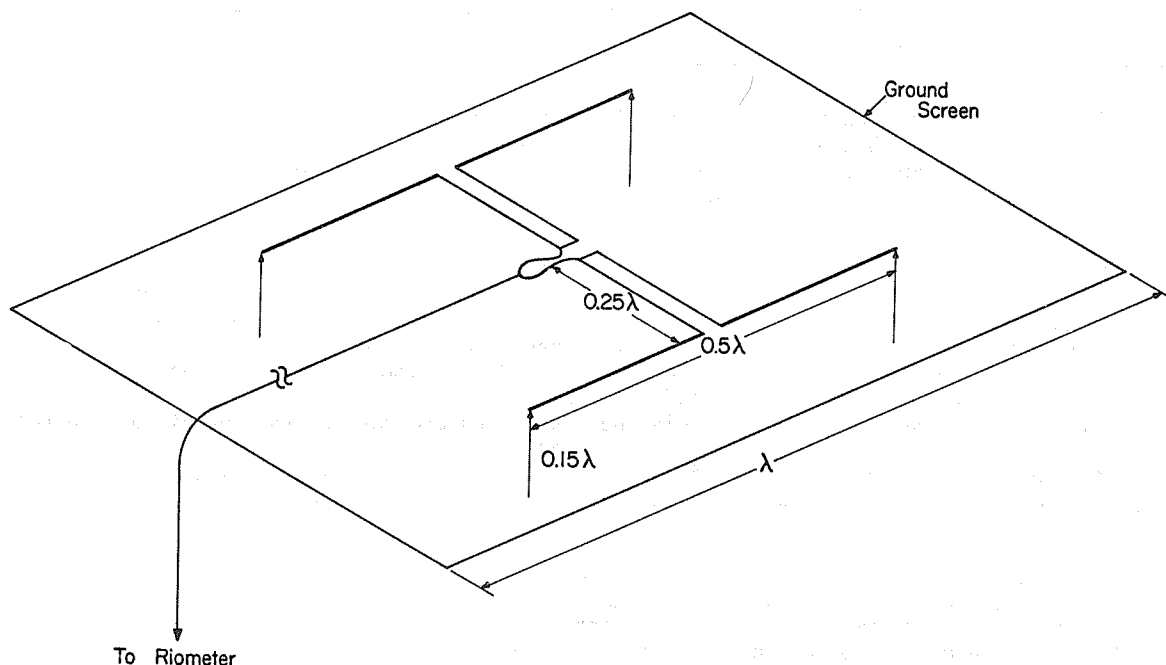


Fig. 5.3 Sketch of a typical double-dipole riometer antenna.

The cosmic noise source has been assumed to be distributed uniformly across the sky. For extreme precision, one would have to apply a correction that varied with sidereal time, since the source is never quite uniform. For most purposes, however, such precision is not required and is indeed almost impossible to attain since neither the source distribution nor the antenna pattern are sufficiently well known. An antenna used at Delhi for 22.4 MHz consists of 4 dipoles spaced 0.3λ apart and $\lambda/4$ above the ground, provided with corner reflectors intersecting at right angles. Its beam widths between half-power points are 34° in the N-S, 48° in the E-W vertical planes. If relatively low operating frequencies (say, 20 MHz) are used, the half-power width of the vertical antenna beam should be sufficiently narrow ($\leq 60^\circ$) in order to avoid the ionospheric "iris effect" described in Section 5.5.1.3 below. On higher frequencies, however, this effect is practically negligible.

For antenna directions towards the celestial pole (see above), a single (folded) dipole with a corner reflector has proved to be suitable. The polar diagram of this type of antenna can be made nearly circularly symmetric [cf., e.g., Schwentek and Gruschwitz, 1970].

5.3.5.2 One of the chief causes of difficulties in maintaining high quality recordings for long periods lies in changes in antenna impedance or in the network that matches the antenna output to the feedline. This is especially true in high latitude locations where severe weather conditions are experienced, and every possible precaution should be taken to avoid changes of this kind.

At some sites, meteorological conditions can cause significant variations in the electrical properties of the ground and consequently in the ground reflection coefficient affecting the resulting antenna impedance. Therefore it is useful to put a metal reflecting screen (usually made of parallel grounded wires) below the antenna.

Adequate weatherproofing of the matching network is essential, as are frequent checks of the input impedance to the receiver. In most operating systems, an input impedance of $50\ \Omega$ (with vanishing blind component) has been chosen, but the choice is in fact quite arbitrary. The essential requirement is that the antenna (plus feedline) present to the receiver the same impedance as the servo diode and the test diode. If for some reason the presence of a capacitive component in the combined antenna feedline impedance is unavoidable, a similar component should be included in the impedances of the two noise sources. In some installations the test noise source is fed in at the antenna end of the feedline, thereby avoiding the effect of the feedline attenuation in the recorded signal. Where practical, it is recommended that this procedure be followed. In any case it is desirable to protect the feedline from strong temperature variations affecting transmission efficiency and impedance.

5.3.5.3 In operation at high latitudes where blowing snow may be a frequent occurrence, the records can be effectively obscured by precipitation static. This is caused by the discharge of the snow particles as they strike the metallic antenna, and can only be avoided by housing the antenna in a radome or by covering it with an insulating coating. If some part of the antenna has no direct current (d.c.) connection to the ground, the charge has been known to accumulate to the point where breakdown of the insulation of the capacitors in the antenna input circuit has occurred. To avoid this, a d. c. path to ground should be provided through a suitable resistor.

5.3.6 In order to achieve maximum sensitivity in the recordings, it is recommended that the peak cosmic noise signal be made to produce a deflection of about 90 per cent of full scale on the output recorder. This is best accomplished by either shunting the recorder with an appropriate resistor in cases where the peak output is likely to exceed this limit, or by inserting an attenuator between the servo noise diode and the radio frequency switch, in cases where the output is below the desired level. In the latter case, care must be taken to insert an identical attenuator in the test diode output for calibration.

5.4 Scaling of the Records or The "Quiet Day Curve"

5.4.0 The determination of ionospheric absorption, A (in decibel), as defined by Eq. (5.1) in Section 5.1.5 above, from the cosmic noise power, P , measured at a given place and time with a fixed receiving system, requires the knowledge of the reference value, P_0 , which would be recorded at the same place and time with the same receiving system in the absence of ionospheric absorption. Since the antenna beam, directed upwards, each day explores the same strip of the sky according to the Earth's rotation, this reference value, P_0 , will be a function of sidereal time. This means, the unattenuated cosmic noise pattern repeats at intervals of one sidereal day, and thus moves forward with respect to solar time by 4 minutes per day.

The first and most important step in reducing the recordings to measurements of absorption is, therefore, the preparation of a "quiet day curve" (QDC) which is the best possible estimate of the reference level, P_0 , as a function of sidereal time. Experience has shown that errors in the QDC constitute the most common source of systematic errors in the measured absorption. Manual preparation with great care and judgment by the scientists themselves is therefore preferable to a mechanical procedure (e.g., computer plotting).

5.4.1 For constructing the "quiet day curve" (QDC) the basic assumption is made that for any given sidereal time there is a certain part of the year in which the absorption becomes negligible (probably

in those months when the given sidereal time falls into the night hours of solar time), so that at least once per year the unattenuated reference value, P_0 , being a point of the QDC, is actually recorded with the receiving system in use.

Consequently, the QDC is usually produced from a mass plot of individual readings of the output level as a function of sidereal time for a period during which there is no reason to suspect any changes in the equipment parameters. The upper envelope of this plot, or alternatively a curve that lies above 95 per cent of the individual values, can be taken as the QDC. The QDC is then expressed in the same measuring units as the regular recordings if these are proportional to the noise power (i.e., equivalent noise temperatures, or noise diode plate current squared), so that the power ratio P_0/P in Eq. (5.1) can be simply replaced by the ratio of the measured output (with absorption) to the corresponding QDC value for the same sidereal time (see Eq. (5.1a) in Section 5.3.2 for currents).

For the high precision required for mid-latitude and low-latitude studies, it is recommended that the local times from which the QDC values are chosen be restricted to the late night hours between about midnight and two hours before sunrise, since the residual absorption is likely to be least then. The construction of a complete QDC from these times alone requires roughly one year's observation with very little variation in equipment parameters. The reliability of the QDC might be further improved by a careful selection of days with minimum interference, magnetically and ionospherically quiet conditions, equipment stability, etc.

5.4.1.1 For a vertical antenna beam which is not crossed by strong localized cosmic radio sources, the QDC shows a smooth double-humped feature, where the humps correspond to those sidereal times when the galactic plane crosses the zenith (see Figure 5.4 for an example). At some sites, however, this picture is complicated by more localized strong cosmic noise sources leading to larger humps with steep slopes. Naturally, the scaling of absorption will be most uncertain at those sidereal times with steep slopes of the QDC. This difficulty can be avoided with the use of an antenna beam directed towards the celestial pole (cf., Section 5.3.5). In the idealized case of circular symmetry of the polar diagram of such an antenna, the sidereal time variation of the QDC should vanish completely.

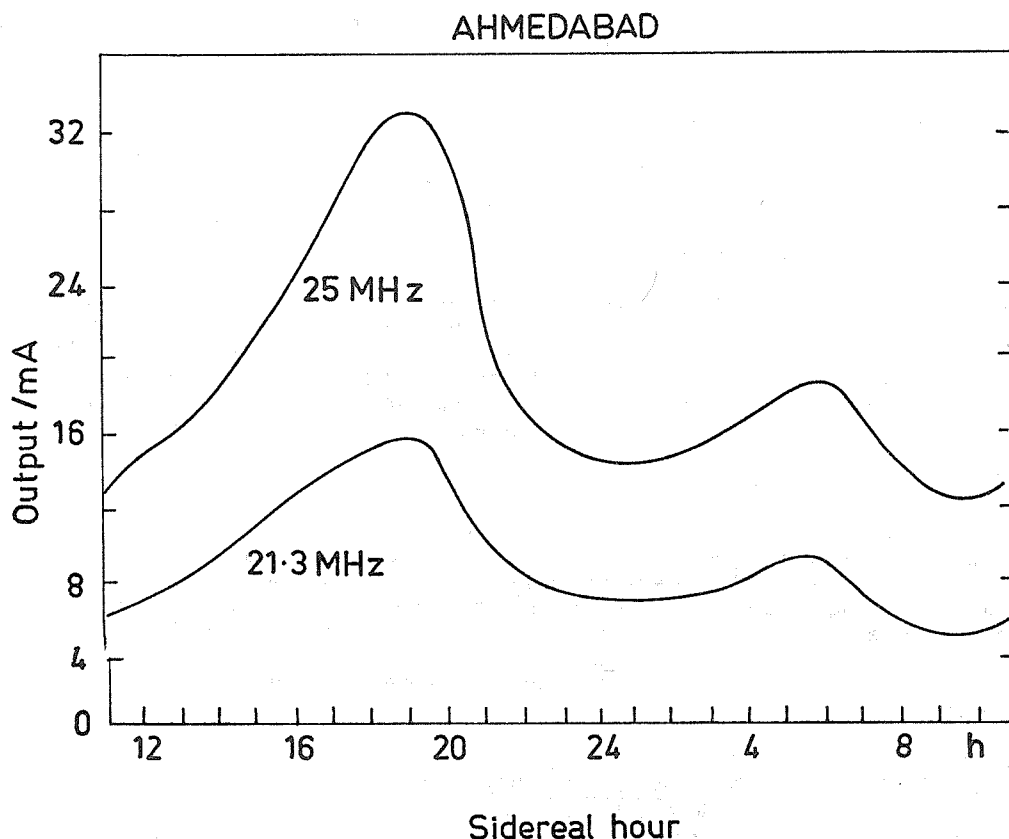


Fig. 5.4 Typical quiet-day curves (QDC) at two frequencies, for vertical antenna beam at low latitudes (Ahmedabad, India).

5.4.1.2 The above basic assumption of vanishing absorption during night may not always be fulfilled. In fact, there might be a residual nighttime absorption, at least for some locations and for certain periods. If this nighttime absorption has a more or less systematic seasonal variation, a QDC constructed in the way described above may be somewhat distorted since different portions of it will have been recorded at different seasons. This can be partially avoided by constructing separate portions of the QDC from each month independently. The sidereal time intervals covered will partially overlap, and the presence of a seasonal variation would be revealed by a systematic change in level in the overlapping portions. A complete QDC could then be constructed from these monthly sections by iteratively moving the curve for each month until it agrees with that of the preceding month.

Long-term measurements carried out in medium latitudes have suggested a significant solar cycle variation in the absolute level of the QDC, amounting to about 0.2 dB per year at 25 MHz, which could be explained by variable nighttime absorption increasing with increasing solar activity. If possible, the QDC should thus be constructed using data from years of minimum solar activity.

5.4.2 In view of the critical dependence of the A2 method on the QDC, several alternative methods have been proposed for constructing the QDC.

5.4.2.1 The first one suggested by Mitra and Sarada [1962] is to plot the recorded cosmic noise absorption as a function of solar time (proceeding from night hours to day hours) for constant sidereal time. The shape of these curves is nearly identical for different sidereal times, and it is often possible to draw a constant value through the nighttime data (see Figure 5.5). This (constant or asymptotic) nighttime value is taken as the QDC value for the given sidereal time.

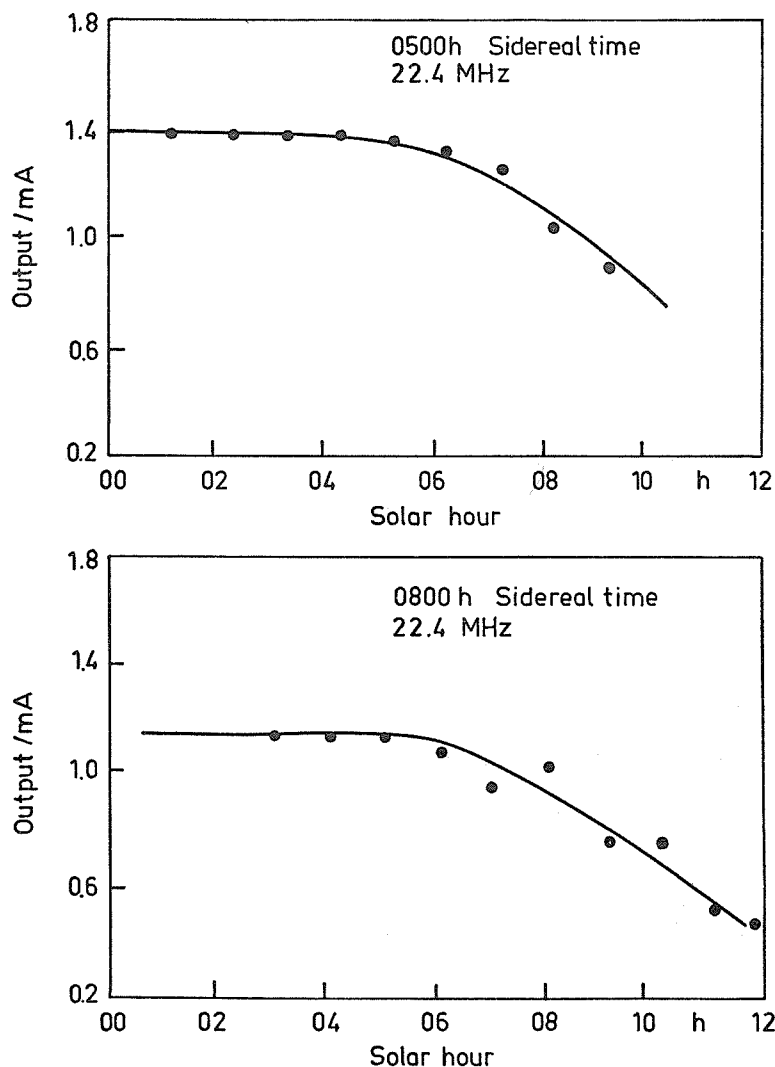


Fig. 5.5 Plot of cosmic noise as a function of solar time for a fixed sidereal time (cf. text).

5.4.2.2 Another possible method, also suggested by Mitra, is to use our knowledge about the frequency variation of cosmic radio noise. Its noise temperature (when no ionospheric absorption is present) varies with $f^{-2.7}$ (see Section 5.2.1). If one uses at least two frequencies, the (lower) operating frequency, f , and a (higher) reference frequency, f_r , the latter being sufficiently high to have negligible ionospheric absorption, then the average noise temperature on the reference frequency, plotted versus sidereal time and scaled up by the factor $(f_r/f)^{2.7}$, provides the QDC for the operating frequency, f .

This method, however, requires either two identical antenna patterns or at least a precise knowledge of the antenna patterns for the two frequencies.

5.4.2.3 Finally, a more sophisticated receiving system which permits measurement of the noise power for the ordinary and extraordinary modes of propagation separately (see Section 5.6.2 below) offers another possibility for improving the QDC: The unattenuated noise power (QDC) is identified with those conditions when the same noise power is recorded for both modes. These are distinguished by applying antenna arrangements which are sensitive to only one or the other "characteristic polarization" which are essentially circular at most locations (see Section 2.2.4 and 4.3.4.2).

5.5 Interpretation and Scientific Use of A2 Absorption Data

5.5.0 Method A2 is less sensitive than methods A1 and A3 since it applies higher operating frequencies. It is therefore ideally suited for the study of excess absorption events under disturbed conditions, i.e., Sudden Cosmic Noise Absorption (SCNA) connected with solar flares, and auroral and polar cap absorption (PCA) effects, since the A1 and A3 techniques often record complete loss of signal under these conditions. Therefore, the A2 method is widely used at high latitude stations. For the study of normal absorption under quiet conditions, however, the A2 method is less suitable than the A1 and A3 methods from the viewpoint of sensitivity, since the rather small magnitude of absorption (one dB or less at 30 MHz in middle latitudes) and its smooth diurnal variation require great effort in order to maintain operation of the equipment as well as reduction and analysis of the records at a high level, as pointed out in the foregoing Sections 5.3 and 5.4. Nevertheless, application of the A2 method to studies of this kind may be convenient at those places where the rather high technical expenses of the A1 method or the rather limiting requirements of path geometry etc. for the A3 method cannot be met, particularly at low (near-equatorial) latitudes where the magnitude of daytime absorption is considerably larger than at medium latitudes.

5.5.1 The analysis of normal ("quiet") absorption and its diurnal and seasonal variations is usually made in terms of the solar zenith angle, χ , and variations with frequency and with latitude. Long series of essentially continuous observations are necessary for establishing the major morphological characteristics of normal absorption, particularly their dependence on solar activity.

5.5.1.1 Mitra and Shain [1953] were the first to show that the quiet absorption measured in this way contains an appreciable contribution from the F region where the critical frequency f_oF2 is high, in addition to the contribution from the quiet D region which forms the essential part in the A1 and A3 techniques. If data of an ionosonde in the vicinity of the A2 observing station are available, one gets by plotting the A2 absorption values against f_oF2 (see Figure 5.6) an increase of absorption with f_oF2 at higher values of f_oF2 , but absorption does not fall to zero at very low values of f_oF2 . This behavior can be used to separate the two contributions to the total absorption, viz., the part A_D which does not depend on f_oF2 and is ascribed to absorption in the lower ionosphere and the part A_F which depends on f_oF2 . The latter is roughly represented by the formula:

$$A_F = A_{\text{tot}} - A_D = K \cdot (f_oF2)^m$$

For details about this procedure see, e.g., Mitra and Shain [1953]; Abdu *et al.* [1967].

The F-region absorption has been shown by Ramanathan *et al.* [1961] to be due to electron-ion collisions, whereas the D-region absorption is almost entirely due to electron-neutral particle collisions. When properly separated from the D-region contribution, the F-region absorption can be used to monitor some physical conditions in the F region, e.g., electron temperatures [Abdu *et al.*, 1967].

5.5.1.2 Comparison of A2 absorption data with simultaneous A1 and/or A3 measurements give a still better possibility to separate the contributions of different ionospheric layers to the total absorption. An excellent opportunity for studies of this kind is given during solar eclipses [e.g., Ohle and Taubenheim, 1967].

5.5.1.3 The F-region absorption derived by the method described in Section 5.5.1.1 above shows a very rapid increase with f_oF2 with a sharp cut-off at high f_oF2 values when the antenna beam is very wide. This is caused by the "iris effect" which occurs when f_oF2 approaches the operating frequency, f_{op} , of the A2 equipment. This effect is explained by the fact that (in the simplified case of a plane ionosphere) a wave of frequency f_{op} cannot penetrate the ionosphere if its angle of incidence, i , is larger than a limiting value, i_0 , given by:

$$\cos i_0 = (f_oF2)/f_{op}$$

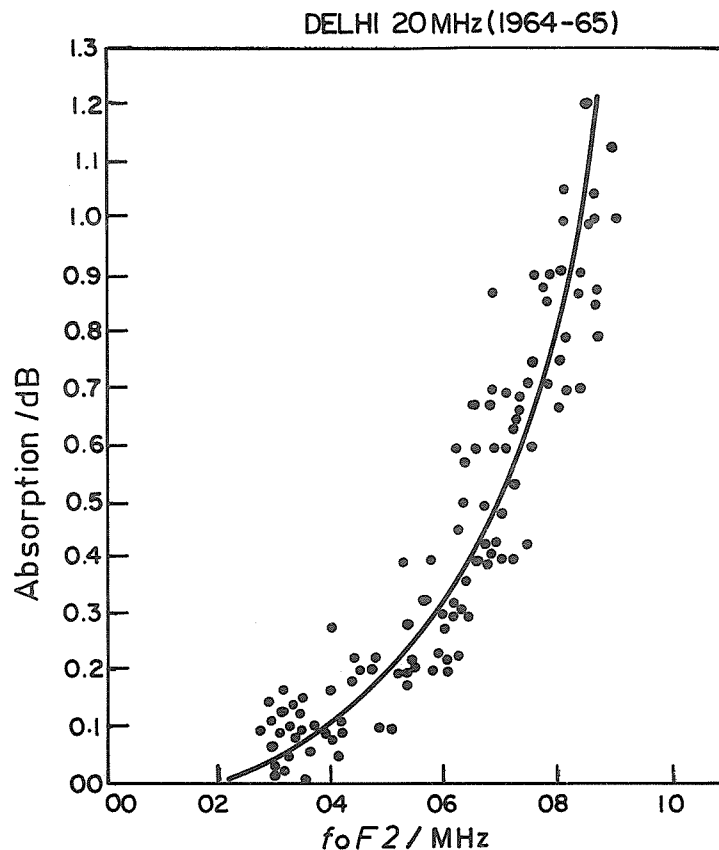


Fig. 5.6 Plot of A2 absorption values versus critical frequency of F2 layer, f_oF2 .

(See Figure 5.7). Table 5.1, giving the angular width of the "iris" for different ratios of f_oF2 to the operational frequency f_{op} , shows that the iris effect will be important only with wide-beam antennas and very low operating frequencies.

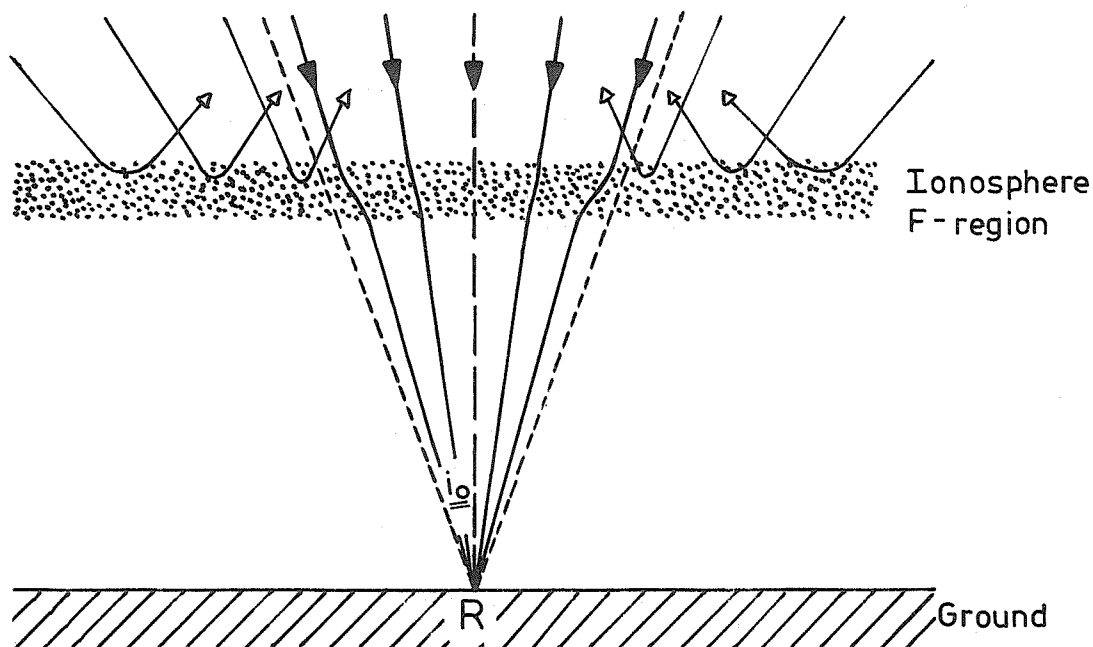


Fig. 5.7 Sketch illustrating the "iris effect" of the ionospheric F layer: Only rays with angle of incidence smaller than i_0 can reach the receiver, R.

Table 5.1

Angular Width (in Degree) of the F-layer "Iris" at Vertical Incidence

| Ratio f_oF2/f_{op} | 0.99 | 0.95 | 0.90 | 0.85 | 0.80 |
|---------------------------|-------|-------|-------|-------|-------|
| Angular width ($=2i_o$) | 16.2° | 36.4° | 51.2° | 63.2° | 73.8° |

5.5.2 Sudden cosmic noise absorption events (SCNAs) are a manifestation of sudden ionospheric disturbances (SIDs) caused by the X-ray induced ionization associated with solar flares. They appear simultaneously over the entire sunlit hemisphere of the Earth and are completely absent in the dark hemisphere. When unobscured by flare-associated radio noise at the riometer frequency, they have the characteristic appearance shown in Figure 5.8a, the onset being rather rapid and the decay rather slow and smooth in most cases. At high magnetic latitudes in sunlight, SCNAs can be confused with auroral absorption events, but the latter normally show much fine structure in the recovery phase.

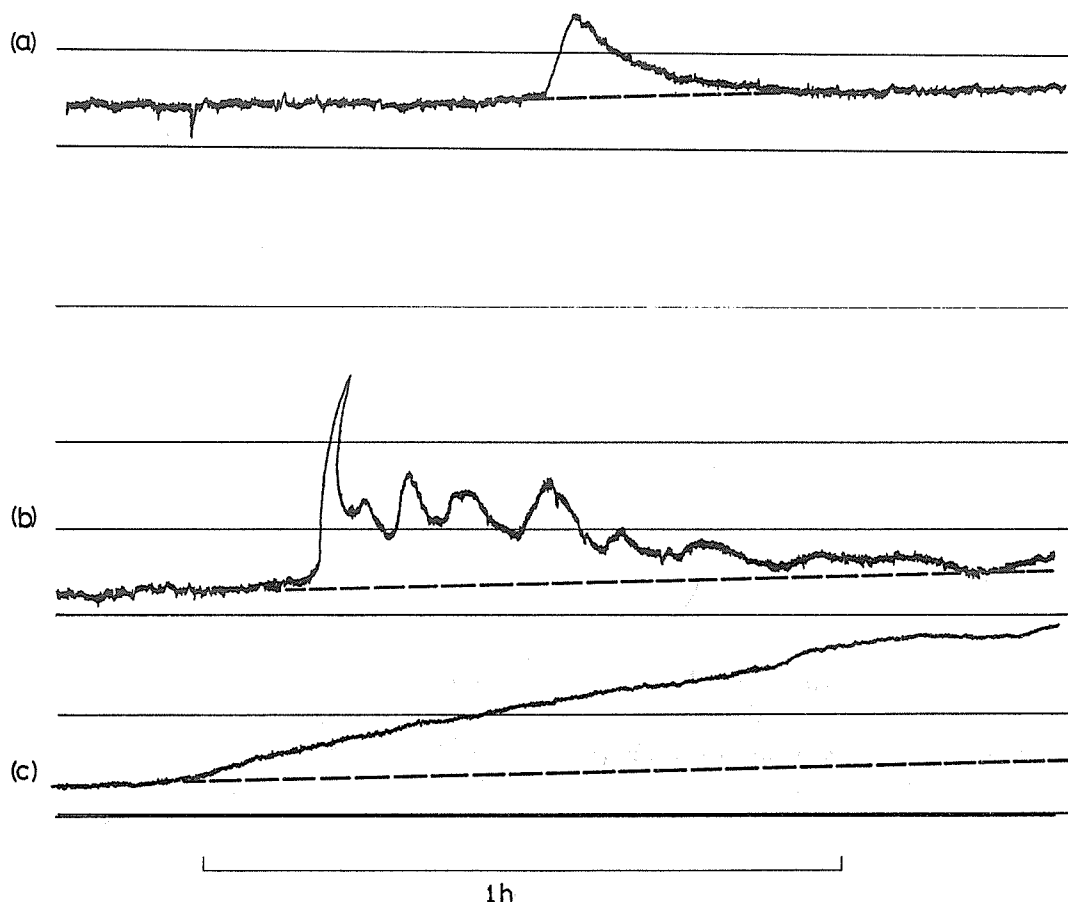


Fig. 5.8 Typical appearances of unusual absorption events:

- (a) sudden cosmic noise absorption (SCNA),
- (b) auroral absorption,
- (c) onset of polar cap absorption (PCA).

Comparison of SCNA records with solar X-ray flux data (desirably with spectral data) allows some investigations in D-region physics, e.g., for the deduction of effective loss rates [Sarada and Mitra, 1960; Mitra, 1966; Subrahmaniyam, 1968], particularly when multifrequency techniques (see Section 5.6.1 below) are applied.

5.5.3 Auroral absorption is the result of increased ionization in the lower ionosphere associated with the energetic electron precipitation during periods of auroral and geomagnetic disturbance. Individual auroral absorption events can display a wide variety of shapes and sizes, and the example shown in Figure 5.8b is only one of many that could have been chosen. The sharp onset is typical of events associated with the breakup phase of visible auroras and the oscillatory nature of the absorption following the onset spike is a fairly common feature. Slowly varying events of relatively long duration commonly occur during the pre-noon hours in the neighborhood of the auroral zone. They are now called "slowly varying absorption events" (SVA). During relatively quiet or only moderately disturbed geomagnetic conditions, auroral absorption is usually confined to magnetic latitudes higher than about 60° , but during intense magnetic storms it frequently appears at much lower latitudes.

5.5.4 Polar cap absorption (PCA) is a result of the bombardment of the lower ionosphere by energetic protons generated by certain major solar flares. Since the protons ionize heavily at low levels in the ionosphere, the absorption recorded during an intense PCA event is greater than that produced by any other natural mechanism, and such events have been known to last for several consecutive days. One of their most characteristic features is a pronounced diurnal variation caused by the photochemical influence of sunlight on the lower ionosphere. During daylight a relatively large electron density is maintained, resulting in strong absorption, while in the absence of sunlight a large fraction of the electrons form negative ions, thereby reducing the absorption by a factor of between 3 and 6. PCA events are relatively uncommon, occurring at a rate of the order of one per month during very high solar activity, and one per year (or less) at solar minimum. The influence of the geomagnetic field on incoming protons normally confines them to magnetic latitudes greater than 60° to 65° , but major reductions in geomagnetic cut-off can take place during the intense magnetic storms that often accompany PCA events and can allow PCA to be observed at magnetic latitudes below 55° . Such medium latitude observations are of great geophysical significance, though unfortunately rare. The example in Figure 5.8c shows the onset of a PCA event and illustrates the relatively structureless nature of typical polar cap absorption.

5.5.5 In low and temperate latitudes the effect of geomagnetic storms is often a decrease of total absorption during the main phase of the storm, since both f_oF_2 and the total electron content of the F region decrease during this time. At the end of the storm, however, the absorption tends to shoot up above normal [Bhonsle and Ramanathan, 1960; Degaonkar and Bhonsle, 1962; Abdu and Degaonkar, 1966]. These results are summarized in Figure 5.9 in a superposed epoch representation for the storms during 1957 and 1965 at Ahmedabad.

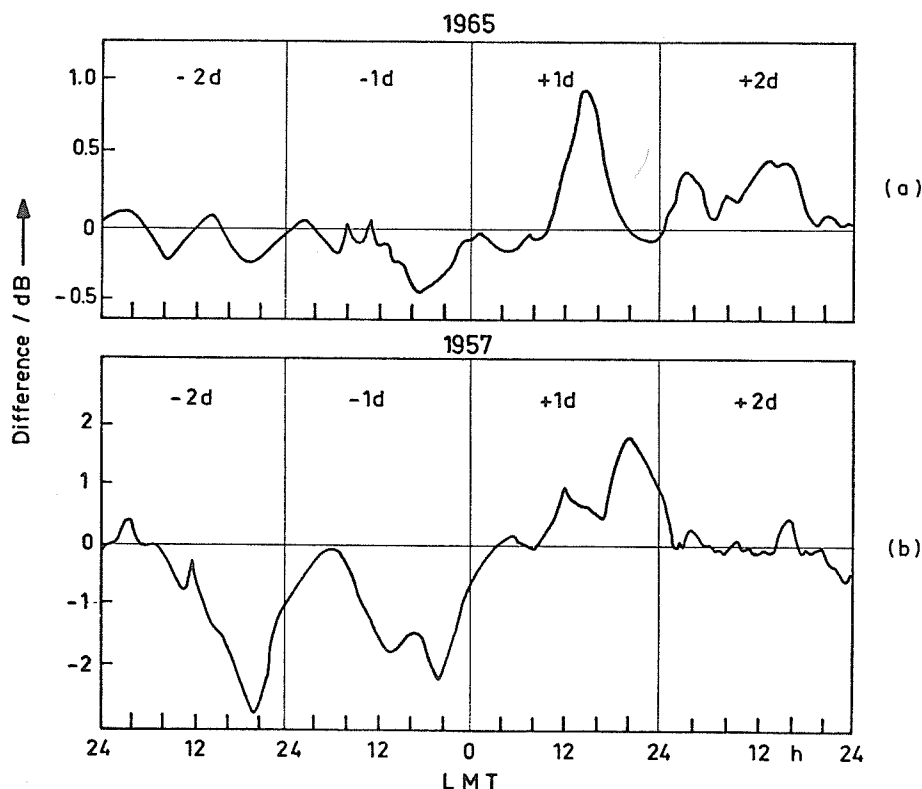


Fig. 5.9 Superposed epoch plots of A2 absorption around the main phase of geomagnetic storms at low latitudes (Ahmedabad, India); (a) 1965, (b) 1957.

5.5.6 Finally, it should be stressed that if A2 measurements are to be used not only as a detector of unusual absorption events but also to obtain quantitative data for ionospheric physics, it is highly desirable to carry out routine A2 observations at sites where also other techniques are applied for the determination of lower ionosphere electron density profiles (e.g., LF sounding, cross modulation and partial reflection methods), or where electron density and electron temperature profiles in the upper ionosphere are obtained with the incoherent scatter technique.

5.6 Specialized Developments of the A2 Technique

5.6.0 During the past decade there appeared several relatively sophisticated developments of the riometer technique aimed at specialized purposes. A few such developments merit some discussion here.

5.6.1 Multifrequency measurements use the frequency dependence of the absorption coefficient which is evident from inspection of Eq. (5.2) above. If the absorption all takes place at altitudes where $\nu^2 \ll (\omega \pm \omega_L)^2$, then κ is proportional to $(\omega \pm \omega_L)^{-2}$, and no information on the height of the absorption region can be derived from the frequency dependence. The same is true if the absorption all takes place at levels where $\nu^2 \gg (\omega \pm \omega_L)^2$, since the frequency dependence then disappears. In a situation between these two extremes, however, it is possible to derive some information on the altitude of the absorbing region from the observed frequency dependence of the absorption and this forms the basis for the multifrequency technique first developed by Parthasarathy, Lerfald, and Little [1964]. See also Section 2.2.5 and Figure 2.2.

5.6.1.1 If one makes the simple assumption that all the absorption is occurring in a thin layer of the ionosphere in which the electron collision frequency is constant, then it can readily be seen that measurement of the absorption at two frequencies can be used to derive the collision frequency, ν , and hence the height of the thin, absorbing layer if the height profile of ν is known. The use of additional frequencies allows one to derive more detailed information on the shape of the absorbing region. For example, if four frequencies are available, it becomes possible to derive a cubic profile of electron density

$$N(h) = a_1 h + a_2 h^2 + a_3 h^3 \quad (5.15)$$

which best fits the observed variation of absorption with frequency.

5.6.1.2 Observations of auroral and polar cap absorption events using this approach have shown that the frequency dependence can display marked departures from the inverse square variation, and hence it is possible to derive some information on the height of the absorbing region. It also appears possible to deduce electron density profiles during SCNA effects by this technique [Mitra *et al.*, 1966] and to compare the results with profiles determined by other methods (partial reflections, cross modulation techniques, etc.). Most of the absorption occurring in the quiet ionosphere, on the other hand, probably takes place at heights where $\nu^2 \ll (\omega \pm \omega_L)^2$, so that the technique would probably not yield any useful information. It should also be pointed out that great care must be taken to ensure that the patterns of the antennas used at the different frequencies are identical or at least that they are sufficiently well known that the vertical pencil-beam absorption can be derived with reasonable accuracy. There is also a natural standard error in measuring the absorption at any one frequency, and the spacing between the operating frequencies should be such that the difference in absorption between two neighboring frequencies is greater than this value. In practice, it is probably hardly justifiable to attempt to use more than four or five frequencies.

5.6.2 Dual polarization measurements utilize the difference of absorption suffered by the ordinary and extraordinary polarization modes, as shown in Section 2.7 above, and by Eq. (5.2) in particular. On the other hand, there is reason to believe that the cosmic noise signal incident on the top of the ionosphere is completely unpolarized, so that equal amounts of power are contained in the two modes. These two facts can be used to obtain two independent sets of absorption data and an improved quiet-day curve (see Section 5.4.2.3 above) by employing a single receiving system with an antenna whose polarization can be switched alternately between the two circular polarizations. This technique has been developed by Little, Lerfald and Parthasarathy [1964], and the interested reader should consult this publication.

In contrast to the multifrequency technique, the dual polarization approach is applicable in the region where $\nu^2 \ll (\omega \pm \omega_L)^2$, and in order to obtain measurable differences in absorption between the two polarizations its use should be restricted to frequencies for which ω_L/ω is greater than about 0.1, i.e., to frequencies below about 15 MHz.

5.6.3 In studies of the latitude dependence of, for example, auroral and polar cap absorption, it is convenient to transmit the data from riometers at several widely spaced locations in real time to a central point and to record all the outputs simultaneously on a multi-channel recorder. A system of this kind has recently been installed in Alaska by NOAA and utilizes a telephone line as a means of transmitting data from a chain of riometers extending from the Arctic coast to southern Alaska. Analog display of the data on a multi-channel recorder located in Anchorage allows comparison between events with completely accurate relative timing, besides permitting continuous real-time monitoring of the quality of operation at the various stations.

5.6.4 There is a general trend towards automatic data processing in geophysics. Since the output of a riometer is in the relatively simple form of measurement of a current as a function of time, it can readily be adapted to digital form. The digital output can then be treated by computer techniques and reduction of the data to values of absorption as a function of time can be carried out much more rapidly than by manual reduction of analog data.

In a system of this kind, sampling of the data can easily be made at intervals of one or two minutes and the output of a digital voltmeter recorded on paper tape, together with timing and calibration information. A quiet-day curve can be generated by the computer (for example by use of the microfilm plotting techniques now available in several computer systems) and can then be fed back into the computer to generate further plots of absorption as a function of time. Automatic systems of this type constitute the only practical means of treating large quantities of data in a reasonable length of time, and there is obviously a great deal of scope for individual approaches to the problem, based on the facilities available.

5.7 International Interchange

At present the international interchange rules for absorption (A2) are as follows:

In addition to exchange for events observed by riometers, stations operating riometers are asked to do the following:

5.7.1 Notify one of the WDCs, annually (e.g., in March) or more often, that riometers are in operation, giving the frequency, antenna arrangement and polarization, and time of beginning of operation and any major gaps in observation, e.g., gaps of more than one day since the last report. The WDC will contact the station if there are requests for copies of original records.

5.7.2 Send to one of the WDCs copies of any systematic scalings which have been made, e.g., monthly tables of the values of absorption in dB during the first minute of every hour together with median, median count and quartiles (scaling Type I); or monthly tables of the maximum absorption occurring each hour (00-01, 01-02 h, etc.) with the time of occurrence of the maximum to the nearest tenth of an hour (scaling Type II).

5.7.3 In addition, for times of special interest, such as auroral absorption events or polar cap absorption events as may be identified by Retrospective World Intervals or other special projects, participating stations may be invited by the WDCs or the special project coordinator to send special reductions or copies of their original records, preferably on 35 mm film together with the best possible estimates of the quiet day curve or equivalent numerical or computerized data.

5.7.4 When the riometer station has no further significant need for the riometer records for any period, it is invited to deposit them at one of the WDCs, together with the information necessary for their use in scientific work, e.g., quiet day curves, calibration information, and description of the experimental arrangement.

CHAPTER 6: METHOD A3 (a) OBLIQUE INCIDENCE FIELD STRENGTH OBSERVATIONS
ON FREQUENCIES ABOVE 2 MHz

by

H. Schwentek
Max Planck-Institut für Aeronomie, Katlenburg-Lindau, F.R.G.

Table of Contents

| | Page |
|--|------|
| 6.1 Introduction | 123 |
| 6.2 Short Description of the Method and Conditions for Its Applicability | 123 |
| 6.3 Theory of Absorption at Oblique Incidence | 124 |
| 6.4 Day and Night Field Strength | 129 |
| 6.5 Detailed Instructions Concerning the Choice of Transmission Distance and Frequency | 131 |
| 6.6 Receiving and Recording Equipment | 134 |
| 6.7 Calibration of the Receiving System | 136 |
| 6.8 Use of an Ionosonde in the Neighborhood of an Absorption Circuit | 139 |
| 6.9 The Use of a Transmission Curve | 139 |
| 6.10 A Few Characteristic Results | 140 |
| 6.11 Program of Observations | 144 |

6.1 Introduction

6.1.1 An earlier description of method A3 for operators has been published by the author in the *IQSY Instruction Manual No. 4* [1963] and *Annals of the IQSY* [1968] - see General References in Section 10.1, also CCIR [1970]. Fundamental descriptions can be found in Gockel [1948], Schwentek [1958], Triska [1962, 1967] and Hense [1969]. Its application will only be valuable and fruitful if the circuit is carefully planned, and if the measurements are carried out with a certain degree of understanding of wave propagation phenomena and ionospheric conditions. Otherwise, wrong interpretations of the records are unavoidable, and comparisons with the results of other circuits will lead to errors. For this reason we first explain some basic principles and theoretical background before giving practical advice.

6.1.2 It is usual to describe power loss due to absorption in optical devices by the power ratio of the light beam before entering and after leaving the absorber, P^*/P . For radio waves, however, the field strength ratio is normally used (see Section 2.3), and the absorption coefficient κ as used in

$$\int \kappa ds = -\ln (E/E^*) \quad [2.10]$$

is defined by the decrease of field strength, not power. There is no danger of confusion because losses, A , are always measured in dB and the conventions for this unit indicate that

$$\frac{A}{\text{dB}} = -10 \log \frac{P}{P^*} = -20 \log \frac{E}{E^*} \quad (6.1)$$

A being positive since the logarithms are negative.

6.1.3 Some examples of transmission paths used for absorption measurements are shown in Figure 6.1. A2 measurement of cosmic noise by riometer measures the absorption of one path through the whole ionosphere, on a rather high frequency; for instance, 27.6 MHz is often used (see Chapter 5). Quite differently method A3 uses either the F layer or the E layer as a reflector so that only absorption in the lower part of the ionosphere is measured, but the wave passes these layers twice, up and down, at oblique incidence. The frequency must be low enough to be suitably reflected. Under these conditions, circuits can be established which are suitable for measuring mainly the absorption of the D layer (see Section 2.6).

Suitable continuous wave (CW) circuits for absorption measurements at oblique incidence use frequencies between 2 and 3 MHz, and around 6 MHz, at distances between 200 and 400 km.

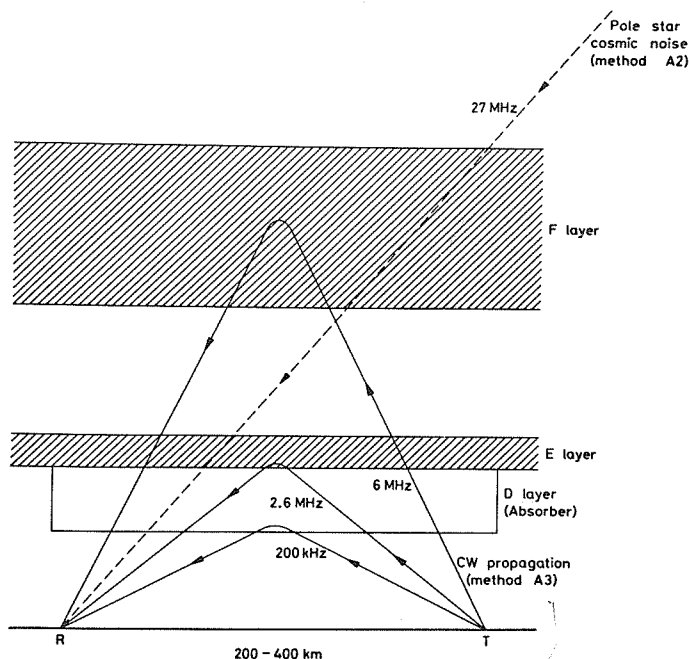


Fig. 6.1 Ray geometry for measurement of absorption in the ionosphere; methods A2 and A3.

6.2 Short Description of the Method and Conditions for Its Applicability

6.2.1 If the frequency can be chosen so that the wave is reflected at oblique incidence from almost constant height in the ionosphere at different times, then the difference of absorption at these times can be determined. In practice, it is possible to arrange the polar diagrams of the transmitting and receiving antennas in such a way that small changes in height are almost unimportant and comparative measurements are feasible provided the wave is always reflected from the same layer. We shall show in

Section 6.3 below that it is desirable to use E-region reflection throughout the day. The main complication in the interpretation of the data arises from the fact that the height of reflection decreases as the ratio of the working frequency to the E-layer maximum usable frequency (MUF) decreases. This should be kept in mind when analyzing the diurnal and annual variation of absorption.

6.2.2 The system needs, at least occasionally, calibration by total reflection from a sporadic-E layer at night. In most areas this is only possible during a limited season of the year. If no satisfactory Es modes occur at night, calibration may still be carried out at night with reflections from the F layer but then it is necessary to know the relative gains of the transmitting and receiving antennas at the E- and F-layer angles of incidence and take into account the difference in path lengths for the E and F modes.

6.2.3 A3 measurements are carried out with continuous wave (CW) transmissions; antennas, frequencies and transmission distance must, however, be chosen so that one mode of reflection is normally much stronger than any other. Some experience is needed to determine the times when this is true and to distinguish between E- and F-mode reflections. The distinctions can be made more easily when ionograms from a nearby station are available; then the propagation conditions can be estimated rather well.

6.2.4 A3 measurements are usually arranged in such a way that non-deviative absorption is most prominent. As shown in Section 2.5, the absorption coefficient is then quickly decreasing with increasing frequency, with $(f \pm f_L)^{-2}$ as seen in Eq. (2.17). Thus, the lower the frequency, the higher the absorption is. Of course, at lower frequencies the influence of double refraction provoked by the Earth's magnetic field is quite important.

6.2.5 Technical requirements for an A3 circuit are: a transmitter with a stable power output, stable receiver and recording unit, well-known transmitting and receiving antennas selected so that

- (i) no appreciable ground-wave signal is picked up;
- (ii) the first E-layer or F-layer reflection is normally much stronger than any other mode;
- (iii) the difference in polarization between the o wave present in the day and the mixed o and x waves present at night does not alter the effective signal strength significantly.

6.2.6 It is usually the main purpose of A3 measurements to monitor the diurnal and day-to-day variations of absorption over a period of years, and thus also monitor the solar activity.

6.2.7 The system described in Section 6.6 below is in fact capable of giving high accuracy over long periods. For more limited objectives, a slightly simpler procedure may be adopted. In fact, most of the complications are needed to establish the absolute values very accurately. With less accurate circuits it is at least possible to record day-to-day and seasonal variations, and to study events, in particular solar flare effects (SIDs), and the excessive absorption occurring on certain groups of winter days (winter anomaly).

6.2.8 The method is rather inexpensive because the only expense is the receiving station. However at some locations it is rather difficult to find a suitable experimental arrangement because this depends mainly on the availability of transmitters. But once achieved, the method needs only a minimum of manpower for observations and data reduction.

6.2.9 With more sophisticated systems more results can be achieved. By using different circuits on different frequencies, for instance 245 kHz, 2.5 MHz, 6 MHz, and 27.6 MHz, and receiving these frequencies at the same location, solar flare effects in a broad range of intensity can be monitored quite accurately (see Chapter 7 for monitoring on low and medium frequencies).

6.3 Theory of Absorption at Oblique Incidence

6.3.1 Because the maximum distance at which accurate data can be obtained is about 500 km, in the analysis of the results a plane Earth approximation may be used.

Model calculations taking account of curvature can be found in the publications on estimation of sky-wave field strength [Rawer, 1952, 1958; Allcock, 1954; Piggott, 1959; Barghausen, 1966; Barghausen *et al.*, 1969]. In 1970 CCIR provisionally recommended the last reference for use [CCIR Report 252-2, 1970a].

6.3.2 The change in absorption from night to day for a wave which is reflected in the same region of the ionosphere may be computed from the daytime and nighttime signal strengths, E_d and E_n , and the corresponding halfpath lengths, s'_d and s'_n . Considering the cymomotoric force (see Section 1.1), i.e. multiplying by s' , compensates for the effect of spatial attenuation.

For waves reflected in the E layer at oblique incidence the equivalent loss at vertical incidence is approximately $\cos \alpha$ times the observed loss, where α is the angle of incidence. The equivalent absorption for a frequency f_d at vertical incidence, $A(f_d, 0)$ in dB, is obtained from

$$\frac{A(f_d, 0)}{dB} = \frac{A(f_d, \alpha)}{dB} \cdot \cos \alpha = -\cos \alpha \cdot 20 \cdot \log \left(\frac{E_d s' d}{E_n s' n} \right) \quad (6.2)$$

For a 1E mode, s'_d/s'_n is very close to unity so that its logarithm may usually be neglected. The value of $\cos \alpha$ is determined by the virtual height of reflection, h' , and the distance between transmitter and receiver, d . Thus,

$$\cos \alpha = \frac{h'}{(h'^2 + d/2)^{1/2}} \quad \text{where } h' = s' \cos \alpha. \quad (6.3)$$

If the nighttime reflection is from the F region, the recorded signal strength E_n must be multiplied by $s'(F)/s'(E)$, and also by a factor determined by the transmitting and receiving antennas polar diagrams for the directions involved. It is, of course, essential to obtain calibration measurements at times when the residual absorption is very small and the waves are totally reflected.

6.3.3 Relative Strength of Different Modes

The distances, frequencies and antennas are chosen so as to make one dominant for as long as possible. It is desirable to calculate the maximum effect on the received signal which is likely to be produced by other modes, particularly during calibration observations.

If the half-path length of one hop is denoted by s' and the gains of the transmitting and receiving antennas by G_t and G_r respectively, and if the suffixes 1 and 2 are used to denote two different modes, and if m is the number of hops of one multihop path, then the ratio E_1/E_2 of the received signals for the two modes in the absence of absorption is given by

$$\frac{E_1}{E_2} = \frac{G_{t1} G_{r1} s'^2_2}{G_{t2} G_{r2} s'^2_1} \cdot m \quad (6.4)$$

If there is no absorption, the average total signal strength E_{tot} is given by

$$E_{tot} = (E_1^2 + E_2^2)^{1/2} = E_1 (1 + E_2^2/E_1^2)^{1/2} \quad (6.5)$$

It is often convenient to use a vertical monopole for the transmitter antenna and a horizontal dipole about $\lambda/4$ above ground for the receiver antenna. For these we can write approximately

$$G_t \propto \sin \alpha = \frac{d/2}{s'}, \quad G_r \propto \cos \alpha = \frac{h'}{s'}$$

Hence for two one-hop paths ($m=1$)

$$\frac{E_1}{E_2} = \left(\frac{h'_1}{h'_2} \right) \left(\frac{s'_2}{s'_1} \right)^3 \quad (6.6)$$

and for a one-hop path and a multihop path (m)

$$\frac{E_1}{E_2} = m^2 \left(\frac{h'_1}{h'_2} \right) \left(\frac{s'_2}{s'_1} \right)^3 \quad (6.7)$$

The relative values of E_{tot} , E_1 and E_2 in some typical cases are given in Table 6.1. When allowance is made for ground losses, the value of E_{tot}/E_1 falls to 1.13 and even less if absorption is present. Thus, for adequate antenna systems the calibration fields are unlikely to be more than about 10 per cent above the value due to the dominant mode on the average.

Table 6.1

Relative Strength of Signals Propagated by Different Modes
($d = 300$ km, $h'E = 100$ km, $h'F = 300$ km, $G_t \propto \sin \alpha$, $G_r \propto \cos \alpha$)

| Modes | E_1/E_2 | | E_{tot}/E_1 | |
|--------|-----------|----|---------------|-----|
| | ratio | dB | ratio | dB |
| 1E, 1F | 2.17 | 6 | 1.10 | 1 |
| 1E, 2E | 1.35 | 3 | 1.25 | 2 |
| 1F, 2F | 3.12 | 10 | 1.05 | 0.5 |

6.3.4 Choice of the Antennas

6.3.4.1 The first principle to be observed in choosing the transmitting and receiving antennas is that the combination must reject high-angle rays and thus minimize the effects of multiple reflections. In practice, it is most convenient to use a vertical monopole at the transmitter and a horizontal dipole at the receiver. Such antennas can excite or receive both magneto-electronic modes. For the frequency bands which are useful for A3 systems, differential absorption reduces the extraordinary (x) wave so that during the day it is negligible compared with the ordinary (o) wave. This is valid to a higher degree for the E mode than for the 1F mode.

6.3.4.2 At most angles of incidence the characteristic polarizations are approximately circular, and hence roughly equal amounts of o and x waves are radiated or picked up by a typical small monopole or dipole antenna. However, when the angle of incidence is such that the direction of the wave normal of the 1E or 1F mode is within about 5° of being perpendicular to the Earth's field, the o wave will be strongly elliptically polarized with the great axis parallel to the direction of the field and thus be almost vertically polarized at most latitudes. The x wave will be polarized perpendicularly to the field. Thus, if the downgoing wave travels nearly at perpendicular direction to the field, the receiving antenna should be vertically polarized; if the upgoing wave is perpendicular to the magnetic field then the transmitting antenna must be vertically polarized. The angles of elevation, ϕ , and azimuth, θ , at which this occurs, when the dip angle of the field is ψ , are shown in Figure 6.2. The values can be calculated using the relation

$$\tan \phi = \cos \theta \cos \psi \quad (6.8)$$

Either polarization may be used, as convenient, for the other antenna, although it is usually best to have one which does not radiate or pick up the ground wave. If the dip angle is near the critical value for the 1E mode and the wrong polarization is used, the signal due to the minor axis of the polarization ellipse for the o wave will be received during the day, and that due to the major axis of the x wave at night. The calibration will then be incorrect, possibly by a factor of 10 or more.

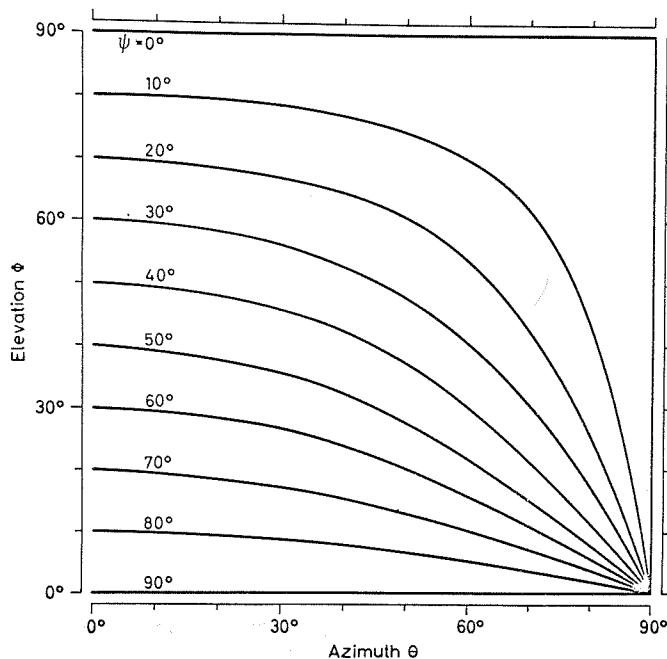


Fig. 6.2 Curves representing the conditions for which the direction of propagation is perpendicular to the geomagnetic field. θ is the azimuth angle, measured from the magnetic meridian; ψ is the geomagnetic dip angle; ϕ is the angle of elevation.

6.3.4.3 The angles of incidence for virtual heights of reflection of 100 km (1E), 300 km (1F) and 600 km (2F) are shown in Figure 6.3. The polar diagrams of typical transmitting and receiving antennas can be taken from Figures 6.4 and 6.5. These show the relative gain as a function of the angle of elevation for a half-wave vertical monopole (Figure 6.4) and for a horizontal half-wave dipole placed a quarter wave above the ground (Figure 6.5). The radiation in the direction of maximum gain when the conductivity of the ground is infinite corresponds to 100 percent.

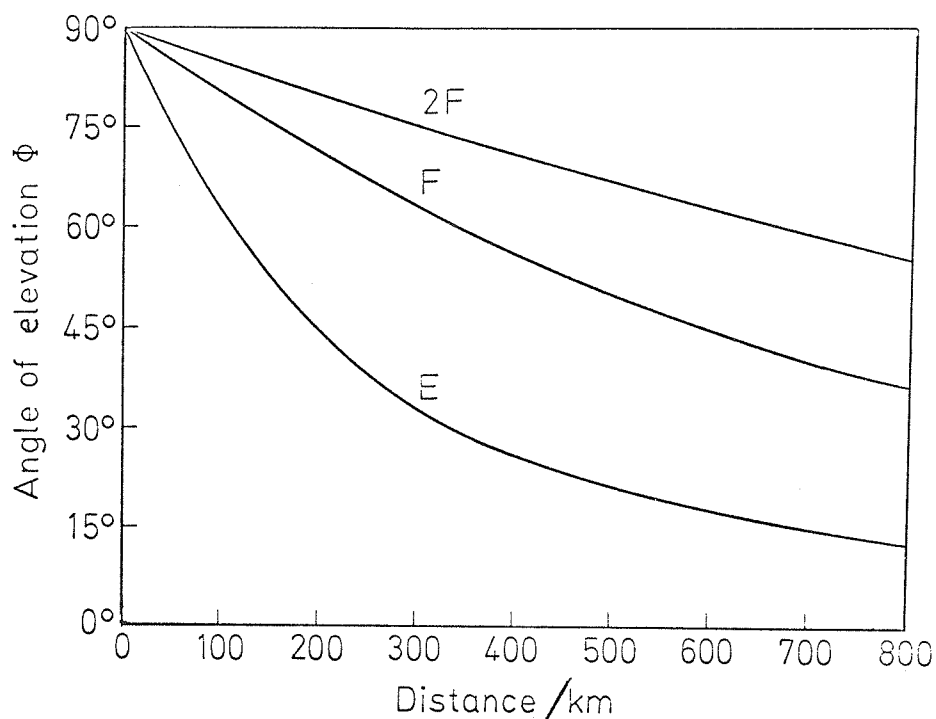


Fig. 6.3 Variation with distance (d) of angle of elevation (ϕ) of incident wave for E- and F-mode reflections.

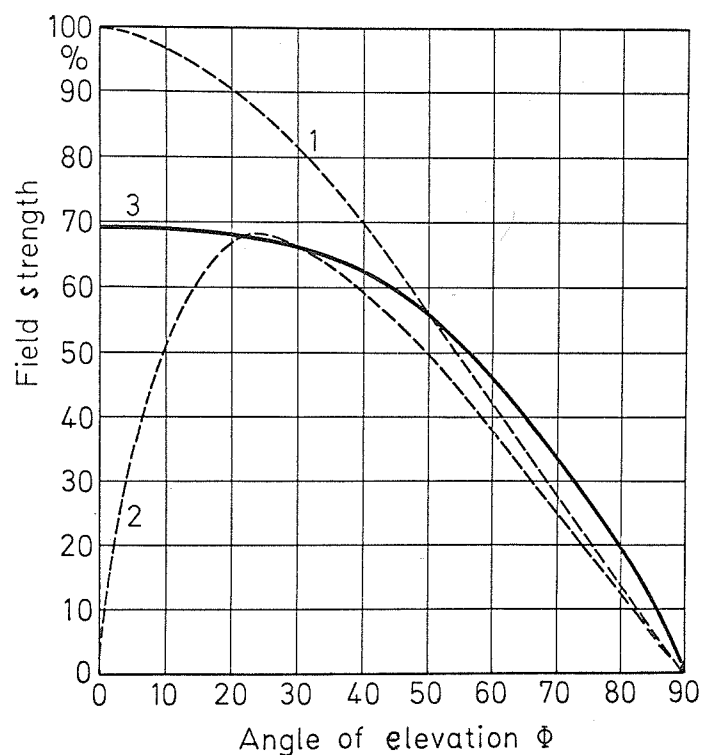


Fig. 6.4 Polar diagrams of a quarter-wave vertical monopole: (1) calculated for infinite ground conductivity; (2) calculated for finite conductivity; (3) measured by aircraft at 0.74 MHz.

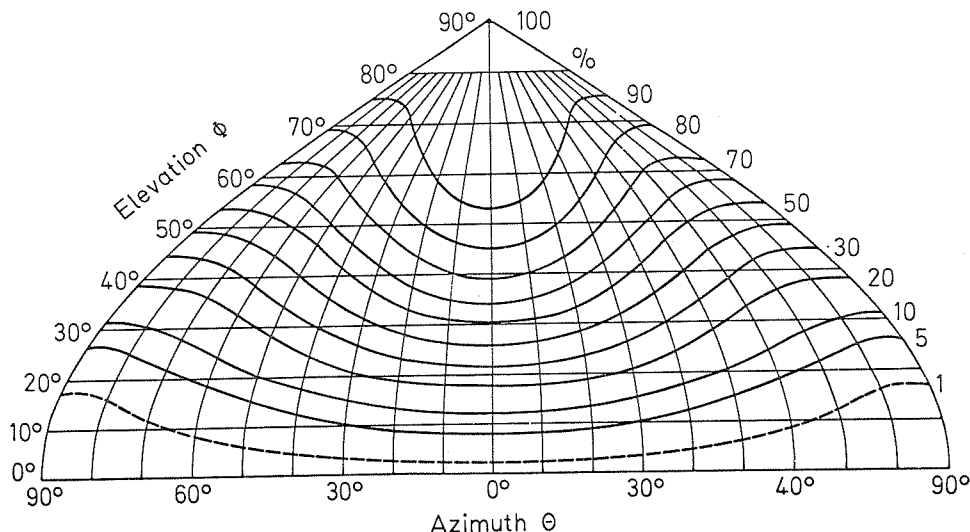


Fig. 6.5 Polar diagram of a horizontal half-wave dipole placed a quarter wavelength above the ground. The angle is measured from the direction of the dipole.

Read relative gain (in %) at the right-hand side for each curve.

6.3.4.4 At vertical incidence it is possible to use a polarimeter to select one magneto-ionic component. This usually consists of two crossed dipoles with a phase-shifting device. A similar system may, in principle, also be used at oblique incidence, but it is difficult to adjust it properly so that one component is suppressed and to confirm that the adjustment is correctly maintained.

6.3.5 Effect of Antenna Diagrams upon Field Strength Comparison

6.3.5.1 If 1F is the dominant mode in daytime, the night value, E_n , can be determined quickly, provided that the height of reflection does not appreciably change. We define as "night" the time between two hours after sunset and one hour before sunrise. If then the critical frequency of the F layer is higher than $f_d \cos \alpha$, the record mainly gives E_n directly. Unfortunately, however, the height of reflection is rather variable, and this fact may lead to a large error because a variation of height implies changes of the angle of departure (see Figure 6.3) so that the antenna diagrams have to be taken into account. If the height of reflection decreases, the signal strength increases because the length of the transmission path decreases also. Depending on the form of the antenna diagrams, the signal strength will increase or decrease when the height of reflection decreases.

In the ideal case the increase of signal strength due to a decrease of absorption for decreasing height of reflection would be compensated by decreasing the gain of the antenna diagrams when the angle of elevation decreases. For the circuit Luxemburg-Lindau, for example, the error is less than 5% for a variation of height of reflection from 230 to 370 km. It follows that for an 1F transmission the height of reflection may play an important role. If so, the height must be determined continuously by applying a transmission curve to the ionograms of an ionosonde station not too far from the midpoint of the circuit (see Section 6.9).

6.3.5.2 As explained in Section 6.3.4 above, it is usually unavoidable to accept a simple system which receives both components and consequently to make allowance for the presence of an x wave at night. A careful comparison of the signals received when one or both components are likely to be present enables the correction to be determined experimentally. In practice, it is usually sufficient to assume a correction factor of 0.8 for a calibration of the 1E mode or 0.7 for one by the 1F mode.

6.3.6 Effects of Polarization

As shown in Section 6.3.2 above, if the wave is reflected in the same region (height) under daytime and nighttime conditions, then the antenna diagrams need not be known in detail. However, the conditions of polarization must be taken into account.

6.3.6.1 Since the absorption is smaller for the ordinary than for the extraordinary component, the antennas should be designed so as to select the ordinary component (see Section 6.3.4 for details). If the extraordinary component were used, the measurement would often be influenced by the stronger ordinary component, especially during high absorption conditions.

6.3.6.2 Close attention must be given to the suppression of the ground wave, especially for the lower frequencies and shorter distances. For this reason propagation paths over sea should not be used. In addition, the antennas can be used to minimize the effects of other modes when it is desired to measure either the 1E or 1F mode alone.

6.3.6.3 Hence, the first step to be taken is to design the antennas in such a way that during the day a 1E path (or a 1F path) dominates; that is, the signal strength of the 1E path (or 1F path) differs from the total signal strength by not more than about, say 1 dB.

6.3.6.4 If antennas on both ends of the circuit can be chosen arbitrarily, the following recommendations can be given: For a 1E circuit it is convenient to use at the transmitter a vertical monopole a quarter or half wavelength high and at the receiver a horizontal folded-dipole a quarter wavelength above the ground.

For a 1F circuit it is convenient to use at the transmitter a system of horizontal dipoles a quarter wavelength above the ground, radiating mainly in the direction to the receiver via 1F, and at the receiver a horizontal folded-dipole a quarter wavelength above ground, pointing to the transmitter.

6.4 Day and Night Field Strength

6.4.1 The nighttime field strength, E_n , is used for signal calibration. If the same height of reflection occurred during day and night, the absorption decrement could simply be written as

$$\frac{A_d(f_d, d)}{\text{dB}} = 20 (\log E_n - \log E_d) \quad (6.9)$$

For the case of a daytime 1E mode this formula is only valid at night on some occasions, namely when a blanketing Es layer happens to be present. In these cases the observed signal strength is just E_n . The problem is to identify the occasions without studying the statistical distribution of nighttime field strength values for many nights.

6.4.2 A rapid way to estimate the value of E_n more or less precisely is extrapolation of the diurnal variation of signal strength. An extrapolation is necessary because for most usable frequencies, due to deviative loss, the absorption is higher than expected during the first two hours after sunrise and two hours before sunset. There are days, however, when an Es layer occurring around sunrise or sunset produces a more regular trend (see Section 4.9.3.4 and Figure 4.23).

The procedure of extrapolation can be made by drawing a pencil line through the maxima of the signal strength recorded during the day. This line represents the average variation of maximum signal strength (Figures 6.6 and 6.7). Thus, the times of sunset and sunrise must be marked by pencil lines. One may take from a calendar the times at the ground but it is much better to compute the times in the E layer at 100 km.

Extrapolation to the unattenuated nighttime value must be made with care because the duration of the transition interval depends on the frequency used and the distance between transmitter and receiver.

6.4.3 It will be found that sometimes, in fact, the observed signal value follows the extrapolated lines, namely when a blanketing Es layer was present around sunset or sunrise, e.g., see Figures 6.6 and 6.7. These cases are most useful but rare. They should be evaluated carefully because they give most valuable information.

6.4.4 When no Es reflections occur around sunrise and sunset, one may also find a nighttime value, E_n , which, however, will be less accurate. The accuracy can be increased by averaging over the data for all days showing regular behavior.

6.4.5 When the F layer has to be used for calibration, the variation of the critical frequency f_oF_2 must be studied so as to determine the upper limit of frequency for which adequate calibration might be obtained at night. For a permanent installation the probable values of f_oF_2 for a complete solar cycle should be considered. These can be found at vertical sounding stations. A monthly median curve of f_oF_2 can also be taken from an ionospheric prediction program. Account must be taken, however, of the day-to-day fluctuation of f_oF_2 which covers a range of about $\pm 20\%$ around the tabulated monthly medians.

For an example, for the period near sunspot minimum we would first select the minimum appropriate value of f_oF_2 from published f_oF_2 values; then reduce it by 20 per cent so as to avoid deviative absorption, and finally multiply it by $\sec \alpha$. Thus, for a transmitter-to-receiver separation of 300 km, let the f_oF_2 value (taken from a suitable table) be 2.7 MHz

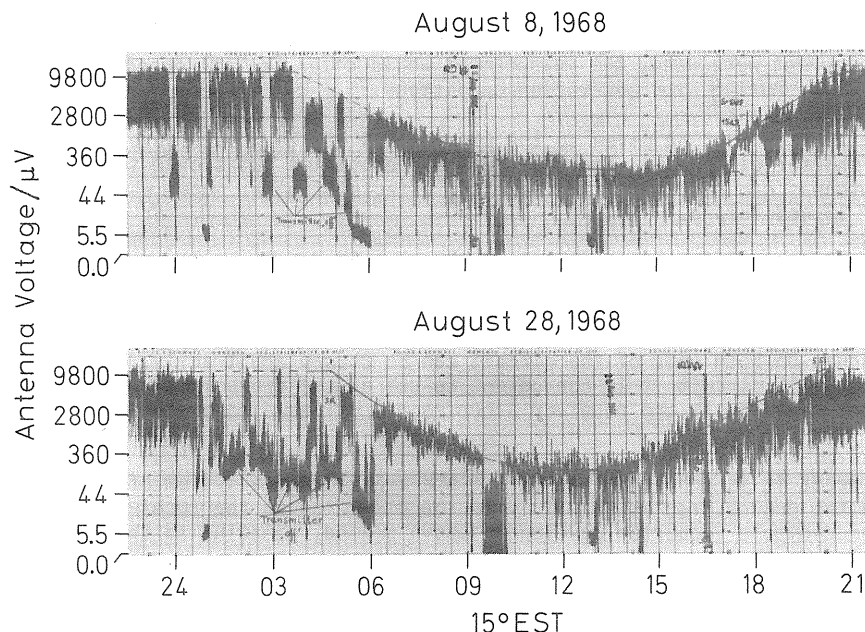


Fig. 6.6 Diurnal variation of signal strength; strong Es layer around sunrise and sunset, representing the ideal case for simple calibration. It should be pointed out that the values E_n and E_d are derived from a smooth curve drawn through the peaks of maximum signal strength (line).

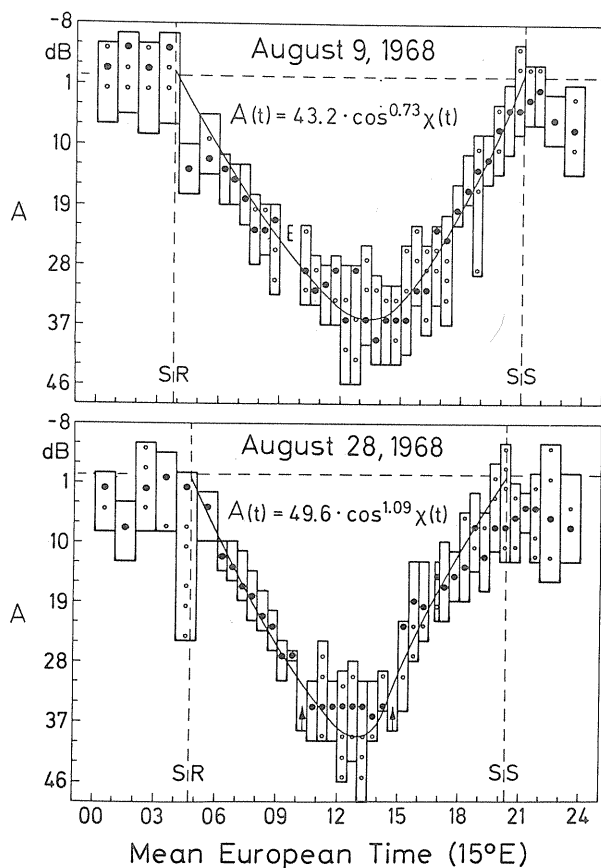


Fig. 6.7 Diurnal variation of signal strength (in dB), reduced to a constant level (1 Es transmission at night). Points indicate absolute maxima of occurrence in the indicated range, circles secondary maxima.

with $h'F = 300$ km, then the limit of the usable frequency range would be $2.7 \cdot 0.8 \cdot 1.12 = 2.4$ MHz. This is the highest frequency that could be used for absorption measurements and also for calibration every month. For long-period measurements with stable equipment, higher frequencies may be used because the calibration is then made only when f_oF2 is high enough. Calibration by means of F-layer transmission should be used as a check even at frequencies for which calibration by Es reflections is possible.

6.4.6 Nighttime data obtained with both techniques should be used together. After studying about 100 cases, the median values of the highest ten values should be used to represent E_n . The usual error of this value will not be greater than ± 3 dB if the procedures are carefully applied. If, in fact, very clear Es transmission occurs during several nights of a month, the median value of the signal strength corresponding to these cases may be compared with the extrapolated value, and thus, step by step, the error in the determination of E_n can be reduced.

6.4.7 The daytime field strength, E_d , can be determined very quickly by drawing the envelope through the peaks of signal strength as shown in Figure 6.6. This procedure implies a simple averaging process. Then, for every half hour or hour a median maximum signal strength can be determined using the calibration curve of the receiver. This is correct because E_n also refers to quasi-maximum values.

It should be emphasized that the procedure of calibration should always be employed when this is possible. The better the calibration, the more reliable are the results.

6.5 Detailed Instructions Concerning the Choice of Transmission Distance and Frequency

6.5.1 General Outline

The considerations which follow are of great importance not only for planning and realizing a circuit, but also for a better understanding of the diurnal variation of the signal strength. Only if they are respected, can one hope to meet the fundamental requirement of method A3, viz. to have one well-defined transmission mode so dominant that any other mode can be disregarded.

6.5.1.1 As described in Section 6.5.2 below, the choice of the optimum transmission distance is mainly determined by the geometric conditions imposed by the requirement that the measured signal strength can be identified with just one mode. The dominant mode should be preferably the 1E mode or the 1F mode; the ground wave must be negligible anyway. Now, when the distance is fixed, the usable frequencies depend on the critical frequencies of the reflecting layers and the angles of incidence for the chosen distance. The geometric model of a circuit is shown in Figure 6.8 which presents the relation between the virtual heights, the frequencies, and the angles of incidence.

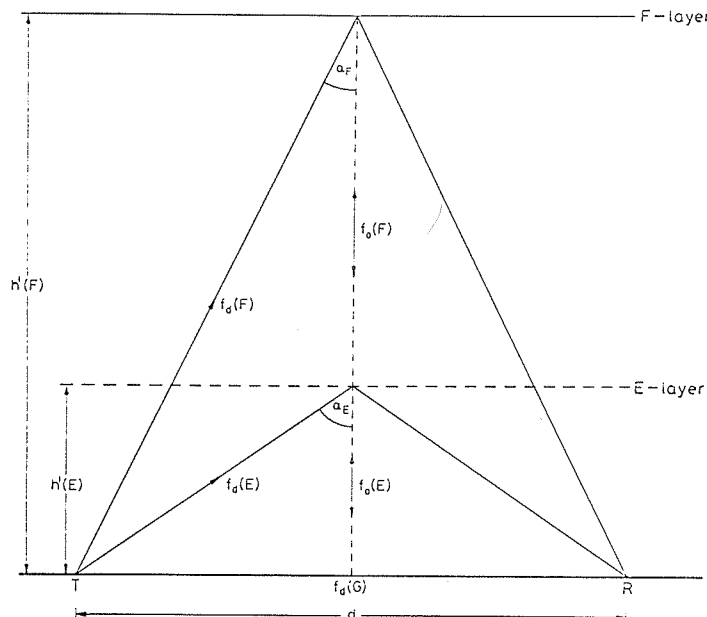


Fig. 6.8 Geometric model for the propagation of ground wave and sky waves at oblique incidence and short distances between a transmitter T and a receiver R. T transmitter, R receiver, d distance between transmitter and receiver, $h'(E)$ (virtual) height of reflection of the wave at the E layer, $h'(F)$ (virtual) height of reflection of the wave at the F layer, $f_d(G)$ frequency of the transmitter (G indicates ground wave), $f_d(E)$ frequency of the transmitter (E indicates reflection at the E layer), $f_d(F)$ frequency of the transmitter (F indicates reflection at the F layer): α_E angle of incidence of the wave at the E layer, α_F angle of incidence of the wave at the F layer, $f_o(E)$ equivalent frequency of the wave for vertical incidence in the E layer, $f_o(F)$ equivalent frequency of the wave for vertical incidence in the F layer.

6.5.1.2 Reflection Condition. For a flat Earth the relationship between frequency f_d which will be reflected at an angle of incidence α to a distance d and a frequency f_0 reflected at vertical incidence from the same virtual height h' is obtained from the refraction law and geometry. Its form for a flat ionosphere is:

$$f_d = f_0 \frac{1}{\cos \alpha} = f_0 \cdot (h'^2 + (d/2)^2)^{1/2} / h' \quad (6.10)$$

It should be noted that the Maximum Usable Frequency (MUF) is related to the critical frequency (f_c) of the reflecting layer by an expression of the same type, that is

$$\text{MUF} \cdot \cos \alpha = f_c. \quad (6.11)$$

Curves giving $\cos \alpha$ or f_0/f_d as a function of distance, d , for reflections at different heights, h' are given in Figure 6.9.

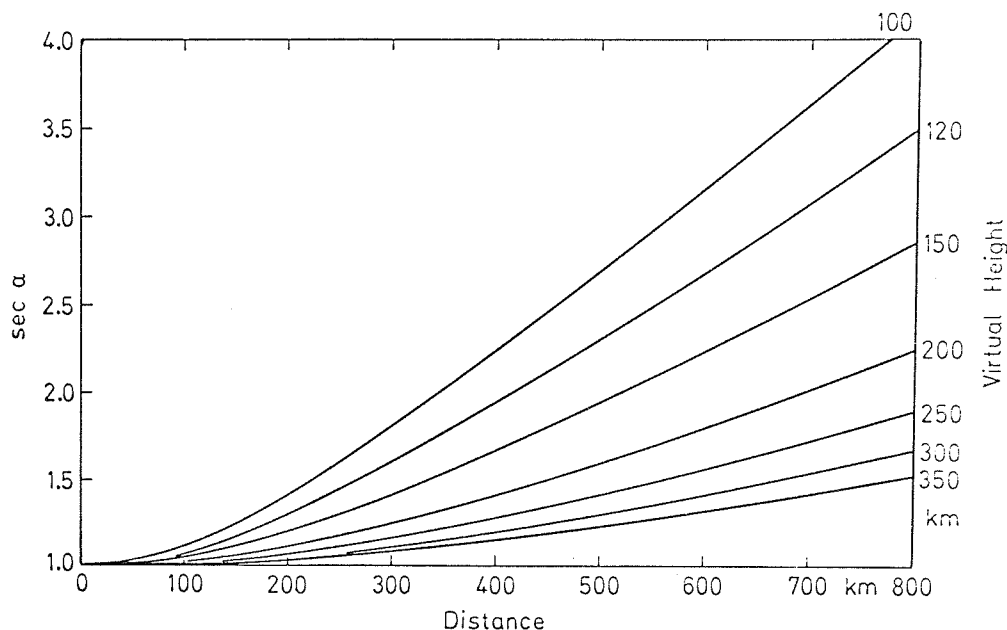


Fig. 6.9. Variation of $\sec \alpha$ with distance (d) and virtual height (h') for E- and F-layer reflections.

6.5.1.3 According to the theory explained in Section 2.5, the absorption of a wave reflected at oblique incidence from the E layer is quite well described by the non-deviative approximation in almost the whole range of frequencies for which reflection occurs at all. There may, however, rather often occur Es layers. These could play an important role by superposing a 1Es signal due to partial reflection on the 1E signal, thus causing fading which on occasions is quite extensive. On the other hand F-layer reflections may be influenced by considerable height changes with time and by the fact that the absorption in the E layer is often deviative. In these cases it is not easy to interpret the observations. For these and other reasons it is desirable, and easier, to use E-region reflections whenever possible. This is, of course, only practical if in the particular configuration used the F-layer reflections, particularly the 1F mode, are much weaker than the 1E mode.

6.5.2 Choice of Distance

To determine a suitable distance between transmitter and receiver, several parameters have to be considered.

6.5.2.1 The shorter the path, the greater the influence of the ground wave is. The ground wave limits the maximum absorption which can be measured during, for example, days of high winter anomaly or a sudden ionospheric disturbance which appears as a short-wave fadeout in the context of A3 measurements. The minimum distance is determined by the signal strength of the ground wave which should be less than the minimum atmospheric noise signal. This minimum distance depends on the conductivity of the ground between the transmitter and the receiver, and on the kind of receiving antenna chosen. For instance, the strength of the ground-wave signal can be reduced very much by using a properly balanced horizontal dipole antenna. For a transmission path over land the ground-wave signal is much weaker than for a path over sea.

6.5.2.2 Angular Selection of Modes. At short ranges ($d \approx 100$ km) the E, F and multiple-order reflections all arrive at approximately the same angle so that it is impossible to separate them by means of the antenna diagram. Between about 100 and 1000 km, the angular separation of the first E and first F echoes is sufficient to enable them to be separated using suitable simple antennas. The greater angular separations are found between 200 and 500 km and this is, therefore, the best range of distances from this point of view (Figure 6.3).

While the E-layer MUF rapidly increases with distance, the usable frequency band increases only slowly, because strong F reflections may be present over much of the band above the screening frequency. Hence the shorter distances near 200 to 300 km are preferred.

6.5.2.3 It is normally essential to use transmitter and receiver antennas which do not radiate vertically so as to minimize the effects of higher order modes when the absorption is small. For this case, it is desirable to keep the distance as short as possible within the limits imposed by the strength of the ground wave.

6.5.2.4 In practice, there is a fairly broad range of useful distances with the optimum near 200 to 300 km. Generally the power required increases with distance, and somewhat greater distances may be used if the available power is sufficient.

6.5.3 Choice of Frequency to Select the 1E Mode. At vertical incidence the upper limit of the range of usable frequencies is determined by the critical frequency, and at oblique incidence by the MUF of the reflecting layer. In practice, deviative losses for vertical incidence become significant within about 20 percent of the critical frequency and prohibitive within 10 percent, whereas for angles of incidence greater than about 45° they are negligible up to the MUF. When the critical frequency is low, this difference is important.

6.5.3.1 In general the critical frequency of the reflecting layer varies with time of day, with season, and with the sunspot cycle, and it is necessary to select a frequency which is reflected for a reasonable part of the day and for all seasons. For instance, at temperate latitudes the critical frequency of the E layer, f_oE , can be estimated approximately from a power law in $\cos \chi$, e.g.,

$$f_oE = (3.25 + 0.0047 \cdot R) \cos^{0.25} \chi \quad (6.12)$$

which has been obtained from the data of the midlatitude station Lindau for the period 1956 to 1966. R is the Zürich sunspot number (generally the monthly median is applied).

6.5.3.2 As to the usefulness in time, frequencies which are adjusted to a constant fraction of the noon MUF will be reflected during the same percentage of total time irrespective of distance; a fixed frequency, however, will be reflected during a longer time as the distance increases. This advantage can only be used if any F-layer reflections present are much weaker than those from the E layer. With simple antennas this is usually only true when the absorption is rather small.

The most important criterion in choosing a frequency is that it should be possible to measure absorption during the whole day. The variations of the E-layer critical frequency during the period when absorption measurements are required should be assessed. In some cases where Es appears regularly and is totally reflecting, the Es layer may also be considered. The minimum blanketing frequency likely to occur in the required period is noted and used to determine the working frequency.

6.5.3.3 The maximum frequency which can be used at any distance is determined by the minimum frequency at which significant F-layer reflections are obtained. This is mainly determined by the E-layer screening frequency f_s which is given by the expression

$$f_s = f_oE \sec \alpha_F \quad (6.13)$$

where α_F is the angle of incidence at the F layer for the required distance d .

In practice, the F-layer absorption is high, up to a frequency 10 percent higher than f_s , so that the maximum frequencies which can be used are rather higher than those given by Eq. (6.13). However, it is indicated to decrease the maximum frequency by 10 percent to allow for day-to-day changes in f_oE . The net result is that the values of f_s given by Eq. (6.13) may be used uncorrected.

6.5.3.4 With low power, the low frequency limit is usually determined by the available sensitivity. At any rate, frequencies lower than $1.5 \cdot \sec \alpha$ MHz are not recommended as these frequencies are often reflected in the D region instead of in the E region. Thus, the highest value of f_oE in the recording period gives a useful lower limit to the desirable frequency band even when high-power transmitters are available.

6.5.3.5 In practice, the critical frequencies deduced above are often too low to be useful and it is necessary to restrict the period of useful observation so that a practical system is obtained. Thus, it is seldom worthwhile to attempt to measure absorption near sunrise and sunset using a frequency which is useful for the remainder of the day.

As an example, let the lowest and highest values of f_oE at noon be 2.0 MHz and 3.4 MHz and suppose that only noon measurements are required. Let the chosen distance be 300 km. Then since $\sec \alpha = 1.12$ as shown in Figure 6.9, the minimum screening frequency for F reflections from a virtual height of 300 km is 2.2 MHz. The available band is then from 1.7 to 2.2 MHz. If the antenna systems could be designed so that the F reflection was negligible, it would be possible to extend this band up to the E-layer minimum MUF, 3.6 MHz. In practice, for such an experiment, a frequency near the lower end of the usable band would be chosen so as to give several hours of useful recording even when f_oE was near its minimum value.

6.5.3.6 When an antenna is used which gives no radiation at vertical direction, such as a vertical monopole, the combination of the effects of antenna polar diagram and the additional spatial attenuation of the 1F mode relative to the 1E mode weakens the 1F mode so much that a totally reflected 1E mode is dominant whenever the absorption is small. It is then unnecessary to depend on screening to weaken the F reflections, and the E reflections can be used until the E or Es MUF is equal to the working frequency. This simplifies the calibration problem at night.

6.5.4 Summary Rules for the Selection of Distance and Frequency

6.5.4.1 In order to select the 1E mode, frequency and distance should be selected in such a way that the observed daytime values of the signal strength, with an error of not more than about 1 dB, are due to the sole one-hop E-layer reflection; F-layer propagation must be excluded by blanketing, higher-order reflections tend to be heavily absorbed. In mid-latitudes, frequencies of 2 to 3 MHz and distances of about 200 to 400 km fulfill these conditions and provide good results.

6.5.4.2 If the 1F mode is desired, i.e. using the F layer as a reflector, frequencies of about 6 MHz and distances of 200 to 400 km can be chosen provided that suitable antennas are employed (see Section 6.6).

6.5.5 Choice of Transmitter

6.5.5.1 The most ideal transmitter would be a crystal controlled continuous wave (CW) transmitter which radiates 24 hours a day and which would be switched off at least for 5 minutes at noon and at midnight so that the noise level at the receiving site can be determined. A convenient power of the transmitter would be 1 to 5 kW.

6.5.5.2 If a double sideband transmitter is recorded, a narrow receiver bandwidth selecting only the carrier frequency should be used, for instance 100 Hz to 500 Hz, provided that the stability of the frequency is high enough (and also there is stability of the local oscillator at the receiver). A narrow bandwidth would also provide a better signal-to-noise ratio; this is particularly important in winter during days when the winter anomaly gives high absorption. Therefore, every care should be taken to have good frequency stability; only in this case can narrow bandwidths and low power be used.

6.5.5.3 If one has a special transmitter, it is convenient to use CW and stop the transmission for some minutes every hour so that the intensity of any interfering signals could be measured. The minimum power for such an unmodulated transmitter depends on the bandwidth of the receiver and the presence of interfering signals. For continuous operation it is recommended that the transmitter be operated with between 25 and 50% of its maximum power.

6.5.5.4 In most cases a commercial transmitter must be used. Such arrangement, of course, reduces considerably the costs of a circuit. But it is necessary to check the transmitted power which should not vary too much. It must be kept in mind here that a 20% change in transmitted power means about 1 dB error of our measurement. Therefore, careful checks must be made.

6.5.6 Availability of Commercial Transmitters

In the frequency range between 2 and 3 MHz coastal communication transmitters are operating in many countries. A world map of such stations exists (*Weltkarte der Küstenfunkstellen für den Sprech-Seefunkdienst auf Grenzwellen*, edited by Deutsches Hydrographisches Institut Hamburg, and similar publications in other countries). There exist also station listings with power indications for nautical radio services. Unfortunately, most of the listed stations do not transmit during 24 hours. Sometimes arrangements can be obtained in view of continuous transmission. This is for example the case of the West German station DAN at Norddeich (2614 kHz). It must be pointed out that in the near future the transmitters of the coastal stations will become nearly useless. Since 1975 some of the transmitters are only on the air when there is a need for communication, that is, the carrier wave is switched on from time to time; the diurnal variation, however, can still be recorded. But beginning in 1978 the coastal transmitters will be operated with single sideband transmission with reduced or even suppressed carrier wave. Then only broadcast transmitters will be available for A3 measurements, but generally not in the frequency band from 1.6 to 6 MHz.

6.6 Receiving and Recording Equipment

The receiving equipment (see Figure 6.10) may be rather simple using four commercially available units.

6.6.1 The receiver is mainly used to select and amplify the nautical frequency. As the measurement is made with automatic volume control (avc), the relevant voltage should be rather large, for example 10 to 30 V.

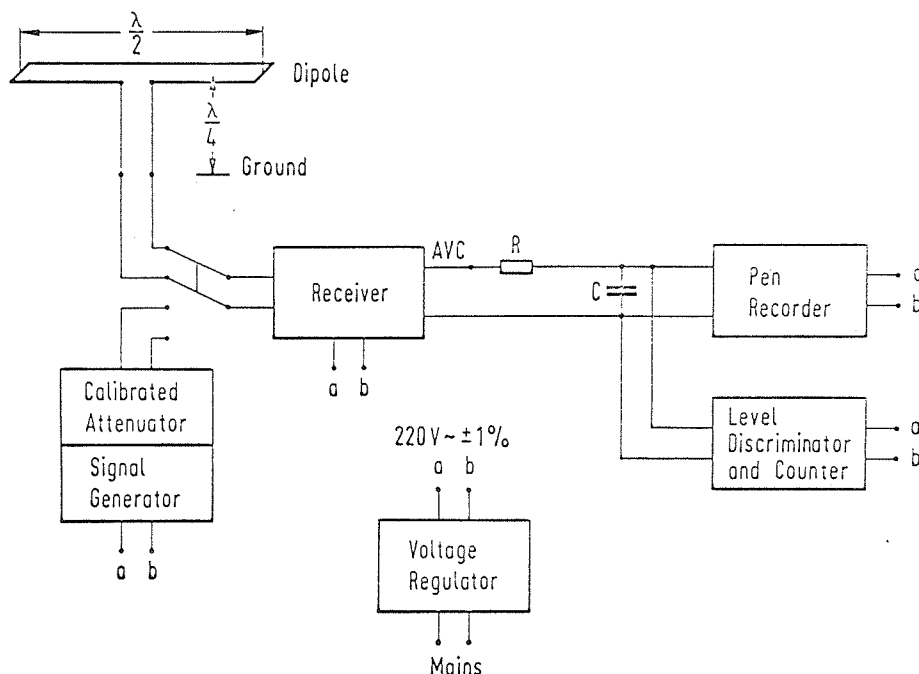


Fig. 6.10 Block diagram of receiving and recording equipment.

6.6.1.1 Tube receivers are generally used, at least in most present day equipment. The commercial receiver BRT 400 T (British General Electric Company) has been found to be suitable provided the voltage regulator tube is replaced by a better voltage regulating device. Unfortunately, this receiver, which is now no longer available, is not insensitive to larger temperature changes. In practice, an important point is to achieve a very good long-term stability of the receiver. This means that the calibration curve of the receiver should be at least approximately logarithmic and have stable working conditions during at least six months. If this can be obtained, the calibration needs only be checked every day at several points, and the data analysis can be performed with the same calibration curve as long as no change occurs.

6.6.1.2 Transistor Receivers

As far as the method A3 is concerned, reports detailing experience with transistor receivers are not yet available. While it is certainly feasible to use such equipment, the stability of the system with temperature and supply voltage should be checked very carefully.

6.6.2 The recorder, usually a pen recorder, should be very reliable. A servo recorder is recommended, as for example the "Enograph" (manufacturer Rhode & Schwarz, Munich). The paper speed may be very low; convenient values are 20 or 60 mm per hour. The width of the paper should be at least about 100 mm corresponding, for example, to a voltage range of 10 or 30 V. It is useful to insert a time constant, determined by a resistor-capacity integrating circuit, between the receiver and recorder; a convenient value of the time constant is between 1 and 5 s.

The noise level may be compensated for by adjusting the pen recorder electrically so that the usual noise level corresponds to zero on the recording paper. The adjustment is made daily by switching off the antenna (and the signal generator for tuning, if just in operation).

6.6.3 The signal generator and calibrated attenuator are usually combined in one unit; the accuracy of the attenuator should be as good as about ± 0.1 dB.

6.6.4 Finally, a voltage regulator for feeding the complete equipment is necessary; its accuracy should be at least $\pm 1\%$.

6.6.5 The recording technique may be extended to give data about fading of signals by adding a level discriminator and a counter so that the frequency distribution of signal strength can be found for convenient periods of time, e.g., with three level discriminators a total dynamic range of 70 dB between the day and nighttime signal strength can be fully covered in 1.5 dB steps. The intervals should be calibrated so as to give exactly logarithmic response. Daily calibration and long term stability are essential.

An interesting feature of half-hourly statistical distributions of signal strength is that the influence of the Es layer can be recognized clearly. Moreover sunrise and sunset changes of absorption can be followed much better. The total time constant of the equipment (receiver plus counter) should not be greater than 5 s.

6.7 Calibration of the Receiving Systems

The receiver should be tuned very carefully to the transmitter and correct tuning checked daily.

After disconnecting antenna and signal generator from the receiver, the recorder is adjusted to zero position to compensate for set noise (see Section 6.6.2).

By recording a chosen transmitter for a couple of days, the most suitable voltage range of the pen recorder can be found. In many cases the optimum coverage of the paper width can be obtained by using a more sensitive voltage range and reducing the avc voltage by the resistor R in Figure 6.10. The highest avc voltage will occur at night when blanketing Es occurs. At middle latitudes the lowest voltages occur around noon in winter (due to the winter anomaly of absorption).

The choice of receiver sensitivity depends on the ground-wave signal and on the noise level.

If the diurnal variation of signal strength is recorded conveniently, accurate calibration can be carried out. The width of the paper which corresponds to a dynamic range of signal strength of about 80 dB should be divided into equal intervals of about 1 dB.

These steps may be drawn on the recording paper. Then, by means of the signal generator the signal strength of each step can be determined. Hence the calibration curve can be drawn.

6.7.1 The method of operation is best illustrated by discussing an existing system, viz, the Norddeich-Lindau Circuit. At Lindau, records are made of the transmission of a German Post Office communications transmitter at Norddeich which operates nearly continuously for 24 hours a day on a frequency of 2.61 MHz. The transmitter-to-receiver distance is 295 km, and the transmitted power is 2.5 kW. (Available power of the transmitter is 10 kW.) A vertical half-wavelength monopole is used at the transmitter and a folded horizontal half-wave dipole placed a quarter wavelength above ground is used at the receiver.

For these conditions the 1E mode will be present whenever f_oE or f_bEs exceeds 1.5 MHz; the 1F path is screened whenever f_oE is above 2.3 MHz. Calibration may be possible using F reflections when these are not screened by E or Es and $f_oF2 \geq 2.8$ MHz. The maximum calibration error (when the absorption is zero) is 10 percent.

6.7.2 Calibration Measurements

In order to calibrate the equipment during conditions of negligible absorption, it is necessary to know the mode of propagation which is then present and the signal strength corresponding to this mode. If the calibration mode of propagation is 1F, it is necessary to determine the equivalent signal strength which would have been received at the angle of incidence corresponding to a 1E mode of reflection.

Provided that one takes measurements during a sufficient number of night hours, the statistical distribution of field strength may be obtained within a few nights. The actual distributions vary with the propagation conditions actually present during the recording periods, but they show certain regular features which identify the main modes of propagation. A convenient sample may be obtained by measuring the maximum signal strength every 3 min from 3 h after sunset until 2 h before sunrise at the ground. Two examples are shown in Figure 6.11. Peaks in the distributions occur at signal strengths which correspond to typical modes of propagation. The interpretation of these peaks is most easily performed with ionograms taken at a nearby station. The most important statement is concerned with the occurrence of Es. For periods with little or no Es, the peak must be due to the 1F reflection mode. The signal strength corresponding to total reflection, E_n , must be determined either for the 1Es or the 1F mode.

6.7.3 Calculation of Calibration Constant

6.7.3.1 If the calibration measurement has been made with the 1Es mode, the median value of $h'Es$ is obtained from the ionograms using the transmission curve, and the corresponding value of s'_n is calculated. The most probable value for E_n for the 1E mode is found from the corresponding maximum in the distributions using the quasipeak values.

If necessary, allowance must be made for the presence of the extraordinary component. On the average, this makes E_n about 1.2 times greater than the true value. Let the appropriate factor be K_c . When the 2E mode gives a significant contribution to the field from Eqs. (6.5) ... (6.7) the correction E_{tot}/E_n is calculated; this is K_d . Then the calibration constant for the 1E mode used during daylight hours is:

$$\frac{C(E)}{dB} = 20 \log (E_n s'_n K_c K_d) \quad (6.14)$$

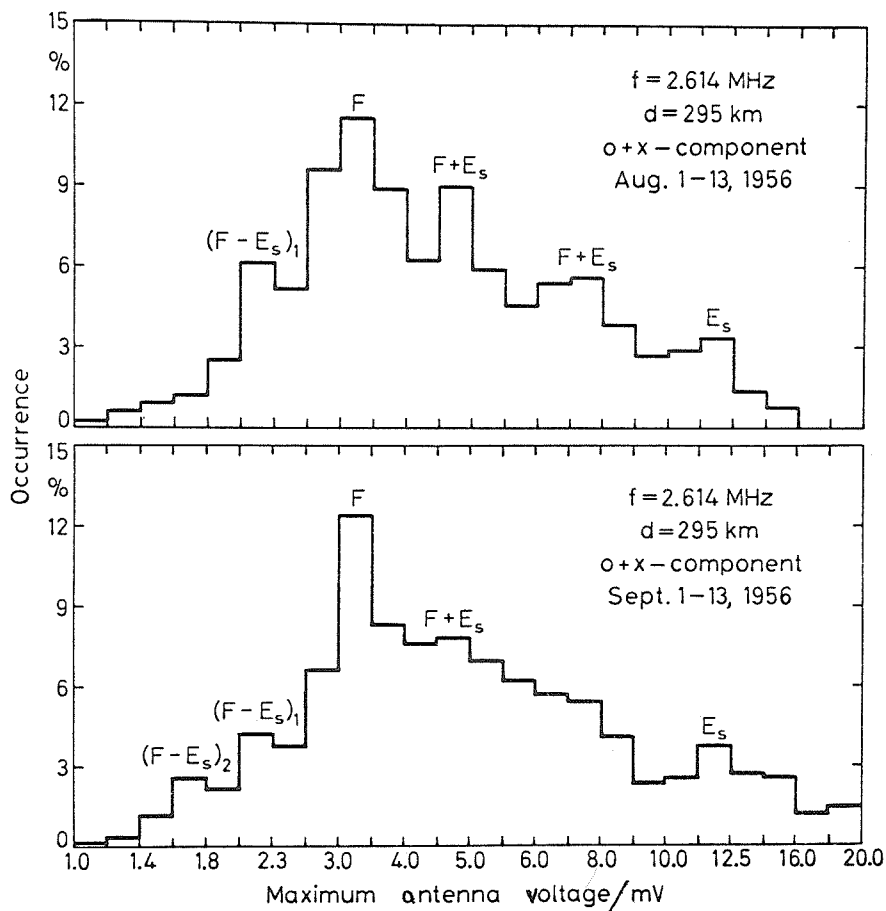


Fig. 6.11 Frequency of occurrence of maximum values of antenna voltage (signal strength) during intervals of 3 min during the night; stronger E_s reflections present. Compare with Figure 6.13.

6.7.3.2 If the calibration measurements have been made with the 1F mode, the most probable value $E_n(F)$ is found using the average $h'F$ for the period of calibration measurements. The value of $s'_n(F)$ is calculated for the adopted mean value of $h'F$. Allowance is made for the presence of the extraordinary 1F mode. This makes $E_n(F)$ about 1.4 times greater on the average than the true value.

The relative gains of the antennas in the directions of the 1E and 1F modes are calculated and from these the following factors are determined:

$$K_a = G_t(1E)/G_t(1F); \quad K_b = G_r(1E)/G_r(1F) \quad (6.15)$$

Then, the calibration constant for the 1F mode is:

$$\frac{C(F)}{dB} = 20 \log \left[E_n(F) s'_n(F) K_a K_b K_c \right] \quad (6.16)$$

In general it is much easier to obtain values of $C(F)$ than of $C(E)$, and there will be many occasions when only the former can be determined.

6.7.3.3 The two values $C(E)$ and $C(F)$ are then compared and used to check the reliability of K_a , K_b , K_c and K_d . The long-term stability of the equipment may be determined by comparing values of $C(F)$ obtained on different occasions, and this should always be done. By suitable inspection a final value, C , of the calibration constant is deduced from $C(E)$ and $C(F)$.

The absolute accuracy of the experiment depends finally on the accuracy of $C(E)$ and $C(F)$. If their magnitudes differ significantly, a special investigation is needed to identify the cause, e.g. by finding the relationship between $C(E)$ or $C(F)$ values at times when it is reasonably certain that both modes are occurring simultaneously and when only one is likely to be present. With simple antennas on a reasonably flat site, it is usually possible to compute K_a and K_b with adequate accuracy.

6.7.3.4 The change in signal strength from day to night is likely to be more than 40 dB in practice. Thus, even if the accumulated error is as much as 3 dB, the absorption can be measured with an accuracy of 10 percent. Clearly, a crude calculation using computed values of antenna gain (K_a , K_b) and 0.8 as an average value for K_c is likely to give a value of $C(F)$ which will be quite adequate for many purposes. However, when good values of $C(E)$ are available, these should be used. Calibration constants should be determined for each month.

6.7.4 Determination of the Absorption Value $A(f)$

6.7.4.1 The values of $A(f)$ are deduced from the daytime values of the cymomotoric force, $E_d s'_d$, and the calibration constant, $C(E)$ or $C(F)$. It is essential to identify E_d in the same way as E_n , i.e., either peak or median values should be adopted in both cases. The calibration is simplest if peak values are used throughout, though this may be slightly misleading on a few occasions when strong fading is present.

6.7.4.2 The value of s'_d is deduced from the value of h' obtained with the transmission curve. The equivalent absorption is then

$$\frac{A(f_d, 0)}{dB} = -\cos \alpha (20 \log E_d s'_d - C) \quad (6.17)$$

where C is the best value of the calibration constant deduced from $C(E)$ and $C(F)$ (see Section 6.7.3.3 above).

6.7.4.3 When E_d is comparable with the ground-wave signal E_g or with the estimated noise level E_r , it is possible to compute E_d approximately from the observed total signal E_c using:

$$E_d = (E_c^2 - E_g^2)^{\frac{1}{2}} \quad \text{or} \quad = (E_c^2 - E_r^2)^{\frac{1}{2}} \quad (6.18)$$

It is very convenient to solve Eq. (6.18) graphically using log-linear graph paper. The relation between $A(f_d, C)$ and $\log E_d$ is linear and determined by the constant.

It is helpful to know the probability distribution of the different virtual heights, h' . For the circuit Norddeich-Lindau ($d=295$ km, $f=2.614$ MHz) the frequency of occurrence, n , was obtained by applying the transmission curve to ionograms of the station Lindau. The result shown in Table 6.2 gives a maximum of probability at $h'=305$ km. This value is used for $h'F$ and only such data E_n are taken from the signal strength records which belong to time periods for which h' is between 280 and 330 km.

Table 6.2

| h' (km) | n | h' (km) | n | h' (km) | n |
|--------------|-----|--------------|-----|--------------|-----|
| 200 | 0 | 280 | 57 | 350 | 30 |
| 210 | 0 | 290 | 66 | 360 | 12 |
| 220 | 4 | 300 | 76 | 370 | 7 |
| 230 | 22 | 310 | 73 | 380 | 6 |
| 240 | 30 | 320 | 62 | 390 | 2 |
| 250 | 26 | 330 | 47 | 400 | 1 |
| 260 | 40 | 340 | 38 | 410 | 0 |
| 270 | 33 | | | | |

6.8 Use of an Ionosonde in the Neighborhood of an Absorption Circuit

6.8.1 In the simplest case the variation of reflection height during the day can be neglected if the 1E mode is dominant in the daytime. The 1Es mode is used for calibration at night. For purposes of calibration the factor s'_n/s'_d in Eq. (6.2) may be assumed to be 1. But it must be taken into account that only a blanketing Es layer occurring at night can meet the necessary condition of $s'_n/s'_d=1$. Otherwise the calibration must be carried out by extrapolating procedure as described in Section 6.4.2 above.

6.8.2 It is difficult to decide from the sole signal strength record whether an Es layer at night is blanketing or not. The uncertainty of the interpretation of the signal strengths received at night can be avoided if ionograms are available from a station within a few hundred km of the midpoint of the path (see Section 6.7). Thus it is most desirable that such ionograms be made available, at least when calibrating the equipment. The shorter the distance between the ionosonde and the midpoint of the path, the more certain it is that the midpoint conditions will be similar to those given on the ionogram. Experience shows that occurrence of Es at the midpoint of the path at night resulting in an increase of signal strength does not mean that Es echoes also occur on ionograms obtained from an ionosonde located at one end of the path. But if a longer sequence of half-hourly ionograms show that little or no Es is present, there is only a small chance of a 1Es mode being present on the oblique path.

The use of an ionosonde for the interpretation of the signal strengths received at night and the determination of approximate reflection heights at oblique incidence is described in the following Section 6.9.

6.8.3 When no ionosonde is available, the deductions about the mode present should be checked using the seasonal variations of Es that are typical for the latitude zone involved. For instance, at temperate latitude Es is quite common in summer but rather rare in winter.

6.9 The Use of a Transmission Curve

Provided that an ionosonde is available in the vicinity of the circuit -- the best place for it would be below the point of reflection -- the heights of reflection and the modes of transmission can be determined.

6.9.1 The ionogram is a plot obtained automatically with photographic recording. It shows virtual height of reflection h' as a function of frequency f_0 of the wave reflected vertically from the ionosphere. Now, for a flat earth and for short distances (up to 500 km or so) there is a simple relation between the oblique incidence frequency, f_d , which will be reflected at an angle of incidence α , the distance d , and the frequency, f_0 , reflected at vertical incidence from the same virtual height h' :

$$f_d = f_0 / \cos \alpha = f_0 / (h^2 + d^2/4)^{1/2} / h' . \quad (6.19)$$

6.9.2 For a given circuit, f_d and d are fixed values. As shown by N. Smith [1937], Eq. (6.19) may be taken as the relationship between f_0 and h' , which when plotted is called the "transmission curve". This curve is placed upon an ionogram so that the frequency for which the transmission curve, Eq. (6.19), goes to infinity coincides with the frequency used at distance d . Then the intersections of the transmission curve with the ionogram trace considered determine the equivalent heights of the "high angle" and the "low angle" ray. In the cases where the A3 method is applied only the low angle ray is of importance (i.e., the lower h' value found by intersection).

6.9.3 In practice, the ionogram can be projected optically on a table bearing the plot $h' = h'(f_0)$ corresponding to the transmission curve as in Eq. (6.19). Modes and the virtual heights of reflection can be determined easily, for instance, at intervals of half an hour if ionograms are taken according to this schedule.

6.9.4 Figure 6.12 shows an ionogram from Lindau with a transmission curve for $d = 295$ km superposed on it to show the virtual heights of reflection for the frequency 2.61 MHz. In this example, a partial reflection from an Es layer at 110 km was present, together with a total reflection from a virtual height of about 300 km in the F layer. When the ionogram shows that the F echoes are screened so that they do not intercept the transmission curve, only Es modes are possible. The virtual heights of reflection must be known in order to evaluate the angles of incidence and oblique path lengths; they may be obtained directly from the heights of interception of the transmission curve and the traces on the ionogram.

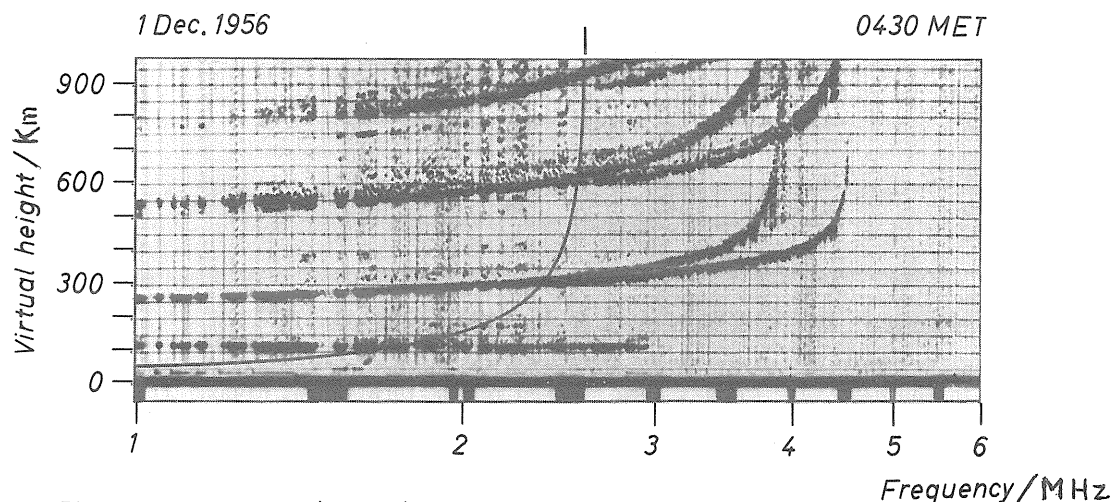


Fig. 6.12 Ionogram (Lindau) with superposed transmission curve.

6.9.5 Determination of Modes In the daytime the CW signal strength should be determined mainly by one mode of propagation, either the 1E or the 1F mode. During the night the 1F propagation will dominate, but 1Es can give considerable signal strength, particularly in the lower frequency range (2 to 3 MHz). If at night both the 1Es and 1F modes are considered, it is necessary to take account of six different types of propagation (Figure 6.13). These differ from each other according to whether one or both modes are present and whether the F mode is weakened (by partial reflection or absorption) at one or both of the points where it penetrates the Es layer.

All the indicated types have occurred in practice in the Norddeich-Lindau experiments. Type 1 is very common; Types 3 to 6 are fairly common; Type 2 is rather rare at most seasons.

6.9.6 Determination of Virtual Heights When F-layer reflections are being used for calibration purposes, it is convenient to restrict the analysis of the signal strength to times when the F-layer virtual height is within certain limits which may be selected using the distribution of virtual heights corresponding to the F-mode propagation at night for a month. An example is shown in Section 6.7.4 (Table 6.2). Since a change of 20 percent in virtual height alters the unabsorbed field by about 10 percent, a range of ± 10 percent about the most probable height may be used without incurring a significant error. Data obtained when $h'F$ lies in this range and Es is absent may be used to determine the calibration values very quickly. When there are seasonal changes in $h'F$ of more than 20 percent, it is, of course, necessary to change the adopted value of $h'F$ accordingly.

6.10 A Few Characteristic Results

Most published A3 investigations were made in Europe [Schwentek, 1958, 1963a,b, 1967, 1968, 1971; Triska, 1962, 1965, 1967; Nitzsche, 1964; Hense, 1969]. Since A3 uses continuous recording, it is very helpful for identifying events like SIDs (see Section 6.10.5) or eclipses [Nitzsche, 1964] and in particular the winter days of anomalously high absorption which seem to be related with stratospheric warmings [Bossolasco and Elena, 1963; Rose and Widdell, 1965; Shapley and Beynon, 1965; Triska, 1965; Dieminger *et al.*, 1966; Schwentek, 1967, 1968, 1971; Labitzke and Schwentek, 1968].

6.10.1 The diurnal variation of absorption is rather easily followed by method A3.

6.10.1.1 If, for instance, the half-hourly signal strength values E_d are plotted vs. time, the diurnal variation of signal strength can be represented. Since the absorption loss is given by

$$A(f_d, \alpha) = 20 \log \frac{E_n s'_n}{E_d s'_d} \quad (6.20)$$

two parameters must be determined in order to find from E_d the absorption value, namely the nighttime value E_n and the ratio s'_n/s'_d ; the latter can be derived exactly only by application of the transmission curve to ionograms taken near the midpoint of the circuit. Otherwise, admitting a certain error, s'_n/s'_d is generally assumed to be one.

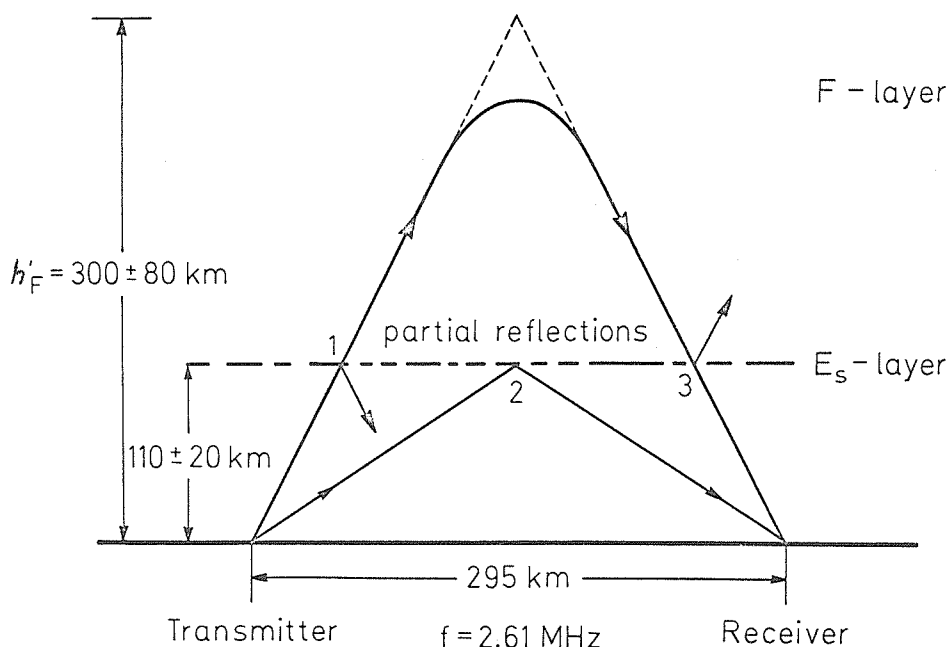


Fig. 6.13 Geometry of the Norddeich-Lindau path and type of propagation at oblique incidence.

1. 1F mode only; no Es layer present;
2. 1 Es mode only; F layer blanketed;
3. 1F mode + 1Es mode (reflection usually partial); reflection at point 2, no reflections at points 1 and 3;
4. (F-Es)₁; reflection at the F layer and partial reflection (or absorption) at (in) the E layer at point 1 or point 3;
5. (F-Es)₂; reflection at the F layer and partial reflection (or absorption) at (in) the E layer at point 1 and point 3;
6. (F-Es)_{1,2} + Es; reflection at the F layer and Es layer (at point 2) and partial reflection (or absorption) at (or in) the Es layer at point 1 or point 3, or at point 1 and point 3. In such cases the distribution of signal strength can be rather involved.

6.10.1.2 Now, it is advisable to plot not only $A(f, \alpha)$ as a function of time, but also $\log A$ against $\log \cos \chi$ using one sheet of mm paper for each day. From the plot $\log A$ vs. $\log \cos \chi$ it is easy to derive the following parameters: subsolar absorption A_0 , exponent n , time delay τ and data with $A(\cos \chi = \text{constant})$. Data can be averaged for groups of several days up to one month. An example is shown in Figure 6.14. Thus, the diurnal variation of absorption is determined.

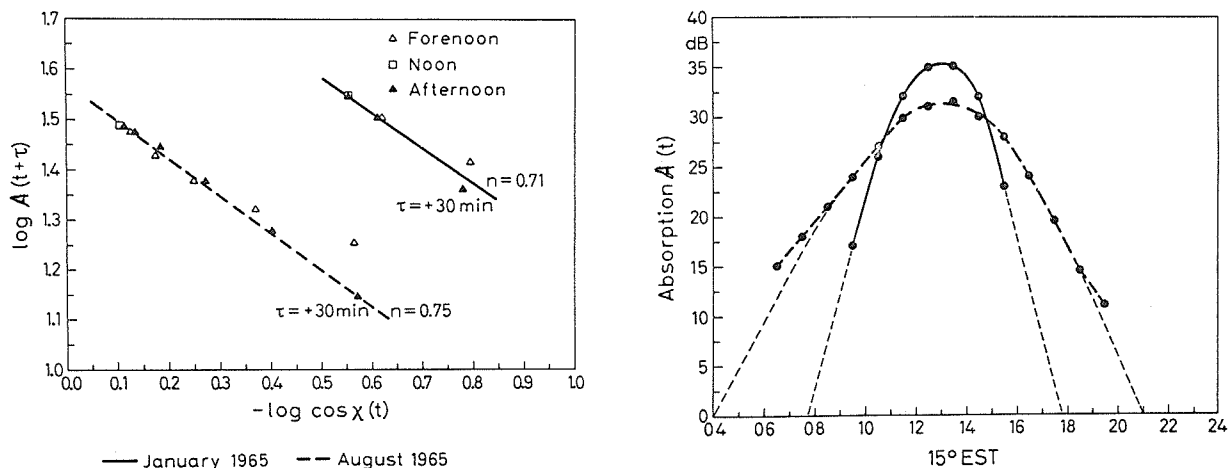


Fig. 6.14 Diurnal variation of absorption loss for January and August 1965 (circuit Norddeich-Lindau; 296 km; 2.61 MHz). Left figure: $\log A(t+\tau)$ vs. $-\log \cos \chi$ as an example for the equation $A(t+\tau) = A_0 \cos^n \chi(t)$; the values for forenoon, noon, and afternoon were separated. Right figure: $A(t)$ vs. t (15° EST).

6.10.1.3 Because the absolute values and the shape of the diurnal variation may vary considerably from day to day, averages should be considered with some caution. Particularly in winter at middle latitudes, monthly averages often give a rather crude picture; this is due to the winter anomaly. There are in fact groups of days showing very high absorption among other days with much smaller but still anomalous absorption. On the northern hemisphere the phenomenon occurs mainly in January and February, but also in October, November, December and March.

6.10.2 Seasonal variation of absorption is either determined from noon values or from values at constant solar zenith angle. Three examples are described by Figures 6.15 and 6.16. In Figure 6.15 daily noon values for a period of one year have been plotted against $\cos \chi$. The values are separated according to season. The occurrence of the winter anomaly appears clearly (see the triangular symbols). This increase occurs only at temperate latitudes; in Europe the range is about 30° to 70° .

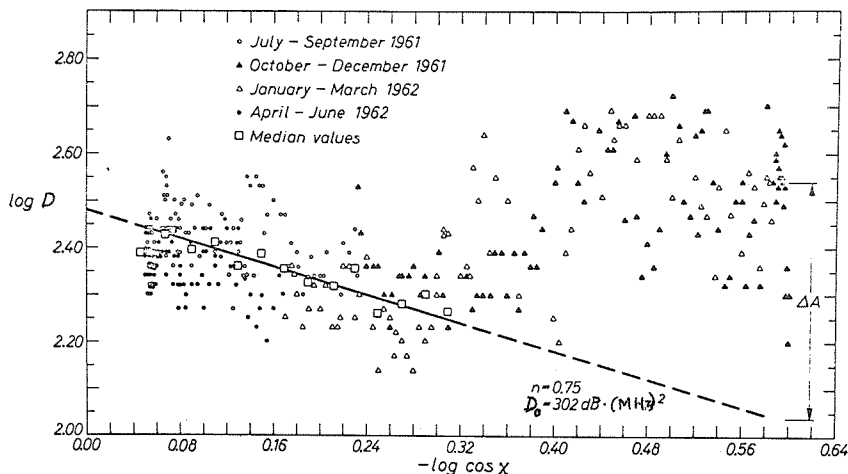


Fig. 6.15 Daily noon values of $\log D$ vs. $-\log \cos \chi$ for one year (1961/62) (circuit Norddeich-Lindau). The exponent found for most of the diurnal variations is the same as that for the seasonal variation for this particular year. See Section 4.7.6.1, Eq. (4.13) for a definition of D .

In Figure 6.16 absorption A at a constant solar zenith angle is plotted vs. time. The forenoon and afternoon values are shown separately. Also the difference between the values is shown, indicating a certain delay between the time of highest absorption and the time of minimum solar zenith angle χ (at local noon).

Since the absorption in the ionosphere is correlated strongly with the solar zenith angle, this should be taken into account in evaluating averages. Therefore such averages should preferably refer to the summer and winter solstices. Median values for periods of 15 (or 16) days around the solstices are recommended.

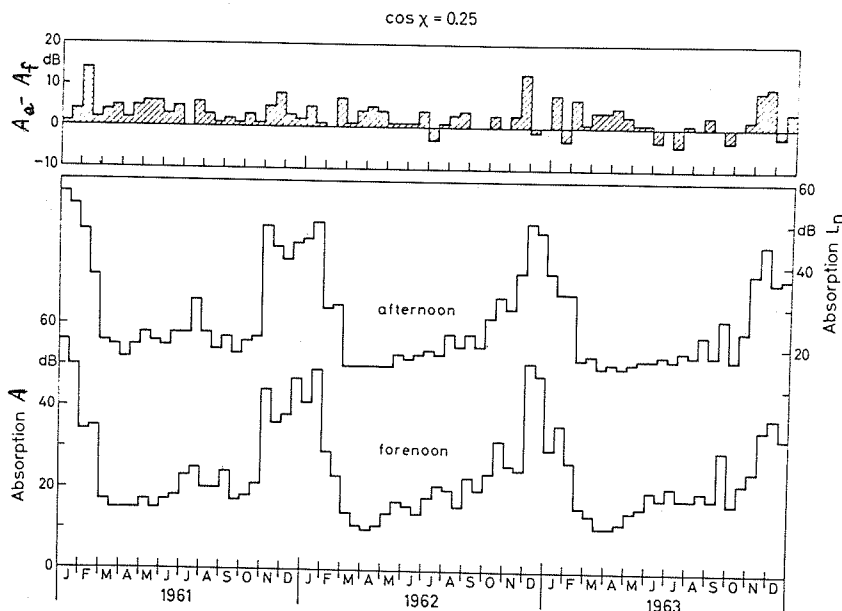


Fig. 6.16 Absorption loss for solar zenith angle = constant ($\cos \chi = 0.25$) plotted vs. time; circuit Norddeich-Lindau (main diagram). The upper small diagram shows the difference between afternoon and forenoon absorption.

6.10.3 Variation of absorption in the sunspot cycle can be monitored very well with method A3 when applied at frequencies around 2.5 MHz. By taking median noon values half-monthly and plotting them vs. time, the sunspot cycle can be followed. A typical example for midlatitudes, the results from the circuit Norddeich-Lindau are presented in Figure 6.17. It should be noted that in summer there is a tendency to lower values which is very probably due to a decrease of the reflection level around noon, an effect which can also be recognized on the daily plots of $\log A$ vs. $-\log \cos \chi$. In winter, the well-known winter anomaly is present but only at "subauroral" latitudes.

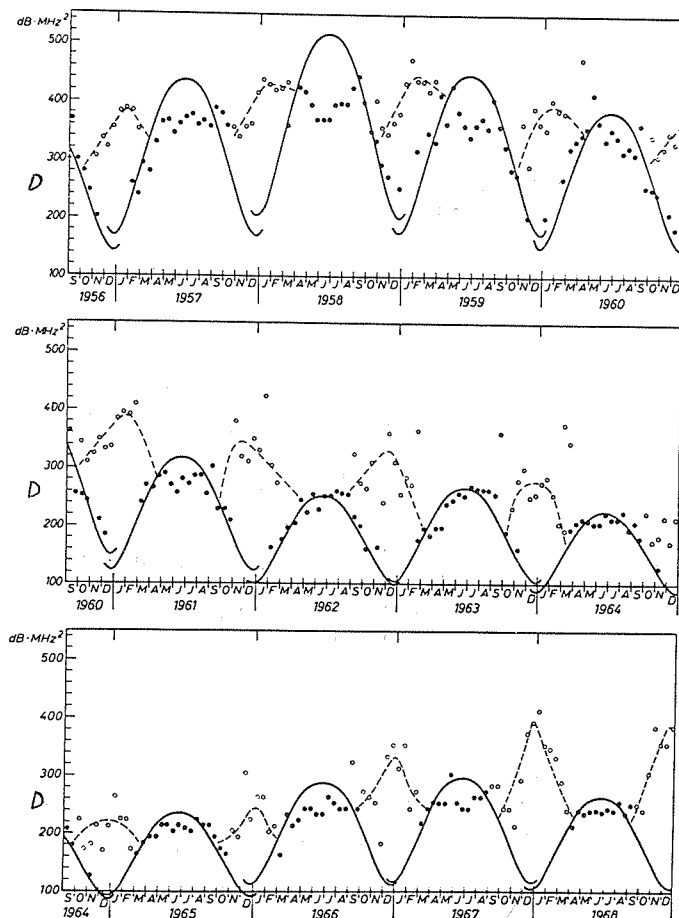


Fig. 6.17 Half-monthly median noon values of absorption from 1956 through 1968, i.e. over more than one sunspot cycle; circuit Norddeich-Lindau. The curves indicate the function $D = D_0 \cos^{0.75} \chi$; D_0 was determined empirically from plots of $\log D$ vs. $-\log \cos \chi$ (see Figure 6.15).

6.10.4 Correlation between ionospheric absorption and other parameters of the atmosphere can be obtained from the theory of wave attenuation by collisions (see Chapter 2). The absorption value A may be interpreted an atmospheric parameter in view of Eqs. (2.12) through (2.17). If the simplifications mentioned in Section 2.5 are valid, we have the easy case of non-deviative absorption. This is largely true for suitably arranged A3 circuits so that, according to Eqs. (2.12) and (2.17),

$$A \propto \int_0^h N \cdot \nu \, dh \quad (6.21)$$

holds, where N is electron density, ν collision frequency, and h height of reflection. Thus absorption is a function of the electron density and electron collision frequency profile. These depend upon the solar radiation and state of the neutral atmosphere. The level of magnetic activity also has an effect. Hence, correlations have been found between the various parameters of the atmosphere and ionospheric absorption, see: Shapley and Beynon [1965], Belrose and Thomas [1968], Bourne and Hewitt [1969], Labitzke and Schwentek [1968], Schwentek [1966, 1968, 1969].

6.10.5 Shortwave fadeouts, also called Sudden Ionospheric Disturbances (SIDs), can most successfully be monitored with A3 continuous recording of signal strength. A frequency of about 2.5 MHz and a distance of about 300 km are suitable for quantitative measurements in case of weak effects. During stronger effects,

however, only the noise level or the ground wave signal is recorded so that the period of strongest attenuation gives no precise numerical data. While this is an inconvenience (avoided by method A2, see Chapter 5) the presence of a strong SID can be seen in the record quite well, and also the period of strong absorption. Strong events are better reproduced with a higher frequency, say 6 MHz.

An example is given in Figure 6.18 where A3 records on three frequencies are shown, together with an A2 record obtained on 27.6 MHz.

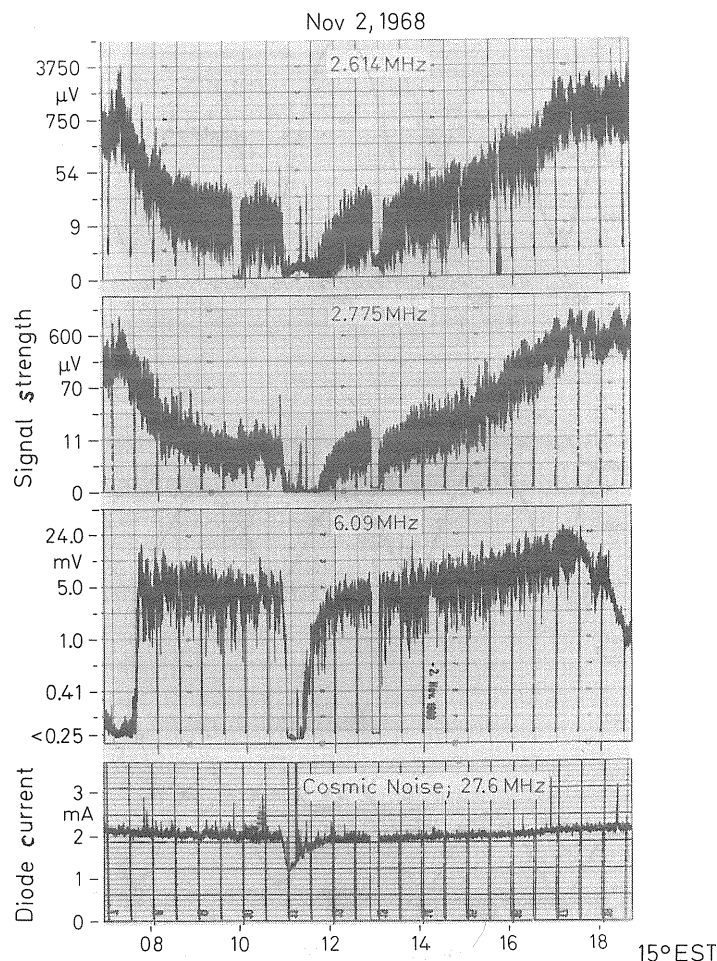


Fig. 6.18 Shortwave fadeout, November 2, 1968. Shown are the records of three different transmission paths and of one riometer. NL Norddeich-Lindau (296 km; 2.614 MHz); KL Kiel-Lindau (300 km; 2.775 MHz); LL Luxemburg-Lindau (339 km; 6.09 MHz). The antenna of the riometer, a horizontal half-wave dipole in a corner reflector, is directed to the pole star. During the strong flare only the riometer gives a complete record. Start of the effect: 0949 UT, maximum at 1001 UT, end at about 1112 UT. Absorption at 6.09 MHz higher than 26 dB, at 27.6 MHz 2.27 dB.

6.11 Program of Observations

6.11.1 Continuous recording should be maintained during the whole day so that the diurnal variation of absorption can be checked in the best possible way. For calibration purposes, it is essential that records are available for the nighttime. When using 1E in the daytime, it is necessary to look for times when E-region reflections are dominant at night (1Es). If there are nights without reflections from the Es layer (at middle latitudes this often occurs during winter), the 1F transmission can be used for calibration provided, however, that the antenna diagrams are known (see Section 6.3.4). On higher frequencies (around 6 MHz), the transmission may be interrupted at night for a couple of hours because of a low critical frequency of the F2 layer. There should at any rate be enough hours of 1F transmission at night for calibration purposes.

6.11.2 Presentation of results should be made uniformly. It is usual that for daylight hours, hourly values (or better half-hourly values) of absorption loss, A (in dB), are presented in monthly tables, one for each frequency. The characteristic parameters of the circuit (frequency, antennas, distance between transmitter and receiver, orientation with respect to geographic North and to the geomagnetic field, method of calibration used) should be indicated on every sheet. Daily plots of $\log A$ vs. $-\log \cos \chi$ are very helpful; using the data on such plots, A ($\cos \chi = 0.1$) can be determined easily. These data seem to be very suitable for correlation with other parameters of the atmosphere. It is recommended strongly that these data also be published in monthly tables giving hourly values. At present the international interchange rules for absorption (A3) are as follows:

Monthly tables should be sent to the WDCs, one for each frequency giving hourly values of the absorption in dB but only for hours when E-region reflections were dominant. Medians, median count and quartiles should also be given. The location of the transmitter and the path length must be specified.

6.11.3 Comparison of continuous wave (CW) and pulse propagation whenever available should be considered as a great help for better understanding the details of method A3.

As an example, Figure 6.19 shows the transition from E- to F-layer transmission around sunset. At about 1710 h the intensity of the 1E pulse signal and the signal strength decrease. Between 1715 and 1730 h the 1F and 1E pulse signals are rather weak resulting in a considerable decrease of signal strength. After 1730 h the dominant mode is 1F. If there had been an Es layer around sunset with a coefficient of reflection $r = 1$, then the series of (relative) maxima of signal strength could have been indicated by the dotted line (in part C of Figure 6.19). This shows again how the nighttime value, E_n , can be derived by extrapolation of the diurnal variation of signal strength.

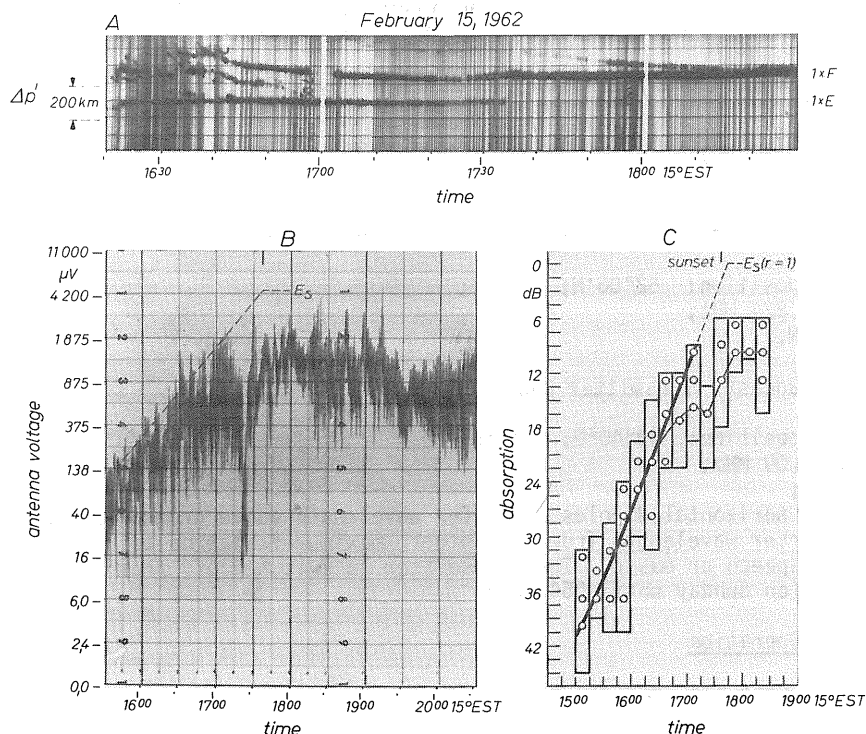


Fig. 6.19 Comparison of pulse propagation (2.5 MHz) and CW propagation (2.61 MHz) over the same transmission path (Norddeich-Lindau; 296 km). (A) Pulse recording. (B) Signal strength recording with CW transmission. (C) Frequency distribution of signal strength derived from a level discriminator. Upper and lower limits of the squares indicate a number of 50% with regard to the maximum number (100%) of counts.

6.11.4 Present State of Application of Method A3

Until now, the method A3 using short waves has been applied predominantly in Europe.

6.11.4.1 Available Transmitters There are some important transmitters in Europe, the signal strength of which is recorded at several locations.

1. Shortwave communication transmitter Norddeich-Radio DAN in Germany (FRG).

Geographic position: 53°36.5'N; 7°8.5'E;
Frequency: 2.614 MHz;
Power: 2.5 kW;
Antenna: Vertical dipole; 5/8 wavelength high;
Modulation: Speech; time signals at 1150 - 1200 UT and 2355 - 2400 UT; transmitter is sometimes switched off, mainly during the night.

2. Shortwave communication transmitter Kiel Radio DAO in Germany (FRG).

Geographical position: 54°26'13.5"N; 10°08'3.6"E;
Frequency: 2.775 MHz;
Power: 2.5 kW;
Antenna: Vertical dipole; 5/8 wavelength high; height of the pole 45 m;
Modulation: Speech.

3. Shortwave time signal transmitter Prague OMA in Czechoslovakia [Třiska, 1962, 1967].

Geographic position: 50°04'24"N; 14°52'55"E;
Frequency: 2.500 MHz;
Power: 1.0 kW;
Antenna: Vertical monopole, height half a wave length;
Modulation: Every hour the transmitter is switched off, between the 40th and 45th minute.
First minute of every quarter of an hour: Call Signal; 2nd to 5th minute: 1 KHz;
15th minute: Time signals; 20th - 25th minute: carrier wave only.

4. Shortwave communication transmitter Oostend (Belgium).

Geographical position: 51°11'N; 2°48'E;
Frequency: 2.761 MHz;
Power: 0.2 kW.

5. Shortwave communication transmitter Scheveningen (Netherlands).

Geographical position: 52°06'N; 4°15'E;
Frequency: 2.824 MHz;
Power: 2.0 kW.

6. Shortwave broadcast transmitter Radio Luxembourg (Luxemburg).

Geographical position: 49°40'N; 6°19'E;
Frequency: 6.09 MHz;
Power: 50 kW;
Antenna: Two horizontal dipoles a quarter wavelength above ground, spaced a quarter wavelength from each other; maximum radiation to 58° (NE);
Modulation: Speech or music. The transmitter is switched off from 0200-0400 UT (on Sunday until 0545 UT).

6.11.4.2 Circuits in Operation

The following circuits are continuously in operation (1968/72):

- 1) Norddeich-Lindau (Germany, FRG); $d = 296$ km.
- 2) Norddeich-DeBilt (Netherlands); $d = 214$ km.
- 3) Norddeich-Neustrelitz (Germany, GDR); $d = 395$ km.
- 4) Norddeich-Panská Ves (Czechoslovakia); $d = 600$ km.
- 5) Norddeich-Leicester (Great Britain); $d \approx 570$ km.
- 6) Kiel-Lindau (Germany, FRG); $d = 317$ km.
- 7) Kiel-Neustrelitz (Germany, GDR); $d = 220$ km.
- 8) Kiel-Panská Ves (Czechoslovakia); $d = 520$ km.
- 9) Kiel-Leicester (Great Britain); $d \approx 760$ km.
- 10) Oostend (Belgium)-Leicester (Great Britain); $d \approx 320$ km.
- 11) Scheveningen (Netherlands)-Leicester (Great Britain); $d \approx 370$ km.
- 12) Luxembourg-Lindau (FRG); $d = 339$ km.
- 13) Stuttgart-Neustrelitz (GDR); $d = 570$ km.

The following circuits have been operated for certain periods:

- 1) Omaruru-Tsumeb (Southwest Africa); $d = 275$ km.
- 2) S. Marinella-Capo S. Lorenzo (Italy); $d = 340$ km.

CHAPTER 7. METHOD A3 (b): OBLIQUE INCIDENCE FIELD STRENGTH OBSERVATIONS ON
FREQUENCIES IN AND BELOW THE MF BROADCASTING BAND

by

E. A. Lauter

Zentral-Institut für Solar-Terrestrische Physik, Obs. Kühlungsborn (G.D.R.)

with the assistance of

J. Bremer, G. Entzian and K. Sprenger

Table of Contents

| | Page |
|--|------|
| 7.0 List of Symbols | 148 |
| 7.1 Introduction | 149 |
| 7.2 Receiving and Recording Equipment | 149 |
| 7.2.1 Description of the Measuring Equipment | |
| 7.2.1.1 Loop antenna | |
| 7.2.1.2 Auxiliary antenna | |
| 7.2.1.3 Ground wave elimination circuit | |
| 7.2.1.4 Receiver | |
| 7.2.1.5 Recording unit | |
| 7.3 Examples of Records | 151 |
| 7.4 The Evaluation of the Sky Wave Records and Determination of Ionospheric Absorption | 152 |
| 7.5 Discussion of the Factor C for the Determination of the Absolute Values of Ionospheric Absorption | 155 |
| 7.6 Choice of Transmitter | 157 |
| 7.7 Choice of Observing Site | 157 |
| 7.8 Observing Program | 157 |
| 7.9 Some Examples of Results from A3 Records in the LF and MF Range | 157 |

7.0 List of Symbols

- E : electric field strength (in general)
- E_G : electric field strength of the ground wave at the observing site
- E_i : effective electric component of the sky wave at the receiving loop antenna
- $\overline{E_i}$: median of E_i
- E_N : electric field strength of the ground wave measured at a point near the transmitter (distance r_N)
- E_0 : reference field strength at 1 km distance from the transmitter
- E_{0G} : ground-wave reference field strength at 1 km distance from the transmitter
- E_{0S} : sky-wave reference field strength at 1 km distance from the transmitter
- E_S : resultant electric field strength of the sky wave
- E_{S1} : "normal" component of the electric sky-wave field strength, oscillating in the plane of incidence
- $\overline{E_{S1}}$: median value of E_{S1}
- E_{S2} : "abnormal" component of the electric sky-wave field strength, oscillating perpendicularly to the plane of incidence
- $\overline{E_{S2}}$: median value of E_{S2}
- h : reflection height
- H_i : effective magnetic component of the sky wave at the receiving loop antenna
- H_{S2} : "abnormal" magnetic component of the sky wave, oscillating in the plane of incidence
- i : angle of incidence on the ionosphere
- K : a factor describing the deviation of the vertical radiation pattern of the transmitting antenna from that of an elementary dipole
- A' : ionospheric absorption (in dB) at oblique incidence
- r : distance from transmitter (km)
- r_G : length of the ground-wave propagation path
- r_N : distance from the transmitter to the nearby measuring point where the field strength E_N has been measured
- r_S : length of the sky-wave propagation path
- η : ground-wave transmission factor over the given measuring path r_G
- η_N : ground-wave transmission factor over the short distance r_N
- ρ : ionospheric reflection coefficient (in general)
- ρ^i : total ionospheric reflection coefficient at oblique incidence
- ρ_1^i : (normal) ionospheric reflection coefficient at oblique incidence
- ρ_2^i : ionospheric conversion coefficient at oblique incidence
- σ : conductivity of the ground
- ϕ : angle of rotation of the loop antenna from its zero position in order to produce a calibration mark
- χ : solar zenith angle

7.1 Introduction

7.1.0 The interest of method A3(b) lies in its ability to follow D-region changes by a rather simple experimental device. Very low and low frequency radio propagation experiments, as initiated over thirty years ago by Ratcliffe and his group at Cambridge [e.g. Best, Ratcliffe and Wilkes, 1936] and then developed further by Lauter and his group at Kühlungsborn, by Belrose at Ottawa, and by some others, have become an important factor in maintaining continuous patrol of the plasma in the mesosphere and at the mesopause level, that is, in the D region. In spite of the rather complicated structure of the D region caused by different ionizing sources, the measurement of absorption at low and medium frequencies provides a full-time patrol of the lower ionosphere between 60 and 90 km. Changes in the ionizing solar wave radiation, incoming high energy particles and seasonal changes in upper atmospheric structure may be determined from the resulting data. Special effects which may be studied from such measurements are:

- a) normal daily and seasonal variations
- b) sunrise effects
- c) sunspot cycle variations
- d) solar flare effects
- e) high energy particle effects (storm-time effects and after-effects)
- f) variations from one day to another of absorption and roughness of the reflecting layer.

7.1.1 In the following sections an improved method for making absorption measurements on low and medium frequencies is described which has now been used for more than two sunspot cycles at one station (Kühlungsborn). A larger network in eastern Europe is being developed. The increasing interest in coupling processes between different upper atmospheric layers makes it necessary to have a more extensive world network. The rather strict conditions for a suitable measuring site which are necessary for the use of this method also during very high absorption and at small solar zenith angles may limit the adoption of a full program at many stations. But there is no serious difficulty in making measurements if the observing time is limited to zenith angles greater than 75° and during the night.

With D-region models that are valid for medium latitudes, the detailed interpretation of such absorption results using full wave equations has now become possible.

7.1.2 A few general considerations should first be reported. Measurements of ionospheric absorption at oblique incidence by means of CW transmitters at short and medium distances (Method A3) are usually made at frequencies greater than 2.5 MHz. For application of this method also at low and medium frequencies, we have a completely different set of conditions insofar as the ground wave is not negligible in this frequency range. This means, on the one hand, that it is necessary to separate the sky wave from the ground wave at the receiving site but, on the other hand, the absorption measurement can be facilitated by a direct comparison of these two components.

The separation of sky wave and ground wave can be achieved by using a vertical loop antenna with its plane perpendicular to the direction of arrival of the ground wave. Oriented in this way (so-called "zero position") the antenna is insensitive to the ground wave, but not to the sky wave which differs from the ground wave because of its angle of incidence, its elliptic polarization and its permanent amplitude fluctuations, the so-called fading.

The comparison of the sky wave with the ground wave can be achieved by rotating the same loop antenna for a short time away from its zero position by a number of known angles ϕ , thus producing calibration marks proportional to $E_G \cdot \sin \phi$ where E_G = ground-wave field strength. Then any recorded e.m.f. E_i , induced by the sky wave can be compared with these calibration marks, i. e., the ratio

$$\frac{E_i}{E_G} = \sin \phi \quad (7.1)$$

7.2 Receiving and Recording Equipment

There are different techniques for recording the sky wave of LF and MF transmitters. In the following paragraphs we describe mainly the measuring device which has been successfully used for many years at the Observatory for Ionospheric Research, Kühlungsborn, of the Heinrich-Hertz-Institute for Solar-Terrestrial Physics of the German Academy of Sciences in Berlin.

7.2.1 Description of the Measuring Equipment

The receiving and recording equipment consists of a loop antenna, an auxiliary antenna, a special input circuit, the receiver and a recording unit. Figure 7.1 shows the block diagram of the whole measuring equipment which will now be described in detail.

7.2.1.1 The configuration of the loop antenna is not at all critical. A square loop with 8 turns and a diagonal of 0.70 m is found to be very satisfactory, regardless of particular frequency used; but instead of a loop antenna a ferrite rod may be used as well.

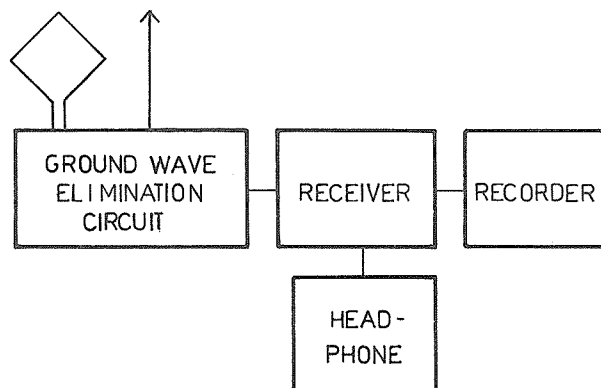


Fig. 7.1 Block diagram of the A3 measuring equipment

Special attention must be given to the mechanical precision of the bearing of the loop axis. The amplitude ratio of sky wave to ground wave may be as low as 10^{-4} during summer noon, and this means that then the loop antenna must be adjusted with an accuracy of about one hundredth degree to the proper direction in order to eliminate effectively the ground wave. The exact control of such tiny displacements of the antenna can easily be achieved using a worm gear, for instance, with a step-down ratio of 1:360. By introducing mechanical stress in the gear, it is possible to eliminate backlash; this is a vital requirement for obtaining the necessary reproducibility within one hundredth degree of loop displacement.

7.2.1.2 Auxiliary antennas are useful in addition to loop antennas. Every normal loop antenna receives even in its zero position not only the desired sky wave but also a small portion of the ground wave. This is due partly to certain asymmetries of the loop antenna in relation to the input circuit, and partly to the fact that because of local environmental influences the ground wave is not exactly planar. If it were not eliminated, due to the residual effect of the ground wave, one could not detect the sky wave in cases where it is very faint. For this elimination an auxiliary antenna is needed which, by suitable coupling in the special input circuit as described in the following paragraph, is designed to supply the necessary "bucking" voltage. In general a vertical whip antenna of 1 to 2 m height in the loop axis may be used for this purpose.

7.2.1.3 A ground wave elimination circuit is also needed in the frequency range we consider. The loop antenna and the auxiliary antenna are interconnected in a special input circuit. Out of the number of different possibilities, one is shown in Figure 7.2. In this case voltage contributed by the vertical rod antenna is adjusted by means of a potentiometer. Instead of a potentiometer a differential tuning capacitor or a variometer coil may equally well be used.

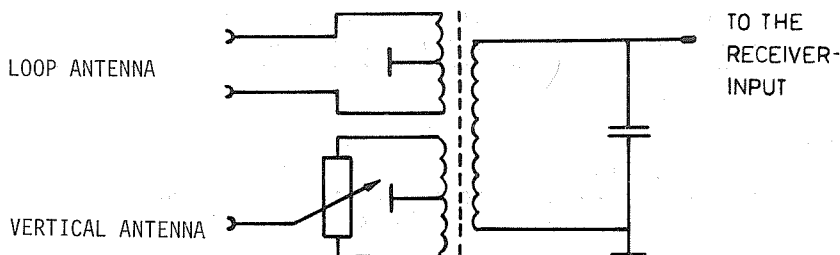


Fig. 7.2 Ground wave elimination circuit

7.2.1.4 As for a receiver, in principle a straightforward or a superheterodyne receiver may be used. It must, however, meet the following demands:

- Considering the dense occupation of the low and medium frequency bands, and in order to obtain a good signal-to-noise ratio, it should have a small bandwidth. The receivers being used at the Observatory at Kühlungsborn have bandwidths from 80 to 500 Hz between the 3 dB points.
- Since the bandwidth must be narrow, a superheterodyne must have a local oscillator with high frequency stability.
- The gain stability must be high.
- The overall sensitivity must be high in order to give usable records also during summer noon when the sky-wave field strength is only of the order of $1 \mu\text{V/m}$.

It is desirable also to have a headphone output in order to simplify the proper adjustment of the loop antenna and the exact elimination of the residual effect of the ground wave.

At the output of the receiver, the a.c. voltage is rectified and fed to a recording unit.

For automatic data processing there should also be the possibility of connecting an analogue-to-digital converter to the output of the receiver.

7.2.1.5 As for a recording unit, it has proved very useful to use a "point recorder" with a relatively rapid stroke sequence (20-30 points/min) instead of a pen recorder. While recordings from a pen recorder can be completely unreadable during disturbances due to thunderstorms or similar electric interference pulses, a recording from a point recorder with sufficiently short response time can normally still be used even under such conditions. Thus even in summer months with frequent thunderstorms, the continuity of the recordings is preserved. A chart speed of 60 mm/h is sufficient in most cases.

7.3 Examples of Records

An example of a low sensitivity sky-wave record (for low height of the Sun and during the night) obtained by an equipment like that described in the preceding paragraphs is shown in Figure 7.3. The recording begins with very small to nearly zero amplitudes in the early afternoon; this is a consequence of the strong daytime absorption of the sky wave and of the elimination of the ground wave by a proper adjustment of the antenna system. Only shortly before sunrise does the sky wave become increasingly noticeable. It finally reaches a nearly constant level during the night, apart from the fading by which the sky wave is always characterized. After sunrise the increasing daytime absorption again causes a gradual disappearance of the sky wave. At the left-hand edge of the record in Figure 7.3 the calibration marks can be seen; these have been obtained from the ground wave by turning the loop antenna out of its zero position by known angles ϕ (5° , 10° through 25°) so that they represent field strengths proportional to $E_G \sin \phi$. It is expedient to make this calibration only during daytime, preferably near noon when the sky-wave absorption is highest. Noon is also the best time for a check on the exact elimination of the ground wave by turning the loop antenna to minimum reception of the ground wave and by totally compensating for the residual effect by means of an appropriate adjustment of the potentiometer in the special input circuit (Figure 7.2).

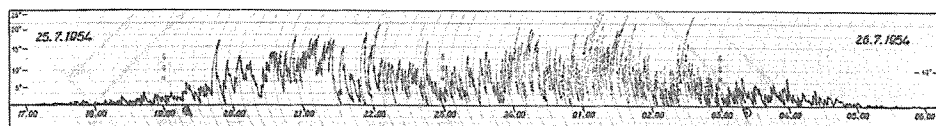


Fig. 7.3 Example of a sky wave record on 245 kHz (transmitter distance 180 km) for the period from two hours before sunset (a) till three hours before sunrise (b).

An extension of the sky-wave records to times also of greater height of the Sun, i.e., of higher absorption, is usually achieved by an appropriate increase of the receiver gain as shown in Figure 7.4.

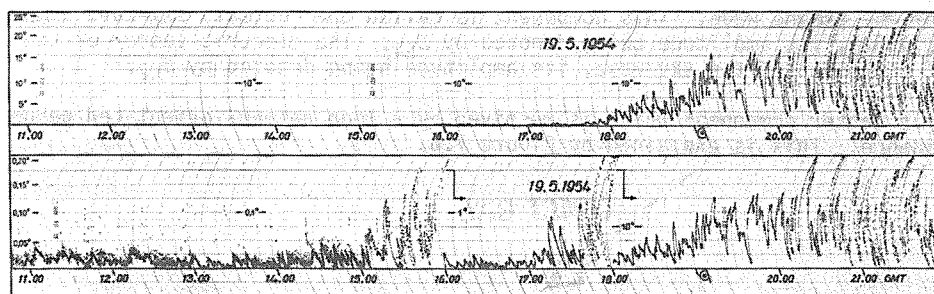


Fig. 7.4 Example of a low sensitivity record (top) and a simultaneous record with higher sensitivity during daytime (bottom) on 245 kHz (the sensitivity is reduced by a factor of 10 at times marked by arrows).

At the top of this Figure there is once more a low sensitivity record, whereas at the bottom a corresponding high sensitivity record for the same day is shown. For the first five hours of this record the sensitivity is 100 times greater than that of the simultaneous low-sensitivity record above, so that the sky wave characterized by its fading is clearly perceptible even during the period of highest absorption around noon. The calibration marks in this case have been obtained by rotating the loop antenna by only 0.05° to 0.2° (!) out of its zero position. The scattered points in this part of the record are due to interference from distant thunderstorms, and they demonstrate the superiority of a point recorder as compared with a pen recorder which would produce a "sea of ink" in this case. As the afternoon advances, there is a systematic increase of the sky wave so that the sensitivity of the record must be reduced by a factor of 10 at about 1600 UT and once more at about 1800 UT; the sensitivity is then the same as in the upper record. Instead of changing the sensitivity of the receiver it is, of course, also possible to use a constant-gain receiver with a logarithmic characteristic (over a range of about 80 dB). It is then possible to follow the diurnal variation of absorption without switching the gain.

In this way a continuous observation of the ionospheric absorption in the LF and MF range is possible during the whole day and in all seasons. At the Kühlungsborn Observatory (54.1°N; 11.8°E) such observations have been made on different frequencies between 100 and 1200 kHz since 1948 at low Sun heights and during the night and, since 1952 also at great Sun heights up to noon. Some examples of results from these measurements are given in Section 7.9 below.

7.4 The Evaluation of the Sky-Wave Records and the Determination of Ionospheric Absorption

7.4.0 The propagation geometry of a typical measuring path in the LF range is illustrated in Figure 7.5. It is assumed that the distance r_G between transmitter and receiver is of the order of about 200 km, so that the curvature of the Earth's surface can be neglected. The height h of the ionospheric reflection level may be about 100 km or less, and thus the angle of incidence i may be of the order of 45° or so. The path length of the sky wave is denoted by r_S . It is known that a linearly polarized electromagnetic wave entering the ionosphere is split into two characteristic polarizations so that after reflection it leaves the ionosphere with an elliptical polarization. The configuration, size and orientation of the polarization ellipse are dependent on the temporally and spatially variable state of the ionosphere in the reflecting area which is caused by permanent random fluctuations and irregularities of the electron concentration; the result is the well-known fading of the reflected wave (see also Chapter 3).

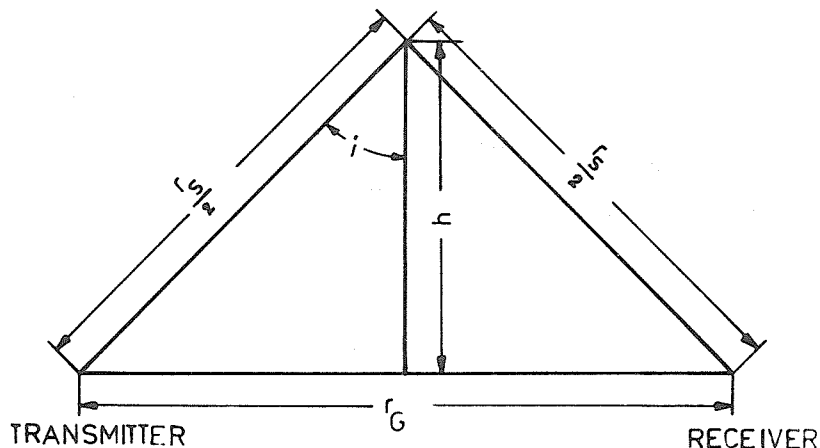


Fig. 7.5 Propagation geometry of a typical measuring path in the LF range.

7.4.1 One may describe the elliptically polarized sky wave by two linearly polarized components. The electric vector of one component oscillates in the plane of incidence, i.e., in the same plane as the electric vector of the ground wave. This component is called the "normal" sky-wave component [e.g. Bracewell *et al.*, 1951], its amplitude being denoted by E_{S1} . The electric vector of the other component is the "abnormal" component of the sky wave, its amplitude being denoted by E_{S2} .

It is only this latter component which is received by a loop antenna orientated perpendicularly to the plane of incidence. This is explained by Figure 7.6.

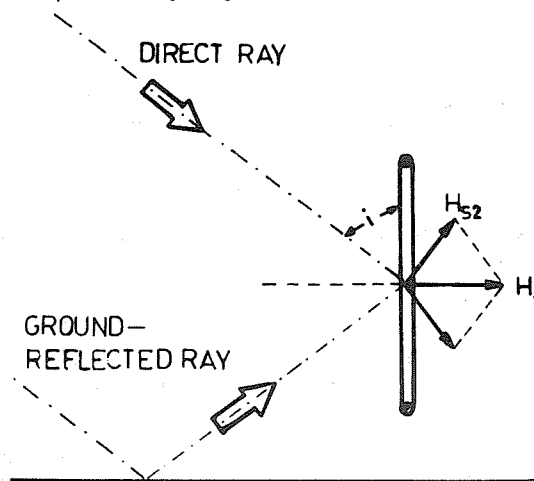


Fig. 7.6 Effective (magnetic) components of the sky wave at the receiving loop antenna.

7.4.2 In this Figure, for the sake of clarity, instead of the electric components (oscillating perpendicularly to the plane of incidence) the corresponding magnetic component (oscillating in the plane of incidence) are shown. We see that in addition to the direct ray of the sky wave a ground-reflected ray must also be considered [e.g. Weeks and Stuart, 1951; Sprenger, 1958] and, therefore, the effective component H_i becomes

$$H_i = 2H_{S2} \cdot \cos i \quad (7.2)$$

In accordance with the relationship between the magnetic and electric fields of an electromagnetic wave, we can formulate in the same way the effective component E_i of the electric field strength:

$$E_i = 2E_{S2} \cdot \cos i \quad (7.3)$$

In fact E_i can be measured directly on the records, namely as the ratio E_i/E_G according to Eq. (7.1), and we can write

$$\frac{E_i}{E_G} = \frac{E_{S2}}{E_G} \cdot 2 \cdot \cos i \quad (7.4)$$

7.4.3 For the determination of ionospheric absorption from the measured ratio of the sky wave to the ground wave, we use the following argument which is generally valid for the propagation of electromagnetic waves:

$$E = E_0 \cdot \frac{1 \text{ km}}{r} \quad (7.5)$$

where E_0 represents the reference field strength at 1 km distance from the transmitter, r the distance in km and E the field strength at distance r from the transmitter.

For an ionospheric reflected wave, E_S , we can write

$$E_S = \frac{E_{0S}}{r_S/\text{km}} \rho \quad (7.6)$$

where ρ is the reflection coefficient of the ionosphere. Since we are dealing with only one component of the sky wave (the abnormal component E_{S2}) we define accordingly

$$E_{S2} = \frac{E_{0S}}{r_S/\text{km}} \rho'_2 \quad (7.7)$$

and call ρ'_2 the "conversion coefficient", a term introduced by Ratcliffe's group [e.g. Bracewell *et al.*, 1951]. The prime is used in order to indicate that the measurements refer to oblique incidence and not to vertical incidence as, for instance, in the A1 method.

By analogy with Eq. (7.6) we write for the ground wave

$$E_G = \frac{E_{0G}}{r_G/\text{km}} \cdot \eta \quad (7.8)$$

where η = ground-wave transmission factor.

7.4.4 From Eqs. (7.4), (7.7) and (7.8) we obtain the following equation for the ionospheric conversion coefficient:

$$\rho'_2 = \frac{E_i}{E_G} \cdot \frac{r_S/r_G}{E_{0S}/E_{0G}} \cdot \frac{\eta}{2 \cdot \cos i} \quad (7.9)$$

For r_S/r_G we find from Figure 7.5

$$\frac{r_S}{r_G} = \frac{1}{\sin i} \quad (7.10)$$

E_{OS}/E_{OG} is determined by the radiation characteristic of the transmitting antenna which in the LF and MF ranges should be approximately similar to that of an elementary dipole, i.e., similar to

$$\frac{E_{OS}}{E_{OG}} = \sin i \quad (7.11)$$

Possible deviations from this characteristic could be allowed for by a correction factor K

$$\frac{E_{OS}}{E_{OG}} = K \cdot \sin i \quad (7.12)$$

Combining Eqs. (7.9), (7.10) and (7.12) we obtain:

$$\rho'_2 = \frac{1}{2 \cdot \sin^2 i \cdot \cos i} \cdot \frac{\eta}{K} \cdot \frac{E_i}{E_G} = C \cdot \frac{E_i}{E_G} \quad (7.13)$$

with

$$C = \frac{1}{2 \cdot \sin^2 i \cdot \cos i} \cdot \frac{\eta}{K} \quad (7.14)$$

7.4.5 In view of the permanent fluctuations of the recorded sky-wave amplitude E_i , it is not reasonable to use an instantaneous value of E_i for the determination of a corresponding conversion coefficient. Instead, so as to obtain a typical value, the conversion coefficient should be based upon a median value of E_i over a sufficiently long time in order to eliminate the fading. At normal fading rates, the averaging time should be at least 10 to 30 min in the LF range, and 5 to 10 min in the MF range. Denoting the median value of E_i by $\overline{E_i}$, we now have to write

$$\rho'_2 = C \cdot \frac{\overline{E_i}}{E_G} \quad (7.15)$$

The factor C for the calculation of ρ'_2 is a quantity which must be determined separately for each measuring path, so as to permit the determination of the absolute level of the conversion coefficient. Investigations of relative variations of ρ'_2 are already possible without an exact knowledge of the magnitude of C since, in each individual case, C can be considered to be nearly constant. A detailed discussion of the determination of C will be given in Section 7.5 below.

7.4.6 The ionospheric conversion coefficient ρ'_2 established by Eq. (7.15) considers only the abnormal component of the sky wave as already mentioned. It is desirable to go a step further in order to obtain a total reflection coefficient, including the normal component as well. This total reflection coefficient, to be denoted by ρ' , could be interpreted as the square root of the ratio of the reflected power compared to the incident power of the wave. For the desired estimation of ρ' from observations of only the abnormal component, some basic considerations are needed.

From statistical investigations of the fading in the LF range it has been shown that to a first approximation the instantaneous amplitude values of the recorded sky-wave component frequently obey a Rayleigh distribution [Sprenger and Lauter, 1966]. If the reflection process is assumed to take place at a "rough" ionospheric surface, it is possible to describe the reflection by the parameter of the Rayleigh distribution which corresponds to the reflectivity of an equivalent smooth surface and is equal to 1.2 times the median value of all the individual values within the sampling period. It is plausible to suppose that the normal and abnormal components E_{S1} , E_{S2} of the sky wave both obey a Rayleigh distribution and, therefore, we can define a resultant field strength

$$E_S = \left((1.2 \overline{E_{S1}})^2 + (1.2 \overline{E_{S2}})^2 \right)^{1/2} \quad (7.16)$$

upon which the total reflection coefficient ρ' should be based. With the preliminary assumption $\overline{E_{S1}} = \overline{E_{S2}}$ (the bar again indicates the median value) we find

$$E_S = 1.7 \overline{E_{S2}} \quad (7.17)$$

so that, by analogy with the procedure used in Eqs (7.7) to (7.15), we find for the total reflection coefficient

$$\rho' = 1.7 \cdot C \cdot \frac{\overline{E_i}}{E_G} \quad (7.18)$$

If the assumptions made above concerning the validity of the Rayleigh distribution and of $\overline{E_{S1}} = \overline{E_{S2}}$ do not completely hold true, the factor in Eqs. (7.17) and (7.18) may be slightly different from 1.7 and may, moreover, possibly depend on frequency path length and direction relative to the Earth's magnetic field. A detailed study of this question would, however, demand special observations. For the present we recommend the use of the factor 1.7 as in Eq. (7.18), especially since the factor C also contains some uncertainties as will be seen in Section 7.6.

The total ionospheric absorption A' at oblique incidence follows from the total reflection coefficient ρ' established by Eq. (7.18) in the usual manner:

$$\frac{A'}{dB} = -20 \log \rho' = \text{const} - 20 \log \frac{\overline{E_i}}{\overline{E_g}}. \quad (7.19)$$

7.5 Discussion of the Factor C for the Determination of the Absolute Values of Ionospheric Absorption

The factor C in Eq. (7.14) must be determined separately for each individual measuring path, as already mentioned. It contains the geometrical term $(2 \cdot \sin^2 i \cdot \cos i)^{-1}$, the ground-wave transmission factor η and a term K describing the radiation characteristic of the transmitting antenna. These terms will now be discussed separately.

7.5.1 The Geometrical Term

The factor $(2 \cdot \sin^2 i \cdot \cos i)^{-1}$ is a function of the transmitter distance x_g and of the reflection height h , and it can be calculated using Figure 7.5. In Figure 7.7 this factor is plotted against transmitter distance (up to 500 km) for different reflection heights (between 70 and 120 km). Of course, the reflection height is not, a priori, known in A3 measurements. But in the low frequency range it should be within the limits of $85 < h < 100$ km by day and night. For this height range and restricting the transmitter distances to the range $180 < x_g < 400$ km, we find from Figure 7.7 only a very small variability of the geometrical factor: hence an exact knowledge of the reflection height and its variations is not crucially important. The possible error should scarcely exceed 10 percent.

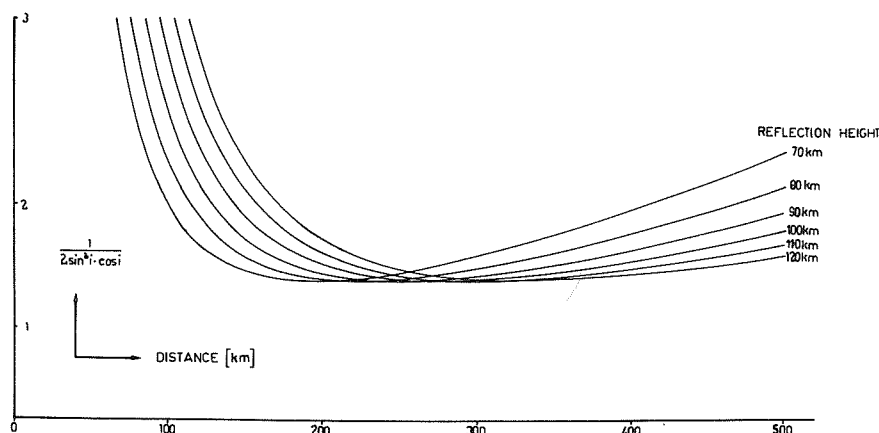


Fig. 7.7 Dependence on transmitter distance and reflection height of the term $(2 \cdot \sin^2 i \cdot \cos i)^{-1}$.

In the medium-frequency range the same should be true, at least as far as reflections from the E region are concerned. However, it may be that in this frequency range during the night a transition to F-region reflections could occur, and this would cause greater uncertainties in the geometrical term.

7.5.2 Ground-wave Transmission Factor

There are several possibilities for determining η . For instance, one can use the well-known CCIR ground-wave propagation curves which are given for different ground conductivities σ_w . From field-strength measurements in central Europe it has been found that ground-wave propagation over land is satisfactorily described by the CCIR curves for $\sigma = 10^{-2.5}$ S/m [Sprenger, 1958]. Adopting this, η can be simply calculated as the ratio between the actual ground-wave field strength, as given by the corresponding CCIR curve, and the ideal field strength which would be observed without loss. This procedure may be satisfactory in the low frequency range and at not too great distances. Over greater distances and at medium frequencies, however, the uncertainty of η when it is determined in this way can become critical.

A more precise method involves two absolute field-strength measurements: one at the receiving site, giving the value $\overline{E_g}$, Eq. (7.8), and the other one near the transmitter, for instance at a distance of about 10 to 20 wavelengths, preferably in the azimuthal direction of the measuring path in order to avoid possible anisotropy from the horizontal radiation pattern of the transmitting antenna.

By analogy with Eq. (7.8) we can write for the measured field strength near the transmitter (subscript N)

$$E_N = \frac{E_{0G}}{r_N} \cdot \eta_N \quad (7.20)$$

and by combination with Eq. (7.8) we obtain

$$\eta = \frac{E_G}{E_N} \cdot \frac{r_G}{r_N} \cdot \eta_N \quad (7.21)$$

According to this equation, η follows in a very simple way from the two measured field strengths, from the two known distances and from the quantity η_N which is the ground-wave transmission factor over the short distance r_N . η_N is very near unity and can be read with sufficient accuracy from the CCIR curves.

It must be taken into consideration, however, that η may not remain constant, for instance during different seasons. In this case a variation of η if not corrected would produce an apparent variation of ionospheric absorption which did not exist in reality. In order to estimate the possible errors due to this influence, we show in Figure 7.8 the results of ground-wave field strength measurements in the low frequency range over several months. In fact there seems to be a slight seasonal variation which has also been found by other authors [e.g. Gerber and Werth-Müller, 1945; Müller, 1962; Hanle, 1967], but its amplitude is so small that we can neglect it. In the MF range the variations may be a little greater. If necessary, the appropriate corrections can be made on the basis of occasional ground-wave field strength measurements.

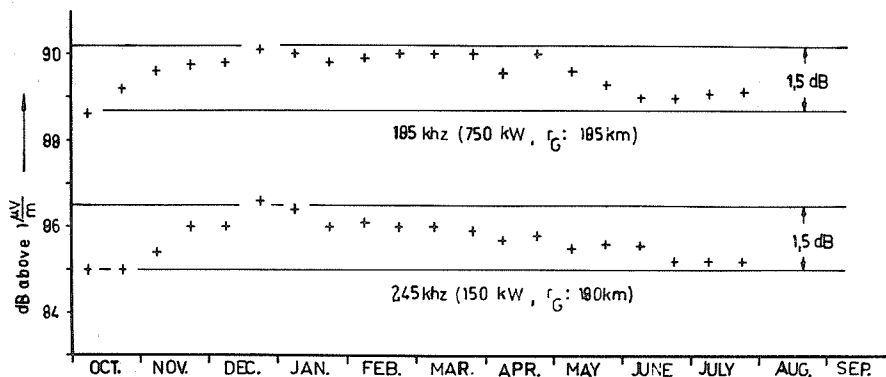


Fig. 7.8 Ground-wave field strength measurements on two frequencies in the LF range (Kühlungsborn, 1967/68).

7.5.3 Radiation Characteristics of the Transmitting Antenna

The factor K describing the transmitter's radiation characteristics in the plane of incidence according to Eq. (7.12) has to be determined from special experimental measurements or from theoretical calculations of the antenna pattern which may be available from the engineers at the transmitting station. If such data are not available, the factor K is somewhat uncertain, but it is not expected to differ much from unity in most cases (in the LF and MF range).

7.5.4 Concluding Remark about the Uncertainties of C

The uncertainties of the individual terms in the factor C , as discussed in the preceding paragraphs, imply a corresponding uncertainty in the absolute value of the ionospheric absorption A' as determined by Eq. (7.19). While the uncertainties due to the contributions of the geometrical term and of η are not critical, say about ± 1 dB, the main contribution can arise from the uncertainty of K if there is no adequate information about the transmitting antenna. However, by careful consideration of all the components of C and excluding extremely unfavorable conditions, the total uncertainty may be expected to lie within about ± 3 dB.

It should be mentioned once more that an exact knowledge of C is only important for the determination of absolute values of ionospheric absorption which are needed, for instance, for comparison of results on different frequencies and at different sites. Relative absorption measurements on a given measuring path can be obtained without an exact knowledge of C and can nevertheless give important results, for instance on the diurnal and seasonal variation of ionospheric absorption.

7.6 Choice of Transmitter

The method under discussion implies the use of normal broadcast communications and navigation transmitters. Unfortunately, there are relatively few transmitters in the LF and MF range with the exclusive right to operate alone on a given frequency; thus the number of choices is limited. The chosen transmitter should work with nearly constant power though, in principle, the described method is independent of the transmitter power provided that possible changes are covered by appropriate ground-wave calibration marks.

The recommended transmitter distances are between about 150 and 400 km in the low-frequency range, and between about 150 and 250 km in the medium-frequency range. On the one hand the lower limit is determined by the decreasing ratio of sky wave to ground wave with decreasing transmitter distance, so that the exact elimination of the ground wave becomes more and more difficult. On the other hand, possible changes in the reflection height have a great influence on the term $(2 \cdot \sin^2 i \cdot \cos i)^{-1}$ at smaller distances, and they make it difficult to obtain an accurate interpretation (Figure 7.7). The upper limit of recommended distances is dependent on frequency because it is determined by the condition that the ratio of sky wave to ground wave must not exceed the value of 1. Beyond this limit the ground wave amplitude is not great enough for calibration of the larger sky-wave amplitudes. If, however, the ratio is not much greater than unity, an extrapolation of the ground-wave calibration marks may be possible using a signal generator.

7.7 Choice of Observing Site

For the recording of the very weak sky-wave signals during daytime, an extremely exact elimination of the ground wave by a proper adjustment of the loop antenna is necessary. This precise elimination can possibly be destroyed by distortion of the phase front of the ground wave (even by only 0.01° or so) due to variable local environmental influences. Therefore the observing site should not be chosen in the vicinity of electric overhead lines or other long wires (e.g. antennas, metallic constructions or metallic fences) with variable or intermittent contacts. Also the immediate vicinity of high trees should be avoided because of their variable conductivity. Further, the observing site should be far away from sources of industrial man-made noise.

7.8 Observing Program

Continuous recordings on one or more frequencies should be maintained for as many hours as possible during the day and night. From these recordings the following data should be derived for each day:

- noon value of absorption, averaged over a period of about one hour around local noon,
- absorption values at times of constant solar zenith angle χ , preferably at $\cos \chi = 0.0, 0.2, 0.4$ etc., averaged as far as possible over an adequate sampling period as described earlier (Eq. (7.15)).
- hourly values of absorption during the night or an averaged value for the whole night, limited by observations taken only between the times when $\chi = 100^\circ$.

7.9 Some Examples of Results from A3 Records in the LF and MF Ranges

In this Section, some examples are given of LF and MF recordings using Method A3. These have all been obtained at the Observatory for Ionospheric Research in K hlungsborn (54.1°N ; 11.8°E). Explanations are given in the captions to Figures 7.9 through 7.15.

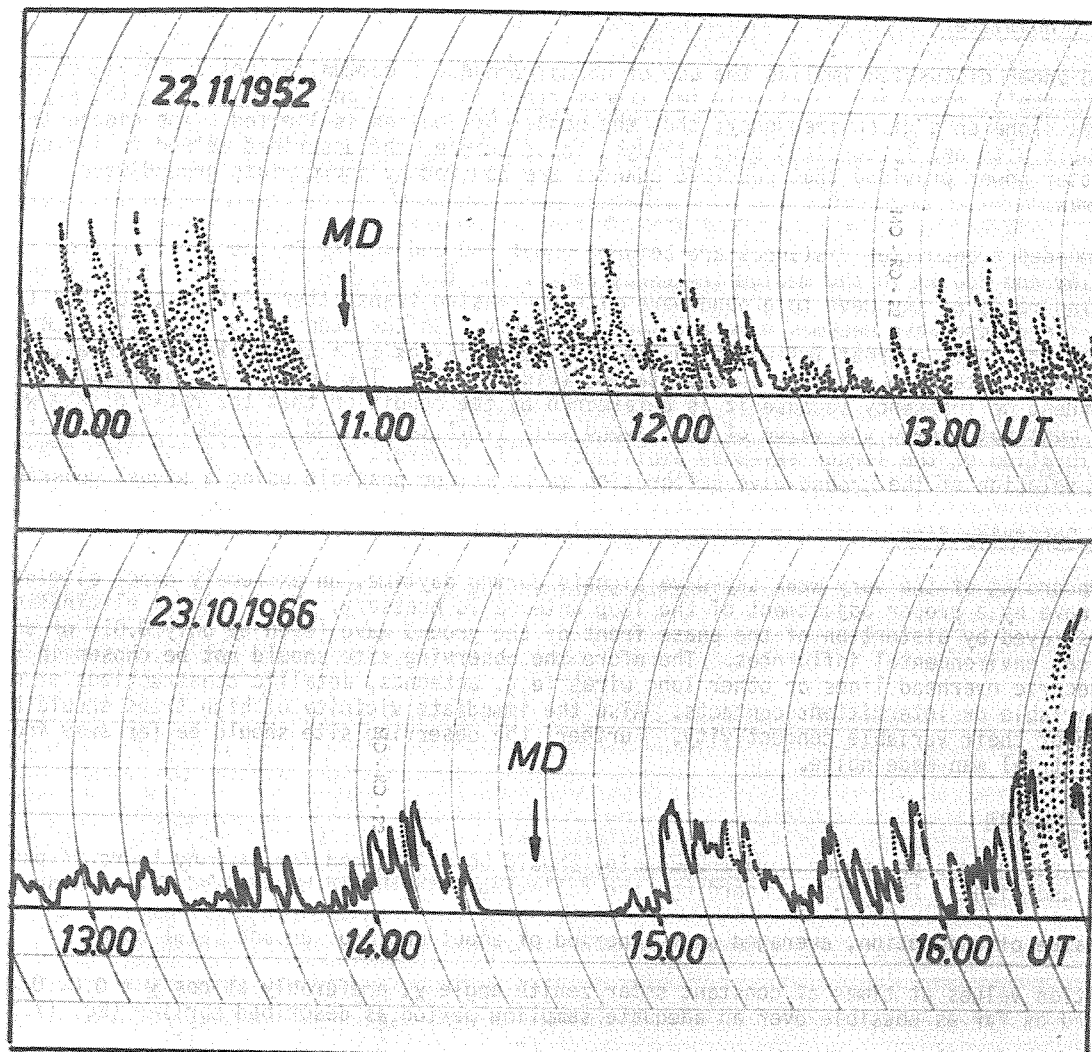


Fig. 7.9 Two examples of the solar flare (Moegel-Dellinger) effect on a 245 kHz path (path length 180 km), indicated by a sudden fade-out of the recorded sky wave for a short period during daytime.

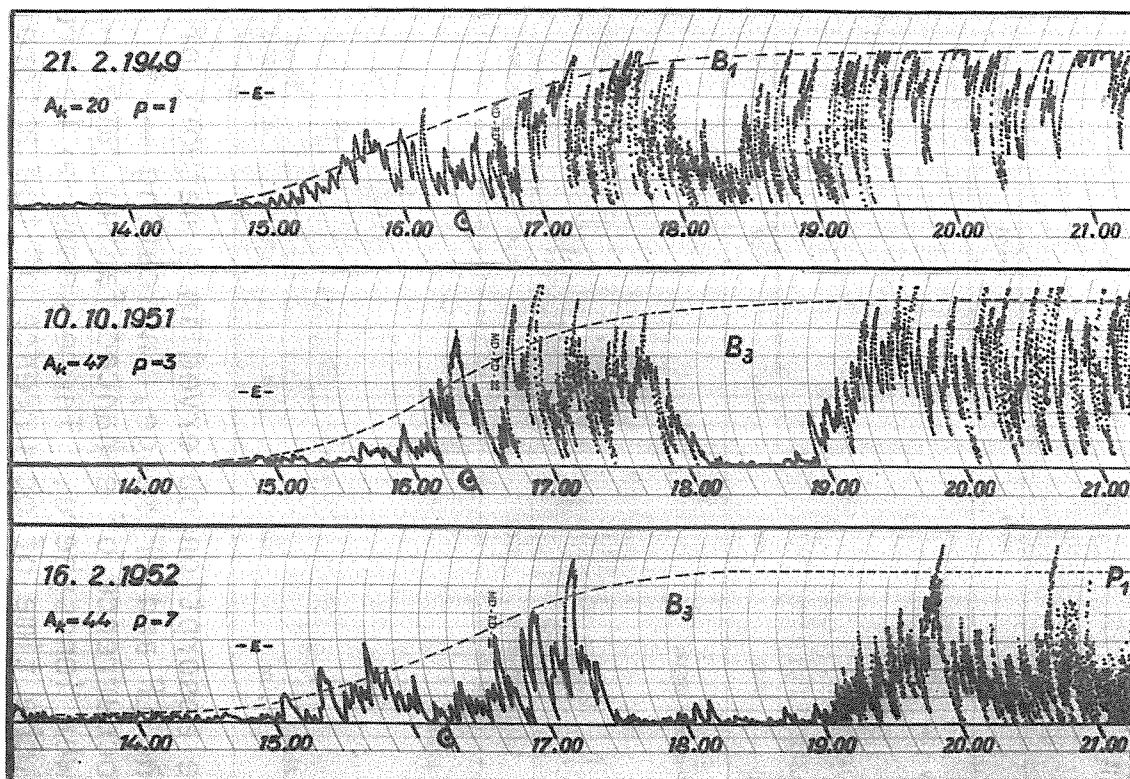


Fig. 7.10 Three examples of transient bay-like absorption anomalies on 245 kHz sky-wave records during nighttime (at sunset) lasting for about one hour, often starting at different times on different propagation circuits in the manner of travelling disturbances.

The dashed lines indicate the normal behavior of sky-wave field strength on this measuring path during the transition from day to night.

The record of 16 February 1952 (16.2.1952) shows the absorption anomaly (B₃). It shows also another form of disturbance, called P₁, which is characterized by the occurrence of an increase in the fading rate for sky wave and is mostly connected with increased geomagnetic activity; it is probably caused by highly different reflection conditions for the ordinary and extraordinary components in the nocturnal E region.

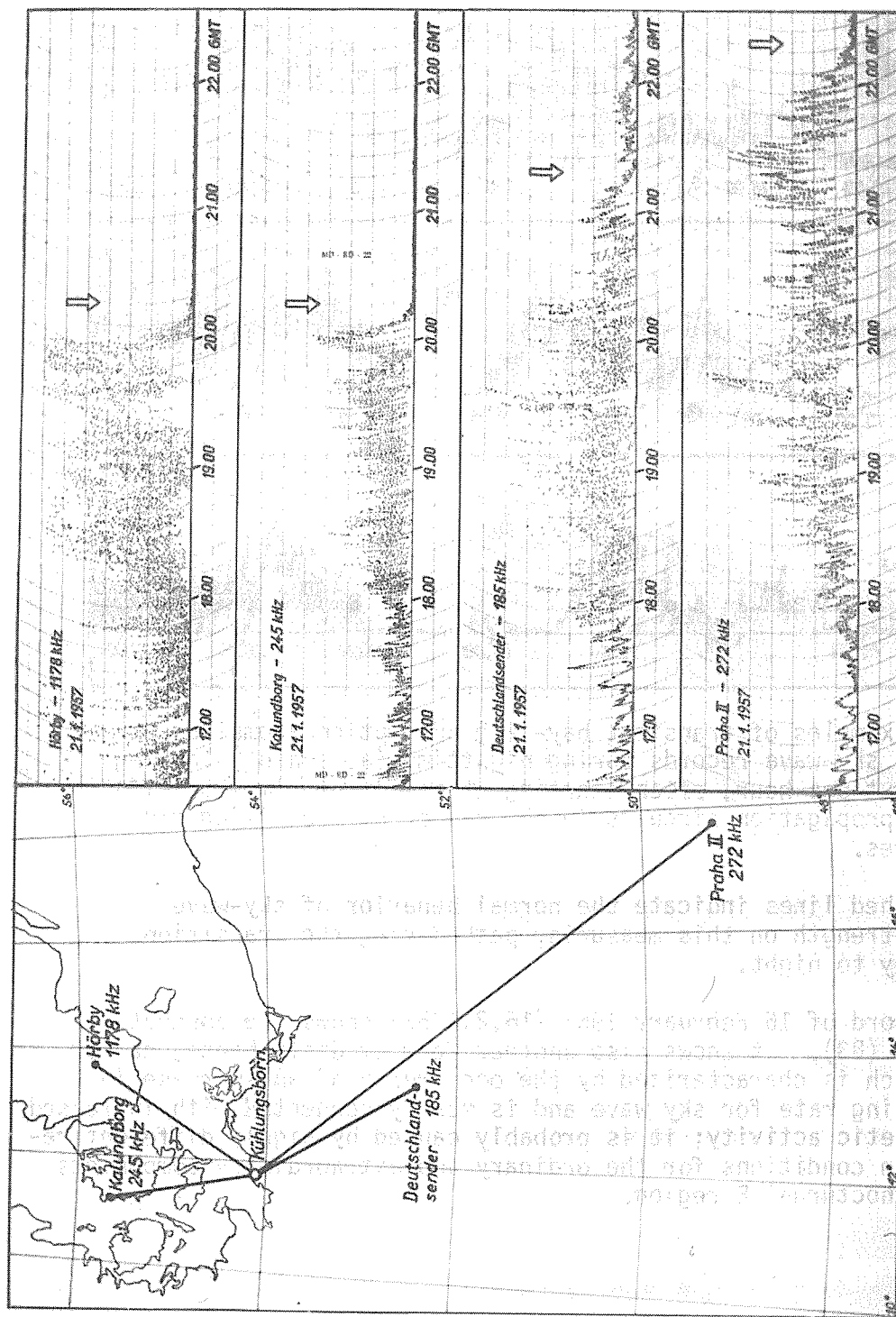


Fig. 7.11 Sudden enhancement of nighttime absorption observed in a network of different measuring paths in the LF and MF range, indicating -- in connection with the preceding occurrence of enhanced fading rate -- a storm commencement in the lower ionosphere. There seems to be pronounced latitudinal control of the time of occurrence of the absorption anomaly as marked by the arrows. [Reproduced from Glöde, Knuth, Lauter 1968].

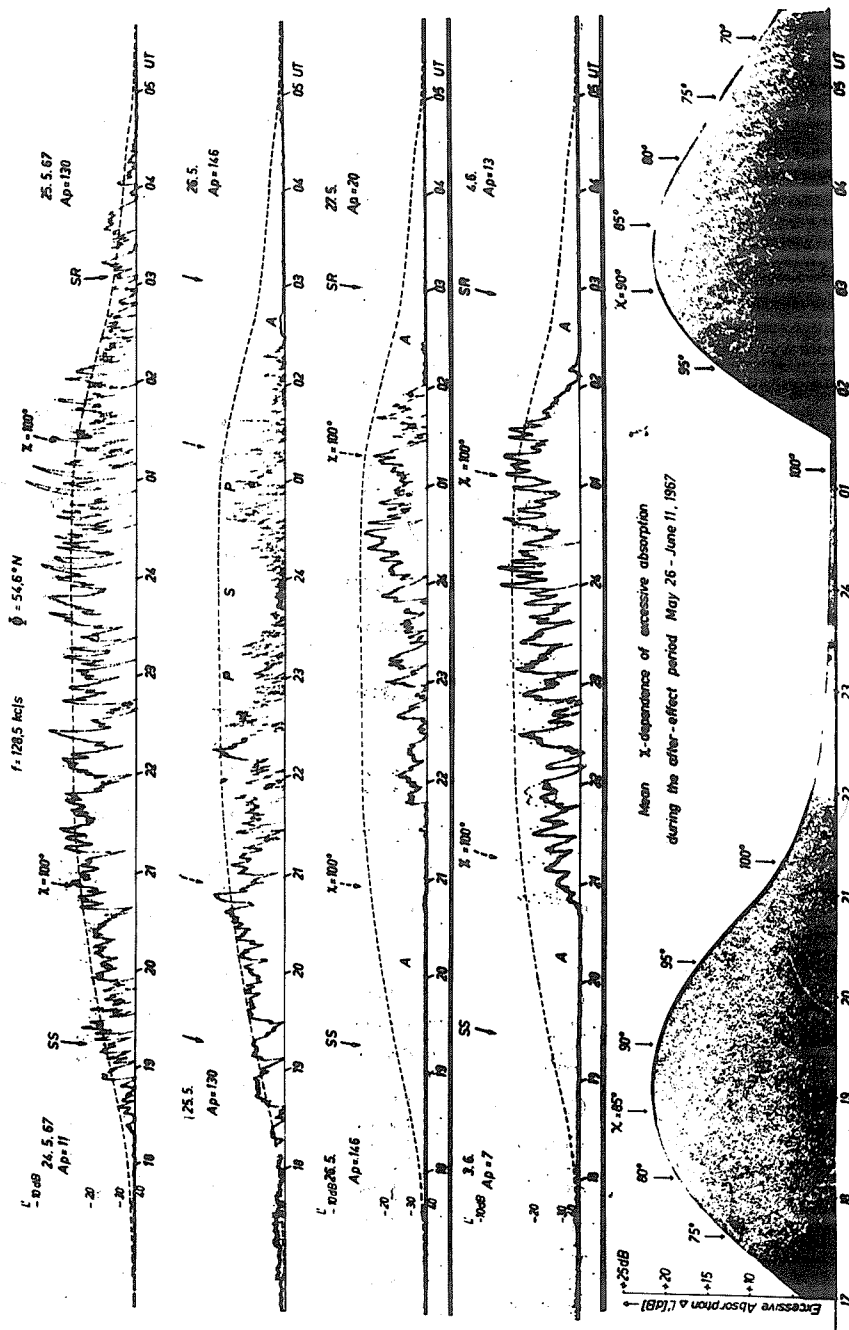


Fig. 7.12 Some examples of sky-wave records on 128.5 kHz during the storm event of May 25, 1967 (25.5.1967) and the following post-storm. The storm is indicated by the occurrence of an enhanced fading rate (P) and increased absorption (S) during the night from May 25 to 26; the after-effect is characterized by excessive absorption around sunset (SS) and sunrise (SR) for many days after the storm.

The record at the top shows the normal behavior of the sky wave during an undisturbed night. The dashed lines indicate the normal mean diurnal variation of the sky-wave field strength, and χ is the solar zenith angle.

The diagram at the bottom shows the mean dependence on χ of the excessive absorption ($\Delta A'$) during the after-effect period from May 26 to June 11, 1967. [Further details have been described by Glöde, Knuth and Lauter [1968].

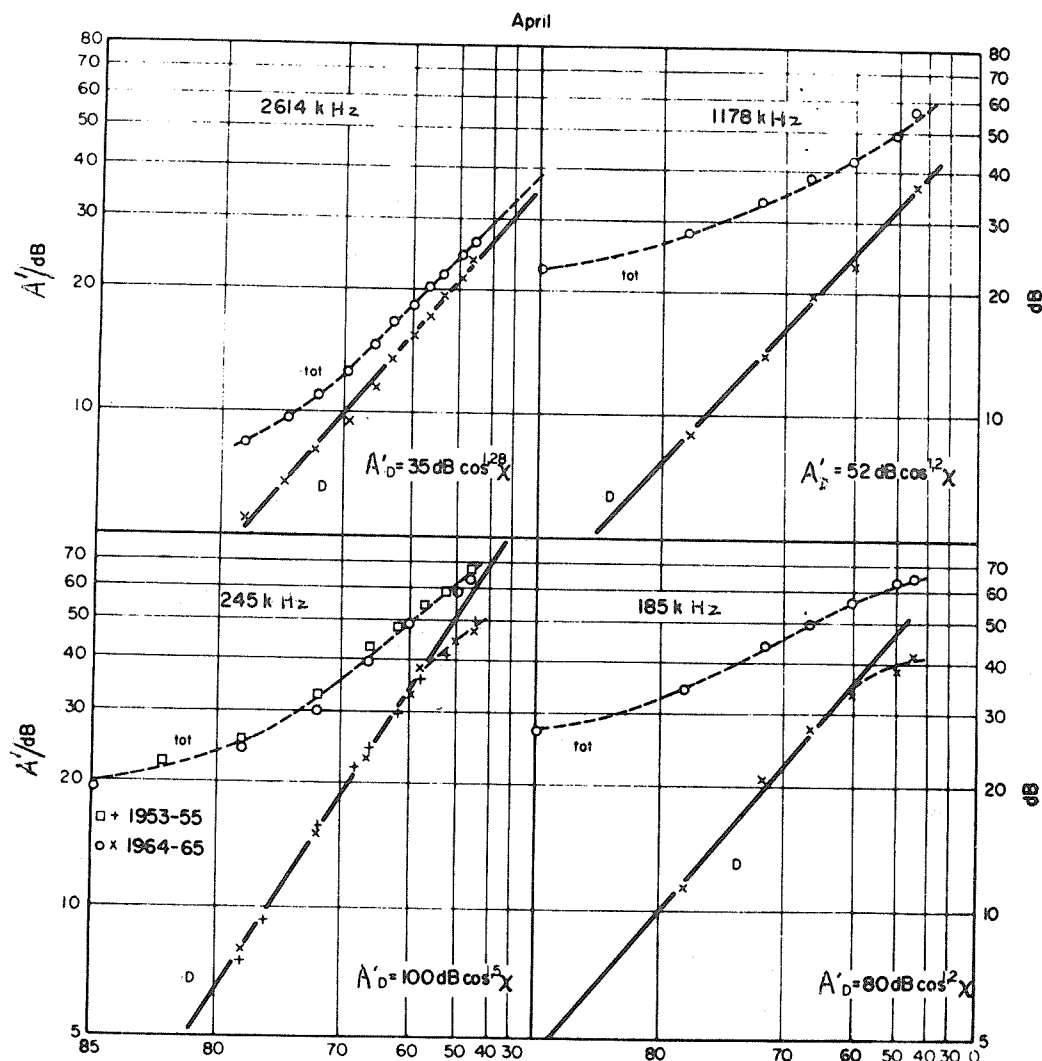


Fig. 7.13 Dependence on solar zenith angle χ (abscissa) of daytime absorption on different frequencies in spring at sunspot minimum conditions. Comparisons of results from A3 measurements in the LF and MF range (185 kHz, 245 kHz, 1178 kHz) by the method described in this manual and from the usual A3 measurements in the HF range (2614 kHz).

A common $\cos^n \chi$ law (giving straight lines in a logarithmic presentation) with exponents $n=1.2$ to 1.5 (in this case) can be achieved by reducing the total absorption A'_{tot} to the pure daytime absorption A'_D , i.e., by subtracting that amount of absorption which is already present at sunrise. (For further results and investigations of this kind, see Lauter and Sprenger [1966]; Lauter and Nitzsche [1967].

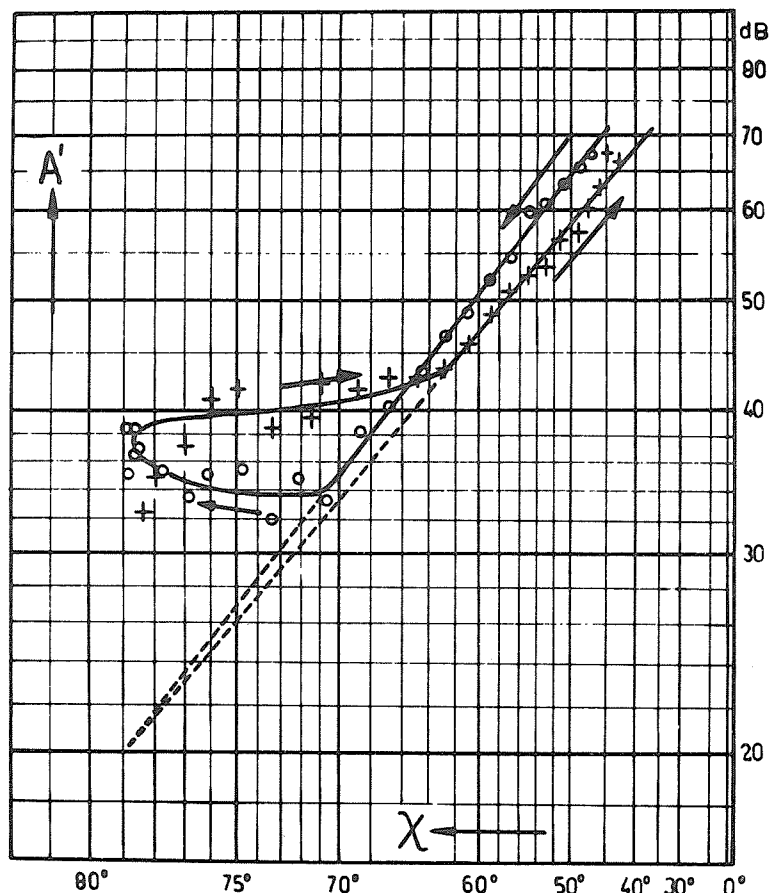


Fig. 7.14 Annual trend of noon absorption (pentad mean values from sunspot minimum years) on 245 kHz from September through December (o) and from January through April (+). The "winter anomaly" of ionospheric absorption is clearly shown by the deviation from the $\cos^2 \chi$ law (straight lines), starting at $\chi=71^\circ$ (early November) and lasting until $\chi=63^\circ$ (late February).

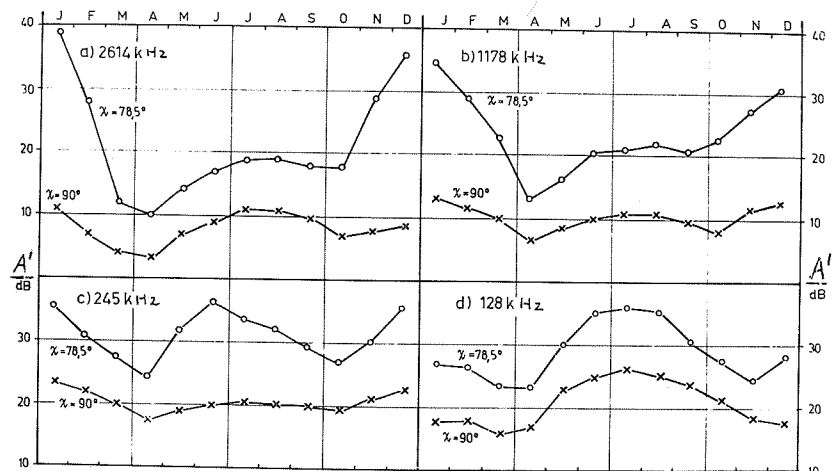


Fig. 7.15 Annual variation of ionospheric absorption at constant solar zenith angle χ in the LF, MF and HF ranges, showing a decrease in the winter anomaly with decreasing frequency and the appearance of enhanced absorption during summer on the lower frequencies. [cf. Lauter and Nitzsche, 1967; Lauter and Sprenger 1968].

CHAPTER 8. THE PARTIAL REFLECTION METHOD

by

W. Dieminger and K. Schlegel
Max-Planck-Institut für Aeronomie, Lindau-Katlenburg, F.R.G.

Table of Contents

| | Page |
|---|------|
| 8.1 Introduction | 165 |
| 8.2 The Principle of Measurements | 165 |
| 8.3 The Theory of the Partial Reflection Method | 165 |
| 8.3.1 The Basic Theory | |
| 8.3.2 Volume Scattering | |
| 8.3.3 Extended Theory of Volume Scattering | |
| 8.3.4 Differential Phase Measurements | |
| 8.4 Choice of the Probing Pulse Parameters | 169 |
| 8.4.1 Probing Frequency | |
| 8.4.2 Probing Pulse Width | |
| 8.4.3 Probing Pulse Sequence | |
| 8.5 Comments on the Equipment | 172 |
| 8.5.1 Experimental System and Operating Sequence | |
| 8.5.2 Transmitter and Receiver | |
| 8.5.3 Antenna System | |
| 8.5.4 Data Recording System | |
| 8.6 Processing of the Partial Reflection Data | 176 |
| 8.7 Facilities and Aims of Partial Reflection Measurements | 176 |
| 8.8 Annex: Partial Reflection Measurements with FM-CW | 177 |
| Appendix 8.A: Table 8.A.1. Operating and Recording Data of Some Partial Reflection Installations | 179 |
| Table 8.A.2. Various Partial Reflection Installations | 180 |

8.1 Introduction

The conventional method of measuring the electron density in the ionosphere, viz. vertical echo sounding, fails for the lowest part of the ionosphere for several reasons. First, the electron density in the D region is so small that the corresponding plasma frequency is in a frequency range where echo soundings are hardly possible for organizational (other services) or technical (expensive antenna systems) reasons. Second, the collision frequency is so high that absorption is very pronounced especially for low frequencies. Third, the interpretation of the observations becomes difficult because of the complex influence of the collisions and the geomagnetic field on the refractive index. Fourth, the ray theory breaks down for frequencies low enough to be totally reflected in the lower part of the D region. Other radio methods, therefore, must be applied for exploring the D region. One of them, the partial reflection method which has been introduced by Gardner and Pawsey [1953], will be discussed in detail in this chapter.

8.2 The Principle of the Measurements

Using conventional ionospheric sounders, the lowest echoes are being recorded at a height of 100 km. These echoes are attributed to total reflections at levels where the refractive index approaches zero. By increasing the overall sensitivity of the equipment (by increasing the power of the transmitter, the efficiency of the receiver, or by selecting locations with very low noise level) more and more echoes become visible at heights down to 60 km (Figure 8.1) [Dieminger, 1968]. The simultaneous occurrence of these low echoes and of echoes from the E region proves that the low height reflections are partial ones. The echoes are most distinct on frequencies below 3 MHz. For most locations the use of frequencies below 1.6 MHz is excluded by the extensive and continuous use of these frequencies by broadcast and other services. Therefore most observations have been carried out between 2 and 3 MHz. In principle they are possible also on higher frequencies [Dieminger and Hoffman-Heyden, 1952].

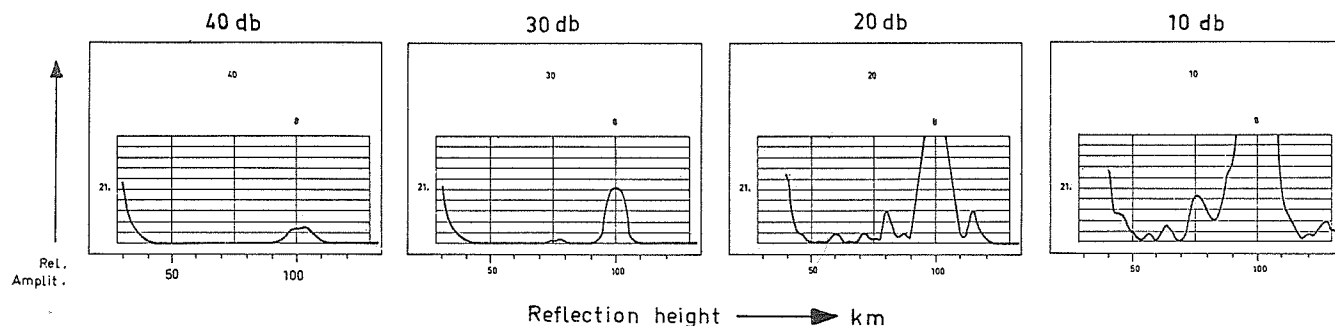


Fig. 8.1 A 2-second sequence of amplitude-reflection height snapshots for different gains of the receiver. More and more partial reflections appear with increasing receiver gain. (Tsumeb, 21 April 1965, 1552 h (15° EMT) frequency 750 kHz, from Elling [1965]).

The information about the D region, especially about the electron density and collision frequency, is extracted from the amplitude of both magneto-ionic components of the downcoming wave. These two amplitudes are measured simultaneously or nearly simultaneously but separately from each other. In most of the experiments the ordinary (o) and extraordinary (x) components are displayed on an A-scope, setting the two amplitudes in the positive and negative y-direction respectively, as shown in Figure 8.2. These pictures are recorded on film and evaluated later by hand. A more sophisticated recording on magnetic tape will be described in Section 8.5.4.

8.3 The Theory of the Partial Reflection Method

There are currently three theories to explain the partial reflection data in terms of electron density and electron collision frequency. The first one, which will be described in the following section, is widely used as a basic theory and yields reasonably good results. The other two are improvements of this basic theory and will be described in Sections 8.3.2 and 8.3.3.

8.3.1 The Basic Theory

This theory was first given by Gardner and Pawsey [1953] and was improved later by Belrose and Burke [1964] who applied the magneto-electronic formula of Sen and Wyller [1960] instead of the Appleton-Lassen formula for the refractive index. This improvement was necessary because of the dominant role of the electron collision frequency in the D region, which requires a thorough treatment. Thus the Sen-Wyller theory, which takes the velocity dependence of the collision frequency into account, was adopted (see Appendix 2.B in Chapter 2).

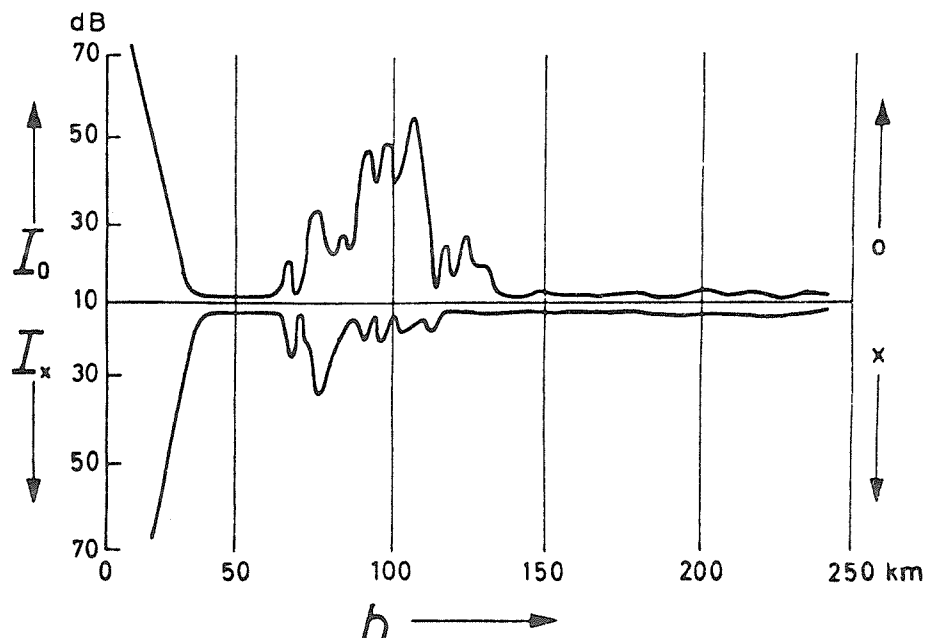


Fig. 8.2 Partially reflected echoes from the D region as shown on an A-scope.
Upper trace: ordinary component; lower trace: extraordinary component.
[Dieminger, 1968].

For many applications the "quasi-longitudinal approximation" of the Sen-Wyller formula as given in Eq. (8.1) is used. The validity of this approximation depends on the geographic location of the station and on the wave frequency used, and has to be checked carefully in every case. If it is not valid, the formula for the general case given in the paper from Sen and Wyller has to be applied. In the following the quasi-longitudinal approximation will be used to explain the basic theory of the partial reflection method. In the general case the formulas look somewhat different, but one has to proceed in the same way.

The complex refractive index n in the quasi-longitudinal approximation given by Sen and Wyller is:

$$n^2 = \left[\mu_{x,o} - j \frac{\sigma_{o,x,o}}{\omega} \right]^2 = 1 - \frac{\omega_N^2}{\omega \hat{\nu}} y_{x,o} C_{3/2}(y_{x,o}) - j \frac{5\omega_N^2}{2\hat{\nu}\omega} C_{5/2}(y_{x,o}) \quad (8.1)$$

where

$\mu_{x,o}$ = real part of the refractive index

$\kappa_{x,o}$ = absorption coefficients; (x = extraordinary, o = ordinary wave component)

$\omega = 2\pi f$, where f is the operating wave frequency

$\omega_N = \sqrt{\frac{Nq^2}{m_e \epsilon_0}}$ plasma frequency (N = electron density)

$\hat{\nu}$ = electron-neutral collision frequency ("most probable" ν)

$y_{o,x} = \frac{\omega \pm \omega_L}{\nu}$

$\omega_L = 2\pi f_H \cos \phi$ longitudinal component of the gyrofrequency

$C_{3/2}, C_{5/2}$ = C-script integrals, see Appendix 2.B in Chapter 2 (tabulated e.g. by Burke and Hara [1963]).

For the reflection mechanism of the upgoing waves in the D region Fresnel reflection from a sharp boundary of infinite dimensions is assumed, where the refractive index changes from n_1 to n_2 over a length that is small compared with a wavelength. In that case the reflection coefficient is given by

$$R = \frac{n_2 - n_1}{n_2 + n_1} \approx \frac{\Delta n}{2n} \quad (8.2)$$

As shown by Belrose and Burke [1964], the formula (8.2) is not only valid for an infinite slab but also for a number of blobs with an enhanced electron density (volume scattering).

This formula is valid for normal incidence of the wave if the wave frequency is sufficiently far away from the plasma frequency. The real amplitudes A_0 and A_X of the ordinary and extraordinary wave components partially reflected at a height h can be described by

$$A_{X,0} \sim |R_{X,0}| \exp \left[-2 \int_0^h \kappa_{X,0} dh \right]$$

(A for amplitude should not be confused with the absorption decrement A .)

$|R_{X,0}|$ being the absolute value of the reflection coefficient for the x- or o-wave component. By forming the ratio A_X/A_0 we get (see Section 2.7 in Chapter 2):

$$\frac{A_X}{A_0} = \frac{|R_X|}{|R_0|} \exp \left[-2 \int_0^h (\kappa_X - \kappa_0) dh \right] \quad (8.3)$$

Since A_X and A_0 are measured in the experiment, $|R_X|$, $|R_0|$, κ_X and κ_0 must be expressed in terms of known quantities such as operating wave pulsation ω , electron density N , and longitudinal component of the gyro-pulsation ω_L .

With Eq. (8.2) we find

$$\frac{R_X}{R_0} = \frac{\Delta n_X}{2n_X} \cdot \frac{2n_0}{\Delta n_0}$$

Assuming that n is a function of N only, i.e. ignoring the change in v at the boundary and assuming further that $n_X = n_0 \approx 1$, we can write:

$$\frac{R_X}{R_0} \approx \frac{dn_X^2}{dN} / \frac{dn_0^2}{dN} \quad (8.4)$$

The assumption that the partial reflections are caused primarily by irregularities in electron density, and that the influence of irregularities in collision frequency is orders of magnitude smaller is justified by calculations of Gallet [1955] and Piggott and Thrane [1966]. Nevertheless, Manson [1966] and recently Jones and Kopka [1971] pointed out that taking into account irregularities in collision frequency could considerably influence the computed electron density under certain circumstances.

Differentiating Eq. (8.1) with respect to N and inserting in Eq. (8.4) yields:

$$\frac{|R_X|}{|R_0|} = \left[\frac{\{y_X C_{3/2}(y_X)\}^2 + \left\{\frac{5}{2} C_{5/2}(y_X)\right\}^2}{\{y_0 C_{3/2}(y_0)\}^2 + \left\{\frac{5}{2} C_{5/2}(y_0)\right\}^2} \right]^{1/2} \quad (8.5)$$

The difference $\kappa_X - \kappa_0$ in terms of ω , ω_L , N , and $\hat{\omega}$ is obtained in a similar way. By comparing the imaginary parts of Eq. (8.1), assuming $\mu_{X,0} \approx 1$, we find

$$\kappa_{X,0} = \frac{5}{4} \frac{Nq^2}{m_e \epsilon_0 c_0 \hat{\omega}} C_{5/2}(y_{X,0})$$

$$\text{and} \quad \kappa_X - \kappa_0 = N \cdot \left\{ \frac{5}{4} \frac{q^2}{m_e \epsilon_0 c_0 \hat{\omega}} [C_{5/2}(y_X) - C_{5/2}(y_0)] \right\} = N \cdot F \quad (8.6)$$

Inserting Eq. (8.6) into Eq. (8.3) we obtain:

$$\frac{A_X}{A_0} = \frac{|R_X|}{|R_0|} \exp \left[-2 \int_0^h N F dh \right]$$

or

$$\ln \left(\frac{A_X}{A_0} \right) = \ln \left(\frac{|R_X|}{|R_0|} \right) - 2 \int_0^h N F dh$$

Measuring the amplitudes A_X and A_0 in two adjacent heights h_1 and h_2 , where $\Delta h = h_2 - h_1$ is sufficiently small, so that N and F in the integral will remain nearly constant with respect to height, we can write

$$\ln \left(\frac{A_X}{A_0} \right)_2 - \ln \left(\frac{A_X}{A_0} \right)_1 = \ln \left(\frac{|R_X|}{|R_0|} \right)_2 - \ln \left(\frac{|R_X|}{|R_0|} \right)_1 - 2NF \Delta h$$

where the indices 1 and 2 correspond to the heights h_1 and h_2 . Thus we find for the desired electron density:

$$N = \frac{1}{2F\Delta h} \left[\ln \left(\frac{A_X}{A_O} \right)_1 - \ln \left(\frac{A_X}{A_O} \right)_2 - \ln \left(\frac{|R_X|}{|R_O|} \right)_1 + \ln \left(\frac{|R_X|}{|R_O|} \right)_2 \right] \quad (8.7)$$

On the right-hand side, this formula contains only known quantities except the collision frequency $\hat{\nu}$, which is in general unknown. To avoid this deficiency we proceed in the following way. For the lower "boundary" of the D region, h_0 , the electron density is close to zero and absorption coefficients $\kappa_{X,0}$ also will be zero, and thus from Eq. (8.3) follows:

$$\left(\frac{A_X}{A_O} \right)_{h_0} = \frac{|R_X|}{|R_O|} = f(\omega, \omega_L[h_0], \hat{\nu}[h_0]) \quad (8.8)$$

Since $(A_X/A_O)_{h_0}$ is known, from Eq. (8.8) we can calculate the collision frequency $\hat{\nu}$ at the height h_0 . This value $\hat{\nu}(h_0)$ is used to construct an exponential $\hat{\nu}(h)$ -profile taking the gradient of this profile from a standard atmosphere or from rocket measurements.

This procedure yields reasonably good results in spite of the uncertainty of h_0 , and several methods are developed by the various groups to avoid errors in estimating h_0 .

A quite different way to get information about the collision frequency is to measure not only the amplitude of the downcoming wave but also its phase. This extension of the partial reflection method is briefly outlined in Section 8.3.4.

8.3.2 Volume Scattering

Though Belrose and Burke [1964] showed that Eq. (8.2) is valid not only for Fresnel scattering but also for volume scattering, their proof was not complete because it was based on an analysis of volume scattering by Booker [1959], which did not take into account the Earth's magnetic field and the electron collisions with neutral particles. In a "revised" and a "most recently revised" theory for partial reflection measurements, Flood [1968, 1969] was able to make some important steps toward a more rigorous analysis of volume scattering. He assumed a scattering medium consisting of a dielectric of mean value ϵ with stochastic fluctuations of the dielectric constant $\Delta\epsilon(r)$. As a scattering volume, he defines a blob with a vertical thickness $\sigma\tau/2$, where τ is the duration of the probing pulse.

Comparing Flood's results with those from the basic theory we find that Eq. (8.3) must be rewritten as:

$$\frac{\overline{A_X^2}}{\overline{A_O^2}} = \frac{|R_X|^2}{|R_O|^2} \exp \left[-4 \int_0^h (\kappa_X - \kappa_O) dh \right] \cdot M(\omega, \omega_L, \hat{\nu}, N, \tau) \quad (8.9)$$

The factor

$$M(\omega, \omega_L, \hat{\nu}, N, \tau) = \frac{C_{5/2}(y_O) \sinh \left[\sigma\tau/4 \left\{ 5C_{5/2}(y_X) \frac{Ne^2\tau}{m\epsilon_0\sigma\hat{\nu}} - \alpha(h) \right\} \right]}{C_{5/2}(y_X) \sinh \left[\sigma\tau/4 \left\{ 5C_{5/2}(y_O) \frac{Ne^2\tau}{m\epsilon_0\sigma\hat{\nu}} - \alpha(h) \right\} \right]} \quad (8.10)$$

arises from the differential absorption within the scattering volume, which was not taken into account in the basic theory. The function $\alpha(h)$ is the intensity variation of the fluctuation spectrum with altitude.

From Eqs. (8.9) and (8.10) it follows that a simple derivation of the electron density N , as it was shown in the basic theory, is no longer possible, when volume scattering is not negligible.

Taking the electron density profile obtained by the basic theory as a first-order solution and computing with that profile the correction term M , one can improve the initial profile step by step. The function $\alpha(h)$ can be estimated by computing the amplitudes of the scattered o wave as a function of altitude with the first-order profile and comparing these amplitudes with the measured data.

There has been a controversy about the magnitude of the correction factor M between Flood and Holt [1969] who showed that this factor is indeed very close to unity in many cases, so that the early profiles of e.g. Belrose and Burke [1964] which were computed with the basic theory are still reliable. Flood agreed, but stated that under certain circumstances, particularly at very low heights, the error in neglecting the correction factor may become considerable.

Thus in practise one has to check carefully if the basic theory is sufficient or not.

8.3.3 Extended Theory of Volume Scattering

The most recent development in partial reflection theories is the work by Cohen [1971] who takes into account the effect of the changing reflection coefficient within the pulse width τ , which was not included in Flood's theory. Similarly as Flood, he starts with a scattering volume, $\sigma\tau/2$, containing a finite number of discrete and independent scatterers. The received amplitudes are the sum of the echoes of all these scatterers located in $\sigma\tau/2$. The receiver output is calculated from probability theory, assuming that each scatterer has a uniform probability distribution. The result of this theory is a complicated integral equation for the electron density profile which will not be given here.

Comparing this theory with the basic theory, it turns out that the computed profiles show a strong dependence on the pulse width τ . While the difference between the basic theory and this theory is negligible at short pulse widths ($\tau \approx 10-25$ μ s), there are considerable differences at pulse widths of $\tau \gtrsim 50$ μ s. Thus the important result of this theory is that the basic theory could be applied if the probing pulse width τ is sufficiently small. The experimental questions concerning the pulse width will be discussed in Section 8.4.2.

8.3.4 Differential Phase Measurements

Not only the amplitude, but also the phase of a wave partially reflected in the D region is altered. Assuming a single scatterer at a height h , we obtain for the phase difference between the two components of the wave,

$$\Delta\phi = \phi_x - \phi_o = \frac{2\omega}{c_o} \int_0^h (n_x - n_o) dh + \eta_o - \eta_x \quad (8.11)$$

$\eta_{o,x}$ being the phase change at the reflection point.

Measuring $\Delta\phi$ and evaluating Eq. (8.11) with the help of Eq. (8.1) is another method to find the electron density profile. Combining these results with those obtained by differential amplitude measurement, it is possible to get the electron density profile and collision frequency profile simultaneously and independently.

Currently there are two methods applied to measure the differential phase. Austin *et al.* [1969] and Austin [1971] measured directly the phase between the upgoing and the downcoming wave for both magneto-electronic components and calculated $\Delta\phi$ from these results. Von Biel, Flood and Camnitz [1970] obtained the phase difference indirectly by measuring the mean square amplitudes of sums and differences of the two wave components.

Both measurements together with those from Belrose [1970] have preliminary character because of the difficulties in exact phase measurements. The authors were not able to derive electron density profiles with the same accuracy as those obtained by differential amplitude measurements. They only use the differential phase measurements as a cross check for the differential amplitude experiment.

Nevertheless the differential phase measurement seems to be a useful complement to the differential amplitude measurements, and it certainly will become more important when the experimenters have more experience in measuring the phase difference with better accuracy.

8.4 Choice of the Probing Pulse Parameters

To install a satisfactorily working partial reflection experiment a careful choice of the appropriate probing pulse parameters needs to be made. Some considerations about this subject are summarized in the following sections.

8.4.1 Probing Frequency

The choice of the probing frequency depends mainly on the height range of the D region which should be explored, and on the geographic location of the installation. From the aim that the measurements of the amplitude A_x/A_o should be as accurate as possible, it follows that the value of this ratio should be as high as possible, since in this case it is the least sensitive to interference. Regarding Eq. (8.3) we can say that A_x/A_o is large if R_x/R_o is large since the exponential expression is always less than 1. If we compute $\frac{|R_x|}{|R_o|}$ with Eq. (8.4) and the CP approximation to the Appleton-Lassen formula (see Section 2.2.4) which is sufficient for this estimation, we get

$$\frac{|R_x|}{|R_o|} = \sqrt{\frac{(\omega + \omega_L)^2 + \nu^2}{(\omega - \omega_L)^2 + \nu^2}}$$

using the notation of Eq. (8.1). This ratio is roughly 1 if $\bar{\nu}$ dominates (at very low heights), and is

$$\frac{|R_X|}{|R_0|} \approx \frac{\omega + \omega_L}{\omega - \omega_L} \quad (8.12)$$

if $(\omega \pm \omega_L)$ dominates.

From Eq. (8.10) it follows that the measurements will be more accurate as ω approaches ω_L , the longitudinal component of the gyropulsation ω_B . This fact is illustrated in Figure 8.3. To get the same accuracy as obtained with the 2.66 MHz installation at Ottawa, one has to take a probing frequency of 0.5 MHz if the installation is to be operated in Brazil. Nevertheless, the probing frequency should not be chosen too near to ω_L because difficulties in the theory might arise. The influence of the probing frequency on the height range of the D region which is covered by the measurements is illustrated in Figure 8.4. With a probing frequency of 2.66 MHz reliable data could be obtained in the height range 65-85 km and with 6.275 MHz in the height range 72-95 km.

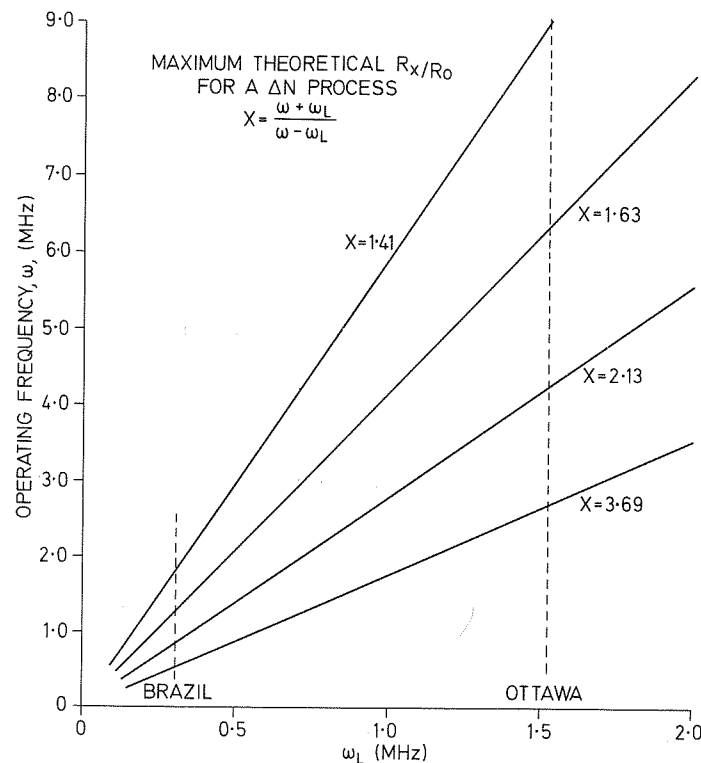


Fig. 8.3 The quantity $(\omega + \omega_L)/(\omega - \omega_L)$ as an index for the accuracy of the A_X/A_0 -ratio measurements depending on the wave frequency and on the longitudinal component of the gyrofrequency. [Belrose, 1970].

In practice the choice of the probing frequency will also depend on the local conditions such as noise and reserved frequency bands.

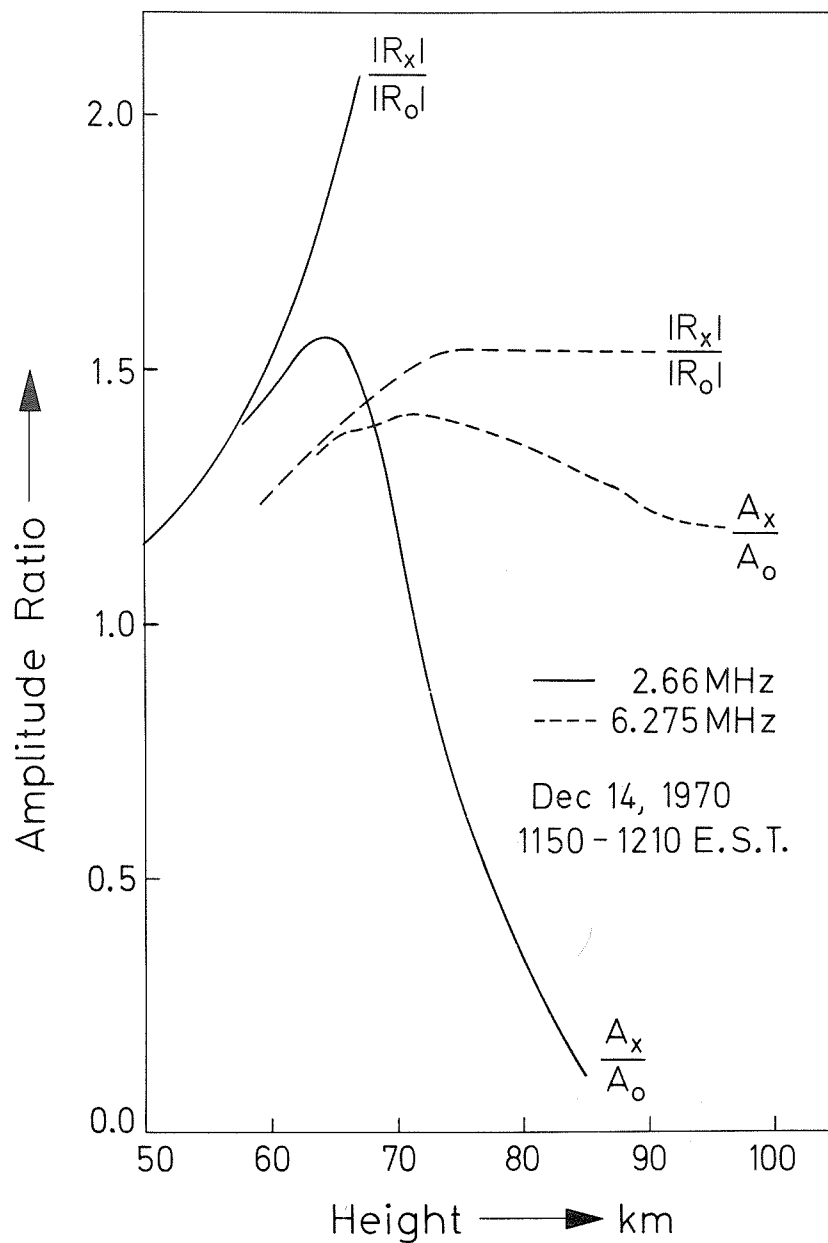


Fig. 8.4 - Computed values $|R_x|/|R_o|$ and measured ratios A_x/A_o for two different probing frequencies on a quiet day (Ottawa, 14 Dec. 1970, 1150-1210 EST).

8.4.2 Probing Pulse Width

The probing pulse width is a very important parameter, especially with regard to the theory which becomes simpler if the pulse width is small, as mentioned in Section 8.3.3. On the other hand small pulses are not always easy to handle from the technical point of view. Moreover to receive the echoes of a small pulse, a greater receiver bandwidth is needed which may be troublesome in the case of high noise. Thus the pulse width generally could not be chosen as small as required by the theory. Only if a pulse width of about 20-30 μ s could be achieved, will the error by using the basic theory be usually within the A_x/A_0 measuring accuracy.

8.4.3 Probing Pulse Sequence

The probing pulse sequence primarily depends on the experimental facilities. From the theoretical point of view it should be as high as possible, since the fluctuations in the D region are quite fast. To obtain a reliable electron density profile some tens of A_x/A_0 profiles are necessary, and it is apparent that the spread of the A_x/A_0 values will be smaller if they are taken within a shorter time.

A high probing pulse sequence moreover implies a short delay time $t_{x,0}$ between transmission of the x-mode and the o-mode pulse. In the ideal case both pulses should be transmitted simultaneously, but this could only be achieved with separate antenna arrays for transmitting and receiving, using a linearly polarized transmitter antenna. The setting up of two separate antenna arrays on the other hand is usually prohibited by the high costs if the antennas are as large as required in Section 8.5.3. Thus the delay time, $t_{x,0}$ has to be shortened as much as possible, which could be realized by using high speed vacuum relays to switch the antenna between the x mode and the o mode. From their switching time of 20-30 ms it follows that a probing pulse sequence of 10-20 Hz could be achieved.

Another limitation for a high probing frequency is the speed of the recording device. With the widely used film recording a maximum recording frequency of 1 to 2 Hz is possible because of the time consuming film exposure and film transportation. A higher recording frequency could only be realized with a fast digital recording system. In Appendix 8.A Table 8.A.1 shows the parameters mentioned in this section for some partial reflection installations.

8.5 Comments on the Equipment

In this chapter some comments on the experimental equipment shall be given. The experimental system has been improved considerably since the early experiments of Gardner and Pawsey [1953]. For comparison in Appendix 8.A, Table 8.A.2, details of the experimental installations for partial reflection measurements of different experimenters are listed.

8.5.1 Experimental System and Operating Sequence

Although there are a lot of different partial reflection experiments, the installations are always variations of a basic arrangement which is shown in Figure 8.5. The operating sequence is the following. After the calibration, the transmitter is triggered and produces a pulse which is radiated from the transmitting antenna in, for example, the extraordinary mode. The receiver is locked during this time. After some hundred microseconds, the wanted echoes from the 50 to 90 km height range are received with the corresponding-polarized receiving antenna and a certain attenuator adjustment. After having recorded the A_x amplitude, this sequence is repeated if necessary once or several times with different attenuator adjustments, depending on the dynamic range of the receiver. After that the polarization is switched to the o mode and the whole procedure, which shall be called a "cycle", is repeated (see also Table 8.A.1 in Appendix 8.A). After having recorded some cycles, the noise is measured by opening the receiver without transmitting a pulse before. In principle one o- and one x-cycle yield one electron density profile, but due to the fading of the echo one profile is not very meaningful. In practice some tens of double-cycles have to be performed to obtain a reliable electron density profile.

8.5.2 Transmitter and Receiver

Since the partial reflections from the D region are very weak, the transmitter has to be quite powerful. In the special case the required transmitting power depends on the site noise and the antenna array used for transmitting and receiving. As one can see from Table 8.A.2 in Appendix 8.A, the transmitter power ranges from 15 to 1000 kW (except the first installation from Gardner and Pawsey). Many of these values are presumably too low, which may account for the unsatisfactory results of some measurements. In the case of low noise 100 kW may be sufficient if a good antenna system is used. The shape of the transmitted pulse is also an important factor of the measurements. In most cases rectangular pulses are used, but it requires a certain expenditure to give the pulse an exact rectangular shape, especially if it is quite short. For this reason Jones [1971] proposes to use Gaussian-shaped pulses. They are easier to realize, much less disturbing and easier for theoretical considerations.

The principal requirements of the receiver are linearity and a sufficient bandwidth according to the width of the probing pulse. The maximum gain of the receiver should be about 120 dB. Since the linearity of this range is nearly impossible to achieve, an attenuator with one or more steps has to be used to fit the received echoes to the linear range of the receiver.

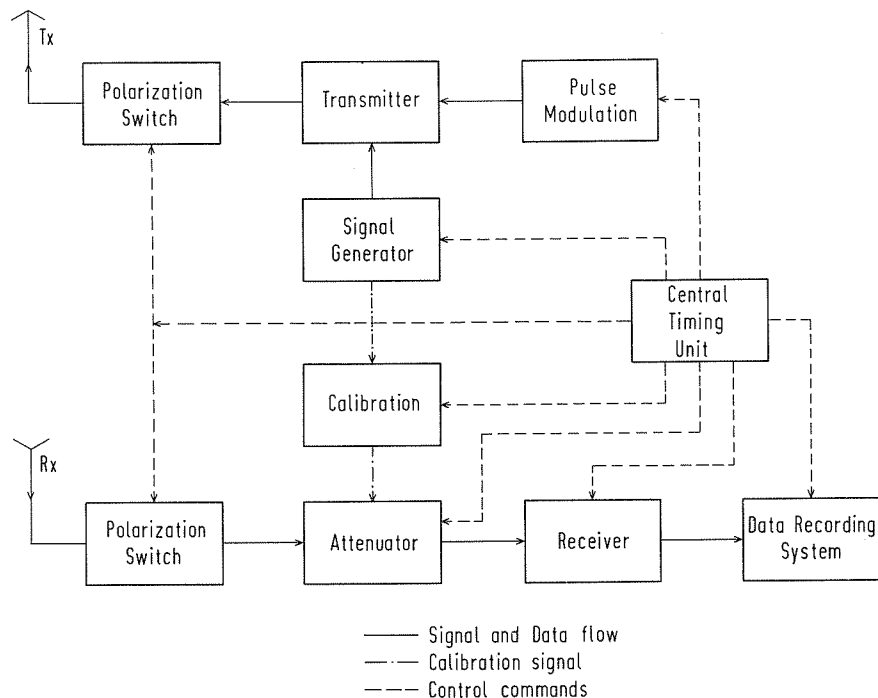


Fig. 8.5 Basic arrangement of a partial reflection experimental equipment.

The minimum theoretical bandwidth of the receiver must be about 40 kHz if a 25 μ s rectangular pulse is used. But in practice the bandwidth has to be greater if the rise time of the pulse is high, and the pulse should be received without great distortion. A greater bandwidth of the receiver naturally implies a higher rate of interference from frequencies adjacent to the probe frequency, which may be very cumbersome if the man-made noise at the receiving station is high. In that case the bandwidth has to be reduced in spite of the associated disadvantages.

8.5.3 Antenna System

A sufficiently large antenna array is one of the most important factors to obtain satisfactory results in partial reflection measurements. One reason for the requirement of a large antenna array is the weakness of the partially reflected waves and the other is the need of a small beamwidth to reduce interferences. While the faintness of the echoes can be amplified by increasing the transmitter power, the required small beamwidth of the antenna could only be achieved with a great number of dipoles.

The need of a small antenna beamwidth is documented in the older publications of nearly all those authors who used only small antennas, and who reported considerable interference by oblique reflections and reflections on mountains, sea waves, and other obstacles. A four dipole square array may only be sufficient if the noise at the receiving station is very low and none of the obstacles mentioned above are present. Since this situation is quite rare, the number of dipoles has to be increased if good data are desired. Figure 8.6 shows the dependence of the power gain over a half-wave dipole and of the beamwidth on the number of dipoles. In practice the number of dipoles is generally limited by financial reasons; from the theoretical point of view it should be as high as possible.

As a result from Table 8.A.2, most of the experimenters use a square array of dipoles which is the most convenient form for receiving circularly polarized waves. In this arrangement, which is shown schematically in Figure 8.7 as a 40-half-wave dipole array, all the dipoles in the rows a, b, c, d, e are fed in phase while the dipoles in the columns A, B, C, D, E are fed similarly but in quadrature. If separate antennas are used for transmitting and receiving, a linearly polarized transmitting antenna may be used. Consequently the polarization switch on the transmitter side can be omitted, but a gain loss of 3 dB has to be taken into account. More convenient from the economical point of view is a single antenna system for transmitting and receiving which was used by Belrose [1970], Feyer and Vice [1959] and Holt *et al.* [1963]. An example of the TR switch which is required in that case is shown in Figure 8.8. This TR switch has the advantage of being a purely passive network which uses no mechanical switching. One can easily realize, taking the phases of signals into account, that the voltage of point R is zero in the transmitting mode and the voltage at point T is zero in the receiving mode, while the voltage at point X and O are separated in phase 90° as required for a circularly polarized wave.

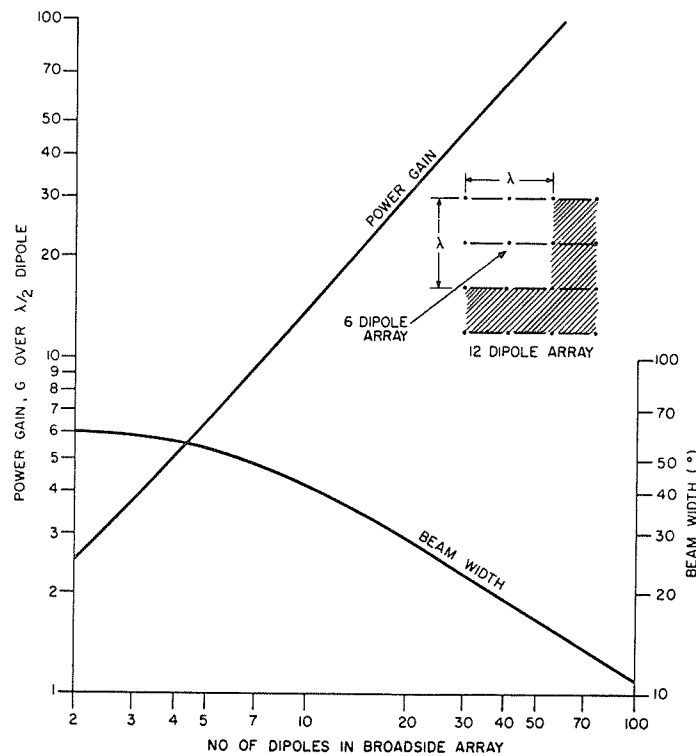


Fig. 8.6 Power gain over a half-wave dipole and beamwidth of an antenna array built of m dipoles. [Belrose, 1971].

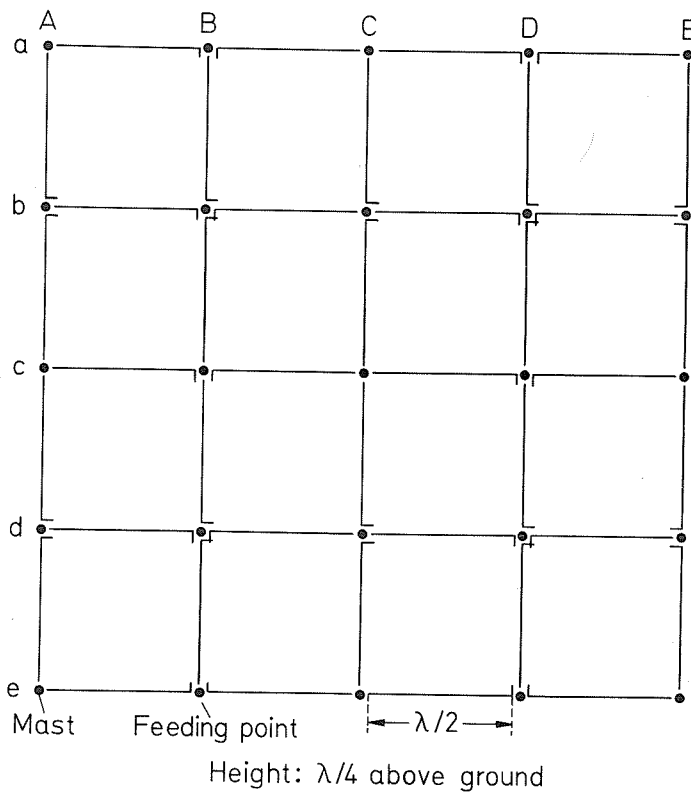


Fig. 8.7 Example of a 40-dipole-square array antenna.

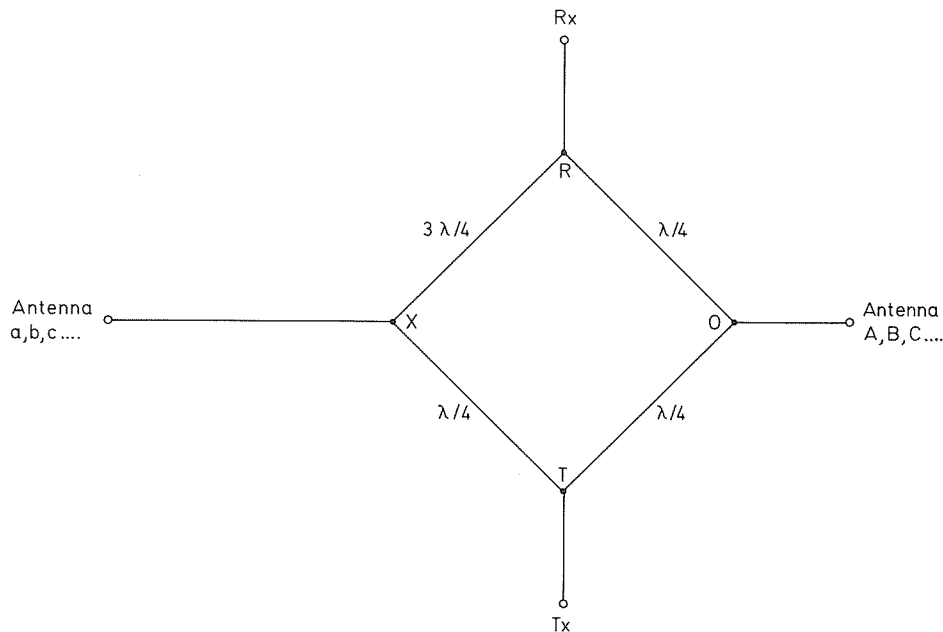


Fig. 8.8 Passive network switch for transmitting and receiving [Belrose, 1970].

8.5.4 Data Recording System

The simplest data recording system which is used by the majority of the experimenters is an A-scope and a camera. The A_x amplitude versus height is displayed in the positive y -direction and the inverted A_o amplitude versus height in the negative y -direction of a cathode ray tube. Since both amplitudes are displayed one after the other (if $t_{x,o} \neq 0$), the film in the camera is transported whenever such a double exposure is performed. Both the cathode ray display and the camera are controlled by the central timing unit shown in Figure 8.5. A more convenient data recording system is presently used at Ottawa [Belrose *et al.*, 1972], Urbana [Birley and Sechrist, 1971] and Armidale [Lehmann, 1971] and will be used at Lindau. A block diagram of this system is shown in Figure 8.9. The analog voltage of the height amplitude echo envelope, which was formerly displayed on an oscilloscope, is now fed into an analog-to-digital converter. In this device one digital amplitude value is formed for each height interval of, for instance, 2 km. These digital amplitude values in a height range from about 40 to 100 km are stored in a memory. This is done for both amplitudes $A_x(h)$ and $A_o(h)$ and also for the noise values. The memory is then read out on an incremental tape recorder. The AD converter, memory and tape recorder are controlled by the same central timing unit which is shown in Figure 8.5. The data on the magnetic tape can be directly analyzed with the help of a computer.

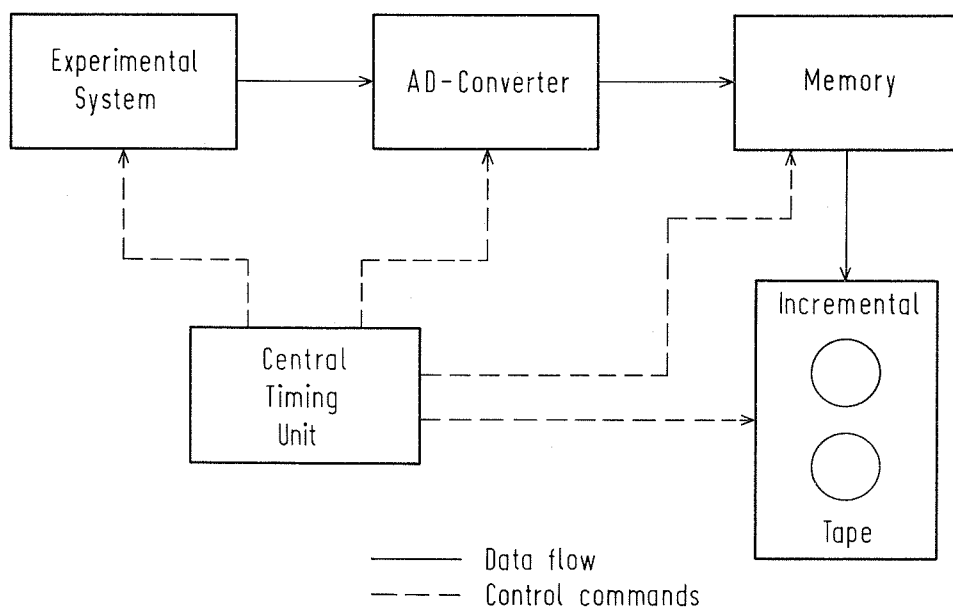


Fig. 8.9 Block diagram of a digital data recording system for partial reflection measurements.

This data recording system is certainly more expensive than the simple A-scope and film recording, but it has the great advantage that the laborious and lengthy manual scaling of the films is avoided which is especially important if the measurements extend over a long time.

8.6 Processing of the Partial Reflection Data

The processing of the partial reflection data does not only imply the application of an appropriate theory as described in Section 8.3, but also preprocessing of the raw data, selection of "good data", and consideration of measuring errors.

To obtain A_x and A_0 values two different methods are applied if the data are on film. One is reading off the amplitudes at small fixed height intervals from the base of the D region, the other by reading the peak amplitudes of echoes which appear at the same height on both modes of polarization. The first method which is called "envelope scaling" is similar to that of Gardner and Pawsey [1953], while the second, which is called "peak scaling", is similar to that used by Fejer and Vice [1959]. Though the peak scaling is more appropriate to the theory which assumes single scatterers in the D region, envelope scaling is also widely used because it allows a more accurate determination of the A_0 and A_x values. Particularly those groups that use digital data recording have adopted the envelope scaling because the peak scaling is very uncertain in that case. Belrose [1970] showed that there are differences between the various methods of scaling, but that the uncertainties are mostly within the standard deviation of the measurements.

If one has the A_0 and A_x values, there are several methods to form the A_x/A_0 ratios, since the amplitudes from a particular height exhibit a considerable scatter as mentioned in Section 8.4.3. One method is to compute the average values of A_0 and A_x separately and then determine the ratio $\overline{A_x}/\overline{A_0}$ as a ratio between these mean values. The other method is to compute the ratio $\overline{A_x/A_0}$ from the corresponding echo pairs. Belrose and Burke [1964] showed that both methods exhibit only small differences.

Regarding the development of the partial reflection theory Flood [1968, 1969] and Cohen [1971] pointed out that the simple ratios $\overline{A_x}/\overline{A_0}$ or $\frac{\overline{A_x}}{\overline{A_0}}$ could involve a considerable error. Instead of this, a ratio of the mean square amplitudes $\overline{A_x^2}/\overline{A_0^2}$ should be used.

The selection of "good" data mainly implies the rejection of those A_0 and A_x values which are not markedly above the noise level or which lie at the upper limit of the measuring range. Moreover the errors caused by off-vertical echoes and by reflections from fixed or moving obstacles (airplanes) have to be taken into account.

Regardless of the stage of the applied theory an adequate $\hat{\nu}(h)$ profile has to be adopted for computing the electron density profile if only differential amplitudes are measured. The simplest way is to take the gradient from a standard atmosphere, combining it with the measured $\hat{\nu}(h_0)$ as described in Section 8.3.1, or to take a mean of different rocket measured profiles which has to be shifted until $\hat{\nu}(h_0)$ fits to this mean profile. Both methods have the disadvantage of neglecting the seasonal variations of $\hat{\nu}(h)$. This inadequacy has been overcome by a thorough analysis of Gregory and Manson [1969a] who studied the seasonal variation of $\hat{\nu}(h)$.

8.7 Facilities and Aims of Partial Reflection Measurements

Historically it was the main aim of partial reflection measurements to obtain electron density profiles in the D region. These profiles could be studies with respect to their daily, seasonal, and sunspot cycle variations [e. g. Coyne and Belrose, 1971; Gregory and Manson, 1969a and b, 1970; Manson and Merry, 1970]. Moreover, the short time variations of the $N(h)$ profile during special events, such as magnetic storms, solar x-ray flares [Montebriand and Belrose, 1971], solar proton events, or high energy particle precipitation events [Schlegel, 1971] could be observed. These results combined with those from riometer, solar x-ray, and absorption measurements yield valuable information about the various processes taking place in the D region during such events. If differential phase measurements become more advanced, all the observations mentioned above could be extended to the electron collision profiles. This could be a step towards the explanation of meteorological effects in the D region and stratospheric-ionospheric coupling effects such as winter anomaly. A further step in this direction are D-region drift measurements, which are already performed by various groups with the partial reflection method [Golley and Rossiter 1971; Fraser, 1968; Haug and Holt, 1968]. These results together with the partial reflection studies of D-region irregularities [Fraser and Vincent, 1970; Manson, Merry and Vincent, 1969] should be able to extend our knowledge of the dynamics and the plasma physics of the D region. All these examples show that the partial reflection method is a powerful tool for investigating the lower ionosphere.

8.8 Annex: Partial Reflection Measurements with FM-CW

During the preparation of this paper a new technique for performing partial reflection measurements was investigated at the Max-Planck-Institut für Aeronomie, Lindau. This technique which was already applied successfully to other ionospheric sounding measurements in this institute is the FM-CW method (frequency modulated continuous waves). The great advantage of this technique in comparison with the so far applied "pulse-technique" is the reduction of the transmitter power by orders of magnitude as will be shown in the following.

Different from the pulse technique, in the FM-CW technique not a single pulse but a continuous wave with linearly increasing frequency is transmitted into the D region (Figure 8.10). The echo signals which arrive at the receiver after the time delays $t_1, t_2, t_3 \dots$ were superimposed by the instantaneous transmitter signal yielding low frequency shifts $F_1, F_2, F_3 \dots$. In this way the time delay spectrum of the received signal is transformed into a low frequency spectrum. By Fourier analyzing the receiver signal after the mixing process, one obtains the spectrum of the frequencies $F_1, F_2, F_3 \dots$, where these frequencies correspond to the heights of the reflecting centers in the D region, and the intensity of the spectrum at those frequencies corresponds to the reflection coefficient of those centers. The obtained frequency profile, $A_{x,o}(F)$, can be easily converted into a height profile, $A_{x,o}(h)$, by the relation

$$h = \frac{c_0}{2} \cdot \left(\frac{\Delta f}{\Delta t} \right)^{-1} \cdot F$$

c_0 being the velocity of light and $\Delta f/\Delta t$ the linear frequency increase of the transmitter signal (Δf is called "frequency sweep" and Δt "sweeptime"). Since the Fourier analysis yields not only the amplitudes but also the phases of the low frequency spectrum, one needs no additional equipment for measuring differential phases. The evaluation of the differential amplitudes, $A_{x,o}(h)$, and differential phases, $\varphi_{x,o}(h)$, by means of the magneto-electronic theory is performed in the same way as in the case of the pulse techniques.

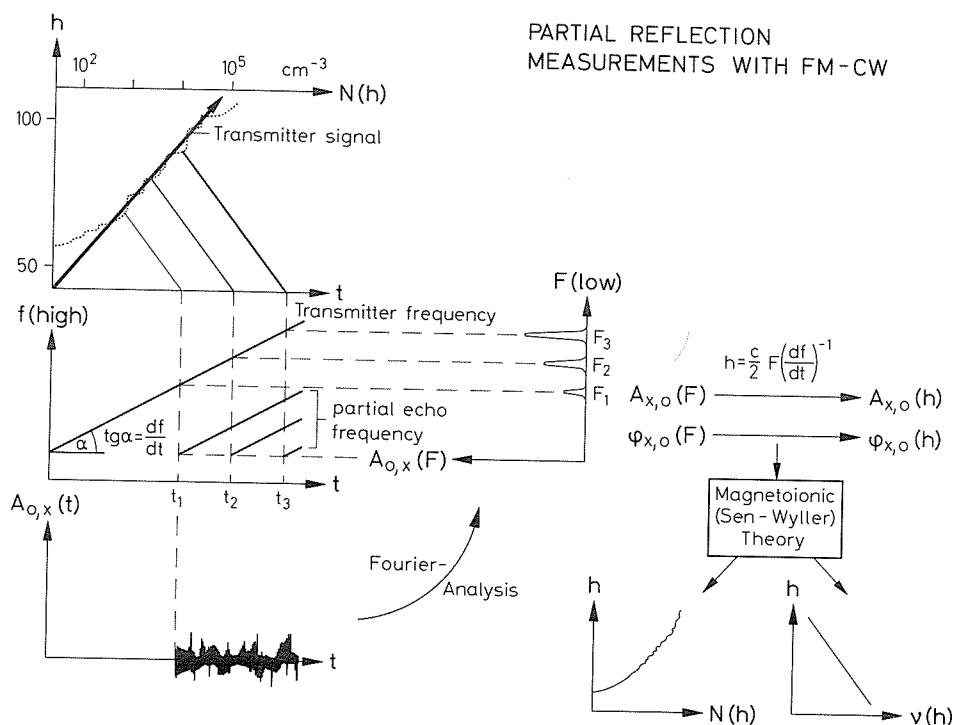
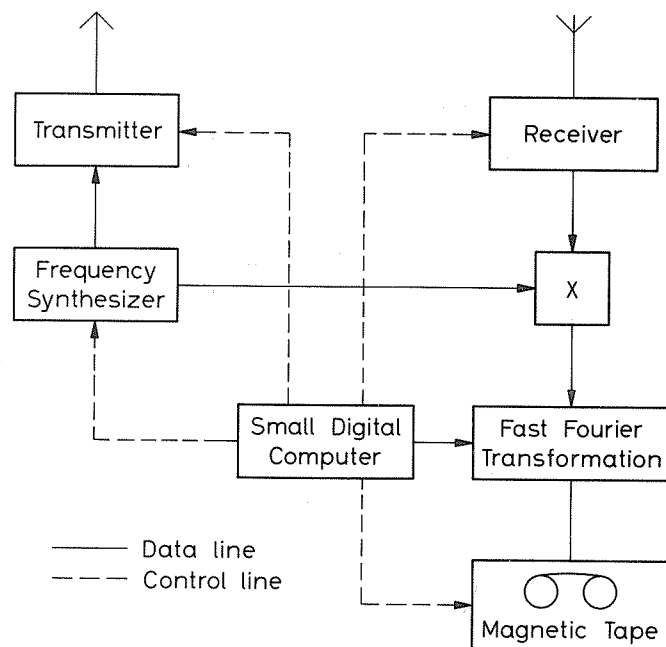


Fig. 8.10 Partial reflection measurements with the FM-CW technique. By transmitting a continuous wave with linearly increasing frequency f and mixing the received signal with the instantaneous transmitter signal, the delay times t_i of the received signals were transformed into low frequencies F_i . Fourier analysis and conversion of the frequencies F_i to altitudes h_i yield the amplitudes $A_{x,o}(h)$ and phases $\varphi_{x,o}(h)$ of the partially reflected signal.

The reduction of the transmitter power mentioned above by applying the FM-CW technique is, of course, the consequence of using a continuous wave instead of a single pulse. Comparing the duration of one pulse of 25 μ s as applied in pulse techniques with a duration of one frequency sweep of 1 s as applied in the FM-CW technique yields a factor of 40,000 by which the transmitter power can be reduced theoretically. Instead of using 400 kW with the pulse technique one obtains theoretically the same signal-to-noise ratio with a transmitter power of 10 W applying the FM-CW technique. In practice, the reduction factor is not so high because of necessary transmitting interruptions for switching from x to o mode or inserting receiving periods if only one antenna system is used for transmitting and receiving.

Our first results of partial reflection measurements with FM-CW technique [Kramm, Schlegel and Weiss, 1972] were so encouraging that we decided to realize the planned partial reflection installation at Lindau with this technique. Figure 8.11 shows a block diagram of the equipment and some data of the operating parameters. The equipment was expected to be in operation in the spring of 1974.

The Lindau Partial Reflection Equipment



Transmitter Frequency: 3.95-4.05 MHz
 Transmitter Power : 2×500 Watt
 Frequency Sweep : 100kHz
 Sweeptime : 1s
 Antenna : 40Dipole Square Array

Fig. 8.11 Block diagram of the Lindau partial reflection equipment and operating parameters.

It should be noted that D-region measurements with a special kind of FM-CW technique were already performed more than 20 years ago by Gnanalingam and Weekes [1955] and later by Titheridge [1962]. But neither the advanced electronics nor the present theoretical knowledge (e.g. Sen-Wyller formula) were at the disposal of those authors, so that their results -- being excellent at that time -- are unsatisfactory from the present point of view. Today, modern electronics enables us to produce highly stable frequency sweeps as well as to perform Fourier analysis very quickly with analog or digital devices. So we are quite optimistic about possible improvements of the partial reflection measurements by this technique.

APPENDIX 8.A

Table 8.A.1 Operating and Recording Data of Some Partial Reflection Installations

| Authors | Delay time between x and o pulse, $t_{x,o}$ | Recording time for one A_X/A_0 Profile (double cycle) | Recording Device |
|---|--|--|------------------|
| Belrose [1970] | 70 ms | 12 s | digital |
| Birley and Sechrist [1971] | 33 ms | 2 s | digital |
| Dieminger, Kramm, Rinnert, Schlegel (planned) | FM-CW technique | highly variable, 0.2 to more than 10 s | digital |
| Fejer and Vice [1959] | 250 ms | 10 s | film |
| von Biel [1966] | 60 ms | 0.72 s | film |
| Falcon [1967] | 0 (lin. pol. wave) | 4.28 s (14 per min) | film |
| Gregory and Manson [1969] | 0 | 0.04 s for one A_X/A_0 value averaged over 10 s | visual and film |
| Thrane <i>et al.</i> , [1968] | 0 | 0.65 s (100 per min) | film |

Table 8.A.2 Various Partial Reflection Installations

| Authors | Location | Transmitter | | | Antenna System* | Theory | Data Recording | Comments |
|--|--|--------------------------|--------------|------------------|---|-------------------------------------|------------------------|--|
| | | Frequency (MHz) | Power (kW) | Pulse width (μs) | | | | |
| Belrose, Burke [1964] Belrose [1970] | Ottawa, Ont. | 2.66 6.275 | 1000 100 | 50 50 | T _x and R _x : 40 dipole square array T _x and R _x : 128 dipole square array | basic | digital | Additional differential phase measurements since summer 1971 |
| Belrose, Bode, Hewitt [1966] | Churchill, Manitoba | 2.66 6.275 | 100 100 | 50 50 | T _x and R _x : 4 dipole square array T _x and R _x : 144 dipole square array | basic | digital | |
| Belrose, Bode, Hewitt [1966] | Resolute Bay, NWT | 2.66 6.275 | 100 100 | 50 50 | T _x and R _x : 4 dipole square array T _x and R _x : 40 dipole square array | basic | digital | |
| Briggs <i>et al.</i> , [1969] | Buckland Park, Australia | 1.98 5.84 | 100 | 25-200 | T _x : 89 dipole array R _x : 89 dipole array | - | - | Originally designed for drift measurements. |
| Cole, Ferraro, Lee [1969] | State College, Penna. | 2.2 4.5 | 1100 | - | T _x : 9 crossed dipole array R _x : 1 fullwave dipole, lin. pol. | basic | A-scope | Installation was designed for wave interaction |
| Dieminger, Kramm, Rinnert, Schlegel | Lindau, W. Germany | 4.0 | 0.5 | cont. wave | T _x and R _x : 40 dipole square array | - | digital | Planned, FM-CW technique (Section 8.8) |
| Falcon [1967] | Boulder, Colo. | 2.666 | 15 | 35 | T _x : 1 dipole, linear polarization R _x : 2 dipoles, perpendicular | basic | A-scope film | |
| Fejer, Vice [1959] | Frankenwald, South Africa | 1.83 2.63 | 70 | 30 | T _x and R _x : 4 dipole square array | basic, but Appleton-Hartree formula | A-scope film | The installation was also used for wave interaction measurements. |
| Gardner, Pawsey [1953] | Burraborang Valley, Australia | 2.28 | 1 | 30 | T _x : 1 dipole, linear polarization R _x : 2 dipoles, perpendicular | basic, but Appleton-Hartree formula | A-scope film | No more publication about this subject since 1953. |
| Gregory, Manson [1967, 1969] | Christchurch, New Zealand | 2.404 | 100 | 10-25 | T _x : 4x2 dipoles, linear polariz. R _x : 4 dipoles square array | basic | A-scope film | Also differential phase measurements Austin [1971] |
| Holt, Landmark, Lied [1963] | Tromsø, Norway | 2.3 2.7 | 50 | 100 | T _x and R _x : 2 crossed dipoles | basic, but Appleton-Hartree formula | A-scope | Together with wave interaction measurements |
| Thrane, Haug, Bjelland, Anastasiades, Tsagakis [1968] Haug, Thrane, Tsagakis, Anastasiades [1970] | Lavangsdalen, Norway | 2.25 2.75 | 20-50 | 50-100 | T _x : 1 dipole, linear polarization R _x : 4 dipole, square array | basic | A-scope film | Together with wave interaction measurements |
| | Kjeller, Norway | 2.75 2.90 | 50 | 50-100 | T _x : 12 dipole, linear polarization R _x : 4 dipole square array | basic | A-scope film | |
| | Mallia, Crete | 2.54 2.60 | 50 | 50-100 | T _x : 6 dipoles, linear polarization R _x : 4 dipole square array | basic | A-scope film | |
| | Tsumeb, South-West-Africa | 2.25 | 30 | 50-100 | T _x : vertical rhombic, lin. pol. R _x : 4 dipole square array | basic | A-scope film | |
| Haug [1975] | Ramfjord, near Tromsø, Norway | 2.75 | 100 | 10-50 | T _x and R _x : 16 crossed dipole array variable | basic | digital | Measurements started in Spring 1975 |
| Pirnat, Bowhill [1968] | Urbana, Ill. | 2.66 | 50 | 50 | T _x : 60 dipole square array R _x : 60 dipole square array | basic | A-scope film | Digital data recording since 1970 [Reynolds, Sechrist, 1970; Birley, Sechrist, 1971] |
| Smith, Bourne, Loch, Setty, Coyne, Barrat, Prasad [1965] Heilbronn [1971] Lehmann [1971] | Armidale, Australia Armidale, Australia | 1.78 2.12 2.12 | 60 50 | 50 5-100 | T _x : 4 dipole square array R _x : 4 dipole square array T _x : 4 dipole square array R _x : 1 fullwave dipole, lin. pol. later 24 dipole square array | basic basic | A-Scope digital | Operated only 6 months in 1962. New installation permits wave interaction and partial reflection measurements in amplitude and phase. |
| von Biel [1966] | Cook Islands | 2.4 | 200 | 25 | T _x : 2 orthogonal 6-element dipoles R _x : 2 orthogonal dipoles | basic | A-scope film | Measurements also during the 1966 solar eclipse at Casino, Brazil [v. Biel, Flood and Camnitz, 1970] |

*Circularly polarized unless stated otherwise.

CHAPTER 9. SATELLITE MEASUREMENTS OF ABSORPTION

by

J. Mass

Radio Observatory
Israel Academy of Sciences and Humanities
Haifa, Israel

Table of Contents

| | Page |
|--|------|
| 9.1 Introduction | 182 |
| 9.2 Differential Height Method | 182 |
| 9.3 Differential Path Method | 183 |
| 9.4 Differential Mode Method | 183 |
| 9.5 Conclusion | 185 |

9.1 Introduction

A satellite-borne HF transmitter would seem to be a simple and promising tool for the measurement of the absorption of radio waves in the ionosphere if one simply recorded the signal strength on the ground and compared it with the calculated signal strength for free-space propagation. This procedure, however, is beset with several technical difficulties which have so far not been completely overcome.

The main difficulties in measuring absorption in this way stem from the uncertainties regarding the characteristics of the wave transmitted from the satellite: its effective radiated power in the direction of the receiver and its polarization. All the beacon satellites in non-synchronous orbits which have so far been used in attempts to measure absorption had such altitudinal instabilities and uncertain antenna radiation patterns that it was practically impossible to calculate a free-space unattenuated field strength. The methods employed had to rely on difference measurements to circumvent this problem. The methods proposed and tested used the following differences:

- a) differences between consecutive passes at different heights with averaging of signal strength [Kazantsev, 1959],
- b) differences between signal strengths for oblique and vertical incidence propagation for the same pass [Vassy 1960, 1961; Mass 1963],
- c) differences between the instantaneous amplitude of the ordinary and extraordinary components [Amayenc 1967, 1968].

9.2 Differential Height Method

Kazantsev [1959] measured median curves of received field strength as a function of satellite distance when the satellite passed at altitudes both below and above the F layer. The satellites recorded were Sputniks 1 and 3 which had sufficiently elliptic orbits to cover different altitude ranges, but the main difficulty was their tumbling which caused very strong amplitude variations. Kazantsev plotted median values of field strength as a function of distance during a pass, and then compared this with the free-space amplitude assuming some constant mean value for transmitted power. The difference in attenuation thus calculated between passes at different altitudes is claimed to be due to the absorption between the altitudes of the passes (see Figure 9.1).

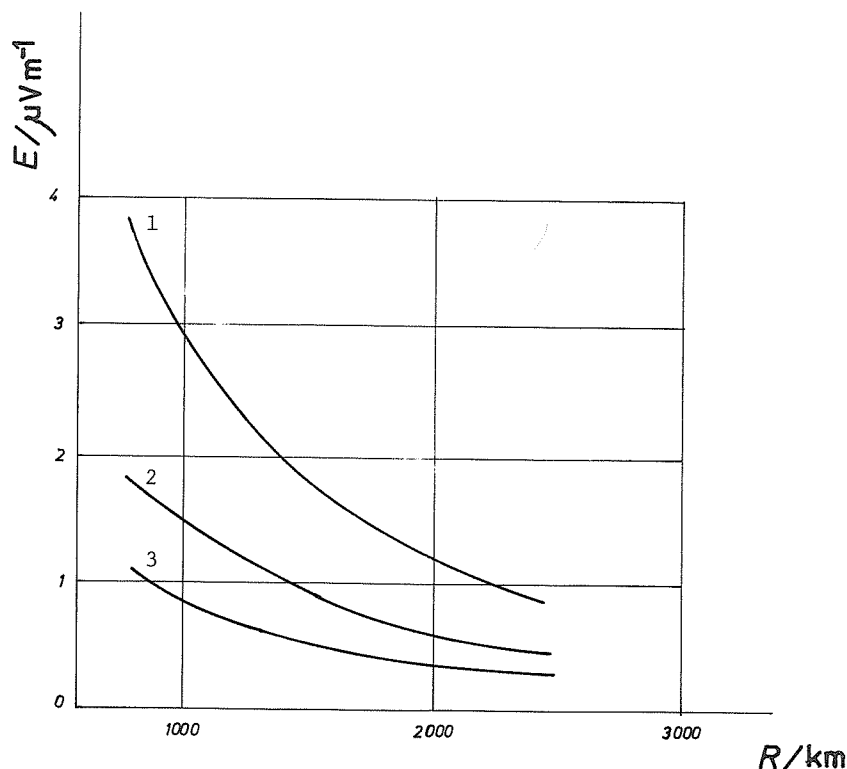


Fig. 9.1 Median curves of received field strength E at 20 MHz as a function of ground distance R . From top to bottom:
1) satellite below F2 Layer, 2) satellite near the F2 maximum,
3) satellite above the F2-Layer maximum, [Kazantsev, 1959].

The values of absorption thus obtained at 20 MHz for the whole F layer was 8-10 dB. This value seems to be exceptionally large as compared with riometer absorption measurements on cosmic noise at the nearby frequencies of 18 or 25 MHz [see Hultqvist, 1963] for an assumed value of $f_oF2 = 11.4$ MHz at the time of the satellite passes.

The causes of the discrepancy between the above and the usual values of F-layer absorption may lie in some attenuation mechanism other than absorption; for instance they may be due to scattering from irregularities [Rawer, 1960] which would not necessarily be detected by a wide angle averaging process or they may be caused by the inherent drawbacks of the method used -- mainly the assumptions that must be made to allow for the averaging of signal strength over the variations due to the satellite's changes in orientation (tumbling). Unfortunately the measurements described were carried out only on a very small number of passes.

9.3 Differential Path Method

A method similar to the Bouguer-Langley method for measuring the absorption of the Sun's rays at optical wavelengths was proposed by Vassy [1961]. This is based on comparisons of the signal amplitude for vertical and oblique transmission paths during the same satellite pass.

It would be especially applicable for beacon-carrying satellites in circular orbits above the main parts of the F layer, like the satellite S-66 (1964-64A). Attempts to use this method as detailed by Mass [1963] (see Figure 9.2) have so far been unsuccessful owing to the difficulty of eliminating the variations due to the satellite antenna radiation pattern and the orientational instability of the satellite. A possible way to overcome these problems would be to orbit a well-stabilized satellite with a well-known radiation pattern and to eliminate polarization difficulties either by receiving on circularly polarized antennas, or by measuring signal amplitudes only at the maxima of the Faraday fadings, at which time the polarization of the receiving antenna lies in the polarization plane of the received wave. It should however, be noted that the total difference in expected attenuation between an oblique path at 45° and a vertical path is only about 0.5 dB (at 20 MHz). Thus extremely high and possibly impractical stability would be required in the other parameters of the system.

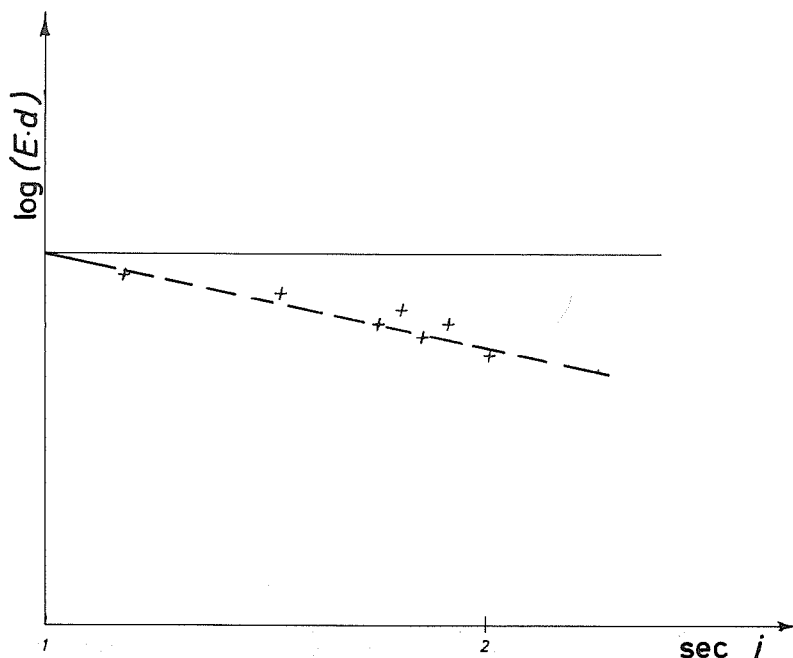


Fig. 9.2 A logarithmic plot of received field E multiplied by the geometric distance to the satellite d , as a function of the secant of the average angle of incidence i_a , should give the total vertical absorption $\int \kappa dz$

$$\text{using } E = \frac{\text{const}}{d} \exp(-\sec i_a \int \kappa dz); \tan \beta = - \frac{hs}{h_i} \int \kappa dz$$

[Mass, 1963].

9.4 Differential Mode Method

Amayenc [1967, 1968] has used the method of comparing the amplitudes of the ordinary and the extraordinary components at the receiving antenna, assuming that the transmitted signal is purely linearly polarized (that is, equal right-hand and left-hand circular components). The attenuations A_o and A_x of the ordinary and extraordinary components differ from each other and can be approximated by:

$$A_{0,x} = \frac{\alpha}{(f \pm f_L)^2} \int N v ds \dots \quad (9.1)$$

in which the upper (lower) signs refer to the ordinary (extraordinary) components respectively, where f is the wave frequency, f_L the gyromagnetic frequency, N the electron density, v the number of collisions per unit volume and time, ds the differential path length [Amayenc, 1967; see also Section 2.7 in Chapter 2]. By measuring the difference $A_X - A_0$ between the signal amplitudes, one can find A itself. Thus:

$$A_X - A_0 = \alpha \int N v ds \left[\frac{1}{(f - f_L)^2} - \frac{1}{(f + f_L)^2} \right] \quad (9.2)$$

in which the terms within the square brackets are known and the left-hand side is measured. Thus the integral can be calculated, and this gives the total attenuation as above.

This experiment was performed with great care, making sure that the crossed dipole receiving antenna was continuously pointed at the passing satellite. Calibration of the receiving system with a balloon-borne transmitter showed that the error in the differential amplitude readings of the two modes was less than ± 1.5 dB.

Using this method (see Figure 9.3) Amayenc found values of total ionospheric absorption to be 3 to 25 dB at 20.005 MHz when the transmitting satellite (1964-64A) was at an altitude of approximately 1000 km. The values of f_oF2 at the time varied between 6 and 11 MHz. The absorption values are much greater than those usually found using the cosmic noise method $A2$, but they agree with the results mentioned earlier obtained by Kazantsev [1959].

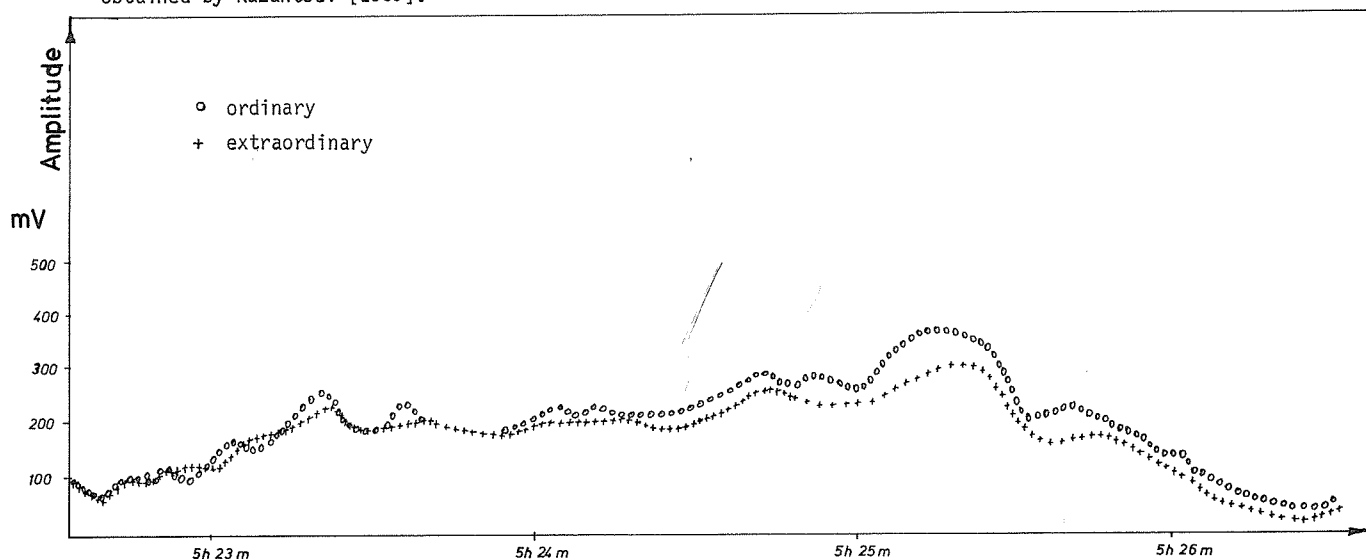


Fig. 9.3 A typical plot of ordinary and extraordinary component amplitudes at 20.005 MHz (revolution 9880, satellite 1964-64A, in September 1966). From the ratio of the amplitudes, the difference in absorption and the total absorption are calculated [Amayenc, 1967].

This method has the inherent advantage over the two previously mentioned ones in that it measures instantaneous absorption over different paths from the satellite, and that it does not require assumptions on constant transmitted power, stable or known satellite attitude, or a stationary ionosphere. It could also be used with a geostationary satellite transmitting at a relatively low frequency (say 20 MHz); it would have the additional advantage of making it possible to use fixed antennas.

Unfortunately there is no adequate explanation as yet for the great discrepancies between the values of absorption measured by this method and the more conventional methods. The difficulty may lie in the slight ellipticity of the polarization of the transmitted wave (which would give rise to a difference in the amplitudes of the received modes even without any absorption) or it may be due to some still unknown factor which would cause a difference between the absorption of a wave from a coherent point source (satellite) and the absorption obtained from measurements averaged over a wide solid angle viewed from the ground. Until this problem is resolved, it will not be possible to use this promising method.

9.5 Conclusion

At the present time it does not seem advisable to encourage routine measurements of the ionospheric absorption of radio waves using satellite transmissions. A method has yet to be developed which will overcome the problems and resolve the discrepancies of the three above-mentioned attempts. If, however, a reliable method can be found, it may provide an easy and cheap way of determining absorption on an average basis, and also of giving information about spatial structure.

CHAPTER 10. REFERENCES AND GENERAL APPENDICES

Table of Contents

| | Page |
|---|------|
| 10.1 General References | 187 |
| 10.2 Individual References | 188 |
| 10.3 Appendix I: Symbols and Abbreviations in Use for Absorption Measurements | 200 |
| 10.4 Appendix II: Abbreviations (Letter Symbols) | 201 |
| 10.5 Appendix III: List of World Data Centers | 202 |

10.1 GENERAL REFERENCES

- | | | |
|--|----------------------------------|--|
| BEYNON, W.J.G. and G. M. BROWN (eds.) [Contributions by W. R. PIGGOTT, C. G. LITTLE and the eds.] | 1957 English | <i>Annals of the International Geophysical Year</i> , Vol. III, Part II, The Measurement of Ionospheric Absorption, Pergamon Press, London. |
| PIGGOTT, W. R. | 1967 English | Collision frequency in the D-region and stratospheric- mesospheric relations, pp. 826-854 in <i>Progress in Radio Sci. 1963-66</i> , Union Radioscientifique Internationale, Brussels. |
| PIGGOTT, W. R. and G. M. BROWN (eds.) | 1963 English | <i>IQSY Instruction Manual No. 4</i> , Ionosphere, IQSY Secretar- iat, London. |
| RAWER, K. (ed.) [Contributions by W. DIEMINGER H. SCHWENKEK, E. A. LAUTER, P. SIMON, M. PICK and J. TAUBENHEIM (with U. HENSE and W. LIPPERT) and the ed.] | 1966 English and French | (Report from a special European meeting held at Brussels), <i>Annals Géophys.</i> , 22, 272-325. |
| RAWER, K. | 1969 English | Synoptic ionospheric observations including absorption, drifts and special programmes, in <i>Annals of the IQSY</i> , Vol. 5, Paper 7, MIT Press, Cambridge, Mass., p. 97. |

See also the following papers for which
references can be found under Section 10.2
below:

| | |
|----------------------|--------|
| APPLETON and PIGGOTT | [1954] |
| PIGGOTT | [1964] |
| MITRA | [1970] |
| GEORGE | [1971] |
| HARNISCHMACHER | [1974] |

10.2. INDIVIDUAL REFERENCES

- | | | |
|---|-----------------|--|
| ABDU, M. A. and S. S. DEGAONKAR | 1966 English | in <i>Proceedings of the IQSY Symposium</i> , New Delhi, p. 151. |
| ABDU, M. A., S. S. DEGAONKAR and K. R. RAMANATHAN | 1967 English | Attenuation of Galactic Radio Noise at 25 MHz and 21.3 MHz in the Ionosphere over Ahmedabad during 1957-1964, <i>J. Geophys. Res.</i> , 72, 1547. |
| ALLCOCK, G. Mc. | 1954 English | Ionospheric absorption at vertical and oblique incidence, <i>Proc. Inst. Electr. Engrs.</i> , 101, Pt. III, 360. |
| AMAYENC, P. | 1967 French | Méthode expérimentale de mesure de l'absorption ionosphérique utilisant des satellites artificiels, <i>C. R. Acad. Sc. Paris</i> , 264, 662. |
| AMAYENC, P. | 1968 French | Caracteristiques des resultats de mesure de l'absorption ionosphérique a l'aide d'un satellite balise, <i>Planet. and Space Sci.</i> , 16, 1415, 163-219. |
| APPLETON, E. V. | 1928 English | Some Notes on Wireless Methods of Investigating the Electrical Structure of the Upper Atmosphere, <i>Proc. Union Radio Sci. Intern. (URSI)</i> , 2, 1. |
| APPLETON, E. V. | 1932 English | Wireless Studies of the Ionosphere, <i>J. Inst. Electr. Engrs.</i> , 71, 642. |
| APPLETON, E. V. and W.J.G. BEYNON | 1955 English | An ionospheric attenuation equivalence theorem, <i>J. Atmos. Terr. Phys.</i> 6, 141. |
| APPLETON, E.V. and W. R. PIGGOTT | 1954 English | Ionospheric absorption measurements during a sunspot cycle, <i>J. Atmos. Terr. Phys.</i> , 5, 141-172. |
| ARGENCE, E., M. MAYOT and K. RAWER | 1950 French | Contribution a l'etude de la distribution électronique de l'ionosphère et de l'absorption des ondes courtes, <i>Annls. Geophys.</i> , 6, 242-285. |
| ARGENCE, E., K. RAWER and K. SUCHY | 1953 French | Influence du champ magnétique terrestre sur l'absorption des ondes courtes dans l'ionosphère (incidence normale), <i>C. R. Acad. Sc. Paris</i> , 236, 190. |
| AUSTIN, G. L. | 1971 English | A direct measuring differential phase experiment, <i>J. Atmos. Terr. Phys.</i> 33, 1667. |
| AUSTIN, G. L., R.G.T. BENNETT and M. R. THORPE | 1969 English | The phase of waves partially reflected from the lower ionosphere, <i>J. Atmos. Terr. Phys.</i> , 31, 1099. |
| BAILEY, V. A. | 1937 English | Motions of Electrons in a Gas in the Presence of Variable Electric Fields and a Constant Magnetic Field, <i>Phil. Mag.</i> , 23, 774. |
| BARGHAUSEN, A. F. | 1966 English | Medium-Frequency Sky Wave Propagation in Middle and Low Latitudes, <i>IEEE Transactions Broadcasting BC-12</i> , 1-14. |
| BARGHAUSEN, A. F., J. W. FINNEY, L. L. PROCTOR and L. D. SCHULTZ | 1969 English | Predicting long-term operational parameters of high-frequency sky-wave telecommunication system, <i>ESSA Techn. Report ERL 110-ITS</i> , 78, U.S. Govnt. Printing Office, Washington, DC, USA. |
| BELROSE, J. S. | 1970 English | Radio wave probing of the ionosphere by the partial reflection of radio waves (from heights below 100 km), <i>J. Atmos. Terr. Phys.</i> , 32, 567. |
| BELROSE, J. S. | 1971 English | Private communication. |

- BELROSE, J. S.,
L. R. BODE and
L. W. HEWITT 1966
English A preliminary investigation of diurnal and seasonal changes in electron number density over Resolute Bay as observed by partial reflections, *Electron Density Profiles in the Ionosphere and Exosphere*, J. Frihagen (ed.), North-Holland Publ. Co., Amsterdam, p. 37.
- BELROSE, J. S. and
M. J. BURKE 1964
English Study of the Lower Ionosphere Using Partial Reflection, *J. Geophys. Res.*, 69, 2799.
- BELROSE, J. S.,
L. W. HEWITT and
R. BUNKER 1970
English in *The Polar Ionosphere and Magnetospheric Processes*, Gordon & Breach Publ., New York.
- BELROSE, J. S.,
M. J. BURKE,
T.N.R. COYNE and
J. E. REED 1972
English D-Region Measurements with the Differential-Absorption, Differential-Phase Partial-Reflection Experiments, *J. Geophys. Res.*, 77, 4829.
- BEST, J. E.,
J. A. RATCLIFFE and
M. V. WILKES 1936
English Experimental Investigations of Very Long Waves Reflected From The Ionosphere, *Proc. Roy. Soc. A*, 156, 614.
- BEYNON, W.J.G. and
G. M. BROWN (eds.) 1957
English The Pulse Reflection Method of Measuring Ionospheric Absorption, *Annals of the Int. Geophys. Year, Vol. III*, Part 175-249 (with contributions by W. R. PIGGOTT, W.J.G. BEYNON and G. M. BROWN (Pulse Reflection Method); by C. G. LITTLE (..with extraterrestrial radio waves); by K. RAWER (absorption intercomparison experiments)).
- BHONSLE, R. V. and
K. R. RAMANATHAN 1960
English Magnetic Storms and Cosmic Radio Noise on 25 Mc/s at Ahmedabad (23°02'N; 72°38'E), *Planet. Space Sci.*, 2, 99.
- BIBL, K. 1971
English U.R.S.I. *Information Bull.*, 178, 51-62.
- BIBL, K.,
A. PAUL and
K. RAWER 1959
German Die Frequenzabhängigkeit der ionosphärischen Absorption, *J. Atmos. Terr. Phys.*, 16, 324.
- BIBL, K.,
A. PAUL and
K. RAWER 1965
English Some results of absorption measurements at Freiburg (Germany), *J. Atmos. Terr. Phys.*, 27, 145.
- BIBL, K. and
K. RAWER 1951
French Les contributions des régions D et E dans les mesures de l'absorption ionosphérique, *J. Atmos. Terr. Phys.*, 2, 51.
- BIRLEY, M. H. and
C. F. SECHRIST 1971
English *Univ. of Illinois Aeronomie Report No. 42*.
- BOOKER, H. G. 1959
English Radio Scattering in the Lower Ionosphere, *J. Geophys. Res.*, 64, 2164.
- BOSSOLASCO, M. and
A. ELENA 1963
French Absorption de la couche D et température de la mésosphère, *C. R. Acad. Sc. Paris*, 256, 4491.
- BOURNE, I. A. and
L. W. HEWITT 1968
English The dependence of ionospheric absorption of MF radio waves at mid-latitudes on planetary magnetic activity, *J. Atmos. Terr. Phys.*, 30, 1381.
- BRACEWELL, R. N.,
K. G. BUDDEN,
J. A. RATCLIFFE,
T. W. STRAKER and
K. WEEKES 1951
English The ionospheric propagation of low - and very-low - frequency radio waves over distances less than 1000 Km, *Proc. Inst. Electr. Engrs.*, 98, Pt. III, 221.
- BRIGGS, B. H.,
W. G. ELFORD,
D. G. FELGATE,
M. G. GOLLEY,
D. E. ROSSITER and
J. W. SMITH 1969
English Buckland Park Aerial Array, *Nature (London)*, 223, 1321.

| | | |
|---|---------------------------------------|--|
| BURKE, M. J. and E. H. HARA | 1963 English | Tables of the Semiconductor integrals $C_p(x)$ and their approximation for use with the generalized Appleton-Hartree magneto-ionic Formulas, <i>Rept. No. 113 Defense Res. Telecomm. Establ.</i> , Radio Phys. Lab., Ottawa, Canada. |
| COHEN, D. J. | 1971 English | Ionosphere Res. Lab., <i>Scientific Report No. 378</i> , University Park, Pennsylvania. |
| COLE, A. R., A. J. FERRARO and H. S. LEE | 1969 English | Comparison of Two Groundbased D-Region Experiments, <i>Nature</i> (London), 222, 761. |
| Comité Consultatif Intern. des Radio- communications (C.C.I.R.) | 1970a English French | C.C.I.R. Interim Method for Estimating Sky-wave Field Strength and Transmission Loss at Frequencies between the approximate Limits of 2 and 30 MHz, <i>Rept. 252-2</i> , Union Internationale des Télécommunications, Genève. |
| Comité Consultatif Internationale des Radiocommunications (C.C.I.R.) | 1970b English French Spanish | Ionospheric Propagation, C.C.I.R. XIIth Plenary Assembly, Vol. II, Pt. 2, Union Intern. des Télécommunications, Genève. In particular: p. 70, <i>Rept. 253-1</i> on Sky-wave Field Strength Measurements (with Annex II on method A3); p. 196, <i>Rept. 266-2</i> on Fading. |
| COSPAR W.G.4 | 1972 English | "CIRA 1972", COSPAR Intern. Reference Atmosphere, Akademie-Verlag, Berlin. |
| COYNE, T.N.R. and J. S. BELROSE | 1972 English | The Diurnal and Seasonal Variation of Electron Densities in the Midlatitude D Region Under Quiet Conditions, in <i>COSPAR Symposium on D- and E-region ion chemistry</i> , Urbana, Illinois, C. F. Sechrist, Jr., and M. A. Geller, eds., <i>Aeronomy Report No. 48</i> . |
| DAVIES, K. | 1965 English | <i>Ionospheric Radio Propagation</i> , NBS Monograph No. 80, Nat. Bur. Stand., Washington, D.C. |
| DEGAONKAR, S. S. and R. V. BHONSLE | 1962 English | in <i>Proc. Intern. Conf. Cosmic Rays and Earth Storms</i> , Kyoto, p. 286. |
| DELOBEAU, F. and K. SUCHY | 1956 French | L'absorption ionosphérique à Dakar, <i>J. Atmos. Terr. Phys.</i> , 9, 45. |
| DIEMINGER, W. | 1968 | in <i>Winds and Turbulence in Stratosphere, Mesosphere and Ionosphere</i> , K. Rawer (ed.), North-Holland Publ., Amsterdam, pp. 178-200. |
| DIEMINGER, W. and A. E. HOFFMANN- HEYDEN | 1952 German | Reflexionen von Kurzwellen aus Höhen unter 100 Km, <i>Naturwiss.</i> , 39, 1. |
| DIEMINGER, W., G. ROSE and U. WIDDEL | 1966 English | On the existence of anomalous radio wave absorption during winter in 40° Northern latitude, <i>J. Atmos. Terr. Phys.</i> , 28, 317. |
| DINGLE, R. B., D. ARNDT and S. K. ROY | 1957 English | The Integrals $C_p(x) = (p!)^{-1} \int_0^\infty e^p (\epsilon^2 + x^2)^{-1} e^{-\epsilon} d\epsilon$ and $D_p(x) = (p!)^{-1} \int_0^\infty e^p (\epsilon^2 + x^2)^{-2} e^{-\epsilon} d\epsilon$ and their tabulation, <i>Appl. Sci. Res.</i> , 6 B, 155. |
| ECKLUND, W. L. and J. K. HARGREAVES | 1968 English | Some measurements of auroral absorption structure over distances of about 300 Km and of absorption correlation between conjugate regions, <i>J. Atmos. Terr. Phys.</i> , 30, 265. |
| FALCON, G. D. | 1967 English | in <i>Proc. Conf. on Ground-Based Radio Wave Propagation studies of the lower Ionosphere</i> , Ottawa, pp. 197-204. |
| FEJER, J. A. and R. W. VICE | 1959 English | An investigation of the ionospheric D-region, <i>J. Atmos. Terr. Phys.</i> , 16, 291. |
| FLOOD, W. A. | 1968 English | Revised Theory for Partial Reflection D-Region Measurements, <i>J. Geophys. Res.</i> , 73, 5585. |

- | | | |
|--|------------------|---|
| FLOOD, W. A. | 1969 English | Reply (from discussion of previous paper by Holt [1969]), <i>J. Geophys. Res.</i> , 74, 5183. |
| FRASER, G. J. | 1968 English | Seasonal variation of southern hemisphere mid-latitude winds at altitudes of 70-100 Km, <i>J. Atmos. Terr. Phys.</i> , 30, 707. |
| FRASER, G. J. and R. A. VINCENT | 1970 English | A study of D-region irregularities, <i>J. Atmos. Terr. Phys.</i> , 32, 1591. |
| GALLET, R. M. | 1955 English | Aerodynamical Mechanisms Producing Electronic Density Fluctuations in Turbulent Ionized Layers, <i>Proc. Inst. Radio Engrs.</i> , 43, 1240. |
| GARDNER, F. F. and J. L. PAWSEY | 1953 English | Study of the ionospheric D-region using partial reflections, <i>J. Atmos. Terr. Phys.</i> , 3, 321. |
| GEORGE, P. L. | 1971 English | The global morphology of the quantity fN_{vdh} in the D- and E regions of the ionosphere, <i>J. Atmos. Terr. Phys.</i> , 33, 1893. |
| GERBER W. and A. WERTHMÜLLER | 1945 German | <i>Techn. Mitt. TT</i> (Switzerland) No. 1, 12. |
| GINZBURG, V. L. | 1944 English | <i>J. Phys.</i> (USSR), 8, 253. |
| GLÖDE, P., R. KNUTH and E. A. LAUTER | 1968 English | Development of storms in the lower ionosphere at medium latitudes, <i>Annls. Géophys.</i> , 24, 317. |
| GNANALINGAM, S. | 1972 English | Equatorial ionospheric Absorption during half a solar Cycle (1964-1970), <i>Rept. X-625-72-276</i> , Goddard Space Flight Center, Greenbelt, MD., USA. |
| GNANALINGAM, S. and K. WEEKES | 1955 English | D-Region Echoes with a Radio Wave of Frequency 1.4 Mc/s, in <i>The Physics of the Ionosphere</i> , Ratcliffe, J. A. (ed.), The Physical Society of London, p. 63. |
| GOCKEL, H. | 1948 French | Mesures d'absorption des ondes courtes par la couche D de l'ionosphère, <i>Annls. Géophys.</i> , 4, 232. |
| GOLLEY, M. G. and D. E. ROSSITER | 1971 English | Some aspects of ionospheric drifts using partial and total reflections from the lower ionosphere, <i>J. Atmos. Terr. Phys.</i> , 33, 701. |
| GREGORY, J. B. and A. H. MANSON | 1967 English | Mesospheric Election Number Densities at 35°S Latitude, <i>J. Geophys. Res.</i> , 72, 1073. |
| GREGORY, J. B. and A. H. MANSON | 1969a English | Seasonal variations of electron densities below 100 Km at mid-latitudes - I. Differential Absorption Measurements, <i>J. Atmos. Terr. Phys.</i> , 31, 683. |
| GREGORY, J. B. and A. H. MANSON | 1969b English | Seasonal variations of electron densities below 100 Km at mid-latitudes - II. Electron densities and atmospheric circulation, <i>J. Atmos. Terr. Phys.</i> , 31, 703. |
| GREGORY, J. B. and A. H. MANSON | 1970 English | Seasonal variations of electron densities below 100 Km at mid-latitudes - III. Stratospheric-ionospheric coupling, <i>J. Atmos. Terr. Phys.</i> 32, 837. |
| GREGORY, J. B. and R. A. VINCENT | 1970 English | Structure of Partially Reflecting Regions in the Lower Ionosphere, <i>J. Geophys. Res.</i> , 75, 6387. |
| GROSSKOPF, J. | 1953 German | <i>Fernmeldetechn. Zeitschr.</i> , 6, 373. |
| HANLE, E. | 1967 German | <i>Nachr. techn. Zeitschr.</i> , 20, 509. |

| | | |
|---|-----------------|---|
| HARA, E. H. | 1963 English | Approximations to the Semiconductor Integrals $C_p(x)$ and $D_p(x)$ for use with the Generalized Appleton-Hartree Magnetoionic Formulas, <i>J. Geophys. Res.</i> , 68, 4388. |
| HARNISCHMACHER, E. | 1974 English | Morphology of the lower ionosphere, The D-region, in <i>Structure and Dynamics of the Upper Atmosphere</i> , F. Verniani (ed.), Elsevier Publ. Co., Amsterdam, 221-244. |
| HARNISCHMACHER, E. and K. RAWER | 1972 English | A summary description of ionospheric absorption measured at Freiburg since 1956, <i>J. Atmos. Terr. Phys.</i> , 34, 947. |
| HARTREE, D. | 1929 English | The Propagation of Electromagnetic Waves in a stratified Medium, <i>Proc. Cambridge Phil. Soc.</i> , 25, 97. |
| HAUG, G. | 1975 | Internal Report of Auroral Observatory Tromsø (January 1975). |
| HAUG, G. and O. HOLT | 1968 English | in Scatter Propagation of Radio Waves, 29 - 1, <i>AGARD Conf. Proc. No. 37</i> . |
| HAUG, A. and H. PETTERSEN | 1970 English | An interpretation of asymmetric cross-correlation functions in D- and lower E-region drift measurements, <i>J. Atmos. Terr. Phys.</i> , 32, 397. |
| HAUG, A., E. V. THRANE, E. TSAGAKIS and M. ANASTASSIADES | 1970 English | Ionospheric observations during the annular solar eclipse of 20 May 1966 - IV. D-region electron densities derived from measurements of partial reflections, <i>J. Atmos. Terr. Phys.</i> , 32, 1865. |
| HEILBRONN, D. J. | 1971 English | <i>Res. Rept. No. 79</i> , Univ. of Melbourne, Academy, Melbourne, Australia. |
| HENSE, U. | 1969 German | Tages-und Jahresgänge der ionosphärischen Absorption im Kurzwellenbereich, <i>Techn. Mitt. RFZ (G.D.R.)</i> , 13, 20. |
| HINČIN (KHINCHIN), A. Ja. | 1949 English | <i>Mathematical Foundations of statistical Mechanics</i> , New York Publ., New York. |
| HOLT, O. | 1969 English | Discussion of Paper by W. A. Flood 'Revised Theory for Partial Reflection D-Region Measurements', <i>J. Geophys. Res.</i> , 74, 5179. |
| HOLT, O., B. LANDMARK and F. LIED | 1961 English | Observations of electron density and collision frequency during polar radio blackout conditions, <i>J. Atmos. Terr. Phys.</i> , 23, 318. |
| HUBER, L. and K. RAWER | 1950 German | Zur Frage des "besten" Impulsempfängers, <i>Archiv. Elektr. Übertragung</i> , 4, 475-484 and 523-536. |
| HULTQVIST, B. | 1963 English | in <i>Radio Astronomical and Satellite Studies of the Atmosphere</i> , J. Aarons (ed.), North-Holland Publ. Co., Amsterdam, pp. 163-219. |
| JONES, M. R. | 1971 English | Private communication |
| JONES, M. R. and H. KOPKA | 1971 English | Preprint (to be published later). |
| KAZANZEV, A. N. | 1947 Russian | <i>Izv. Akad. Nauk SSSR, OTN 1947, No. 9.</i> |
| KAZANZEV, A. N. | 1956 Russian | <i>Izv. Akad. Nauk SSSR, OTN 1956, No. 9.</i> |
| KAZANZEV (KAZANTSEV), A. N. | 1959 English | Absorption and Electron Distribution in the F ₂ Layer Determined from Measurements of Transmitted Radio Signals from Earth Satellites, <i>Planet. and Space Sci.</i> , 1, 130. |

| | | |
|---|-----------------|---|
| KELLY, D. C. | 1960 English | Microwave Conductivity of a Plasma in a Magnetic Field, <i>Phys. Rev.</i> , 119, 27. |
| KLEEN, W. and K. POESCHL | 1968 German | in <i>Taschenbuch d. Hochfrequenztechnik</i> , Third ed., by H. Meinke and F. W. Gundlach, Springer-Verlag, Berlin. |
| KONOPLEVA, E. N. | 1964 Russian | Nadvozhnost svyazi ineobkhodimye otnosheniya signal/pomekha v Kanalye Radiosvyazi na Korotkikh Volnakh, <i>Elektrosvyaz</i> , 5. |
| KOTADIA, K. M. and B. M. PATEL | 1969 English | Lunar variation of ionospheric absorption of radio waves at different frequencies, <i>J. Atmos. Terr. Phys.</i> , 31, 621. |
| KRAMM, R., K. SCHLEGEL and W. WEISS | 1972 English | Partial Reflection Measurements with FM-CW - A Preliminary Investigation, <i>Zeitschr. f. Geophys.</i> , 38, 953. |
| LABITZKE, K. and H. SCHWENKE | 1968 English | Midwinter warmings in the stratosphere and lower mesosphere and the behaviour of ionospheric absorption, <i>Zs. f. Geophys.</i> , 34, 555. |
| LASSEN, H. | 1927 German | Über den Einfluss des Erdmagnetfeldes auf die Fortpflanzung der Elektrischen Wellen der drahtlosen Telegraphie in der Atmosphäre, <i>Elektr. Nachr. Technik</i> , 4, 324. |
| LAUTER, E. A. and P. NITZSCHE | 1967 English | Seasonal variations of ionospheric absorption deduced from A-3 measurements in the frequency range 100-2000 Kc/s, <i>J. Atmos. Terr. Phys.</i> , 29, 533. |
| LAUTER, E. A. and B. SCHÄNING | 1970 English | On the low-latitude boundary of the winter anomaly of ionospheric absorption, <i>J. Atmos. Terr. Phys.</i> , 32, 1619. |
| LAUTER, E. A. and K. SPRENGER | 1966 German | <i>Kleinheubacher Berichte</i> , 11, 211. |
| LAUTER, E. A. and K. SPRENGER | 1968 English | D-region phenomena and stratospheric-mesospheric coupling, <i>Met. Monogr. No. 31</i> . |
| LEHMANN, P. | 1971 English | <i>Rept. No. 78</i> , Univ. of Melbourne, Academy Res., Melbourne, Australia. |
| LITTLE, C. G. and H. LEINBACH | 1959 English | The Riometer - A Device for the Continuous Measurement of Ionospheric Absorption, <i>Proc. Inst. Radio Engrs.</i> , 47, 315. |
| LITTLE, C. G., G. M. LERFALD and R. PARTHASARATHY | 1964 English | Extension of Cosmic Noise Absorption Measurements to Lower Frequencies, Using Polarized Antennas, <i>Radio Science, J. Res. NBS</i> , 68 D, 859. |
| MACHIN, K. E., M. RYLE and D. D. VONBERG | 1952 English | The design of an equipment for measuring small radio-frequency noise powers, <i>Proc. Inst. Electr. Engrs.</i> , 99, (Pt. III), 1927, p. 127. |
| MAJUMDAR, R. C. | 1938 German | Die Theorie der Ionosphäre, <i>Z. Physik</i> , 107, 599. |
| MANSON, A. H. | 1966 English | Comments on the Theory of the Differential Absorption Experiment, <i>J. Geophys. Res.</i> , 71, 3783. |
| MANSON, A. H. and M.W.J. MERRY | 1970 English | Particle influx and the 'winter anomaly' in the mid-latitude ($L = 2.5 - 3.5$) lower ionosphere, <i>J. Atmos. Terr. Phys.</i> , 32, 1169. |
| MANSON, A. H. and M.W.J. MERRY | 1971 English | Seasonal variations of electron densities below 100 Km at mid latitudes - IV. Preliminary model calculations, <i>J. Atmos. Terr. Phys.</i> , 33, 413. |

- | | | |
|---|-----------------|---|
| MANSON, A. H., M.W.J. MERRY and R. A. VINCENT | 1969 English | Relationship between the Partial Reflection of Radio Waves from the Lower Ionosphere and Irregularities as Measured by Rocket Probes, <i>Radio Sci.</i> , 4, 955. |
| MARTYN, D. F. | 1935 English | The Propagation of Medium Radio Waves in the Ionosphere, <i>Proc. Phys. Soc. (London)</i> , 47, 323. |
| MASS, J. | 1963 English | in <i>Radio Astronomical and Satellite studies of the Atmosphere</i> , J. Aarons (ed.), North-Holland Publ. Co., Amsterdam, pp. 255-288. |
| McNICHOL, R. W. | 1949 English | The fading of radio waves of medium and high frequencies, <i>Proc. Inst. Electr. Engrs.</i> , 96, Pt. III, 517. |
| MECHTLY, E. A. | 1959 English | A Computer Program for obtaining refractive Indices and Polarizations from the Appleton-Hartree Equations and magneto-ionic Tables for Cape Canaveral, <i>Sci. Rept. No. 116</i> , Pennsylvania State Univ., Ionospheric Res., University Park, Pa., U.S.A. |
| MILLINGTON, G. | 1954 English | Ray-path characteristics in the ionosphere, <i>Proc. Inst. Electr. Engrs.</i> , 101 (IV), 235. |
| MITRA, A. P. | 1966 English | A Comparative Study of Solar Flare X-Ray Measurements from Satellites and Sudden Ionospheric Disturbances, in <i>Space Res. VI</i> , R. L. Smith-Rose, (ed.), Spartan Books, Washington, DC, p. 558. |
| MITRA, A. P. | 1970 English | HF and VHF absorption techniques in radio wave probing of the ionosphere, <i>J. Atmos. Terr. Phys.</i> , 32, 623. |
| MITRA, A. P. and K. A. SARADA | 1961 English | Determination of the electron content of the outer ionosphere from measurements of cosmic radio noise absorption, <i>J. Atmos. Terr. Phys.</i> , 23, 348. |
| MITRA, A. P. and C. A. SHAIN | 1953 English | The measurement of ionospheric absorption using observations of 18.3 Mc/s cosmic radio noise, <i>J. Atmos. Terr. Phys.</i> , 4, 204. |
| MITRA, A. P., C. V. SUBRAHMANYAM and V. C. JAIN | 1966 English | Multifrequency Observations of Sudden Cosmic Noise Absorption and X-Ray Flares, <i>Radio Sci.</i> , 1, 1188. |
| MONTBRIAND, L. W. and J. S. BELROSE | 1972 English | Effective Electron Loss Rates in the Lower D Region During the Decay Phases of Solar X-ray (SXR) Flare Events, in <i>COSPAR Symposium on D- and E-region ion chemistry</i> , Urbana, Illinois, C. F. Sechrist, Jr. and M. A. Geller (eds.), Aeronomy Report No. 48, p. 290. |
| MÜLLER, K. | 1962 German | Zur Frage der Abhängigkeit von Bodenleitfähigkeit und Feldstärke im Mittelwellenbereich, <i>Techn. Mitt. RFZ (G.D.R.)</i> , 6, 11. |
| NAKAGAMI, M. | 1943 English | <i>J. Inst. Electr. Comm. Engrs. (Japan)</i> , 27, 145. |
| NAKAGAMI, M. | 1960 English | The <i>m</i> - Distribution - A General Formula of Intensity Distribution of Rapid Fading, in <i>Statistical Methods in Radio Wave Propagation</i> , W. C. Hoffman (ed.), Pergamon Press, Oxford, p. 3. |
| NITZSCHE, P. | 1964 German | <i>Gerlands Beiträge zur Geophysik</i> , 73, 266. |
| NITZSCHE, P. | 1969 English | The dependence of ionospheric absorption of radio waves on equivalent frequency, with special emphasis on the winter anomaly, <i>Z. Geophys.</i> , 35, 303-310. |
| OHLE, K. H. and J. TAUBENHEIM | 1967 English | Effect of the solar eclipse of May 20, 1966, on the ionospheric absorption of cosmic noise on 25 Mc/s, <i>J. Atmos. Terr. Phys.</i> , 29, 1663. |

| | | |
|--|------------------|--|
| ORCHARD, H. J. | 1950 English | <i>Wireless Engr.</i> , 27, 27. |
| PARTHASARATHY, R. G. M. LERFALD and C. G. LITTLE | 1963 English | Derivation of Electron-Density Profiles in the Lower Ionosphere Using Radio Absorption Measurements at Multiple Frequencies, <i>J. Geophys. Res.</i> , 68, 3581. |
| PAUL, A. K. | 1964 English | A Method for the Determination of Es-Gradients, in <i>Electron Density Distribution in Ionosphere and Exosphere</i> , E. Thrane (ed.), North-Holland Publ. Co., Amsterdam, pp. 17-20. |
| PFISTER, W. | 1953 English | Magneto-Ionic Multiple Splitting Determined with the Method of Phase Integration, <i>J. Geophys. Res.</i> , 58, 29. |
| PFISTER, W. | 1965 English | Non-Deviative Absorption, in <i>Handbook of Geophysics and Space Environment</i> , S. L. Valley (ed.), McGraw-Hill Book Co., New York, Sect. 12.4, pp. 12.15 - 12.28. |
| PHELPS, A. V. and J. L. PACK | 1959 English | Electron Collision Frequencies in Nitrogen and in the Lower Ionosphere, <i>Phys. Rev. Letters</i> , 3, 340. |
| PIGGOTT, W. R. | 1953 English | The reflection and absorption of radio waves in the ionosphere, <i>Proc. Inst. Electr. Engrs.</i> , 100, Pt. III, 61. |
| PIGGOTT, W. R. | 1955a English | <i>Wireless Engr.</i> , 32, 164. |
| PIGGOTT, W. R. | 1955b English | On the variation of ionospheric absorption at different stations, <i>J. Atmos. Terr. Phys.</i> , 7, 244. |
| PIGGOTT, W. R. | 1956 English | <i>J. Atmos. Terr. Phys.</i> , 6, Special Supplement, 106. |
| PIGGOTT, W. R. | 1959 English | The calculation of the median sky wave field-strength in tropical regions. DSIR, Radio Research, <i>Special Rept. No. 27</i> , H. M. Stationary Office, London. |
| PIGGOTT, W. R. | 1960 English | Discrepancies in the Ionospheric Absorption Deduced from the First Order and Multiple Order Reflections, in <i>Some Ionospheric Results Obtained during the I.G.Y.</i> , W.J.G. Beynon (ed.), Elsevier Publ. Co., Amsterdam, p. 263. |
| PIGGOTT, W. R. | 1964 English | in <i>Studies of Ionospheric Absorption</i> , MIT Press, Cambridge, Mass., U.S.A., pp. 277-295. |
| PIGGOTT, W. R. and K. RAWER | 1972 English | U.R.S.I. Handbook of Ionogram Interpretation and Reduction, 2nd Edition, <i>Report UAG-23</i> , World Data Center A for Solar-Terrestrial Physics, NOAA, Boulder, Colorado, 80302, U.S.A. |
| PIGGOTT, W. R. and E. V. THRANE | 1966 English | The effect of irregularities in collision frequency on the amplitude of weak partial reflections, <i>J. Atmos. Terr. Phys.</i> , 28, 311. |
| PILLET, G. | 1960 French | Contribution a l'etude de l'absorption ionosphérique sur une fréquence fixe, <i>Annls. Télécomm.</i> , 15, pp. 157-184 and 198-219. |
| PILLET, G. | 1962 French | Anomalies dans les mesures de l'absorption ionosphérique, <i>J. Atmos. Terr. Phys.</i> , 23, 57. |
| PIRNAT, C. R. and S. A. BOWHILL | 1968 English | Electron Densities in the Lower Ionosphere Deduced From Partial Reflection Measurements, <i>Aeronomy Rept. No. 29</i> , University of Illinois, Urbana, Illinois. |
| RAMANATHAN, K. R., R. V. BHONSLE and S. S. DEGAONKAR | 1961 English | Effect of Electron-Ion Collisions in the F-Region of the Ionosphere on the Absorption of Cosmic Radio Noise at 25 Mc/sec at Ahmedabad, <i>J. Geophys. Res.</i> , 66, 2763. |
| RATCLIFFE, J. A. | 1948 English | Diffraction from the Ionosphere and the Fading of Radio Waves, <i>Nature</i> (London), 162, 9. |

| | | |
|--|------------------|--|
| RATCLIFFE, J. A. | 1956 English | Some Aspects of Diffraction theory and their Application to the Ionosphere, in <i>Reports on Progress in Physics</i> , 19, 188, (Proc. Phys. Soc., London). |
| RAWER, K. | 1947 French | <i>Revue scientifique</i> , 85, 361. |
| RAWER, K. | 1948 French | <i>Revue scientifique</i> , 86, 585. |
| RAWER, K. | 1950 English | Geometrical Optics of Ionospheric Propagation, <i>Nature</i> (London), 166, 316. |
| RAWER, K. | 1951 French | Comparaison des resultats de mesures de l'absorption ionosphérique effectuées par deux stations européennes, <i>J. Atmos. Terr. Phys.</i> , 2, 38. |
| RAWER, K. | 1952 English | Calculation of Sky-Wave Field Strength, <i>Wireless Engr.</i> , 29, 287. |
| RAWER, K. | 1955 English | Some Remarks Concerning Ionospheric Absorption Work, <i>J. Geophys. Res.</i> , 60, 534. |
| RAWER, K. | 1956 English | Solar Eclipses in the Ionosphere, <i>J. Atmos. Terr. Phys.</i> , 6, Special Supplement, 102. |
| RAWER, K. | 1958 English | in <i>Electromagnetic Propagation</i> , Désirant (ed.), Academic Press, New York, p. 647. |
| RAWER, K. | 1960 English | Radio Propagation Between a Space Vehicle and the Earth in the Presence of the Ionosphere, in <i>Space Research 1</i> , H. Kallmann-Bijl (ed.), North-Holland Publ. Co., Amsterdam, pp. 245-271. |
| RAWER, K., K. BIBL and E. ARGENCE | 1952b French | Mesures de Nombre de Chocs dans les Regions E et F2 de l'Ionosphere, <i>Mém. Soc. Roy. Sci. Liège</i> (12), 269. |
| RAWER, K., K. BIBL and E. THEISSEN | 1952a English | An Improved Method for the Calculation of the Field-Strength of Waves Reflected by the Ionosphere, <i>Nature</i> (London), 169, 147. |
| RAWER, K. and K. SUCHY | 1958 German | Äquivalenztheoreme bei der Wellenabsorption im Plasma, <i>Annalen der Physik</i> (7), 1, 255. |
| REYNOLDS, D. A. and C. F. SECHRIST | 1970 English | Measurement of Average Electron Density between 75 and 80 Kilometers, Univ. of Illinois, <i>Aeronomy Report No. 36</i> . |
| RICE, S. O. | 1948 English | Reflections from Circular Bends in Rectangular Wave Guides - Matrix Theory, <i>Bell System Techn. J.</i> , 27, 305. |
| RICE, S. O. | 1958 English | Distribution of the Duration of Fades in Radio Transmissions: Gaussian Noise Model, <i>Bell System Techn. J.</i> , 37, 581. |
| ROSE, G. | 1970 German | Zur Bestimmung der Elektronendichten und Elektronenstosszahlen mit Hilfe des Differenz-Dopplers u.d. Absorptionsverfahrens in der D-Schicht d. Ionosphäre, <i>Int. Rept. MPI Aeronomie...</i> Katlenburg (F.R.G.). |
| ROSE, G. and H. U. WIDDEL | 1965 German | <i>Kleinheubacher Berichte</i> , 11, 249. |
| SAMUEL, J. C. and P. A. BRADLEY | 1975 English | A new Form of representation of the diurnal and solar-cycle variations of ionospheric absorption, <i>J. Atmos. Terr. Phys.</i> , 37, 131. |

| | | |
|---|------------------|--|
| SARADA, K. A. and A. P. MITRA | 1960 English | Measurement of Cosmic Noise Absorption at Delhi on 22.4 Mc/s, in <i>Some Ionospheric Results obtained during the International Geophysical Year</i> , W.J.G. Beynon, ed., Elsevier Publ. Co., Amsterdam, p. 270. |
| SCHLEGEL, K. | 1971 German | <i>Kleinheubacher Berichte</i> , 15, 143. |
| SCHULTZ, L. D. and R. M. GALLET | 1970 English | A Survey and Analysis of normal ionospheric Absorption Measurements obtained from Radio Pulse Reflections, <i>ESSA Professional Paper No. 4</i> , U.S. Govt. Printing Office, Washington, D.C. |
| SCHWENKEK, H. | 1958 German | Bestimmung eines Kennwertes für die Absorption der Ionosphäre aus einer automatisch-statistischen Analyse von Feldstärkeregistrierungen, <i>Archiv. Elektr. Übertragung.</i> , 12, 301. |
| SCHWENKEK, H. | 1963a German | Ein Analysierzähldruckgerät für die Feldstärkeregistrierung und zur Bestimmung der Absorption der Ionosphäre, <i>NTZ Nachrichtentechn. Zeitschr.</i> , 16, 76. |
| SCHWENKEK, H. | 1963b English | The variation of ionospheric absorption from 1956 till 1963, <i>J. Atmos. Terr. Phys.</i> , 25, 733. |
| SCHWENKEK, H. | 1967 English | The trend of the amount of winter anomaly of ionospheric absorption from 1956 to 1966, <i>J. Atmos. Terr. Phys.</i> , 29, 1169. |
| SCHWENKEK, H. | 1968 German | Zum Auftreten der Winteranomalie der ionosphärischen Absorption von Kurzwellen, <i>NTZ Nachrichtentechn. Zeitschr.</i> , 21, 32. |
| SCHWENKEK, H. | 1971 English | Regular and irregular behaviour of the winter anomaly in ionospheric absorption, <i>J. Atmos. Terr. Phys.</i> , 33, 1647. |
| SCHWENKEK, H. and E. H. GRUSCHWITZ | 1970 English | Measurement of absorption in the ionosphere on 27.6 MHz at 52°N by means of a riometer and a corner reflector antenna directed to the Pole Star, <i>J. Atmos. Terr. Phys.</i> , 32, 1385. |
| SELLMEIER, W. | 1872 German | <i>Poggendorff's Annalen der Physik und Chemie</i> , 147, 386. |
| SEN, H. K. and A. A. WYLLER | 1960 English | On the Generalization of the Appleton-Hartree Magnetoionic Formulas, <i>J. Geophys. Res.</i> , 65, 3931. |
| SHAIN, C. A. | 1951 English | Galactic Radiation at 18.3 Mc/s, <i>Austral. J. Sci. Res.</i> , 4, 258. |
| SHAPLEY, A. H. and W.J.G. BEYNON | 1965 English | 'Winter Anomaly' in Ionospheric Absorption and Stratospheric Warmings, <i>Nature</i> , 206, 1242. |
| SHIRKE, J. S. and G. W. HENRY | 1967 English | Geomagnetic anomaly in ionospheric absorption at low latitude observed on board USNS Croatan, <i>Annls. Géophys.</i> , 23, 517. |
| SHKAROVSKY, I. P. | 1961 English | Values of the Transport Coefficients in a Plasma for any Degree of Ionization based on a Maxwellian Distribution, <i>Canad. J. Phys.</i> , 39, 1619. |
| SMITH, N. | 1937 English | Extension of Normal-Incidence Ionosphere Measurements to Oblique-Incidence Radio Transmission, <i>Nat. Bur. Stand. J. Res.</i> , 19, 89. |
| SMITH, R. A., I. A. BOURNE, R. G. LOCH, C. S. SETTA, T.N.R. COYNE, P. H. RARRAT and B.S.N. PRASAT | 1965 English | Radio Wave Interaction Using Gyro-waves, <i>Rept. No. 65</i> , Air Force Cambridge Res. Lab., Cambridge, Mass., 460. |

| | | |
|---|------------------|--|
| SPRENGER, K. | 1958 German | Die Erschliessung jahreszeitlicher Strukturänderungen der ionosphärischen D-Region aus mehrjährigen Beobachtungen der Tagesdämpfung auf 245 kHz, Doctoral Thesis, Univ. Leipzig. |
| SPRENGER, K. and E. A. LAUTER | 1966 German | Verfahren zur Messung der ionosphärischen Absorption (A3-Methode) im Lang- und Mittelwellenbereich, <i>Schriftenreihe National Komm. fuer Geodäsie und Geophysik, Reihe II</i> , H.1,47. |
| SUBRAHMANIAM, C. V. | 1968 English | Ph. D. Thesis, Delhi Univ., New Delhi. |
| SUCHY, K. | 1964 German | <i>Ergebn. exakt. Naturw.</i> , 35, pp. 103-294. |
| SUCHY, K. and K. RAWER | 1971 English | The definition of collision frequencies and their relation to the electron conductivity of the ionosphere, <i>J. Atmos. Terr. Phys.</i> , 33, 1853. |
| SULANKE, H. and F. TÄUMER | 1967/8 German | Die Eigenschaften von Häufigkeitsverteilungen der Raumwellenfeldstärke im Frequenzbereich zwischen 15... 1600 KHz, <i>Techn. Mittlg. der RFZ (G.D.R.)</i> , 11, 131 and 12, 32. |
| TAUBENHEIM, J. | 1969 German | <i>Statistische Auswertung geophysikalischer und meteorologischer Daten</i> , Akadem. Verlagsgesellsch. Geest u. Portig, Leipzig. |
| THRANE, E. V., A. HAUG, B. BJELLAND, M. ANASTASSIADES and E. TSAGAKIS | 1968 English | Measurements of D-region electron densities during the International Quiet Sun Years, <i>J. Atmos. Terr. Phys.</i> , 30, 135. |
| THRANE, E. V. and W. R. PIGGOTT | 1966 English | The collision frequency in the E- and D-regions of the ionosphere, <i>J. Atmos. Terr. Phys.</i> , 28, 721. |
| TITHERIDGE, J. E. | 1962a English | The electron density in the lower ionosphere, <i>J. Atmos. Terr. Phys.</i> , 24, 269. |
| TITHERIDGE, J. E. | 1962b English | The stratification of the lower ionosphere, <i>J. Atmos. Terr. Phys.</i> , 24, 283. |
| TRISKA, P. | 1962 English | Measurements of Ionospheric Absorption Using Obliquely Incident Radio Waves, <i>Studia Geoph. et Geod.</i> , 6, 235. |
| TRISKA, P. | 1965 English | <i>Geofysikální Sborník No. 238</i> , 603. |
| TRISKA, P. | 1967 English | <i>Geofysikální Sborník No. 287</i> , 495. |
| VASSY, E. | 1960 French | Nouveau principe de mesure de l'absorption ionosphérique, <i>C. R. Acad. Sc. Paris</i> , 250, 4189. |
| VASSY, E. | 1961 French | Sur un nouveau principe de mesure de l'absorption ionosphérique, <i>J. Atmos. Terr. Phys.</i> , 23, 85. |
| VON BIEL, H. A. | 1966 English | <i>Proc. Conf. on Ground-Based Radio Wave Propagation studies of the lower Ionosphere</i> , Ottawa, pp. 216-224. |
| VON BIEL, H. A. | 1971 English | Determination of D-Region Electron Densities within the Scattering Region, <i>J. Geophys. Res.</i> , 76, 5365. |
| VON BIEL, H. A., W. A. FLOOD and H. G. CAMNITZ | 1970 English | Differential-Phase Partial-Reflection Technique for the Determination of D-Region Ionization, <i>J. Geophys. Res.</i> , 75, 4863. |

- | | | |
|--------------------------------|-----------------|---|
| WEEKES, K. and R. D. STUART | 1951 English | The ionospheric propagation of radio waves with frequencies near 100 kc/s over short distances, <i>Inst. Electr. Engrs., Monograph, No. 15.</i> |
| WIENER, N. | 1949 English | <i>The Extrapolation, Interpolation and Smoothing of Stationary Time Series</i> , MIT Press, Cambridge, Mass., U.S.A. |
| WYLLER, A. A. | 1962 English | in <i>Proc. 5th Internat. Conf. on Ionization Phenomena in Gases</i> , H. Maecker (ed.), North-Holland Publ. Co., Amsterdam, pp. 940-954. |

10.3. APPENDIX I

Symbols and Abbreviations in Use for Absorption Measurements

(1) Symbols

The standard symbols for electrical quantities have recently been revised by the appropriate international bodies. Unfortunately the new symbols differ from those which have been used in absorption work in the past. We therefore give the recommended new symbols. The relations are as follows:

| | | | | | | |
|------|-------|-----|-----|--------------------|-------------------|-------------------|
| old: | f_H | L | A | $I(\text{linear})$ | $I(\text{in dB})$ | $G(\text{in dB})$ |
| new: | f_B | A | D | E | F | (F_0) |

With these changes the new symbols are now given in alphabetic order.

| | |
|--|--|
| c_0 | Velocity of light in a vacuum ($= 3 \cdot 10^8$ m/s $= 3 \cdot 10^5$ km/s) |
| f | Frequency of radio wave |
| f_B | Gyro-frequency (Natural frequency of rotation of free electrons around the magnetic field lines) |
| f_L | $f_B \cdot \cos \theta$ = longitudinal component of gyro-frequency |
| f_N | Plasma frequency (proportional to electron density N) |
| f_{oE} | Critical frequency of the normal E layer (o mode) |
| $\left. \begin{matrix} f_{oF1} \\ f_{oF2} \end{matrix} \right\}$ | Critical frequency of layers F1 and F2, respectively (o mode) |
| h'_d | Virtual height of effective reflection of the echo considered (usually in km) |
| d | Distance (usually in km) |
| A | Ionospheric absorption: Logarithmic decrement measured in dB |
| B | Absorption parameter referring to non-deviative absorption only, Eq. (2.20) |
| C | Absorption parameter referring to deviative absorption, Eq. (2.20) |
| D | $= (f + f_L)^2 A$ = Global absorption parameter, Eq. (4.13) |
| E | Electric field strength (usually in μ V/m) |
| F | Logarithmic measure of E , in dB (usually over 1 μ V/m) |
| F_0 | Reference value (see Section 4.5.3) |
| N | Electron (number) density (usually in m^{-3}); also called plasma density |
| P | Radiated power |
| R | Solar activity measured by Zürich sunspot number |
| T | Absolute temperature (of electrons in the ionospheric plasma) |
| X | $= (f_N/f)^2$ = reduced electron density |
| Y | $= f_B / f$ = reduced gyro-frequency |
| Z | $= \bar{\nu} / 2\pi f$ = reduced collision frequency |
| α | Angle between wave normal and the vertical |
| κ | Absorption coefficient of a radio wave in the ionosphere (Local parameter: Frequency, mode and angle θ to be specified) |
| μ | Refractive index in the ionosphere (Local parameter: Frequency, mode and angle θ to be specified) |
| $\bar{\nu}$ | Effective collision frequency. (Different from gas-kinetic effective collision frequency) |
| ν_c | Critical collision frequency (Unique value at a given location, see Figure 2.8) |
| ρ | The apparent reflection coefficient of the ionosphere. |
| (also ρ_i) | This is defined as the ratio of the amplitude actually observed to the amplitude which would have been observed if there had been no collisional losses along the wave trajectory. (Frequency, mode and ray path to be specified.) |
| ρ_g | The apparent reflection coefficient of the ground |
| θ | Angle between wave normal and Earth's magnetic field |
| Φ | Solar activity measured by solar microwave radiation (10.7 cm), also called Covington index. As designated by CCIR, this index is a dimensionless number between the approximate limits 20 and 500. |

10.4. APPENDIX II

Abbreviations (Letter Symbols)

Similar to their use in ionogram reduction, letter symbols are used to describe, to qualify, or to replace a numerical value. Qualifying letters may be considered as special orders to be followed during the statistical treatment of data. Descriptive letters indicate the presence of a particular difficulty (when added to a situation where a letter stands alone with the numerical value), the cause of uncertainty (when accompanied by a qualifying letter and the numerical value) or the reason why it was not possible to obtain a measurement (when replacing a numerical value). The definitions of the letter symbols used in absorption measurements mainly agree with those in use for ionograms.

(Since most of the letter symbols are descriptive, we present them all in alphabetical order, indicating those which are used as qualifying letter symbols.)

| Letter symbol: | Meaning: |
|----------------|---|
| A | Measurement influenced by, or impossible because of, the presence of a lower thin layer, for example Es. |
| B | Measurement influenced by, or impossible because of, absorption in the vicinity of f_{min} . |
| C | Measurement influenced by, or impossible because of, any non-ionospheric reason. |
| D | (Qualifying letter symbol): Greater than ... Note: If no echo is received owing to very high absorption, the absorption decrement x is computed from the observed noise level y (see E) and this value is qualified by D, and described by B. |
| E | (Qualifying letter symbol): Less than ... Note: When no echo is received owing to very high absorption, the measured amplitude is written E_y , where y is the amplitude equivalent to the noise level. |
| F | Measurement influenced by, or impossible because of, the presence of spread echoes. |
| H | Measurement influenced by, or impossible because of, the presence of a stratification. Note: Used only when a stratification which is likely to modify the apparent absorption appreciably is observed in or below the reflecting layer. This symbol applies to ledges but should not be used where the sporadic Es letter A is more appropriate. |
| I | (Qualifying letter symbol): Missing value has been replaced by an interpolated value. |
| J | Ordinary component characteristic deduced from the extraordinary component. |
| L | Measurement influenced by, or impossible because of, insufficient ionization in the reflecting layer. |
| M | Ordinary wave measurement influenced by presence of overlapping extraordinary wave signal. Note: This is usually appropriate only when the absorption is small. |
| N | Conditions are such that the measurement cannot readily be interpreted, for example in the presence of oblique echoes. Also used when the pattern is changing too rapidly with time to permit absorption measurements to be made. Note: N is replaced by the symbol denoting the immediate cause of the difficulty when this is known, e.g., by A, B, F, L, R. |
| O | Measurement refers to the ordinary component. |
| R | Measurement influenced by, or impossible because of, absorption in the vicinity of a critical frequency. To be used also when the echo pattern changes rapidly with time owing to small changes in critical frequency. |
| S | Measurement influenced by, or impossible because of, interference or atmospherics. |

Letter symbol:

Meaning:

- | | |
|---|--|
| U | (Qualifying letter symbol): Uncertain or doubtful numerical value. (a) when described: uncertain because the amplitude may have been affected by the phenomenon denoted by the descriptive symbol; (b) when not described: uncertain because the observations are not internally consistent. |
| W | Measurement influenced or impossible because the echo lies outside the height range recorded. |
| X | Measurement refers to the extraordinary component. Note: To be used when it is not appropriate to convert the absorption to the equivalent ordinary component absorption (symbol J). |
| Z | Measurement refers to the third magneto-electronic component (z component). Note: It is usually not appropriate to convert such measurements to another component. |

10.5. APPENDIX III

List of World Data Centers

The following centers archive ionospheric absorption measurements:

- WDC-A : World Data Center A for Solar-Terrestrial Physics
National Oceanic and Atmospheric Administration (NOAA)
Boulder, Colorado 80302, U.S.A.
- WDC-B : World Data Center B 2
Solar Terrestrial Physics
Uliza Molodežnaja, Moskva B-296, U.S.S.R.
- World Data Center B for SID
Observatory
Ondrejov-u-Prahy, C.S.R.
- WDC-C1: World Data Center C1 for Ionosphere
Appleton Laboratory
Ditton Park, Slough, SL3 9JX, England
- WDC-C2: World Data Center C2 for Ionosphere
Radio Research Laboratories
2-1, Nukui-Kitamachi, 4-chome, Koganei-shi
Tokyo 184, Japan

UAG Series of Reports

Prepared by World Data Center A for Solar-Terrestrial Physics, NOAA, Boulder, Colorado, U.S.A.

These reports are for sale through the National Climatic Center, Federal Building, Asheville, NC 28801, Attn: Publications. Subscription price: \$25.20 a year; \$12.00 additional for foreign mailing; single copy price varies. These reports are issued on an irregular basis with 6 to 12 reports being issued each year. Therefore, in some years the single copy rate will be less than the subscription price, and in some years the single copy rate will be more than the subscription price. Make check or money order payable to: Department of Commerce, NOAA.

Some issues are now out of print and are available only on microfiche as indicated. Requests for microfiche should be sent to World Data Center A for Solar-Terrestrial Physics, NOAA, Boulder, CO 80302, with check or money order made payable to Department of Commerce, NOAA.

- UAG-1 "IQSY Night Airglow Data", price \$1.75.
- UAG-2 "A Reevaluation of Solar Flares, 1964-1966", price 30 cents.
- UAG-3 "Observations of Jupiter's Sporadic Radio Emission in the Range 7.6-41 MHz, 6 July 1966 through 8 September 1968", microfiche only, price 45 cents.
- UAG-4 "Abbreviated Calendar Record 1966-1967", price \$1.25.
- UAG-5 "Data on Solar Event of May 23, 1967 and its Geophysical Effects", price 65 cents.
- UAG-6 "International Geophysical Calendars 1957-1969", price 30 cents.
- UAG-7 "Observations of the Solar Electron Corona: February 1964-January 1968", price 15 cents.
- UAG-8 "Data on Solar-Geophysical Activity October 24-November 6, 1968", price (includes Parts 1 & 2) \$1.75.
- UAG-9 "Data on Cosmic Ray Event of November 18, 1968 and Associated Phenomena", price 55 cents.
- UAG-10 "Atlas of Ionograms", price \$1.50.
- UAG-11 "Catalogue of Data on Solar-Terrestrial Physics" (now obsolete).
- UAG-12 "Solar-Geophysical Activity Associated with the Major Geomagnetic Storm of March 8, 1970", price (includes Parts 1-3) \$3.00.
- UAG-13 "Data on the Solar Proton Event of November 2, 1969 through the Geomagnetic Storm of November 8-10, 1969, price 50 cents.
- UAG-14 "An Experimental, Comprehensive Flare Index and Its Derivation for 'Major' Flares, 1955-1969", price 30 cents.
- UAG-15 "Catalogue of Data on Solar-Terrestrial Physics" (now obsolete).
- UAG-16 "Temporal Development of the Geographical Distribution of Auroral Absorption for 30 Substorm Events in each of IQSY (1964-65) and IASY (1969)", price 70 cents.
- UAG-17 "Ionospheric Drift Velocity Measurements at Jicamarca, Peru (July 1967-March 1970)", microfiche only, price 45 cents.
- UAG-18 "A Study of Polar Cap and Auroral Zone Magnetic Variations", price 20 cents.
- UAG-19 "Reevaluation of Solar Flares 1967", price 15 cents.
- UAG-20 "Catalogue of Data on Solar-Terrestrial Physics" (now obsolete).
- UAG-21 "Preliminary Compilation of Data for Retrospective World Interval July 26 - August 14, 1972", price 70 cents.
- UAG-22 "Auroral Electrojet Magnetic Activity Indices (AE) for 1970", price 75 cents.
- UAG-23 "U.R.S.I. Handbook of Ionogram Interpretation and Reduction", price \$1.75.
- UAG-24 "Data on Solar-Geophysical Activity Associated with the Major Ground Level Cosmic Ray Events of 24 January and 1 September 1971", price (includes Parts 1 and 2) \$2.00.
- UAG-25 "Observations of Jupiter's Sporadic Radio Emission in the Range 7.6-41 MHz, 9 September 1968 through 9 December 1971", price 35 cents.
- UAG-26 "Data Compilation for the Magnetospherically Quiet Periods February 19-23 and November 29 - December 3, 1970", price 70 cents.
- UAG-27 "High Speed Streams in the Solar Wind", price 15 cents.
- UAG-28 "Collected Data Reports on August 1972 Solar-Terrestrial Events", price (includes Parts 1-3) \$4.50.
- UAG-29 "Auroral Electrojet Magnetic Activity Indices AE (11) for 1968", price 75 cents.
- UAG-30 "Catalogue of Data on Solar-Terrestrial Physics", price \$1.75.
- UAG-31 "Auroral Electrojet Magnetic Activity Indices AE (11) for 1969", price 75 cents.
- UAG-32 "Synoptic Radio Maps of the Sun at 3.3 mm for the Years 1967-1969", price 35 cents.
- UAG-33 "Auroral Electrojet Magnetic Activity Indices AE (10) for 1967", price 75 cents.
- UAG-34 "Absorption Data for the IGY/IGC and IQSY", price \$2.00.
- UAG-35 "Catalogue of Digital Geomagnetic Variation Data at World Data Center A for Solar-Terrestrial Physics", price 20 cents.
- UAG-36 "An Atlas of Extreme Ultraviolet Flashes of Solar Flares Observed Via Sudden Frequency Deviations During the ATM-SKYLAB Missions", price 55 cents.
- UAG-37 "Auroral Electrojet Magnetic Activity Indices AE (10) for 1966", price 75 cents.
- UAG-38 "Master Station List for Solar-Terrestrial Physics Data at WDC-A for Solar-Terrestrial Physics", price \$1.60.
- UAG-39 "Auroral Electrojet Magnetic Activity Indices AE (11) for 1971", by Joe Haskell Allen, Carl C. Abston and Leslie D. Morris, National Geophysical and Solar-Terrestrial Data Center, Environmental Data Service, February 1975, 144 pages, price \$2.05.
- UAG-40 "H-Alpha Synoptic Charts of Solar Activity For the Period of Skylab Observations, May, 1973-March, 1974", by Patrick S. McIntosh, NOAA Environmental Research Laboratory, February 1975, 32 pages, price 56 cents.
- UAG-41 "H-Alpha Synoptic Charts of Solar Activity During the First Year of Solar Cycle 20, October, 1964 - August, 1965", by Patrick S. McIntosh, NOAA Environmental Research Laboratory, and Jerome T. Nolte, American Science and Engineering, Cambridge, Massachusetts, March 1975, 25 pages, price 48 cents.
- UAG-42 "Observations of Jupiter's Sporadic Radio Emission in the Range 7.6-80 MHz 10 December 1971 through 21 March 1975", by James W. Warwick, George A. Dulk, and Anthony C. Riddle, Department of Astro-Geophysics, University of Colorado, Boulder, Colorado 80302, April 1975, 49 pages, price \$1.15.
- UAG-43 "Catalog of Observation Times of Ground-Based Skylab-Coordinated Solar Observing Programs", compiled by Helen E. Coffey, World Data Center A for Solar-Terrestrial Physics, May 1975, 159 pages, price \$3.00.

- UAG-44 "Synoptic Maps of Solar 9.1 cm Microwave Emission from June 1962 to August 1973", by Werner Graf and Ronald N. Bracewell, Radio Astronomy Institute, Stanford University, Stanford, California 94305, May 1975, 183 pages, price \$2.55.
- UAG-45 "Auroral Electrojet Magnetic Activity Indices AE (11) for 1972", by Joe Haskell Allen, Carl C. Abston and Leslie D. Morris, National Geophysical and Solar-Terrestrial Data Center, Environmental Data Service, May 1975, 144 pages, price \$2.10.
- UAG-46 "Interplanetary Magnetic Field Data 1963-1974", by Joseph H. King, National Space Science Data Center, NASA Goddard Space Flight Center, Greenbelt, Maryland 20771, June 1975, 382 pages, price \$2.95.
- UAG-47 "Auroral Electrojet Magnetic Activity Indices AE (11) for 1973", by Joe Haskell Allen, Carl C. Abston and Leslie D. Morris, National Geophysical and Solar-Terrestrial Data Center, Environmental Data Service, June 1975, 144 pages, price \$2.10.
- UAG-48A "Synoptic Observations of the Solar Corona during Carrington Rotations 1580-1596 (11 October 1971 - 15 January 1973)"; [Reissue with quality images] by R. A. Howard, M. J. Koomen, D. J. Michels, R. Tousey, C. R. Detwiler, D. E. Roberts, R. T. Seal and J. D. Whitney, E. O. Hulbert Center for Space Research, NRL, Washington, D. C. 20375 and R. T. and S. F. Hansen, C. J. Garcia and E. Yasukawa, High Altitude Observatory, NCAR, Boulder, Colorado 80303, February 1976, 200 pages, price \$4.27.
- UAG-49 "Catalog of Standard Geomagnetic Variation Data", prepared by Environmental Data Service, NOAA, Boulder, Colorado, August 1975, 125 pages, price \$1.85.
- UAG-50 "High-Latitude Supplement to the URSI Handbook on Ionogram Interpretation and Reduction", by W. R. Piggott, British Antarctic Survey, c/o SRC, Appleton Laboratory, Ditton Park, Slough, England, October 1975, 292 pages, price \$4.00.
- UAG-51 "Synoptic Maps of Solar Coronal Hole Boundaries Derived from He II 304Å Spectroheliograms from the Manned Skylab Missions", by J. D. Bohlín and D. M. Rubenstein, E. O. Hulbert Center for Space Research, Naval Research Laboratory, Washington, D. C. 20375 U.S.A., November 1975, 30 pages, price 54 cents.
- UAG-52 "Experimental Comprehensive Solar Flare Indices for Certain Flares, 1970-1974", compiled by Helen W. Dodson and E. Ruth Hedeman, McMath-Hulbert Observatory, The University of Michigan, 895 Lake Angelus Road North, Pontiac, Michigan 48055 U.S.A., November 1975, 27 pages, price 60 cents.
- UAG-53 "Description and Catalog of Ionospheric F-Region Data, Jicamarca Radar Observatory (November 1966 - April 1969)", by W. L. Clark and T. E. Van Zandt, Aeronomy Laboratory, NOAA, Boulder, Colorado 80302 and J. P. McClure, University of Texas at Dallas, Dallas, Texas 75230, April 1976, 10 pages, price 33 cents.
- UAG-54 "Catalog of Ionosphere Vertical Soundings Data", prepared by Environmental Data Service, NOAA, Boulder, Colorado 80302, April 1976, 130 pages, price \$2.10.
- UAG-55 "Equivalent Ionospheric Current Representations by a New Method, Illustrated for 8-9 November 1969 Magnetic Disturbances", by Y. Kamide, Cooperative Institute for Research in Environmental Sciences, University of Colorado, Boulder, Colorado 80302 and Geophysical Institute, University of Alaska, Fairbanks, Alaska 99701, H. W. Kroehl, Data Studies Division, NOAA/EDS/NGSDC, Boulder, Colorado 80302, M. Kanamitsu, Advanced Study Program, National Center for Atmospheric Research, Boulder, Colorado 80303, J. H. Allen, Data Studies Division, NOAA/EDS/NGSDC, Boulder, Colorado 80302, and S.-I. Akasofu, Geophysical Institute, University of Alaska, Fairbanks, Alaska 99701, April 1976, 91 pages, price \$1.60.
- UAG-56 "Iso-intensity Contours of Ground Magnetic H Perturbations for the December 16-18, 1971 Geomagnetic Storm", by Y. Kamide, Cooperative Institute for Research in Environmental Sciences, University of Colorado, Boulder, Colorado 80302 and Geophysical Institute, University of Alaska, Fairbanks, Alaska 99701 (currently Guest worker at Data Studies Division, NOAA/EDS/NGSDC, Boulder, Colorado 80302), April 1976, 37 pages, price \$1.39.